



January 2015

Syntheses And Characterization Of Bis(amino)cyclodiphosphazane Complexes Of Group 4- And -15 Elements

Mathew Etang Otang

[How does access to this work benefit you? Let us know!](#)

Follow this and additional works at: <https://commons.und.edu/theses>

Recommended Citation

Otang, Mathew Etang, "Syntheses And Characterization Of Bis(amino)cyclodiphosphazane Complexes Of Group 4- And -15 Elements" (2015). *Theses and Dissertations*. 1942.
<https://commons.und.edu/theses/1942>

This Dissertation is brought to you for free and open access by the Theses, Dissertations, and Senior Projects at UND Scholarly Commons. It has been accepted for inclusion in Theses and Dissertations by an authorized administrator of UND Scholarly Commons. For more information, please contact und.common@library.und.edu.

SYNTHESES AND CHARACTERIZATION OF
BIS(AMINO)CYCLODIPHOSPHAZANE COMPLEXES OF GROUP 4- AND -15
ELEMENTS

By

Mathew E. Otang
Bachelor of Science, University of Buea, 2004
Master of Science, University of Buea, 2008

A Dissertation

Submitted to the Graduate School

of the

University of North Dakota

In partial fulfilment of the requirements

for the degree of

Doctor of Philosophy

Grand Forks, North Dakota

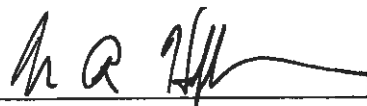
December

2015

This dissertation, submitted by Mathew Etang Otang in partial fulfilment of the requirements for the Degree of Doctor of Philosophy from the University of North Dakota, has been read by the Faculty Advisory Committee under whom the work has been done, and is hereby approved.



Dr. Lothar Stahl



Dr. Mark Hoffmann



Dr. Harmon Abrahamson



Dr. Guodong Du



Dr. Mike Poellot

This dissertation is being submitted by the appointed advisory committee as having met all of the requirements of the Graduate School at the University of North Dakota and is hereby approved.



Wayne Swisher
Dean of the Graduate School



Date

PERMISSION

Title SYNTHESES AND CHARACTERIZATION OF
 BIS(AMINO)CYCLODIPHOSPHAZANE COMPLEXES OF
 GROUP 4- AND -15 ELEMENTS

Department Chemistry

Degree Doctor of Philosophy

In presenting this dissertation in partial fulfilment of the requirements for a graduate degree from the University of North Dakota, I agree that the library of this University shall make it freely available for inspection. I further agree that permission for extensive copying for scholarly purposes may be granted by the professor who supervised my dissertation work or, in his absence, by the chairperson of the department or the dean of the Graduate School. It is understood that any copying or publication or other use of this dissertation or part thereof for financial gain shall not be allowed without my written permission. It is also understood that due recognition shall be given to me and to the University of North Dakota in any scholarly use which may be made of any material in my dissertation.

Mathew Ftang Utang

11/30/2015

TABLE OF CONTENTS

LIST OF FIGURES	x
LIST OF TABLES	xv
LIST OF SCHEMES.....	xvii
LIST OF SYMBOLS AND ABBREVIATIONS	xix
ACKNOWLEDGEMENTS	xxiii
ABSTRACT	xxiv
CHAPTER	
I. GENERAL INTRODUCTION	1
1. Overview of Cyclodiphosphazanes	1
2. Literature Review	3
2.1. Synthesis of Bis(amino)cyclodiphosph(III)azanes	3
2.2. Synthesis of Bis(amino)cyclodiphosph(V)azanes	6
2.3. Synthesis of Metal Complexes of Bis(amino)cyclodiphosph(V)azanes.....	8
2.4. Applications of Cyclodiphosphazanes.....	10

II. ZIRCONIUM- AND -HAFNIUM BIS(AMINO)CYCLODIPHOSPH(V)AZANES COMPLEXES.....	15
1. Introduction	15
2. Experimental	16
Description of Techniques and Chemicals Used.....	16
Description of Instrumentation.....	17
X-ray Crystallography	17
3. Syntheses of Compounds	18
Synthesis of $\{[(^t\text{BuNP})_2(^t\text{BuN})_2]\text{Zr}(\text{O}^t\text{Bu})_2\}$, 35	18
Synthesis of $\{[(^t\text{BuNP})_2(^t\text{BuN})_2]\text{Hf}(\text{O}^t\text{Bu})_2\}$, 36	18
Synthesis of $\{[(^t\text{BuNP}=\text{S})_2(^t\text{BuN})_2]\text{Zr}(\text{O}^t\text{Bu})_2\}$, 37	19
Synthesis of $\{[(^t\text{BuNP}=\text{S})_2(^t\text{BuN})_2]\text{Hf}(\text{O}^t\text{Bu})_2\}$, 38	20
Synthesis of $\{[(^t\text{BuNP}=\text{S})_2(^t\text{BuN})_2]\text{ZrCl}_2\}$, 39	20
Synthesis of $\{[(^t\text{BuNP}=\text{S})_2(^t\text{BuN})_2]\text{HfCl}_2\}$, 40	21
4. Results and Discussions	22
Synthesis and Spectroscopic Analysis of $\{[(^t\text{BuNP})_2(^t\text{BuN})_2]\text{Zr}(\text{O}^t\text{Bu})_2\}$, 34	22
Synthesis and Spectroscopic Analysis of $\{[(^t\text{BuNP})_2(^t\text{BuN})_2]\text{Hf}(\text{O}^t\text{Bu})_2\}$, 36	24
Synthesis and Spectroscopic Analysis of $\{[(^t\text{BuNP}=\text{S})_2(^t\text{BuN})_2]\text{Zr}(\text{O}^t\text{Bu})_2\}$, 37	26
Solid-state Structure of $\{[(^t\text{BuNP}=\text{S})_2(^t\text{BuN})_2]\text{Zr}(\text{O}^t\text{Bu})_2\}$, 37	27

Synthesis and Spectroscopic Analysis of {[(^t BuNP=S) ₂ (^t BuN) ₂]Hf(O ^t Bu) ₂ }, 38	32
Solid-state Structure of {[(^t BuNP=S) ₂ (^t BuN) ₂]Hf(O ^t Bu) ₂ }, 38	33
Synthesis and Spectroscopic Analysis of {[(^t BuNP=S) ₂ (^t BuN) ₂]ZrCl ₂ }, 39	37
Solid-state Structure of {[(^t BuNP=S) ₂ (^t BuN) ₂]ZrCl ₂ }, 39	39
Synthesis and Spectroscopic Analysis of {[(^t BuNP=S) ₂ (^t BuN) ₂]HfCl ₂ }, 40	42
Solid-state Structure of {[(^t BuNP=S) ₂ (^t BuN) ₂]HfCl ₂ }, 40	43
Polymerization Studies.....	47
5. Summary and Conclusion.....	47
III. REACTIONS OF DIANIONIC BIS(ALKYLAMIDO)CYCLODIPHOSPH(III)AZANES WITH ELECTROPHILES: <i>N</i> VERSUS <i>P</i> ELECTROPHILIC ATTACK.....	49
1. Introduction.....	49
2. Experimental.....	52
Description of Techniques and Chemicals Used.....	52
Description of Instrumentation.....	52
X-ray Crystallography.....	53
3. Syntheses of Compounds.....	53
Synthesis of [(PPh ₂) ^t BuNP(μ-N ^t Bu) ₂ PN ^t Bu(PPh ₂)], 52A and 52B	53
Synthesis of <i>cis</i> -[(^t BuNP) ₂ (CyNLi·THF) ₂], 54	54

Synthesis of <i>cis</i> -{[P(μ -N ^t Bu)] ₂ (CyNPCl ₂) ₂ }, 55	55
Synthesis of <i>cis</i> -[(MeSiN ^t Bu) ₂ (N ^t BuPCl ₂) ₂], 57	56
Synthesis of <i>cis</i> -{[(^t BuNPMe) ₂ (^t BuN) ₂ Li ₂ I ₂]}, 58	56
Synthesis of <i>trans</i> -[(MeSiN ^t Bu) ₂ (N ^t BuLi·thf) ₂], 60	57
4. Results and Discussions	58
Synthesis and Spectroscopic Analysis of [(PPh ₂) ^t BuNP(μ -N ^t Bu) ₂ PN ^t Bu(PPh ₂)] 52A and 52B	58
Kinetic Studies for the Conversion of Isomer 52B to Isomer 52A	63
Solid-state Structure of 52A	67
Solid-state Structure of 52B	71
Synthesis and Spectroscopic Analysis of <i>cis</i> -[(^t BuNP) ₂ (CyNLi·thf) ₂], 54	75
Solid-state Structure of <i>cis</i> -[(^t BuNP) ₂ (CyNLi·thf) ₂], 54	77
Synthesis and Spectroscopic Analysis of <i>cis</i> -{[P(μ -N ^t Bu)] ₂ (CyNPCl ₂) ₂ }, 55	82
Solid-state Structure of <i>cis</i> -{[P(μ -N ^t Bu)] ₂ (CyNPCl ₂) ₂ }, 55	84
Synthesis and Spectroscopic Analysis of <i>cis</i> -[(MeSiN ^t Bu) ₂ (N ^t BuPCl ₂) ₂], 57	89
Solid-state Structure of <i>cis</i> -[(MeSiN ^t Bu) ₂ (N ^t BuPCl ₂) ₂], 57	91
Synthesis and Spectroscopic Analysis of <i>cis</i> -{[(^t BuNPMe) ₂ (^t BuN) ₂ Li ₂ I ₂]}, 58	95
Synthesis and Spectroscopic Analysis of <i>trans</i> -[(MeSiN ^t Bu) ₂ (N ^t BuLi·thf) ₂], 60	97
Solid-state Structure of <i>trans</i> -[(MeSiN ^t Bu) ₂ (N ^t BuLi·thf) ₂], 60	98

5. Summary and Conclusion	102
IV. SYNTHESSES AND CHARACTERIZATION OF CYCLODIPHOSPHAZANE COMPLEXES OF PHOSPHORUS AND ANTIMONY	103
1. Introduction	103
2. Experimental	105
Description of Techniques and Chemicals Used.....	105
Description of Instrumentation	105
X-ray Crystallography	106
3. Syntheses of Compounds	106
Synthesis of [(^t BuNP=S) ₃ N], 66	106
Synthesis of [(^t BuNP) ₂ (^t BuN) ₂ P] ⁺ SO ₃ CF ₃ ⁻ , 67	107
Synthesis of {[(^t BuNP) ₂ (^t BuN) ₂]PPh}, 68	107
Synthesis of {[(^t BuNP) ₂ (^t BuN) ₂](P=S)Ph}, 69	108
Synthesis of {[(^t BuNP) ₂ (^t BuN) ₂]PO ^t Bu}, 70	109
Synthesis of {[(^t BuNP) ₂ (^t BuN) ₂]SbPh}, 71	110
Synthesis of {[(^t BuNP) ₂ (^t BuN) ₂]SbO ^t Bu}, 72	110
4. Results and Discussions	111
Synthesis and Spectroscopic Analysis of [(^t BuNP=S) ₃ N], 66	111
Solid-state Structure of [(^t BuNP=S) ₃ N], 66	113

Synthesis and Spectroscopic Analysis of [(^t BuNP) ₂ (^t BuN) ₂ P] ⁺ SO ₃ CF ₃ ⁻ , 67	118
Solid-state Structure of [(^t BuNP) ₂ (^t BuN) ₂ P] ⁺ SO ₃ CF ₃ ⁻ , 67	120
Synthesis and Spectroscopic Analysis of {[(^t BuNP) ₂ (^t BuN) ₂]PPh}, 68	125
Synthesis and Spectroscopic Analysis of {[(^t BuNP) ₂ (^t BuN) ₂](P=S)Ph}, 69	127
Solid-state Structure of {[(^t BuNP) ₂ (^t BuN) ₂](P=S)Ph}, 69	130
Synthesis and Spectroscopic Analysis of {[(^t BuNP) ₂ (^t BuN) ₂]PO ^t Bu}, 70	135
Synthesis and Spectroscopic Analysis of {[(^t BuNP) ₂ (^t BuN) ₂]SbPh}, 71	137
Solid-state Structure of {[(^t BuNP) ₂ (^t BuN) ₂]SbPh}, 71	140
Synthesis and Spectroscopic Analysis of {[(^t BuNP) ₂ (^t BuN) ₂]SbO ^t Bu}, 72	146
5. Summary and Conclusion	149
APPENDICES	
APPENDIX I.....	152
APPENDIX II.....	154
APPENDIX III.....	155
REFERENCES	158

LIST OF FIGURES

Figure	Page
1. Formulas of linear (A), cyclic (B), and polymeric (C), phosphazenes.....	1
2. General structure of bis(amino)cyclodiphosphazanes.	3
3. Examples of macrocycles containing two (26), four (27), five (28), and six (29) P ₂ N ₂ units synthesized from cis-[CIP(μ -NR)] ₂	11
4. Examples of known anti-cancer cyclodiphosphazanes.....	14
5. ¹ H NMR Spectrum of 35	22
6. ¹³ C{ ¹ H} NMR Spectrum of 35	23
7. ³¹ P{ ¹ H} NMR Spectrum of 35	24
8. ¹ H NMR Spectrum of 36	25
9. ¹³ C{ ¹ H} NMR Spectrum of 36	25
10. ³¹ P{ ¹ H} NMR Spectrum of 36	25
11. ¹ H NMR Spectrum of 37	26
12. ¹³ C{ ¹ H} NMR Spectrum of 37	27
13. ³¹ P{ ¹ H} NMR Spectrum of 37	27
14. Solid-state structure and partial labelling scheme of 37 . With the exception of carbon (35 %) all atoms are drawn at the 50 % probability level.	29
15. ¹ H NMR spectrum of 38	32
16. ¹³ C{ ¹ H} NMR Spectrum of 38	32
17. ³¹ P{ ¹ H} NMR Spectrum of 38	33

18. Solid-state structure and partial labelling scheme of 38 . With the exception of carbon (35 %) all atoms are drawn at the 50 % probability level.	34
19. ^1H NMR Spectrum of 39	38
20. $^{13}\text{C}\{^1\text{H}\}$ NMR Spectrum of 39	38
21. $^{31}\text{P}\{^1\text{H}\}$ NMR Spectrum of 39	38
22. Solid-state structure and partial labelling scheme of 39 . With the exception of carbon (35 %) all atoms are drawn at the 50 % probability level.	39
23. ^1H NMR Spectrum of 40	42
24. $^{13}\text{C}\{^1\text{H}\}$ NMR Spectrum of 40	42
25. $^{31}\text{P}\{^1\text{H}\}$ NMR Spectrum of 40	42
26. Solid-state structure and partial labelling scheme of 40 . With the exception of carbon (35 %) all atoms are drawn at the 50 % probability level.	44
27. Coordination modes of cyclodiphosphazanes.....	50
28. ^1H NMR Spectrum of 52 showing both isomers present.	59
29. $^{31}\text{P}\{^1\text{H}\}$ NMR Spectrum of 52 showing both isomers present.	59
30. ^1H NMR Spectrum of 52A	60
31. $^{31}\text{P}\{^1\text{H}\}$ NMR Spectrum of 52A	61
32. $^{13}\text{C}\{^1\text{H}\}$ NMR Spectrum of 52A	61
33. ^1H NMR Spectrum of 52B	62
34. $^{31}\text{P}\{^1\text{H}\}$ NMR Spectrum of 52B	62
35. $^{13}\text{C}\{^1\text{H}\}$ NMR Spectrum of 52B	63
36. Conversion of isomer 52B to isomer 52A at 70 °C.	64
37. Graph of $\ln[\text{isomer } \mathbf{52B}]$ against time.	65
38. Solid-state structure and partial labelling scheme of 52A . With the exception of carbon (35 %) all atoms are drawn at the 50 % probability level.	68

39. Solid-state structure and partial labelling scheme of 52B . With the exception of carbon (35 %) all atoms are drawn at the 50 % probability level.	72
40. ^1H NMR Spectrum of 54	76
41. The $^{13}\text{C}\{^1\text{H}\}$ NMR Spectrum of 54	77
42. The $^{31}\text{P}\{^1\text{H}\}$ NMR Spectrum of 54	77
43. Solid-state structure and partial labelling scheme of 54 . With the exception of carbon (35 %) all atoms are drawn at the 50 % probability level.	78
44. ^1H NMR Spectrum of 55	83
45. $^{13}\text{C}\{^1\text{H}\}$ NMR Spectrum of 55	84
46. $^{31}\text{P}\{^1\text{H}\}$ NMR Spectrum of 55	84
47. Solid-state structure and partial labelling scheme of 55 With the exception of carbon (35 %) all atoms are drawn at the 50 % probability level.	86
48. ^1H NMR Spectrum of 57	90
49. $^{13}\text{C}\{^1\text{H}\}$ NMR Spectrum of 57	90
50. $^{31}\text{P}\{^1\text{H}\}$ NMR Spectrum of 57	91
51. Solid-state structure and partial labelling scheme of 57 . With the exception of carbon (35 %) all atoms are drawn at the 50 % probability level.	92
52. ^1H NMR Spectrum of 58	96
53. $^{31}\text{P}\{^1\text{H}\}$ NMR Spectrum of 58	96
54. ^1H NMR Spectrum of 60	97
55. $^{13}\text{C}\{^1\text{H}\}$ NMR Spectrum of 60	98
56. Solid-state structure and partial labelling scheme of 60 . With the exception of carbon (35 %) all atoms are drawn at the 50 % probability level.	99
57. ^1H NMR Spectrum of 66	112
58. $^{13}\text{C}\{^1\text{H}\}$ NMR Spectrum of 66	112
59. $^{31}\text{P}\{^1\text{H}\}$ NMR Spectrum of 66	113

60. Solid-state structure and partial labelling scheme of 66 . With the exception of carbon (35 %) all atoms are drawn at the 50 % probability level.	114
61. Top view of 66 showing C_s symmetry.....	115
62. ^1H NMR Spectrum of 67	119
63. $^{13}\text{C}\{^1\text{H}\}$ NMR Spectrum of 67	119
64. $^{31}\text{P}\{^1\text{H}\}$ NMR Spectrum of 67	120
65. Solid-state structure and partial labelling scheme of 67 . With the exception of carbon (35 %) all atoms are drawn at the 50 % probability level.	121
66. Solid-state structure of 67 showing C_3 symmetry.....	122
67. ^1H NMR Spectrum of 68	126
68. $^{13}\text{C}\{^1\text{H}\}$ NMR Spectrum of 68	127
69. $^{31}\text{P}\{^1\text{H}\}$ NMR Spectrum of 68	127
70. ^1H NMR Spectrum of 69	129
71. $^{13}\text{C}\{^1\text{H}\}$ NMR Spectrum of 69	130
72. $^{31}\text{P}\{^1\text{H}\}$ NMR Spectrum of 69	130
73. Solid-state structure and partial labelling scheme of 69 . With the exception of carbon (35 %) all atoms are drawn at the 50 % probability level.	132
74. ^1H NMR Spectrum of 70	136
75. $^{13}\text{C}\{^1\text{H}\}$ NMR Spectrum of 70	137
76. $^{31}\text{P}\{^1\text{H}\}$ NMR Spectrum of 70	137
77. ^1H NMR Spectrum of 71	139
78. $^{13}\text{C}\{^1\text{H}\}$ NMR Spectrum of 71	140
79. $^{31}\text{P}\{^1\text{H}\}$ NMR Spectrum of 71	140
80. Solid-state structure and partial labelling scheme of 71 . With the exception of carbon (35 %) all atoms are drawn at the 50 % probability level.	142

81. Front view of 71 showing C_s symmetry.	143
82. ^1H NMR Spectrum of 72	147
83. $^{13}\text{C}\{^1\text{H}\}$ NMR Spectrum of 72	148
84. $^{31}\text{P}\{^1\text{H}\}$ NMR Spectrum of 72	148
85. ^1H NMR Spectrum of 74	153
86. $^{13}\text{C}\{^1\text{H}\}$ NMR Spectrum of 74	153

LIST OF TABLES

Table	Page
1. Crystal and structure refinement data for compound 37	30
2. Selected bond lengths (Å) and angles (°) for 37	31
3. Crystal and structure refinement data for compound 38	35
4. Selected bond lengths (Å) and angles (°) for 38	36
5. Crystal and structure refinement data for compound 39	40
6. Selected bond lengths (Å) and angles (°) for 39	41
7. Crystal and structure refinement data for compound 40	45
8. Selected bond lengths (Å) and angles (°) for 40	46
9. Crystal and structure refinement data for compound 52A	69
10. Selected bond lengths (Å) and angles (°) for 52A	70
11. Crystal and structure refinement data for compound 52B	73
12. Selected bond lengths (Å) and angles (°) for 52B	74
13. Crystal and structure refinement data for compound 54	80
14. Selected bond lengths (Å) and angles (°) for 54	81
15. Crystal and structure refinement data for compound 55	87
16. Selected bond lengths (Å) and angles (°) for compound 55	88
17. Crystal and structure refinement data for compound 57	93
18. Selected bond lengths (Å) and angles (°) for 57	94
19. Crystal and structure refinement data for compound 60	100

20. Selected bond lengths (Å) and angles (°) for 60	101
21. Crystal and structure refinement data for compound 66	116
22. Selected bond lengths (Å) and angles (°) for 66	117
23. Crystal and structure refinement data for compound 67	123
24. Selected bond lengths (Å) and angles (°) for 67	124
25. Crystal and structure refinement data for compound 69	133
26. Selected bond lengths (Å) and angles (°) for 69	134
27. Crystal and structure refinement data for compound 71	144
28. Selected bond lengths (Å) and angles (°) for 71	145
29. Crystal and structure refinement data for compounds, 35 and 36	154

LIST OF SCHEMES

Scheme	Page
1. Syntheses of 3 and 4	3
2. Synthesis of 5	4
3. Syntheses of 6 and 7	4
4. Synthesis of 8	5
5. Syntheses of 9 , 10 , and 11	5
6. Syntheses of 11 , 12 , and 13 by Oxidation.	6
7. Synthesis of 2 by thermolysis.	7
8. Syntheses of 2 and 16 by direct condensation/substitution.	7
9. Synthesis of 18 by metallation.	8
10. Synthesis of 19 by metathesis.	9
11. Syntheses of 21 and 22 by aminolysis.	9
12. Syntheses of 24 and 25 by oxidation.	10
13. N-aryl-amination of aryl bromides and chlorides catalyzed by 5	12
14. Suzuki cross-coupling reaction of alkyl halides and arylboronic acid by the binuclear cyclodiphosphazane palladium(II) complex (30).	13
15. Syntheses of 35 and 36	22
16. Syntheses of 37 and 38	26
17. Syntheses of 39 and 40	37
18. Syntheses of 49 , 50 , and 51	51

19. Syntheses of 52A and 52B	58
20. Isomerization of 52B to 52A via intramolecular nucleophilic attack.....	67
21. Synthesis of 54	75
22. Synthesis of 55	82
23. Synthesis of 57	89
24. Synthesis of 58	95
25. Synthesis of 60	97
26. Synthesis of bis(amino)cyclodiphosphazanes from two aminophosphazenes.	103
27. Syntheses of 61–65 reported previously.....	104
28. Synthesis of 66	112
29. Synthesis of 67	118
30. Synthesis of 68	125
31. Synthesis of 69	128
32. Synthesis of 70	135
33. Synthesis of 71	138
34. Synthesis of 72	146
35. Synthesis of 74	152

LIST OF SYMBOLS AND ABBREVIATIONS

1. Chemical Symbols and Abbreviations

Ar = Aryl

^tBu = tertiary butyl

Cy = cyclohexyl

dba = dibenzylideneacetone

E = chalcogen or organic azide

Et = ethyl

M = molar

MAO = methylaluminumoxane

Me = methyl

Ph = phenyl

R = alkyl or aryl group

THF = tetrahydrofuran

X = halogen

2. General Symbols and Abbreviations

A = frequency factor

Å = angstrom (1×10^{-10} m)

atm = atmosphere

Avg. = Average

°C = degrees Celsius

d = day

dec. = decomposition

E_a = activation energy

Σ = summation

fw = formula weight

g = gram

h = hour

HeLa = human cervical cancer cell line

k = rate constant

K = degrees Kelvin

μ = bridging

M = metal

mL = milliliter

mmol = millimole

M_p = melting point

R = gas constant (8.314 J/K/mol)

RT = room temperature

s = second

S_N2 = bimolecular nucleophilic substitution

Subl. = sublime

T = temperature

3. Nuclear Magnetic Resonance Symbols and Abbreviations

br = broad

d = doublet

dd = doublet of doublets

dt = doublet of triplets

δ = chemical shift

Hz = hertz (cycles per second)

J = coupling constant

m = multiplet

NMR = nuclear magnetic resonance

ppm = parts per million

s = singlet

t = triplet

td = triplet of doublets

{ ^1H } = proton decoupled

4. Infrared Spectroscopy Symbols and Abbreviations

m = medium

s = strong

vs = very strong

vw = very weak

w = weak

5. Crystallographic Symbols and Abbreviations

a = unit cell length

b = unit cell width

c = unit cell height

α = unit cell angle between b and c

β = unit cell angle between a and c

γ = unit cell angle between a and b

λ = wavelength

μ = absorption coefficient

ρ = density

L_p = Lorentz and polarization correction

ORTEP = Oak Ridge Thermal Ellipsoid Program

R = conventional residual factor

V = volume of unit cell

$wR2(F^2)$ = weighted residual factor

Z = number of molecules per unit cell

ACKNOWLEDGEMENTS

I would like to first of all convey my most profound gratitude to the almighty God for the strength, wisdom, and good health He accorded me to pursue and finish this Ph.D. program.

My earnest appreciation goes to my advisor, Dr. Stahl, for not only accepting me into his research group, but also for his ceaseless efforts and keen supervision in guiding me through my research program. I am also grateful for the invaluable technical assistance and feedback provided by all my graduate committee members.

I remain grateful for the financial assistance (Graduate Teaching Assistantship) that I received from the Graduate School through the Department of Chemistry. This assistantship was a huge privilege for me and it enabled me to effectively pursue my graduate program without worrying about how to pay my tuition/fees and to take care of my daily expenses.

I sincerely thank all the staff of the Department of Chemistry at UND for their various contributions that provided me with the platform necessary for the completion of this work. Thanks also to my former research group members, Dr. Edmond Njua and Dr. Joseph West, for helping me learn the use of the Schlenk line and other air-sensitive techniques. I appreciate all my fellow graduate students for their camaraderie and exchange of ideas that made my graduate school experience a worthwhile adventure.

Finally, I thank my uncles and relatives, who after my parents' death, contributed the little they had to make sure I go to college. May God reward them immensely.

ABSTRACT

In the first part of this work, the interaction of sodium *tert*-butoxide and sulfur with Group 4 metal bis(*tert*-butylamido)cyclodiphosph(III)azanes dichlorides, $\{[{}^t\text{BuNP})_2{}^t\text{BuN})_2\text{MCl}_2\}$, where M is Zr or Hf, is reported. The reaction of two equivalents of NaO^tBu with $\{[{}^t\text{BuNP})_2{}^t\text{BuN})_2\text{MCl}_2\}$, M = Zr, Hf, resulted in the isolation of the first metal alkoxide complexes $\{[{}^t\text{BuNP})_2{}^t\text{BuN})_2\text{M}(\text{O}^t\text{Bu})_2\}$, **35** (M = Zr) and **36** (M = Hf) of cyclodiphosphazanes. The oxidation of compounds **35** and **36** with elemental sulfur yielded $\{[{}^t\text{BuNP}=\text{S})_2{}^t\text{BuN})_2\text{M}(\text{O}^t\text{Bu})_2\}$, **37** (M = Zr) and **38** (M = Hf), respectively. Similarly, the oxidation of $\{[{}^t\text{BuNP})_2{}^t\text{BuN})_2\text{MCl}_2\}$, M = Zr, Hf, with elemental sulfur led to the isolation of $\{[{}^t\text{BuNP}=\text{S})_2{}^t\text{BuN})_2\text{MCl}_2\}$, **39** (M = Zr) and **40** (M = Hf). The structures of compounds **37–40** were determined by X-ray crystallography and confirmed by multi-nuclear NMR spectroscopy and elemental analysis.

In part two, the attack of two equivalents of the electrophiles Ph₂PCl, PCl₃, and CH₃I on the dianionic bis(alkylamido)cyclodiphosph(III)azanes, {R = *tert*-butyl (**48**), cyclohexyl (**54**)} is described. The reaction of $[({}^t\text{BuNP})_2({}^t\text{BuNLi}\cdot\text{thf})_2]$ with Ph₂PCl led to the isolation of two products: an asymmetric P, N product, **52A** and a symmetric P, P substituted heterocycle, **52B**. Treatment of *cis*- $[({}^t\text{BuNE})_2(\text{RNLi}\cdot\text{thf})_2]$, E = P, SiCH₃ and R = ^tBu, Cy, with PCl₃ yielded *cis*- $\{[\text{E}(\mu\text{-N}^t\text{Bu})_2(\text{RNPCl}_2)_2]\}$, **55** (E = P, R = Cy) and **57** (E = SiCH₃, R = ^tBu). While the reaction of MeI with compound **48** resulted in the isolation of the symmetrical product *cis*- $\{[({}^t\text{BuNPMe})_2({}^t\text{BuNLi}\cdot\text{thf})_2]\text{I}_2\}$, **58**. Also, the lithiation of compound **59** with *n*-BuLi yielded **60**. Compounds **52A**, **52B**, **54**, **55**, **57**, and

60 were characterized by multi-nuclear NMR spectroscopy, X-ray crystallography, and elemental analysis.

The last part of this work describes the syntheses and characterization of compounds derived from the reactions of $\{[(^t\text{BuNP})_2(^t\text{BuN})_2]\text{ECl}\}$, E = P, Sb, with various reagents. Treatment of $\{[(^t\text{BuNP})_2(^t\text{BuN})_2]\text{PCl}\}$ with excess sulfur, AgSO_3CF_3 , PhMgCl , and NaO^tBu led to the isolation of the compounds $[(^t\text{BuNP}=\text{S})_3\text{N}]$, **66**, $[(^t\text{BuNP})_2(^t\text{BuN})_2\text{P}]^+\text{SO}_3\text{CF}_3^-$, **67**, $\{[(^t\text{BuNP})_2(^t\text{BuN})_2]\text{PPh}\}$, **68**, and $\{[(^t\text{BuNP})_2(^t\text{BuN})_2]\text{PO}^t\text{Bu}\}$, **70**, respectively. Meanwhile, oxidation of compound **68** with elemental sulfur resulted in $\{[(^t\text{BuNP})_2(^t\text{BuN})_2](\text{P}=\text{S})\text{Ph}\}$, **69**. Also, the reaction of $\{[(^t\text{BuNP})_2(^t\text{BuN})_2]\text{SbCl}\}$ with PhMgCl and NaO^tBu yielded $\{[(^t\text{BuNP})_2(^t\text{BuN})_2]\text{SbPh}\}$, **71** and $\{[(^t\text{BuNP})_2(^t\text{BuN})_2]\text{SbO}^t\text{Bu}\}$, **72**, respectively. The structures of compounds **66**, **67**, **69**, and **71** were determined by X-ray crystallography and confirmed by multi-nuclear NMR spectroscopy and elemental analysis.

CHAPTER I

GENERAL INTRODUCTION

1. Overview of Cyclodiphosphazanes

Cyclodiphosphazanes are four-membered ring compounds of the form $[XP(\mu-NR)]_2$, featuring alternating phosphorus and nitrogen atoms in a $(P-N)_2$ ring. Phosphorus and nitrogen form more compounds of greater structural variety than any other two congeners in the periodic table.^{1,2} This is not only because of the ability of nonmetals to form single-, double- and triple bonds with each other, but it is also a result of the high thermal stability of most phosphorus-nitrogen compounds resulting from the strength of P-N bonds. Among all compounds formed by nitrogen and phosphorus, the phosphazenes (Figure 1) have received the most attention because they are used as precursors for P-N polymers and hybrid materials.³⁻⁶

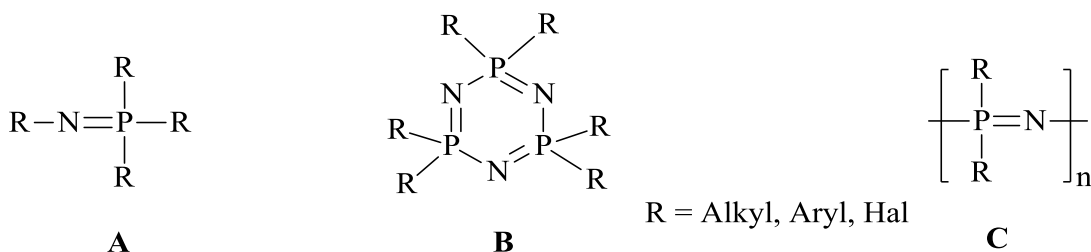


Figure 1. Formulas of linear (A), cyclic (B), and polymeric (C) phosphazenes.

The phosphazenes, both acyclic and cyclic, on the other hand are also a class of P-N compounds with an established chemistry and are well-known for their high stability and ease of synthesis.⁷⁻¹² Whereas phosphazenes have three-coordinate nitrogen atoms,

only two-coordinate nitrogen atoms exist in phosphazenes. Although cyclodiphosphazanes were first reported in the late 19th century,¹³ they were only fully characterized in the early 1960s,^{7, 14} albeit with limited acceptance of the presence of the four-membered ring structure.¹⁵ However, single-crystal X-ray studies in the early 1970s,¹⁶ verified the central (P–N)₂ and served as a stimulus on the research interest on cyclodiphosphazanes. The variety of synthetic and mechanistic studies in the past four decades has led to a better understanding of the structures and reactivity of these saturated phosphorus–nitrogen heterocycles.^{9, 10, 17-40}

Aminocyclodiphosphazanes are neutral molecules, which upon deprotonation with a base yields dianionic amidocyclodiphosphazanes. In the (P–N)₂ ring of bis(amino)cyclodiphosph(III)azanes (**1**) the phosphorus atoms are P(III) centers while bis(amino)cyclodiphosph(V)azanes (**2**) contain P(V) centers (Figure 2). Each atom in the (P–N)₂ ring of cyclodiphosphazanes bears an exocyclic substituent. The substituents of the ring nitrogen atoms usually lie almost in the plane of the ring while the amino substituents of the phosphorus atoms are approximately perpendicular to the ring. Although this arrangement of substituents on the phosphorus atoms makes *cis*- and *trans*-isomers possible, only the *cis*-isomer is usually isolated.³⁸ An important characteristic of bis(amino)cyclodiphosph(III)azanes is that they can react at the exocyclic amines, as dianions, or at the phosphorus centers as cations– or neutral molecules. Also, chirality maybe incorporated at the phosphorus centers or nitrogen substituents, and these systems can easily be modified to furnish a wide range of mixed donor ligands.

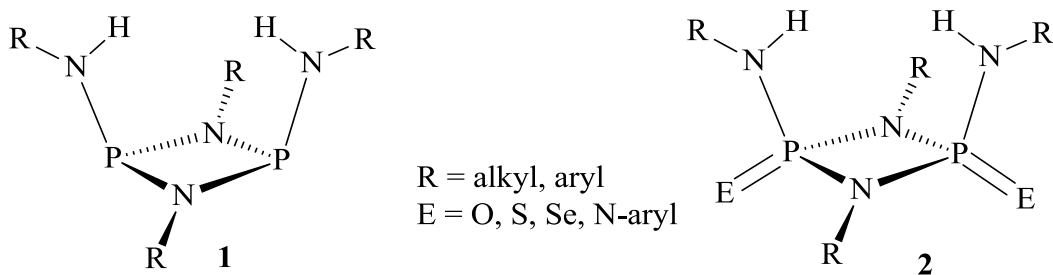


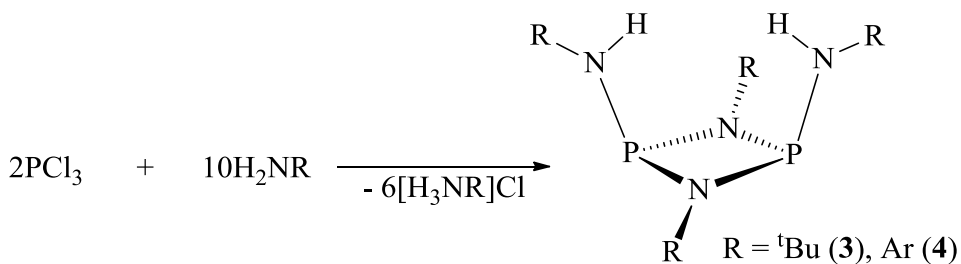
Figure 2. General structure of bis(amino)cyclodiphosphazanes.

2. Literature Review

2.1. Synthesis of Bis(amino)cyclodiphosph(III)azanes

2.1.1 Reaction of Phosphorus Trichloride with Primary Amines

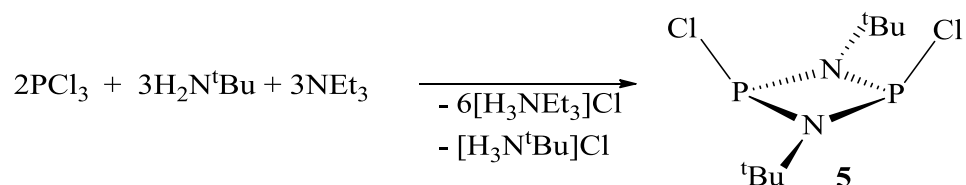
This method is the oldest and easiest means of preparing symmetrically-monosubstituted bis(amino)cyclodiphosph(III)azanes.^{7, 14} It involves the reaction of PCl_3 with a five-fold excess of a primary amine, as shown in Scheme 1. The excess primary amine serves as a Brønsted base to remove the HCl acid generated in the reaction. A modified procedure to obtain **3** was later reported by Schranz *et al.*³⁷ The compound $[\text{Ph}(\text{H})\text{N}(\text{PhNP})_2\text{N}(\text{H})\text{Ph}]$ (**4**) can also be obtained by the transamination of tris(diethylamino)phosphine with aniline.⁴¹



Scheme 1. Syntheses of **3** and **4**.

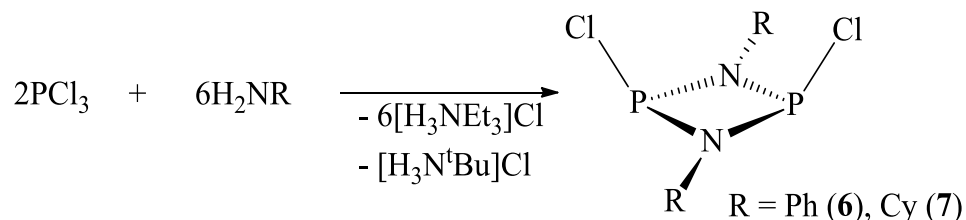
2.1.2 Reaction of Phosphorus Trichloride with Primary Amines in the Presence of Triethylamine

Due to the difficulty involved in using method I to synthesize hetero-substituted bis(amino)cyclodiphosph(III)azanes, alternative routes have been sought, and the first most efficient one (Scheme 2) used to prepare *cis*-[ClP(μ -N^tBu)₂PCl] (**5**) was reported by Moser *et al.*³³



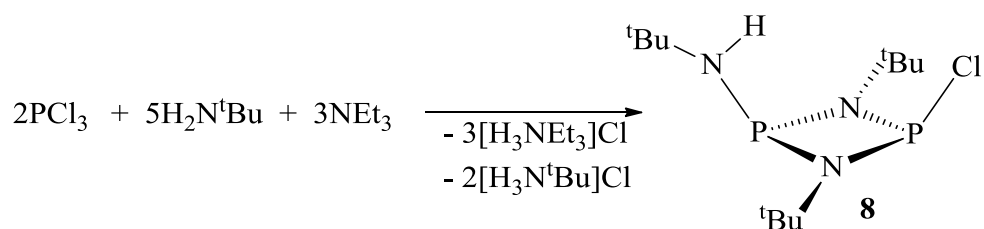
Scheme 2. Synthesis of **5**.

However, in the absence of triethylamine, analogues of compound **5** can also be obtained by treating PCl₃ with a three-fold excess of the respective primary amine as shown in Scheme 3.^{42, 43}



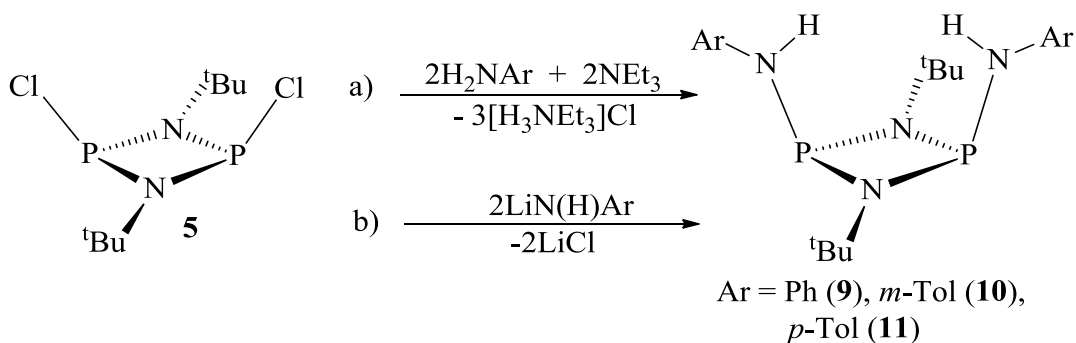
Scheme 3. Syntheses of **6** and **7**.

Hetero-substituted asymmetrical bis(amino)cyclodiphosph(III)azanes, such as [tBuN(H)N(tBuNP)₂Cl] (**8**), have also been prepared by treating two equivalents of PCl₃ with five equivalents of the respective primary amine and three equivalents of NEt₃, as shown in Scheme 4. In each case, the structures of the dichlorides were confirmed by X-ray crystallography.



Scheme 4. Synthesis of **8**.

The chlorine atoms in *cis*-[CIP(μ -N^tBu)₂PCl] (**5**) have been replaced with amino groups using two different approaches. The first involves treatment of compound **5** with two equivalents of a primary amine and two equivalents of triethylamine, as shown in equation (a), Scheme 5. While in the second method, compound **5** is treated with the corresponding lithium amide (equation (b), Scheme 5). Although the second approach requires one additional step, it gives the cleanest products.^{33, 36}



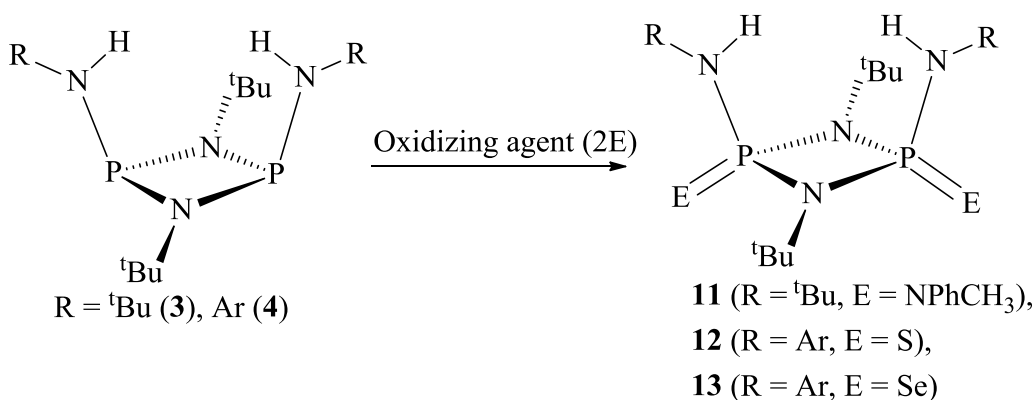
Scheme 5. Syntheses of **9**, **10**, and **11**.

2.2. Synthesis of Bis(amino)cyclodiphosph(V)azanes

Although several synthetic approaches have been used to prepare bis(amino)cyclodiphosph(V)azanes, there are three common general routes.

2.2.1 Oxidation of bis(amino)cyclodiphosph(III)azanes

This method involves the oxidation of bis(amino)cyclodiphosph(III)azanes with elemental chalcogens (E = S, Se or Te), a hydroperoxide (E = O), or an organic azide (E = NR) as shown in Scheme 6.^{29, 30, 32, 44-46}

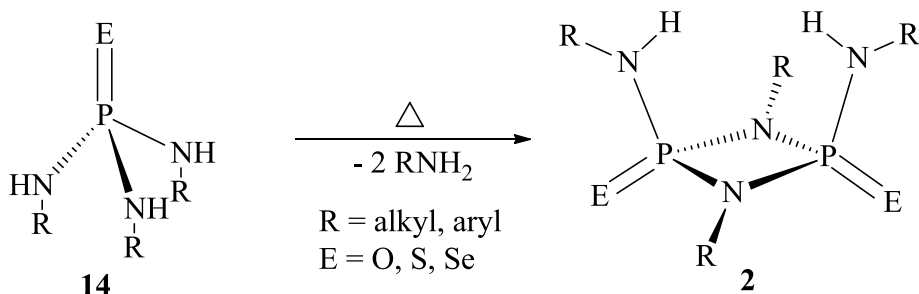


Scheme 6. Syntheses of **11**, **12**, and **13** by Oxidation.

This oxidation occurs via an S_N2 attack by the phosphorus(III) lone pair of electrons on the oxidizing agent, therefore there is usually retention of configuration at the phosphorus center.^{8, 18, 44} This means that *cis*-bis(amino)cyclodiphosph(III)azanes are oxidized solely to obtain the corresponding *cis*-bis(amino)cyclodiphosph(V)azanes while *trans*-bis(amino)cyclodiphosph(III)azanes are oxidized solely to obtain the corresponding *trans*-bis(amino)cyclodiphosph(V)azanes.

2.2.2 Thermolysis (Condensation) of Tris(amino)phosphates

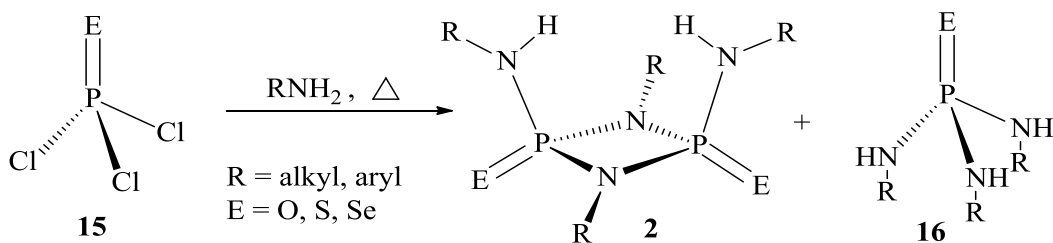
In this method, bis(amino)cyclodiphosph(V)azanes are obtained through direct condensation by thermolysis of tris(amino)phosphates and tris(amino)thiophosphates (Scheme 7).^{44, 47}



Scheme 7. Synthesis of **2** by thermolysis.

2.2.3 Direct Condensation/Substitution

Although this method is similar to method II, it differs in that condensation of the trichlorophosphine with a primary amine takes place *in situ*, followed by heating the reaction mixture (thermolysis) to obtain a mixture of the tris(amino)thiophosphate and the corresponding bis(amino)cyclodiphosph(V)azane at lower temperatures (Scheme 8).⁴⁴



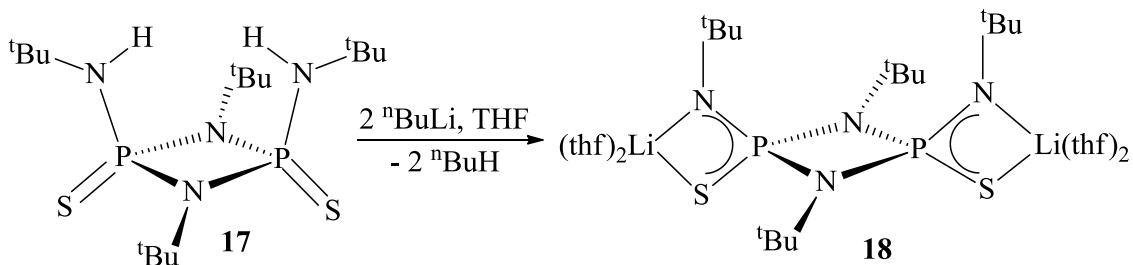
Scheme 8. Syntheses of **2** and **16** by direct condensation/substitution.

2.3. Synthesis of Metal Complexes of Bis(amino)cyclodiphosph(V)azanes

There are four commonly used methods to synthesized metal complexes of bis(amino)cyclodiphosph(V)azanes. These methods include metalation, metathesis, aminolysis, and oxidation.

2.3.1 Metallation

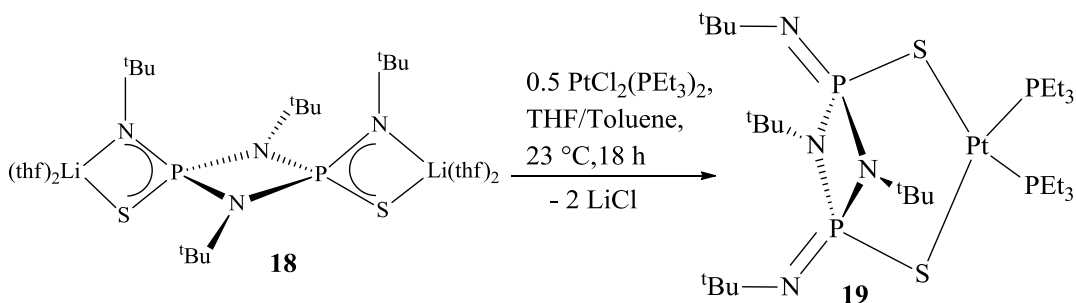
Metallation is the first and most widely used synthetic approach to metal complexes of bis(amino)cyclodiphosph(V)azanes.^{33, 37, 48-50} It involves the deprotonation of the ligand with a reactive organometallic compound, a metal amide, or metal alkoxide reagent (Scheme 9). This method is mostly employed for the preparation of alkali-metal salts of cyclodiphosphazanes, although it is also used in the syntheses of zinc and aluminum complexes.³⁰



Scheme 9. Synthesis of **18** by metallation.

2.3.2 Metathesis

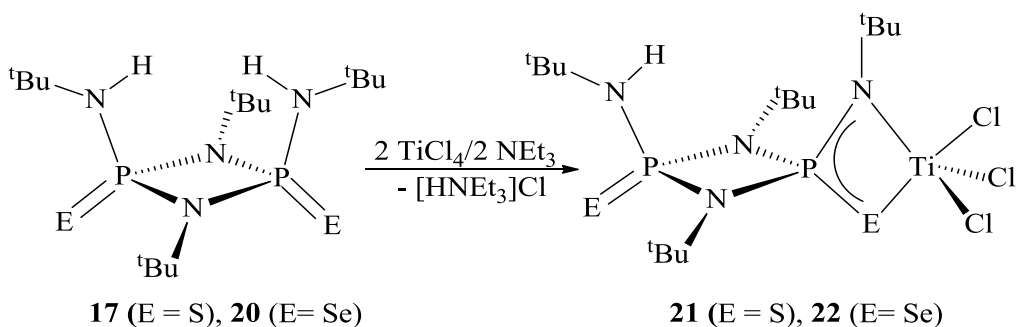
Metathesis involves the reaction between an anionic ligand, such as an alkali metal salt, and a metal halide (Scheme 10). This method is commonly used in the preparation of transition metal complexes.^{34, 36, 51, 52}



Scheme 10. Synthesis of **19** by metathesis.

2.3.3 Aminolysis

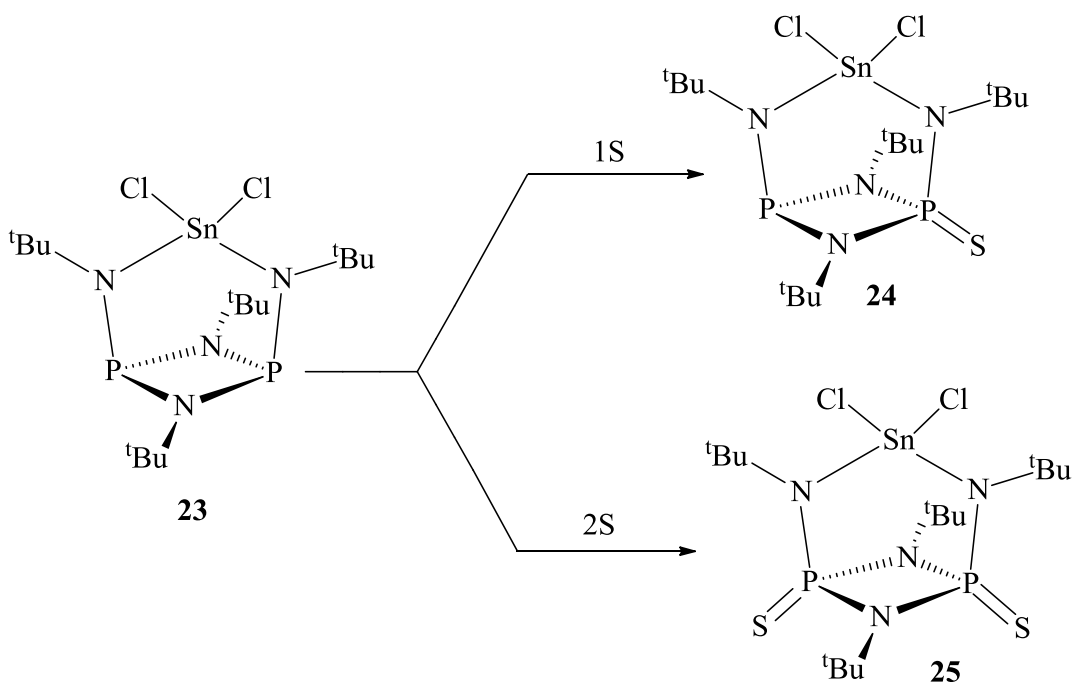
Aminolysis involves the direct reaction of a neutral ligand with a metal halide and a weak base (Scheme 11).^{32, 33, 53} The base functions as a proton scavenger. Structural analysis shows that compound **21** and **22** are *N, E*-chelated TiCl_3 complexes.³²



Scheme 11. Syntheses of **21** and **22** by aminolysis.

2.3.4 Oxidation

Oxidation of metal complex with elemental chalcogens or organic azides usually gives the corresponding P(V) metal complex (Scheme 12).^{32, 54, 55} This method is often the least commonly employed. However, oxidation is important because it does not disrupt the coordination mode of the ligand.



Scheme 12. Syntheses of **24** and **25** by oxidation.

2.4. Applications of Cyclodiphosphazanes

Cyclodiphosphazanes are used in a variety of areas ranging from material precursors to potential anti-cancer agents. Below is a brief review of the current areas in which cyclodiphosphazanes are used.

2.4.1 Scaffolds for Building Clusters, Cages, and Macrocycles

There has been a growing interest in the use of cyclodiphosphazanes in the synthesis of a variety of inorganic clusters, cages, and macrocycles with both main group and transition metal incorporation.^{23-26, 34-37, 56-63} This is not only because of the rigid nature of the P_2N_2 ring, but also due to the presence of the *cis*-oriented and reactive nature of the two P–Cl bonds in bis(chloro)cyclodiphosphazanes, *cis*-[ClP(μ -NR)]₂. The *cis*-orientation of the P–Cl bonds provides a favorable pre-organization for the formation of cyclic structures.⁶⁴ Nucleophilic substitution at the phosphorus center has

predominantly been utilized resulting in macrocycles with varying number of P_2N_2 rings, ranging from two to six as shown in Figure 3.^{25, 60, 64-66} These macrocycles have the ability to host neutral or ionic molecules within their core cavities similar to what is observed for crown ethers, calixarenes, cryptands, and porphyrins.⁶⁷⁻⁷¹ These metallamacrocycles are very important supramolecular structures that are used in catalysis, sensors and molecular electronics.⁷²⁻⁷⁴

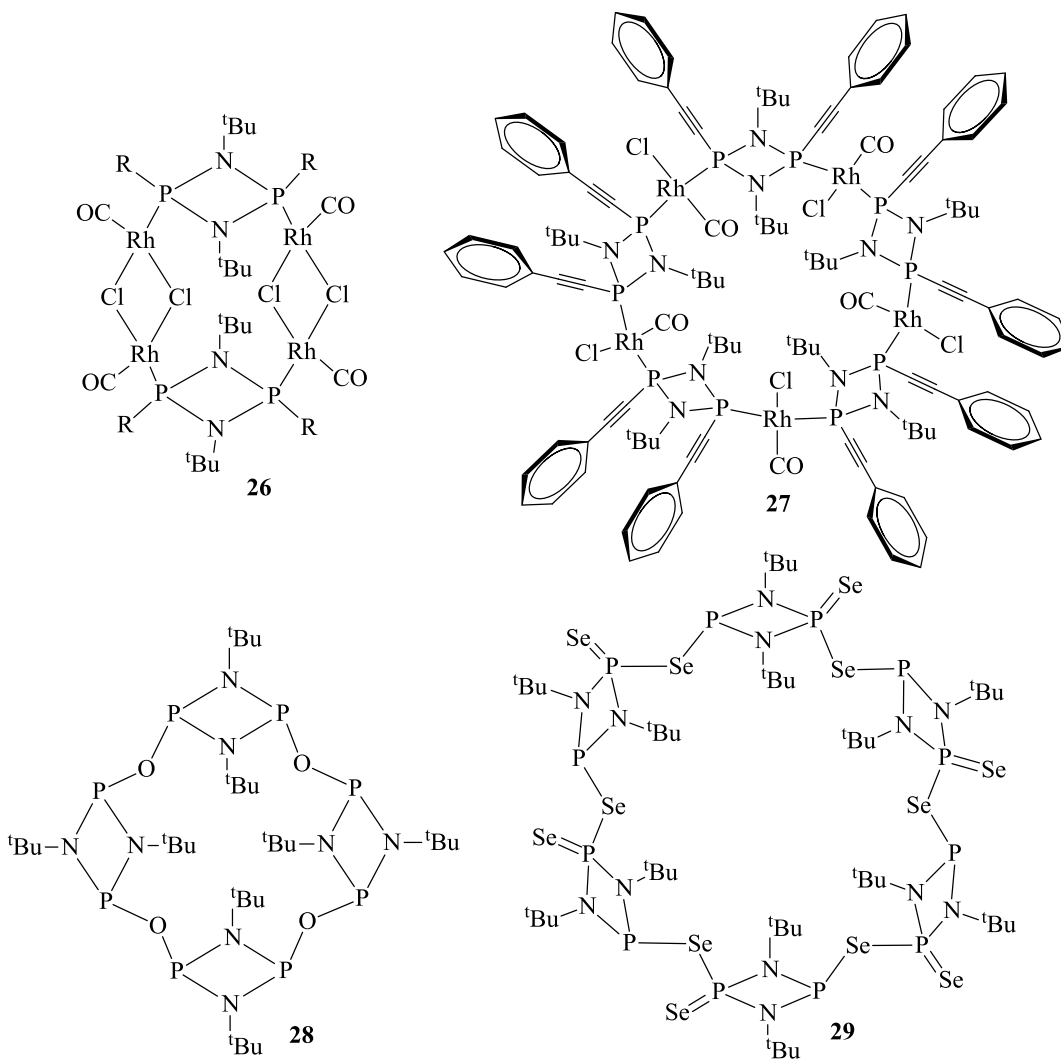
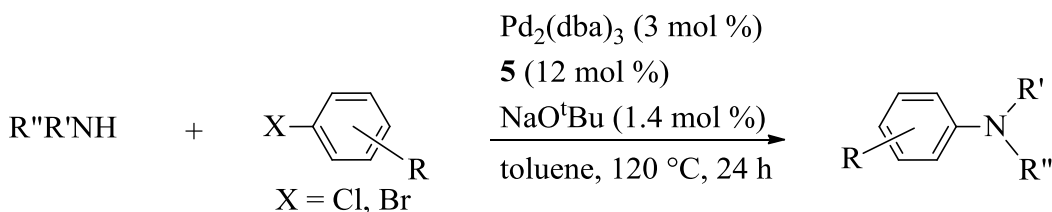


Figure 3. Examples of macrocycles containing two (**26**), four (**27**), five (**28**), and six (**29**) P_2N_2 units synthesized from $cis-[ClP(\mu-NR)_2]_2$.

2.4.2 Ligands in Palladium-Catalyzed Cross-Coupling Reactions

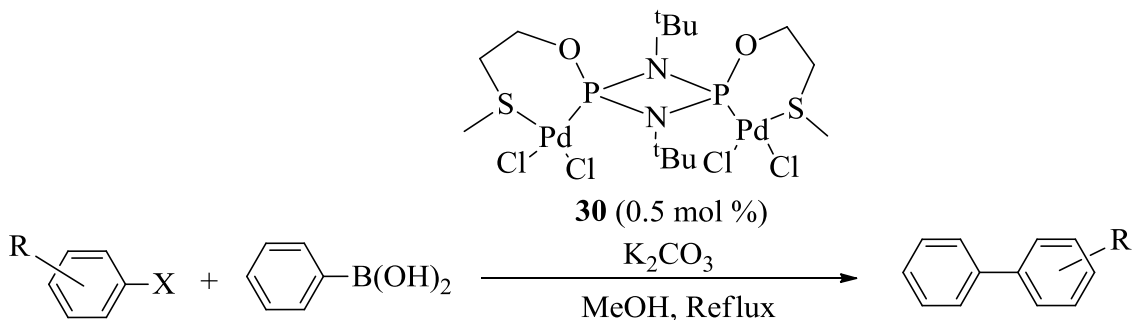
C–N bond formation by palladium-catalyzed cross-coupling reaction is a powerful synthetic technique in organic chemistry. It has been widely used in pharmaceutical, biological, and material sciences for various application.⁷⁵⁻⁷⁸ This reaction is often used for the N-arylation of nitrogen nucleophiles with aryl halides. Swamy and co-workers demonstrated that the inexpensive dichlorocyclodiphosphazane (**5**) can be used as a ligand in the palladium-catalyzed N-arylation of various amines with aryl halides.⁷⁹ The optimum condition for the reaction was the use of 12 mol % of **5**, 3 mol % of Pd₂(dba)₃ at 120 °C, resulting in a 94 % yield of the coupled product (Scheme 13).



Scheme 13. N-aryl-amination of aryl bromides and chlorides catalyzed by **5**.

Although the palladium-catalyzed cross-coupling reaction is known with a variety of transmetallating agents, the Suzuki-Miyaura cross-coupling for the C–C bond formation is the most attractive and practical protocol because of its tolerance for a variety of functional groups.⁸⁰⁻⁸³ In the work of Mague and co-workers,⁸⁴ they found that the bischelated binuclear palladium(II) complex of cyclodiphosphazane (**30**) is an attractive catalyst for the Suzuki cross-coupling reaction of arylboronic acid with aryl bromides. They used 0.5 mol % of **24** at 60 °C in the presence of K₂CO₃ (Scheme 14) as a base and obtained yields ranging from 65–100 %. The homogenous nature of this

catalysis was confirmed by the classical mercury test – addition of a drop of mercury to the reaction mixture did not affect the conversion rate of the reaction, since heterogeneous catalysis would form an amalgam resulting in the poisoning of the catalyst.⁸⁵



Scheme 14. Suzuki cross-coupling reaction of alkyl halides and arylboronic acid catalyzed by the binuclear cyclodiphosphazane palladium(II) complex (**30**).

Apart from being used as catalysts for palladium catalyzed cross-coupling reactions, some cyclodiphosphazanes have been used to study other organic reaction mechanisms like the Mitsunobu reaction,⁸⁶ and Umpolung addition reactions via phosphine activation of alkynes.⁸⁷⁻⁹⁰

2.4.4 Anti-Cancer Biological Studies

In 1994 Abd-Ellah *et al.*⁹¹ reported that some aminocyclodiphosphazane derivatives showed antimicrobial activity. Recently, Balakrishna and co-workers have utilized some cyclodiphosphazanes in anti-cancer studies.^{92, 93} In their studies they observed that the gold(I) cyclodiphosphazane complex (**31**) and the selenol-derived cyclodiphosphazane (**32**) (shown in Figure 4) were effective anti-cancer drugs which inhibited the proliferation of a human cervical cancer cell line (HeLa). Compound **25** exhibited about 38 ± 4 and 83 ± 6 % inhibition of proliferation with 5 and 20 μM , respectively, while compound **26** exhibited about 53 ± 8 and 93 ± 7 % inhibition of

proliferation with 5 and 20 μM , respectively. Under similar experimental conditions, they observed that the anti-cancer drug cisplatin inhibited HeLa cell proliferation with half-maximal inhibitory concentration of $8 \pm 1 \mu\text{M}$. From their findings the anti-proliferative activities of these water-soluble compounds **31** and **32** were superior to that of cisplatin.

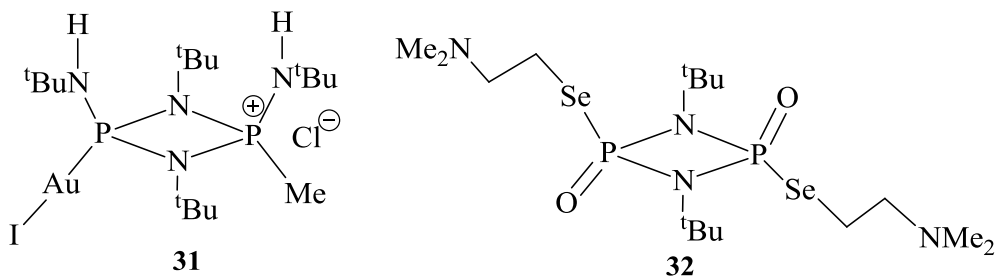


Figure 4. Examples of known anti-cancer cyclodiphosphazanes.

Cyclodiphosphazanes have also been used as ligands for catalysts active in olefin polymerization reactions (Chapter II) and as ligands in coordination chemistry (Chapter III).

3. Scope of Dissertation

In this work we investigated the chemistry of cyclodiphosph(III)azanes and cyclodiphosph(V)azanes as ligands for transition metal and main group elements. This dissertation is divided into four chapters. Chapter I contains the general introduction and review of related literature. The next three chapters contain our findings on three different projects. In Chapter II we report our observations on the syntheses and characterization of bis(amino)cyclodiphosph(V)azanes complexes of zirconium and hafnium. The study of the reactions of anionic bis(alkylamido)cyclodiphosph(III)azanes with electrophiles is reported in Chapter III. The syntheses and characterization of new cyclodiphosphazanes complexes of phosphorus and antimony is described in Chapter IV.

CHAPTER II

ZIRCONIUM- AND -HAFNIUM BIS(AMIDO)CYCLODIPHOSPH(V)AZANES COMPLEXES

1. Introduction

Our interest in bis(amino)cyclodiphosphazane ligands is due to the fact that as chelating ligands with substantial steric bulk, they can generate metal complexes with low coordination numbers. Low coordination numbers for metal complexes are necessary if the complexes are to be used for catalysis. This is because one of the most important property of any catalyst is the availability of an open coordination site.⁹⁴

Metals bearing bis(amido)cyclodiphosphazane ligands are potential catalysts precursors for olefin polymerization because of the *cis*-disposition of the halides on the metal and the tetrahedral coordination geometry about the metal center.^{38, 53, 95, 96} In particular, bis(amido)cyclodiphosph(III)azane complexes derived from group 4 metals have garnered a considerable research interest over the last two decades because they exhibit substantial catalytic activity for ethylene polymerization.^{27, 33, 95} Group 4 bis(amido) complexes are of interest for the following reasons. First, they are less electron rich (12-electron species) than their metallocene analogues (16-electron species). This decreased electron density results in a more Lewis acidic catalyst with improved catalytic activity because activation by the co-catalyst is enhanced. Second, the steric and electronic environment around the metal center can be conveniently altered. This can lead to changes in the physical properties of the polymers produced.

However, the activity of cyclodiphosph(III)azane catalysts decreases significantly after being activated with the co-catalyst methylalumoxane (MAO).³² This observation has been attributed to the occurrence of side reactions and the ring opening of the cyclodiphosphazane.⁴⁵ Side reactions take place because relatively less bulky substituents (R = ^tBu) do not sufficiently protect the Lewis acidic metal center. While the ring opening and destruction of the catalyst occurs because the Lewis acidic MAO reacts with the lone pair of electrons present on the P(III) centers. However, when the P(III) centers are oxidized with elemental chalcogens or organic azides, less Lewis basic cyclodiphosph(V)azanes, which can potentially have higher activities, are obtained.⁵³ The goal of this study is therefore to synthesize group 4 metal complexes with cyclodiphosph(V)azanes *N*- and *S*-donor chelating ligands, and to fully characterize these complexes by NMR spectroscopy, X-ray crystallography, and elemental analysis.

2. Experimental

Description of Techniques and Chemicals Used

General

All experimental procedures were carried out under an atmosphere of argon, using standard Schlenk lines. Prior to use, all solvents were dried and freed of molecular oxygen by distillation under a nitrogen atmosphere from sodium- or potassium benzophenone ketyl.

Chemicals used

Phosphorus trichloride, *tert*-butylamine, NaO^tBu, ZrCl₄, HfCl₄, and sulfur were purchased from either Sigma Aldrich or Alfa Aesar, and they were used without further purification. The compounds *cis*-[(^tBuNP)₂(^tBuNLi·thf)₂],³⁷ {[(^tBuNP)₂(^tBuN)₂]ZrCl₂},²⁷

³³ and $\{[(^t\text{BuNP})_2(^t\text{BuN})_2]\text{HfCl}_2\}$,^{27, 33} were synthesized according to published procedures.

Description of Instrumentation

NMR spectra were recorded on a Bruker AVANCE-500 NMR spectrometer. The ¹H and ¹³C NMR spectra were referenced relative to C₆D₅H (7.15 ppm) and C₆D₆ (128.0 ppm), respectively, as internal standards, while the ³¹P spectra were referenced relative to P(OEt)₃ (137.0 ppm) as external standard in C₆D₆. In all cases positive chemical shift values represent higher frequencies and downfield shifts. Melting points were recorded on Mel-Temp melting point apparatus; they are uncorrected. IR analyses were obtained on an ATI Mattson Genesis Series FTIR spectrometer. Elemental analyses on crystalline samples were performed by ALS Life Sciences Division Environmental, Tucson, AZ.

X-ray Crystallography

Suitable, single crystals were coated with Paratone oil, affixed to Mitegen or Litholoop crystal holders, and centered on the diffractometer in a stream of cold nitrogen. Reflection intensities were collected with a Bruker Apex diffractometer, equipped with an Oxford Cryosystems, 700 Series Cryostream cooler, operating at 173 K. Data were measured using ω scans of 0.3° per frame for 20 seconds until a complete hemisphere of data had been collected. Cell parameters were retrieved using SMART⁹⁷ software and refined with SAINT⁹⁸ on all observed reflections. Data were reduced with SAINTplus, which corrects for Lorentz polarization effects and crystal decay. Empirical absorption corrections were applied with SADABS.⁹⁹ The structures were solved by direct methods with SHELXS-90¹⁰⁰ program and refined by full-matrix least squares methods on F² with SHELXL-97¹⁰¹ incorporated in SHELXTL Version 5.10.¹⁰²

3. Syntheses of Compounds

Synthesis of $\{[(^t\text{BuNP})_2(^t\text{BuN})_2]\text{Zr}(\text{O}^t\text{Bu})_2\}$, **35**

In a 100 mL two-neck flask equipped with a gas inlet and magnetic stirring bar, was combined $\{[(^t\text{BuNP})_2(^t\text{BuN})_2]\text{ZrCl}_2\}$, **33**, (0.230 g, 0.450 mmol) and NaO^tBu (0.0900 g, 0.890 mmol) in 40 mL of toluene. The resulting colorless solution was stirred at 70 °C for 24 h, cooled in an ice bath for 1 h, filtered with a medium-porosity frit, concentrated *in vacuo* to about 15 mL and stored at -12 °C for 3 days. This produced colorless, rod-shaped crystals. Yield: (0.220 g, 0.370 mmol), 84 %.

Mp: 315–317 °C subl. ^1H NMR (500.1 MHz, benzene- d_6 , 25 °C): 1.50 (s, 18H, O^tBu), 1.45 (s, 18H, N^tBu), 1.42 (s, 18H, N^tBu). $^{13}\text{C}\{^1\text{H}\}$ NMR (125.8 MHz, benzene- d_6 , 25 °C): 77.3 (s, $\text{OC}(\text{CH}_3)_3$), 55.7 (d, $J_{\text{PC}} = 17.2$ Hz, $\text{NC}(\text{CH}_3)_3$, amido), 53.7 (t, $J_{\text{PC}} = 12.2$ Hz, $\text{NC}(\text{CH}_3)_3$, imido), 33.7 (d, $J_{\text{PC}} = 9.41$ Hz, $\text{NC}(\text{CH}_3)_3$, amido), 33.5 (s, $\text{OC}(\text{CH}_3)_3$), 30.8 (t, $J_{\text{PC}} = 5.95$ Hz, $\text{NC}(\text{CH}_3)_3$, imido). $^{31}\text{P}\{^1\text{H}\}$ NMR (202.5 MHz, benzene- d_6 , 25 °C): 103.5 (s). Anal. Calcd for $\text{C}_{24}\text{H}_{54}\text{N}_4\text{O}_2\text{P}_2\text{Zr}$: C, 49.36; H, 9.32; N, 9.60. Found: C, 49.60; H, 9.33; N, 9.03.

Synthesis of $\{[(^t\text{BuNP})_2(^t\text{BuN})_2]\text{Hf}(\text{O}^t\text{Bu})_2\}$, **36**

$\{[(^t\text{BuNP})_2(^t\text{BuN})_2]\text{HfCl}_2\}$, **34**, (0.290 g, 0.490 mmol) and NaO^tBu (0.0900 g, 0.980 mmol) were dissolved in 40 mL of toluene in a 100 mL two-neck flask equipped with a gas inlet and magnetic stir bar. The resulting colorless solution was stirred at 70 °C for 24 h, cooled in an ice bath for 1 h, and filtered with a medium-porosity frit. The filtrate was concentrated *in vacuo* to about 15 mL and stored at -20 °C for 3 days. This produced colorless, hexagonal crystals. Yield: (0.290 g, 0.430 mmol), 87 %.

Mp: 300–302 °C subl. ^1H NMR (500.1 MHz, benzene- d_6 , 25 °C): 1.49 (s, 18H, O^tBu), 1.45 (s, 18H, N^tBu), 1.44 (s, 18H, N^tBu). $^{13}\text{C}\{^1\text{H}\}$ NMR (125.8 MHz, benzene- d_6 , 25 °C): 77.4 (s, OC(CH₃)₃), 55.6 (d, $J_{\text{PC}} = 16.2$ Hz, NC(CH₃)₃, amido), 53.9 (t, $J_{\text{PC}} = 12.2$ Hz, NC(CH₃)₃, imido), 34.9 (d, $J_{\text{PC}} = 9.96$ Hz, NC(CH₃)₃, amido), 33.7 (s, OC(CH₃)₃), 30.7 (t, $J_{\text{PC}} = 6.23$ Hz, NC(CH₃)₃, imido). $^{31}\text{P}\{^1\text{H}\}$ NMR (202.5 MHz, benzene- d_6 , 25 °C): 103.4 (s). Anal. Calcd for C₂₄H₅₄HfN₄O₂P₂: C, 42.95; H, 8.11; N, 8.35. Found: C, 43.08; H, 8.15; N, 8.12.

Synthesis of $\{[(^t\text{BuNP}=\text{S})_2(^t\text{BuN})_2]\text{Zr}(\text{O}^t\text{Bu})_2\}$, **37**

Samples of **33** (0.200 g, 0.340 mmol), and excess sulfur (0.0250 g, 0.780 mmol) were combined in 25 mL of toluene in a 100 mL two-necked flask equipped with a gas inlet and magnetic stir bar, stirred at 80 °C for 2 d, cooled in an ice bath for 1 h, and filtered using a medium-porosity frit. The filtrate was concentrated in *vacuo* to about 10 mL and stored at –20 °C for 5 d. This produced colorless, hexagonal crystals. Yield: (0.180 g, 0.270 mmol), 81 %.

Mp: 315 °C dec. ^1H NMR (500.1 MHz, benzene- d_6 , 25 °C): 1.84 (s, 18H, O^tBu), 1.58 (s, 18H, N^tBu), 1.26 (s, 18H, N^tBu). $^{13}\text{C}\{^1\text{H}\}$ NMR (125.8 MHz, benzene- d_6 , 25 °C): 79.9 (s, OC(CH₃)₃), 59.5 (s, NC(CH₃)₃, amido), 57.5 (s, NC(CH₃)₃, imido), 32.9 (s, OC(CH₃)₃), 32.7 (t, $J_{\text{PC}} = 4.23$ Hz, NC(CH₃)₃, amido); 30.1 (t, $J_{\text{PC}} = 4.65$ Hz, NC(CH₃)₃, imido). $^{31}\text{P}\{^1\text{H}\}$ NMR (202.5 MHz, benzene- d_6 , 25 °C): 37.0 (s). IR (cm⁻¹): 2952 (vs), 2865 (vs), 1594 (vw), 1461 (s), 1377 (m), 1362 (m), 1252 (w), 1233 (m), 1192 (m), 1091 (m), 1049 (w), 1021 (m), 992 (m), 933 (w), 869 (m), 842 (m), 777 (m), 746 (w), 666 (vw), 643 (vw), 598 (vw), 511 (vw), 533 (w). Anal. Calcd for C₂₄H₅₄N₄O₂P₂S₂Zr: C, 44.48; H, 8.40; N, 8.65. Found: C, 44.86; H, 8.71; N, 8.46.

Synthesis of $\{[(^t\text{BuNP}=\text{S})_2(^t\text{BuN})_2]\text{Hf}(\text{O}^t\text{Bu})_2\}$, **38**

Samples of **34** (0.170 g, 0.250 mmol), and excess sulfur (0.0192 g, 0.600 mmol) were combined in 40 mL of toluene in a 100 mL two-necked flask equipped with a gas inlet and magnetic stir bar. The ensuing mixture was stirred at 80 °C for 3 d, cooled in an ice bath for 1 h and filtered using a medium-porosity frit. The filtrate was concentrated in *vacuo* to about 18 mL and stored at -20 °C for 5 d. This produced light yellow, block-shaped crystals. Yield: (0.150 g, 0.200 mmol), 83 %.

Mp: 300 °C dec. ^1H NMR (500.1 MHz, benzene- d_6 , 25 °C): 1.82 (s, 18H, O^tBu), 1.56 (s, 18H, N^tBu), 1.26 (s, 18H, N^tBu). $^{13}\text{C}\{^1\text{H}\}$ NMR (125.8 MHz, benzene- d_6 , 25 °C): 79.7 (s, OC(CH₃)₃), 59.6 (s, NC(CH₃)₃, amido), 57.2 (s, NC(CH₃)₃, imido), 33.1 (s, OC(CH₃)₃), 32.8 (t, $J_{\text{PC}} = 4.11$ Hz, NC(CH₃)₃, amido); 30.0 (t, $J_{\text{PC}} = 4.57$ Hz, NC(CH₃)₃, imido). $^{31}\text{P}\{^1\text{H}\}$ NMR (202.5 MHz, benzene- d_6 , 25 °C): 36.2 (s). Anal. Calcd for C₂₄H₅₄HfN₄O₂P₂S₂: C, 39.20; H, 7.40; N, 7.62. Found: C, 39.20; H, 7.71; N, 7.95.

Synthesis of $\{[(^t\text{BuNP}=\text{S})_2(^t\text{BuN})_2]\text{ZrCl}_2\}$, **39**

$\{[(^t\text{BuNP})_2(^t\text{BuN})_2]\text{ZrCl}_2\}$, **33**, (1.00 g, 1.94 mmol) and excess sulfur (0.127 g, 3.98 mmol) were dissolved in 35 mL of toluene and refluxed for 5 d in a 100 mL two-necked flask equipped with a gas inlet and stir bar. After cooling, unreacted sulfur was filtered off using a medium-porosity frit and the filtrate was concentrated in *vacuo* and stored at -20 °C. After several days colorless, hexagonal crystals were obtained. Yield: (0.950 g, 1.66 mmol), 85 %.

Mp: 270 °C dec. ^1H NMR (500.1 MHz, benzene- d_6 , 25 °C): 1.63 (s, 18H, N^tBu), 1.53 (s, 18H, N^tBu). $^{13}\text{C}\{^1\text{H}\}$ NMR (125.8 MHz, benzene- d_6 , 25 °C): 61.9 (s, NC(CH₃)₃, amido), 60.7 (s, NC(CH₃)₃, imido), 31.8 (t, $J_{\text{PC}} = 3.96$ Hz, NC(CH₃)₃, amido), 29.6 (t, J_{PC}

= 4.31 Hz, NC(CH₃)₃, imido). ³¹P{¹H} NMR (202.5 MHz, benzene-d₆, 25 °C): 33.1 (s). IR (cm⁻¹): 2954 (vs), 2872 (vs), 2722 (w), 1463 (vs), 1391 (m), 1367 (s), 1235 (m), 1178 (s), 1094 (vw), 1067 (s), 1047 (m), 1038 (m), 954 (s), 934 (m), 845 (vs), 789 (s), 742 (m), 720 (m), 601 (w), 588 (w), 556 (m), 533 (w). Anal. Calcd for C₁₆Cl₂H₃₆N₄P₂S₂Zr: C, 33.56; H, 6.34; N, 9.78. Found: C, 33.66; H, 6.36; N, 9.35.

Synthesis of {[^tBuNP=S]₂(^tBuN)₂]HfCl₂}, **40**

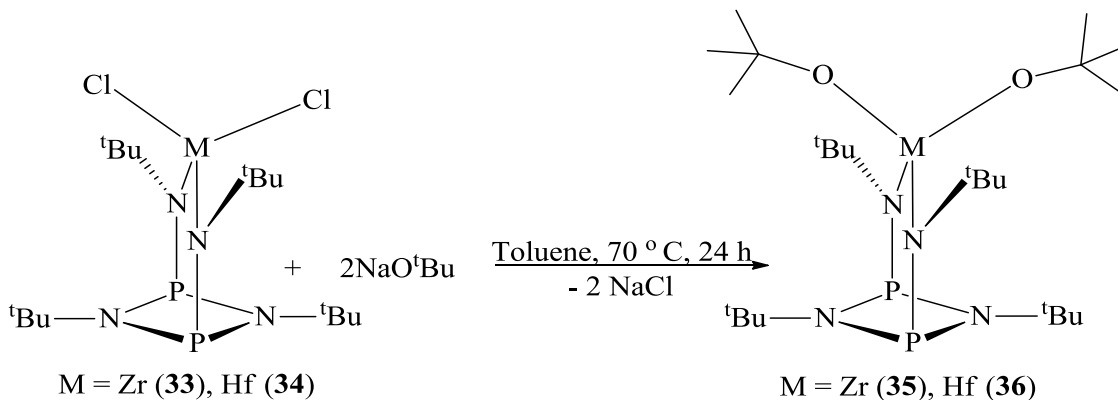
{[^tBuNP)₂(^tBuN)₂]HfCl₂}, **34**, (1.39 g, 2.33 mmol) and excess sulfur (0.152 g, 4.76 mmol) were dissolved in 40 mL of toluene and refluxed for 5 d in a 100 mL two-necked flask, equipped with a gas inlet and stir bar. After cooling, unreacted sulfur was filtered off with medium-porosity frit, and the filtrate was concentrated in *vacuo* and stored at -20 °C for several days to afford colorless, hexagonal crystals. Yield: (1.26 g, 1.91 mmol), 82 %.

Mp: 240 °C dec. ¹H NMR (500.1 MHz, benzene-d₆, 25 °C): 1.64 (s, 18H, N^tBu), 1.51 (s, 18H, N^tBu). ¹³C{¹H} NMR (125.8 MHz, benzene-d₆, 25 °C): 61.8 (s, NC(CH₃)₃, amido), 60.6 (s, NC(CH₃)₃, imido), 32.1 (t, *J*_{PC} = 3.63 Hz, NC(CH₃)₃, amido), 29.5 (t, *J*_{PC} = 4.04 Hz, NC(CH₃)₃, imido). ³¹P{¹H} NMR (202.5 MHz, benzene-d₆, 25 °C): 33.0 (s). IR (cm⁻¹): 2915 (vs), 2725 (w), 1600 (w), 1459 (vs), 1372 (s), 1236 (m), 1181 (s), 1094 (vw), 1070 (s), 1046 (m), 952(s), 934 (m), 852 (vs), 813 (m), 792 (s), 749 (m), 722 (m), 601 (w), 588 (w), 556 (m), 533 (w). Anal. Calcd for C₁₆Cl₂H₃₆HfN₄P₂S₂: C, 29.12; H, 5.50; N, 8.49. Found: C, 29.69; H, 6.06; N, 8.51.

4. Results and Discussions

Synthesis and Spectroscopic Analysis of $\{[(^t\text{BuNP})_2(^t\text{BuN})_2]\text{Zr}(\text{O}^t\text{Bu})_2\}$, **34**

Heating a mixture of **33** and NaO^tBu in toluene at $70\text{ }^\circ\text{C}$ for 24 h yielded compound **34** (Scheme 15). NaCl was filtered off, and the subsequent colorless filtrate crystallized to afford pure **34**.



Scheme 15. Syntheses of **35** and **36**.

The ^1H NMR spectrum, which is shown in Figure 5, exhibits three distinct singlets at 1.49, 1.44, and 1.41 ppm representing the *tert*-butoxy, *tert*-butyl amido and *tert*-butyl imido groups respectively.

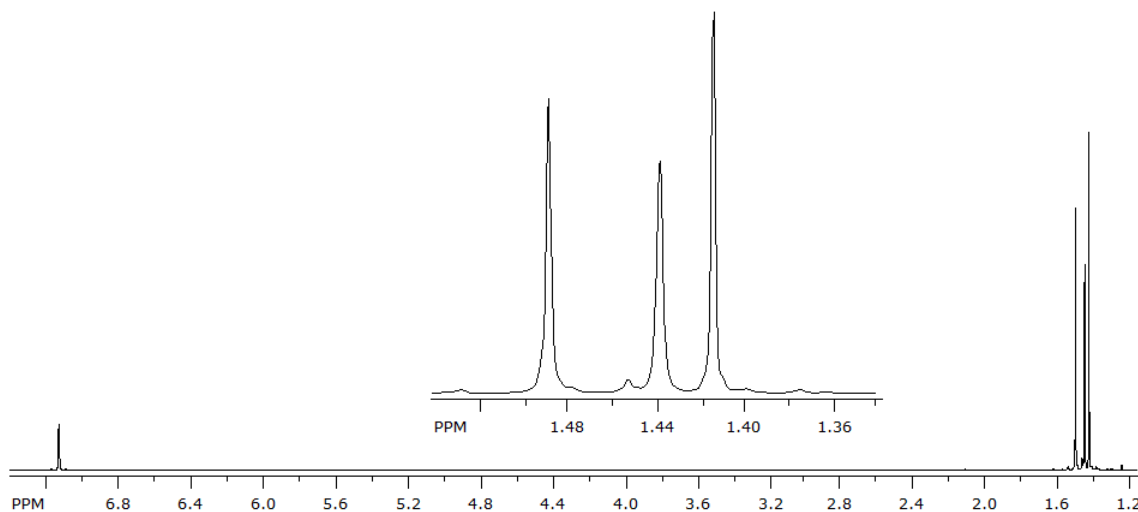


Figure 5. ^1H NMR Spectrum of **35**.

As expected, the $^{13}\text{C}\{^1\text{H}\}$ spectrum (Figure 6) shows two triplets at 53.7 and 30.5 ppm, and these are assigned to the *tert*-butyl imido carbons. The triplets are due to the splitting of these carbons by the two phosphorus centers. There are two doublets at 55.7 and 34.7 ppm for the *tert*-butyl amido carbons since they are split by one phosphorus atom. The two singlets at 77.3 and 33.5 ppm are assigned to the *tert*-butoxy carbons because they are not coupled to any phosphorus center. The $^{31}\text{P}\{^1\text{H}\}$ spectrum (Figure 7) shows a singlet at 103.4 ppm indicative of a P(III) derivative. X-ray data for **35** were collected, but the structure could not be solved because the compound crystallized twinned, (Crystal and structure refinement data are listed on Table 29 in Appendix II.)

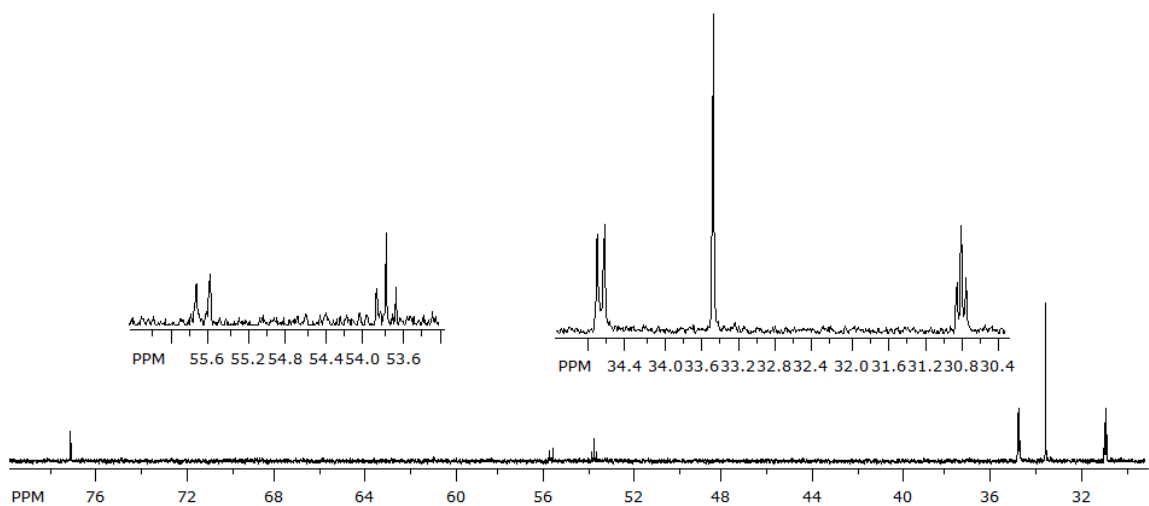


Figure 6. $^{13}\text{C}\{^1\text{H}\}$ NMR Spectrum of **35**.

Figure 7. $^{31}\text{P}\{^1\text{H}\}$ NMR Spectrum of **35**.

Synthesis and Spectroscopic Analysis of $\{[(^t\text{BuNP})_2(^t\text{BuN})_2]\text{Hf}(\text{O}^t\text{Bu})_2\}$, **36**

In a manner similar to **35**, compound **36** was obtained (92 %) as colorless, flat, hexagonal crystals by stirring a 1:2 mixture of **34** and NaO^tBu in toluene at 70 °C for 24 h (Scheme 15). The analysis of **36** by ^1H , $^{13}\text{C}\{^1\text{H}\}$, and $^{31}\text{P}\{^1\text{H}\}$ NMR (shown in Figures 8, 9, and 10, respectively) gave similar chemical shifts and splitting patterns as those obtained for its zirconium analogue **35**. Both **35** and **36** crystallized twinned, which prevented a structure solution, (Crystal and structure refinement data are listed on Table 29 in Appendix II.)

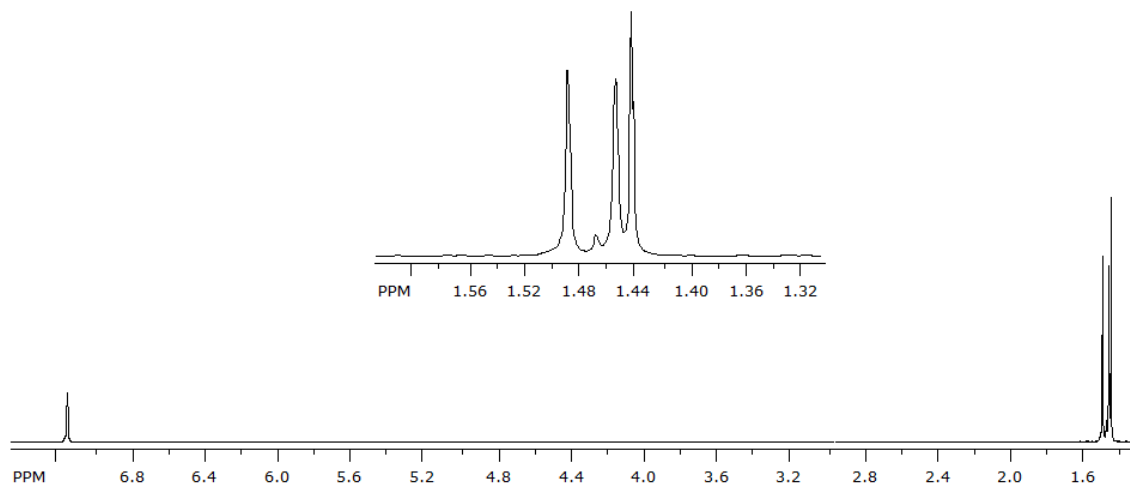


Figure 8. ^1H NMR Spectrum of **36**.

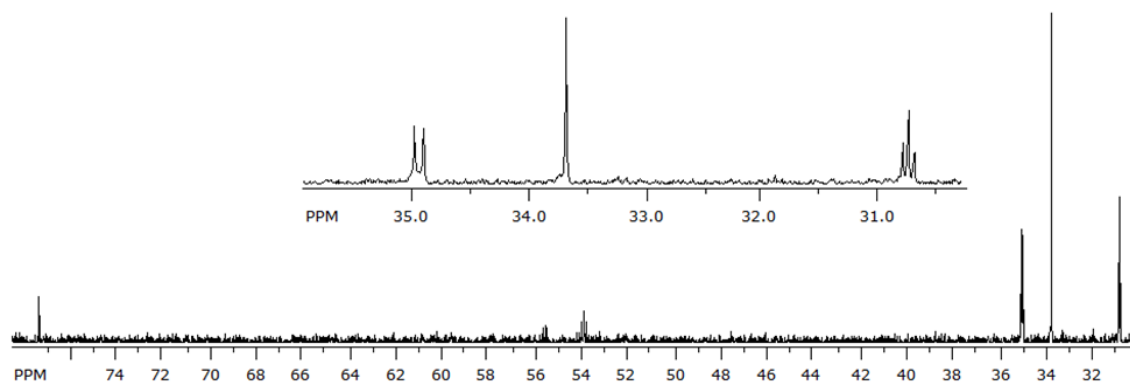


Figure 9. $^{13}\text{C}\{^1\text{H}\}$ NMR Spectrum of **36**.

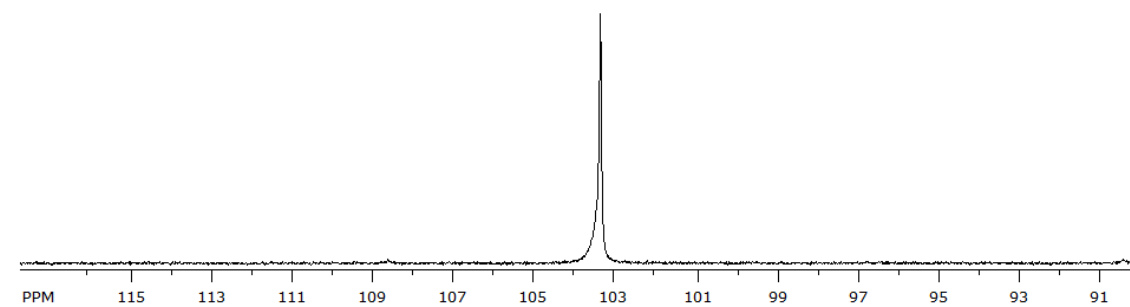
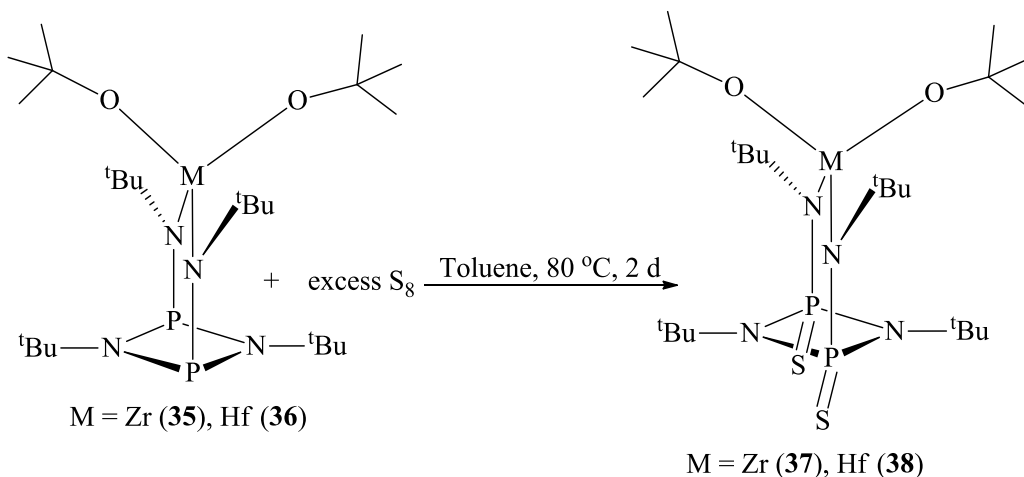


Figure 10. $^{31}\text{P}\{^1\text{H}\}$ NMR Spectrum of **36**.

Synthesis and Spectroscopic Analysis of $\{[(t\text{BuNP}=\text{S})_2(t\text{BuN})_2]\text{Zr}(\text{O}^t\text{Bu})_2\}$, **37**

The oxidation of **35** with excess sulfur in hot toluene (80 °C) for 2 d afforded **37**, as shown in Scheme 16. Pure **37** was separated from unreacted sulfur by fractional crystallization from a concentrated toluene solution.



Scheme 16. Syntheses of **37** and **38**.

The ¹H NMR spectrum of **37**, presented in Figure 11, shows three distinct singlets at 1.84, 1.58, and 1.26 ppm representing the *tert*-butoxy, *tert*-butyl amido and *tert*-butyl imido protons, respectively.

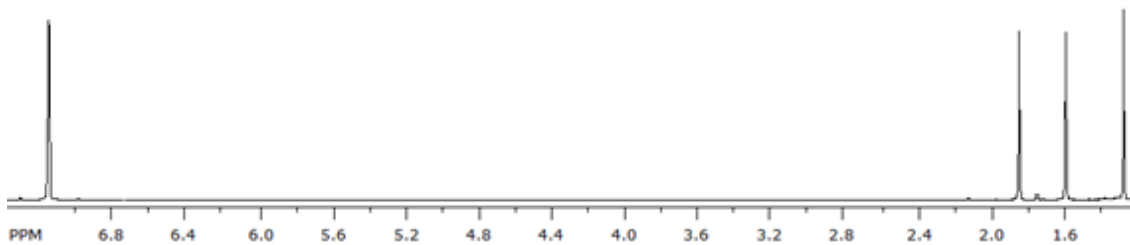


Figure 11. ¹H NMR Spectrum of **37**.

The ¹³C{¹H} and ³¹P{¹H} NMR of compound **37** are shown in Figures 12 and 13 respectively. In the ¹³C{¹H} NMR of **37**, there are four singlets and two triplets. The two singlets at 79.9 and 32.9 ppm are assigned to the *tert*-butoxy carbons, while the triplets at

32.7 and 30.1 ppm represent the imido *tert*-butyl carbons because they each couple with two phosphorus(V) atoms. The remaining singlets at 59.5 and 57.5 ppm represent the *tert*-butyl amido carbon atoms, which do not couple with the phosphorus(V) atom connected to them – a feature we observed with all *tert*-butyl amido carbons for compounds that had been oxidized with sulfur. As with **35**, compound **37** showed a distinct singlet in the $^{31}\text{P}\{^1\text{H}\}$ NMR spectrum, with a chemical shift of 37.0 ppm – a value which is farther upfield than that for **35** as a result of the oxidation. This signal, as expected, is in a region characteristic for P(V) derivatives.

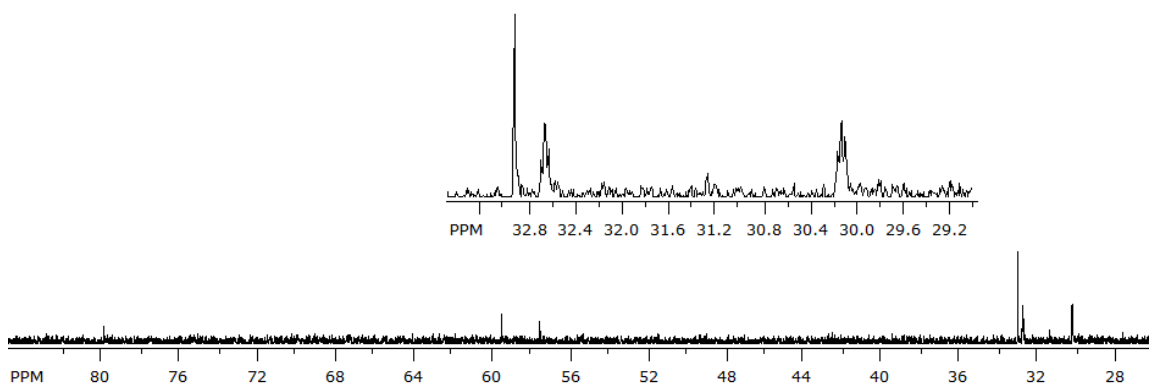


Figure 12. $^{13}\text{C}\{^1\text{H}\}$ NMR Spectrum of **37**.

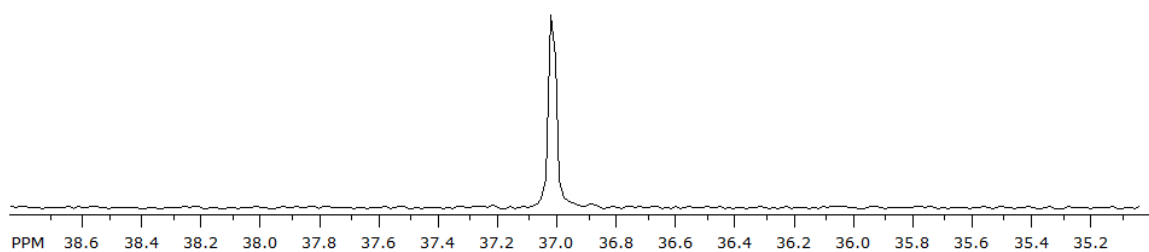


Figure 13. $^{31}\text{P}\{^1\text{H}\}$ NMR Spectrum of **37**.

Solid-state Structure of $\{[(^t\text{BuNP}=\text{S})_2(^t\text{BuN})_2]\text{Zr}(\text{O}^t\text{Bu})_2\}$, **37**

Colorless, rod-shaped crystals of **37** were isolated from cold ($-20\text{ }^\circ\text{C}$) toluene solutions. The solid-state structure of **37** with a partial atom numbering scheme is shown

in Figure 14, while the crystal data and selected bond parameters are listed in Tables 1 and 2, respectively. A single-crystal X-ray study of **37** depicts a pseudo-tetrahedral geometry around the zirconium atom. The compound crystallized in the orthorhombic space group $Cmc2_1$ with four molecules per unit cell. The solid-state structure of **37** shows that it is C_{2v} -symmetric, with the zirconium atom being a recipient of a donor bond from each of the ring-nitrogen atoms.

The endocyclic P–N bonds in **37**, 1.7289(12) and 1.7286(12) Å, are expectedly longer than the exocyclic P–N bonds, 1.6211(5) and 1.6229(14) Å. Both the endocyclic and exocyclic bonds in **37** are shorter than the corresponding bonds in related compounds, $[(Bu^iNP)_2(BN)_2ZrCl_2]$ (P–N(endo): 1.785(3) and 1.736(6) Å, P–N(exo): 1.682(3) Å),³³ and *cis*- $[Me_2Si(\mu-N^tBu)_2PCH_2]_2NiCl_2$ (P–N(endo): 1.688(3) Å).¹⁰³ The two almost identical Zr–N bonds in **37**, 2.1727(15) and 2.1763(15) Å, are similar to those in $[N_2NMe]ZrMe_2$ (2.095(4)–2.173(5) Å),¹⁰⁴ but they are slightly longer than those in $(Me_2N)Zr(NPh_2)_3$ (range from 2.007(4)–2.071(4) Å),¹⁰⁵ and those in the zirconium anion $[(Me_2N)_3Zr(SiPh_2Bu^t)_2]^-$, 2.039(3)–2.063(5) Å.¹⁰⁶ The long Zr–N donor bonds, 2.7042(10) Å, between the Zr atom and each of the ring-nitrogen atoms suggest a weak interaction between the zirconium and nitrogen atoms.

Due to symmetry there are two identical Z–O^tBu bonds in **37** with bond lengths of, 1.9090(10) Å, which are comparable to the Zr–O^tBu bonds in $Zr_3O(O^tBu)_{10}$, 1.900(9) to 1.938(11) Å,¹⁰⁷ $Zr(thd)_3(O^tBu)$ (1.874(7)–2.176(7) Å),¹⁰⁸ and *fac*- $[Ge(\mu-O^tBu)_3ZrCl(O^tBu)_2]$ (1.918(4)–2.144(3) Å),¹⁰⁹ but they are shorter than the Zr–O^tBu bonds reported for $Cp_2Zr(OCHPh_2)_2$ (1.961(2) and 1.984(2) Å),¹¹⁰ and $(Me_4taen)Zr(O^tBu)$, 1.945(2) and 1.948(2) Å.¹¹¹ Each of the *tert*-butoxy groups in **37** has

a geometry that deviates slightly from linearity with the Zr–O–C angle being equal to 170.01°.

The compound has two P=S bonds, whose lengths of 1.9286(7) and 1.9281(7) Å, are similar to the corresponding P=S bond lengths in $\text{TeCl}_2[\text{}^t\text{Bu}(\text{H})\text{N}(\text{S})\text{P}(\mu\text{-N}^t\text{Bu})_2\text{P}(\text{S})\text{N}(\text{H})^t\text{Bu}]_2$, 1.924(1) Å,¹¹² and *cis*-[$(^t\text{BuN})\text{P}(\text{S})\text{N}^t\text{Bu}]_2$, 1.917(1) and 1.933(1) Å.⁸

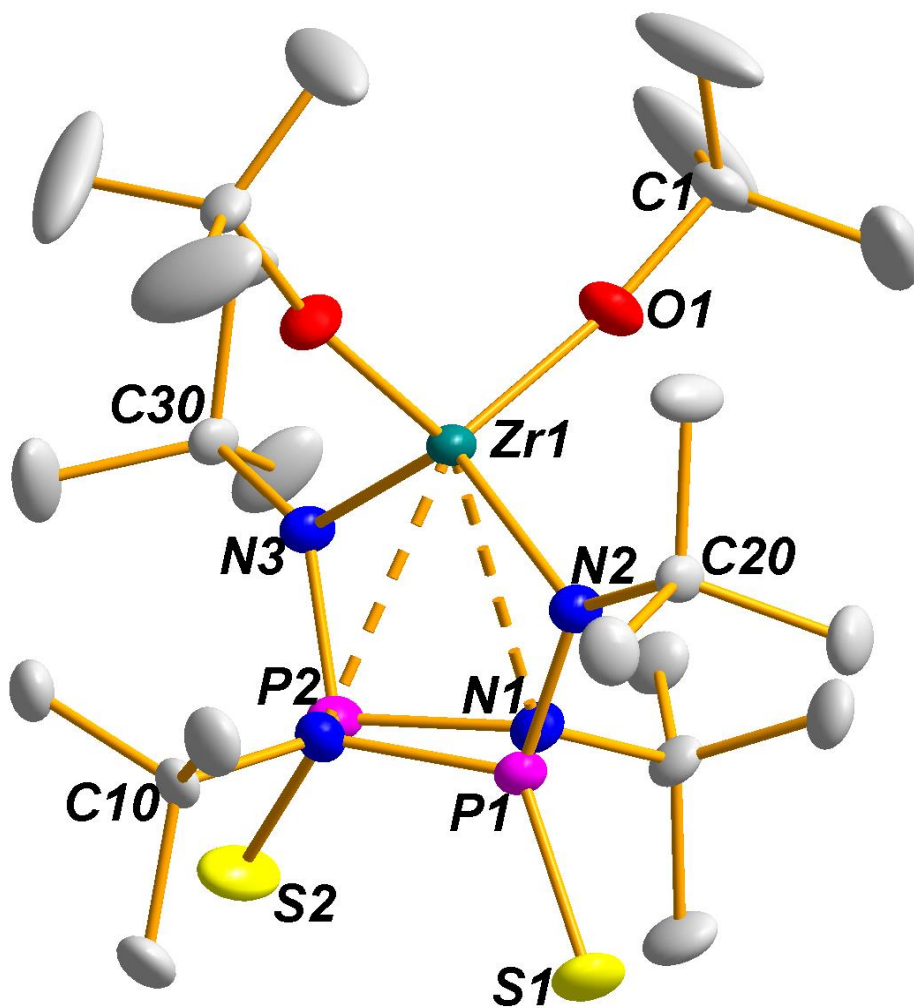


Figure 14. Solid-state structure and partial labelling scheme of **37**. With the exception of carbon (35 %) all atoms are drawn at the 50 % probability level.

Table 1. Crystal and structure refinement data for compound **37**.

Chemical Formula	C ₂₄ H ₅₄ N ₄ O ₂ P ₂ S ₂ Zr
fw	647.99
T/K	173(2)
$\lambda/\text{\AA}$	0.71073
Crystal system	Orthorhombic
Space group	<i>Cmc</i> 2 ₁
$a/\text{\AA}$	16.9585(3)
$b/\text{\AA}$	11.1273(2)
$c/\text{\AA}$	17.7635(3)
$\alpha/^\circ$	90
$\beta/^\circ$	90
$\gamma/^\circ$	90
$V/\text{\AA}^3$	3352.01(10)
Z	4
$\rho(\text{calc}) \text{ g cm}^{-3}$	1.284
μ/mm^{-1}	0.574
F(000)	1376
Completeness (%)	99.90
Reflections collected	30543
Independent reflections	6480 [$R_{\text{int}} = 0.0155$]
$R_w(F^2)^b$ [$I > 2\sigma(I)$]	$R_1 = 0.0228$, $wR_2 = 0.0634$
$R(F)^a$ (all data)	$R_1 = 0.0236$, $wR_2 = 0.0642$

^a $R = \sum |F_o - F_c| / \sum |F_o|$. ^b $R_w = \{ [\sum w(F_o^2 - F_c^2)] / [\sum w(F_o^2)^2] \}^{1/2}$; $w = 1 / [\sigma^2(F_o)^2 + (xP)^2 + yP]$, where $P = (F_o^2 + 2F_c^2) / 3$.

Table 2. Selected bond lengths (Å) and angles (°) for **37**.

Bond Lengths			
Zr1–O1	1.9090(10)	P2–N1	1.7286(12)
Zr1–N1	2.7042(10)	P2–N3	1.6211(15)
Zr1–N2	2.1727(15)	P2–S2	1.9281(7)
Zr1–N3	2.7763(15)	N1–C10	1.4938(17)
P1–N1	1.7289(12)	N2–C20	1.494(2)
P1–N2	1.6229(14)	N3–C30	1.485(2)
P1–S1	1.9286(7)	O1–C1	1.4313(17)
Bond Angles			
O1#–Zr1–O1	108.82(7)	P1–Zr1–P2	53.934(13)
O1#–Zr1–N2	106.78(4)	N2–P1–N1	102.22(5)
O1#–Zr1–N1	150.08(4)	N1#–P1–N1	80.87(2)
O1–Zr1–N1	101.09(4)	N2–P1–S1	121.91(6)
N2–Zr1–N1	63.61(4)	N2–P1–P2	111.17(6)
O1#–Zr1–N1#	101.09(4)	N1#–P1–P2	40.69(4)
N2–Zr1–N1#	63.61(4)	N1–P1–Z1	66.24(4)
O1#–Zr1–P1	121.40(3)	P2–N1–P1	98.61(6)
N2–Zr1–P2	87.72(4)	C10–N1–P2	128.58(9)
O1#–Zr1–P2	87.65(4)	C20–N2–P1	131.29(12)
N3–Zr1–P1	87.65(4)	C30–N3–Zr1	130.65(12)
N3–Zr1–P2	121.09(3)	P2–N3–Zr1	98.10(7)

Synthesis and Spectroscopic Analysis of $\{[(^t\text{BuNP}=\text{S})_2(^t\text{BuN})_2]\text{Hf}(\text{O}^t\text{Bu})_2\}$, **38**

Similar to **37**, compound **38** was obtained by the oxidation of **36** with excess sulfur in hot toluene for two days (Scheme 16). As expected the ^1H , $^{13}\text{C}\{^1\text{H}\}$, and $^{31}\text{P}\{^1\text{H}\}$ NMR spectra of **38** displayed similar chemical shifts and splitting patterns as those observed in the analogous compound **37**. The spectra are shown in Figures 15, 16, and 17 respectively.

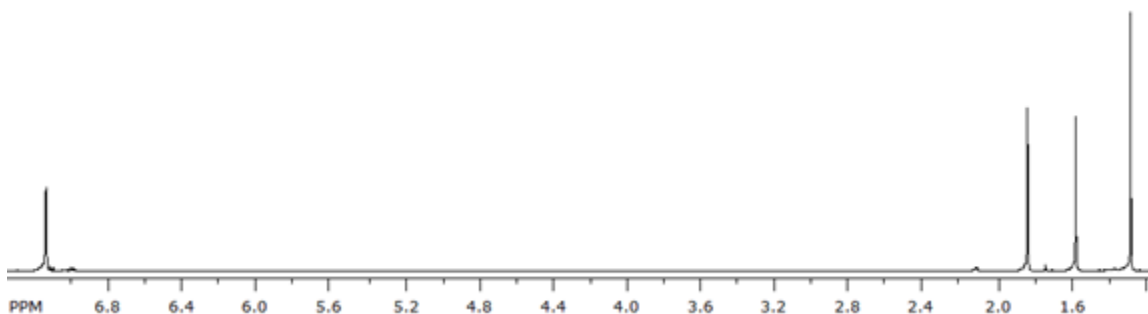


Figure 15. ^1H NMR Spectrum of **38**.

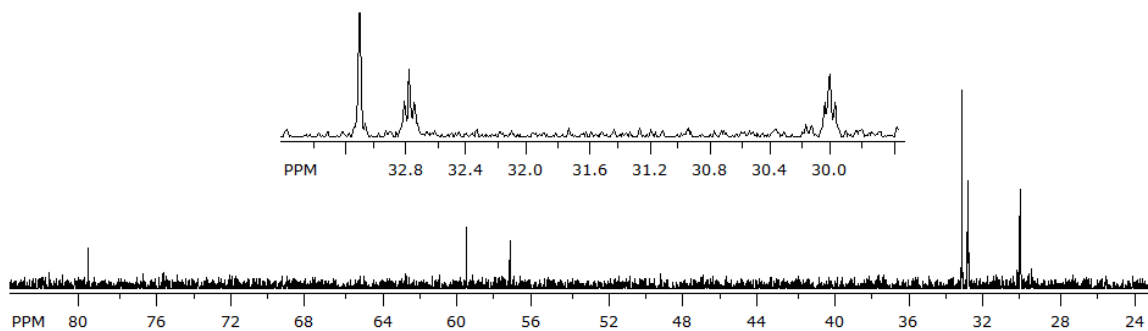


Figure 16. $^{13}\text{C}\{^1\text{H}\}$ NMR Spectrum of **38**.

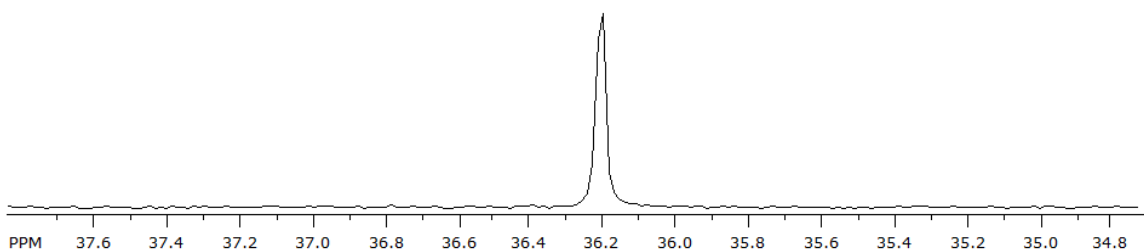


Figure 17. $^{31}\text{P}\{^1\text{H}\}$ NMR Spectrum of **38**.

Solid-state Structure of $\{[(^t\text{BuNP}=\text{S})_2(^t\text{BuN})_2]\text{Hf}(\text{O}^t\text{Bu})_2\}$, **38**

Light-yellow, block-shaped, crystals of **38** were obtained from a concentrated solution of toluene at $-20\text{ }^\circ\text{C}$. The solid-state structure of **38** with a partial atom numbering scheme is shown in Figure 18, while the crystal data and selected bond parameters are listed in Tables 3 and 4, respectively. A single-crystal X-ray study of **38** shows that the compound is identical to its zirconium analogue **37** in that it not only displays a pseudo-tetrahedral geometry around the hafnium atom, but it also crystallized isostructurally to **37** in the orthorhombic space group $Cmc2_1$ with four molecules per unit cell.

A detailed discussion has already been given above for the zirconium analogue **37** and will not be repeated here for **38**, because both compounds are isostructural. Both compounds, **37** and **38** have similar bond lengths and angles, except that the Hf–N bond lengths in **38**, $2.1557(2)\text{ \AA}$, are slightly shorter than those in **37**. The compound has two almost identical P=S bonds, whose lengths of $1.9286(11)$ and $1.9251(10)\text{ \AA}$, are similar to the corresponding P=S bond lengths in $\text{TeCl}_2[{}^t\text{Bu}(\text{H})\text{N}(\text{S})\text{P}(\mu\text{-N}^t\text{Bu})_2\text{P}(\text{S})\text{N}(\text{H})^t\text{Bu}]_2$, $1.924(1)\text{ \AA}$,¹¹² and *cis*- $[{}^t\text{BuN})\text{P}(\text{S})\text{N}^t\text{Bu}]_2$, $1.917(1)$ and $1.933(1)\text{ \AA}$.⁸

Compound **38** possesses a similar slightly puckered, angle sum = 358.9° , P_2N_2 ring like that found in its zirconium analogue **37**.

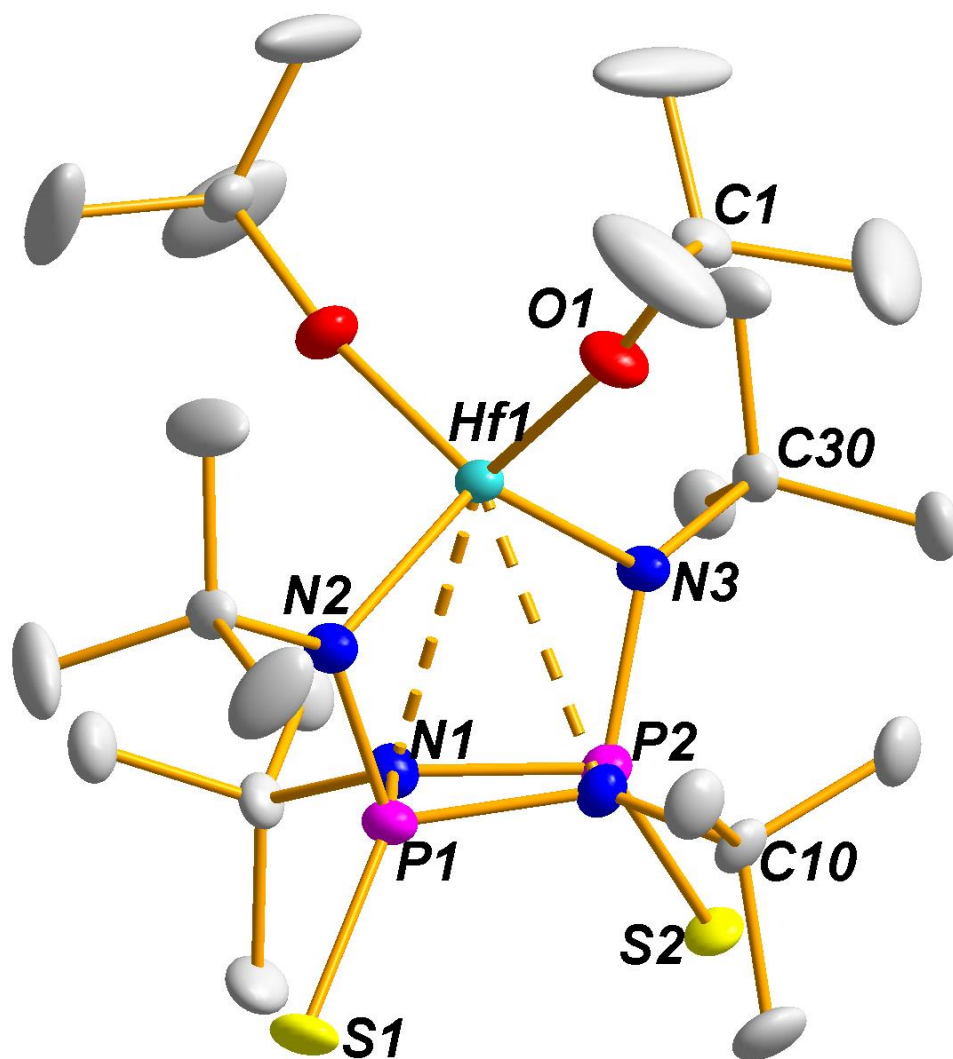


Figure 18. Solid-state structure and partial labelling scheme of **38**. With the exception of carbon (35 %) all atoms are drawn at the 50 % probability level.

Table 3. Crystal and structure refinement data for compound **38**.

Chemical Formula	C ₂₄ H ₅₄ N ₄ O ₂ P ₂ S ₂ Hf
fw	735.26
T/K	173(2)
$\lambda/\text{\AA}$	0.71073
Crystal system	Orthorhombic
Space group	<i>Cmc</i> 2 ₁
$a/\text{\AA}$	16.9610(5)
$b/\text{\AA}$	11.1223(3)
$c/\text{\AA}$	17.7295(3)
$\alpha/^\circ$	90
$\beta/^\circ$	90
$\gamma/^\circ$	90
$V/\text{\AA}^3$	3344.59(18)
<i>Z</i>	4
$\rho(\text{calc}) \text{ g cm}^{-3}$	1.460
μ/mm^{-1}	3.365
F(000)	1504
Completeness (%)	99.00
Reflections collected	25551
Independent reflections	5862 [<i>R</i> _{int} = 0.0218]
$R_w(F^2)^b$ [<i>I</i> > 2 σ (<i>I</i>)]	<i>R</i> ₁ = 0.0182, <i>wR</i> ₂ = 0.0449
$R(F)^a$ (all data)	<i>R</i> ₁ = 0.0189, <i>wR</i> ₂ = 0.0452

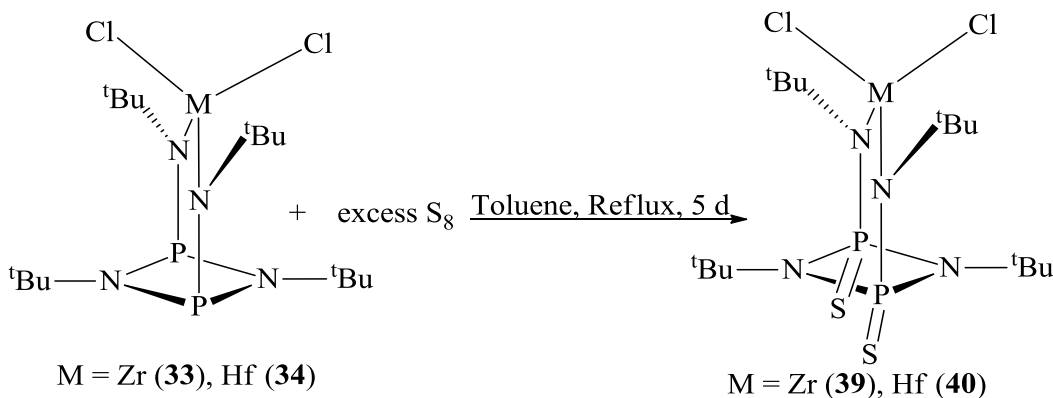
^a $R = \sum |F_o - F_c| / \sum |F_o|$. ^b $R_w = \{ [\sum w(F_o^2 - F_c^2)] / [\sum w(F_o^2)] \}^{1/2}$; $w = 1 / [\sigma^2(F_o)^2 + (xP)^2 + yP]$, where $P = (F_o^2 + 2F_c^2) / 3$.

Table 4. Selected bond lengths (Å) and angles (°) for **38**.

Bond Lengths			
Hf1–O1	1.9007(18)	P2–N1	1.7284(17)
Hf1–N3	2.155(2)	P2–N3	1.633(2)
Hf1–N1	2.6903(16)	P2–S2	1.9251(10)
Hf1–P2	2.8759(7)	N1–C10	1.495(3)
P1–N1	1.7297(17)	N2–C20	1.488(3)
P1–N2	1.627(2)	N3–C30	1.492(3)
P1–S1	1.9286(11)	O1–C1	1.431(3)
Bond Angles			
O1–Hf1–O1#	108.81(12)	N1–P2–N1	80.89(11)
O1#–Hf1–N2	106.04(6)	N2–P1–N1	101.89(9)
O1#–Hf1–N1	100.94(4)	S1–P1–Hf1	169.83(4)
O1–Hf1–N1	150.24(7)	N1#–P1–N1	80.89(11)
N2–Hf1–N1	63.97(6)	N2–P1–S1	121.92(9)
O1#–Hf1–N3	106.50(5)	P1–N1–P2	98.54(9)
N2–Hf1–N1#	63.97(6)	C10–N1–P2	127.47(13)
O1#–Hf1–P1	121.04(6)	C20–N2–P1	131.1(2)
O1#–Hf1–P2	121.37(5)	C30–N3–P2	130.95(17)
N1–P2–S2	120.75(6)	C30–N3–Hf1	131.24(16)
N3–P2–N1	101.97(8)	P2–N3–Hf1	98.10(7)

Synthesis and Spectroscopic Analysis of $\{[(^t\text{BuNP}=\text{S})_2(^t\text{BuN})_2]\text{ZrCl}_2\}$, **39**

An initial attempt to obtain compound **39** by refluxing compound **33** with excess sulfur in toluene for two days resulted in only one of the phosphorus atoms of compound **33** being oxidized. However, prolonged refluxing for five days resulted in complete oxidation of **33** to give compound **39** (Scheme 17). The increased difficulty in the oxidation of **33** is probably due to the fact that the high electronegativity of the chlorine atoms in **33** causes an overall inductive effect that makes the lone pairs of electrons on the phosphorus atoms less available for bonding. Although oxygen is more electronegative than chlorine, via resonance the lone pairs of electron on oxygen might be donated to cause an overall effect that makes the lone pairs of electrons on phosphorus atoms in compound **35** more available for bonding. Therefore, it is easier to oxidize compound **35** than compound **33**.



Scheme 17. Syntheses of **39** and **40**.

The ^1H NMR spectrum of **39** shows two singlets at 1.63 and 1.54 ppm for the *tert*-butylamido and *tert*-butylimido protons, respectively (Figure 19). In the $^{13}\text{C}\{^1\text{H}\}$ NMR spectrum of **39**, Figure 20, there are two singlets at 61.9 and 60.7 ppm for the *tert*-butylamido carbons, while there are two triplets at 31.8 and 29.6 ppm for the *tert*-

butylimido carbon atoms. The triplets occur because each *tert*-butylimido carbon is coupled to two phosphorus(V) atoms in the P₂N₂ ring. The ³¹P{¹H} NMR spectrum of **39** (Figure 21) shows only a single peak at 33.1 ppm, whose chemical shift indicates a phosphorus(V) center.

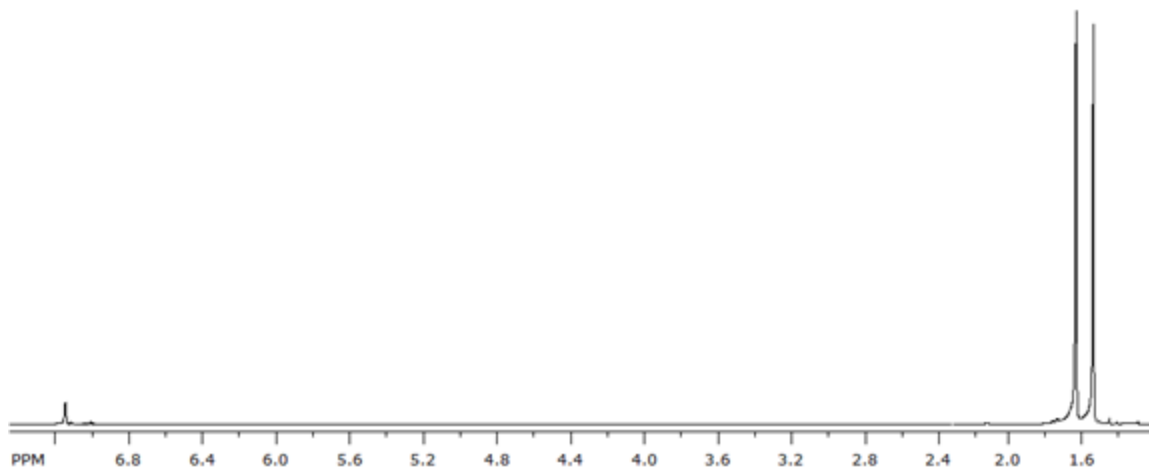


Figure 19. ¹H NMR Spectrum of **39**.

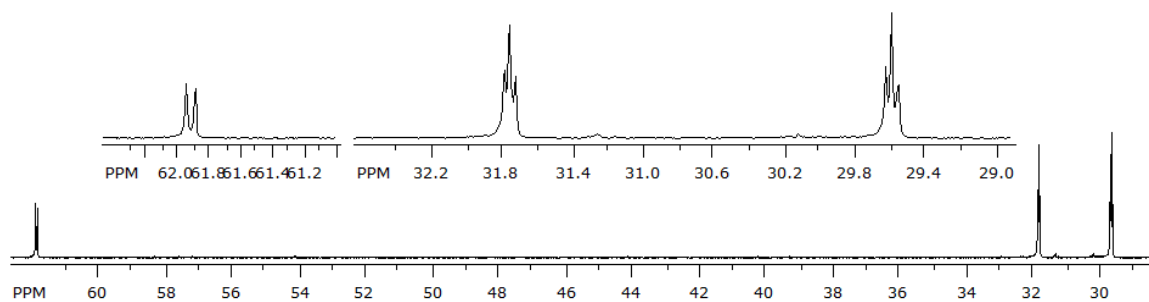


Figure 20. ¹³C{¹H} NMR Spectrum of **39**.

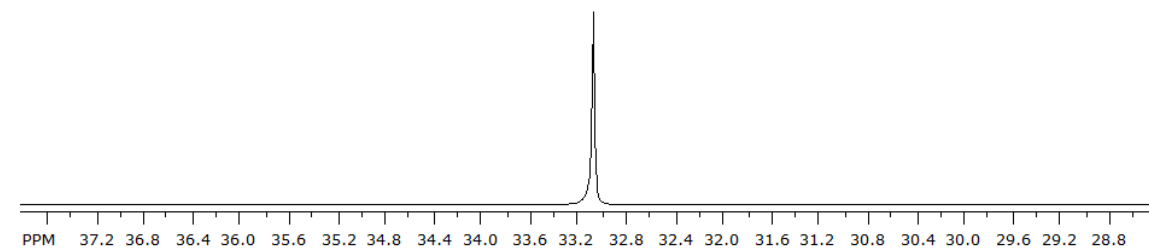


Figure 21. ³¹P{¹H} NMR Spectrum of **39**.

Solid-state Structure of $\{[(^t\text{BuNP}=\text{S})_2(^t\text{BuN})_2]\text{ZrCl}_2\}$, **39**

Colorless, hexagonal crystals of **39** were obtained from a concentrated solution of toluene at $-20\text{ }^\circ\text{C}$. The solid-state structure of **39** and a partial numbering scheme is shown in Figure 22, while the crystal data and selected bond parameters are listed in Tables 5 and 6, respectively. Compound **39** crystallized in the orthorhombic space group *Pbcm*. The solid-state structure of **39** shows that it has an approximate C_{2v} symmetry and a pseudo-tetrahedral geometry around the zirconium atom. Just like in its hafnium analogue, the P_2N_2 ring in **39** is slightly puckered, angle sum = 357° . Because both **39** and **40** are isostructural with identical crystallographic parameters, only compound **40** will be discussed in detail (see below).

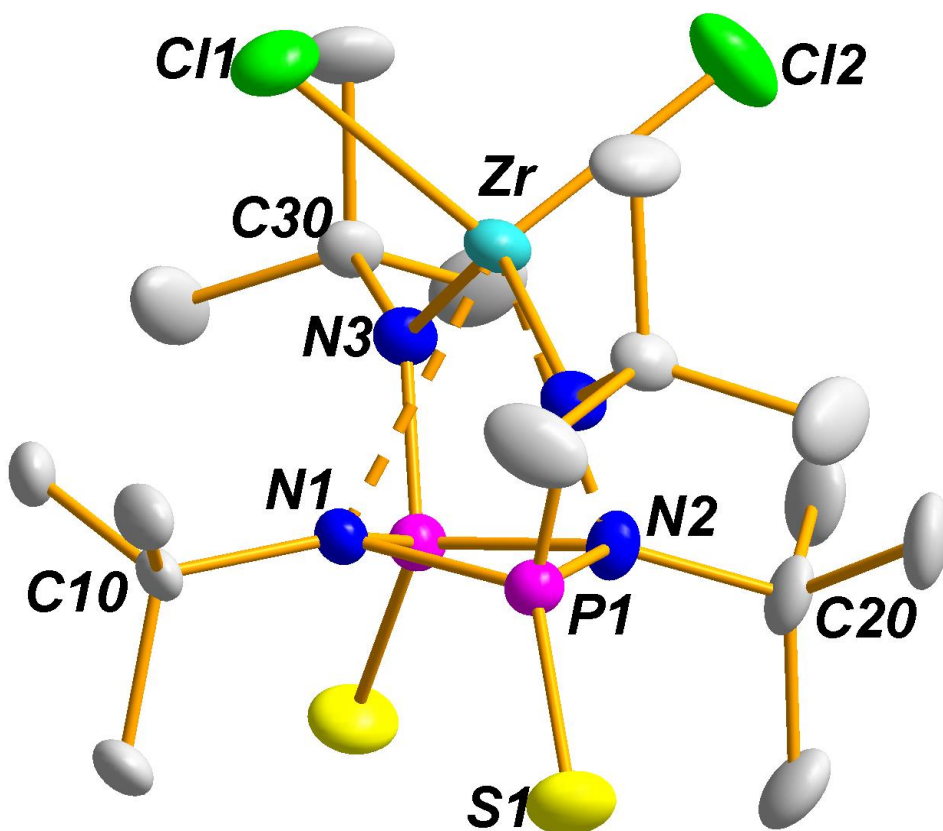


Figure 22. Solid-state structure and partial labelling scheme of **39**. With the exception of carbon (35 %) all atoms are drawn at the 50 % probability level.

Table 5. Crystal and structure refinement data for compound **39**.

Chemical Formula	C ₁₆ H ₃₆ Cl ₂ N ₄ P ₂ S ₂ Zr
fw	572.67
T/K	173(2)
$\lambda/\text{\AA}$	0.71073
Crystal system	Orthorhombic
Space group	<i>Pbcm</i>
$a/\text{\AA}$	13.4729(14)
$b/\text{\AA}$	13.7273(14)
$c/\text{\AA}$	14.0401(14)
$\alpha/^\circ$	90
$\beta/^\circ$	90
$\gamma/^\circ$	90
$V/\text{\AA}^3$	2596.67(46)
<i>Z</i>	4
$\rho(\text{calc}) \text{ g cm}^{-3}$	1.465
μ/mm^{-1}	0.923
F(000)	1184
Completeness (%)	99.50
Reflections collected	57054
Independent reflections	3922 [$R_{\text{int}} = 0.0231$]
$R_w(F^2)^b$ [$I > 2\sigma(I)$]	$R_1 = 0.0253$, $wR_2 = 0.0669$
$R(F)^a$ (all data)	$R_1 = 0.0278$, $wR_2 = 0.0692$

^a $R = \sum |F_o - F_c| / \sum |F_o|$. ^b $R_w = \{ [\sum w(F_o^2 - F_c^2)] / [\sum w(F_o^2)^2] \}^{1/2}$; $w = 1 / [\sigma^2(F_o)^2 + (xP)^2 + yP]$, where $P = (F_o^2 + 2F_c^2) / 3$.

Table 6. Selected bond lengths (Å) and angles (°) for **39**.

Bond Lengths			
Zr1–N3	2.1179(11)	P1–N1	1.7412(10)
Zr1–Cl1	2.3821(6)	P1–N2	1.7361(10)
Zr1–Cl2	2.3734(6)	P1–S1	1.9080(5)
Zr1–N2	2.5734(16)	P1–P1#	2.6299(7)
Zr1–N1	2.5590(15)	N2–C20	1.520(2)
Zr1–P1	2.8210(4)	N1–C10	1.512(2)
P1–N3	1.6414(11)	N3–C30	1.4946(17)
Bond Angles			
N3#–Zr1–N3	126.21(6)	Cl2–Zr1–P1#	123.94(2)
N3–Zr1–Cl1	105.33(3)	N3–Zr1–P1#	90.89(3)
Cl1–Zr1–Cl2	106.55(3)	Cl2–Zr1–P1#	123.94(2)
N3–Zr1–N2	65.94(3)	N3–P1–N1	99.13(6)
Cl1–Zr1–N2	151.45(4)	N1–P1–N2	80.37(5)
Cl2–Zr1–N2	103.35(4)	N3–P1–S1	123.09(4)
N3–Zr1–N1	66.04(3)	N1–P1–S1	122.59(5)
Cl2–Zr1–N1	155.19(4)	N3–P1–P1#	110.47(4)
N1–Zr1–N2	51.85(5)	P1–N2–P1#	98.08(7)
N3–Zr1–P1#	90.89(3)	S1–P1–N1	122.26(6)
Cl1–Zr1–P1#	121.053(16)	P1–N3–Zr1	96.43(5)

Synthesis and Spectroscopic Analysis of $\{[(^t\text{BuNP}=\text{S})_2(^t\text{BuN})_2]\text{HfCl}_2\}$, **40**

In a manner similar to compound **39**, compound **40** was obtained by prolonged (5 d) oxidation of **34** with sulfur in hot toluene (Scheme 17). The ^1H , $^{13}\text{C}\{^1\text{H}\}$, and $^{31}\text{P}\{^1\text{H}\}$ NMR spectra are shown in Figures 23, 24, and 25 respectively. Being analogous to **39**, compound **40** shows similar chemical shift values and splitting patterns to those observed for compound **39**.

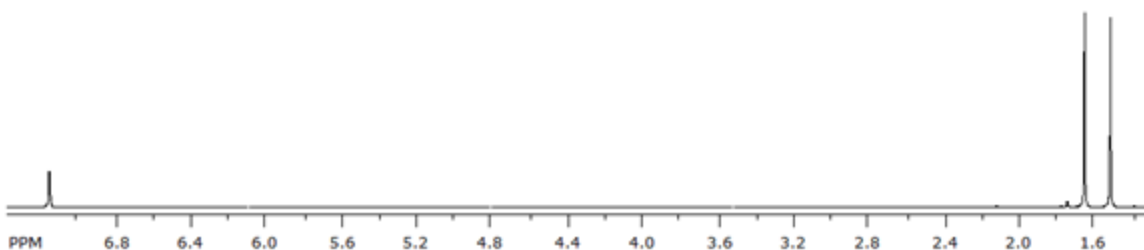


Figure 23. ^1H NMR Spectrum of **40**.

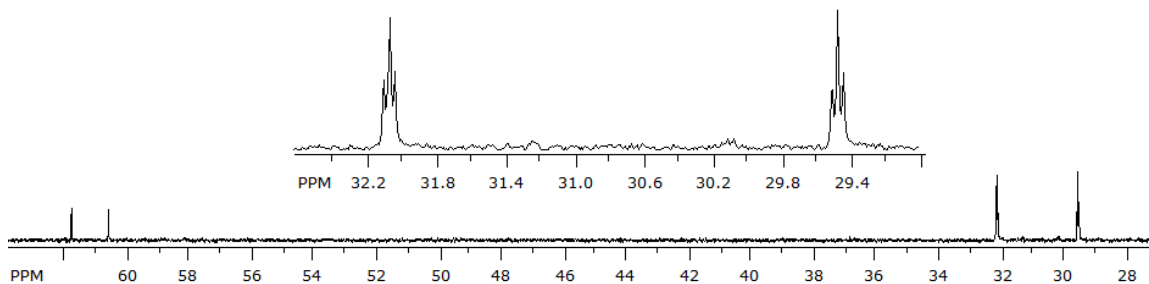


Figure 24. $^{13}\text{C}\{^1\text{H}\}$ NMR Spectrum of **40**.

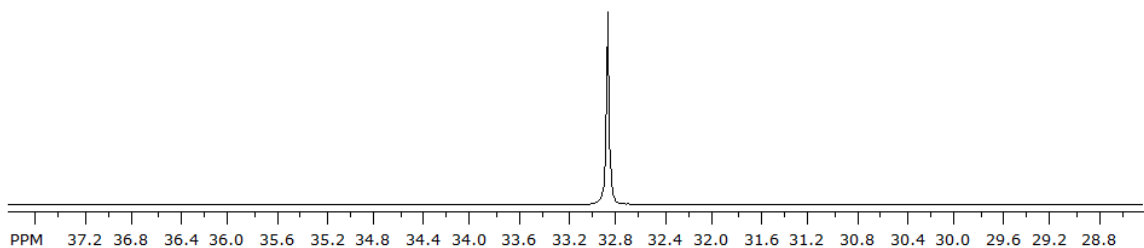


Figure 25. $^{31}\text{P}\{^1\text{H}\}$ NMR Spectrum of **40**.

Solid-state Structure of $\{[(^t\text{BuNP}=\text{S})_2(^t\text{BuN})_2]\text{HfCl}_2\}$, **40**

Like its zirconium counterpart **39**, compound **40** afforded colorless, block-shaped crystals from a concentrated solution of toluene at $-20\text{ }^\circ\text{C}$. The solid-state structure of **40** with a partial atom numbering scheme is shown in Figure 26, while the crystal data and selected bond parameters are listed in Tables 7 and 8, respectively. The solid-state structure of **40** shows a similar pseudo-tetrahedral geometry around hafnium like that depicted in its zirconium analogue **39**. Compound **40** crystallizes in the orthorhombic space group *Pbcm* with four molecules per unit cell and an approximate C_{2v} symmetry.

Both the exocyclic P–N bonds, $1.6363(19)\text{ \AA}$, and the endocyclic P–N bonds, $1.7416(18)$ and $1.7354(18)\text{ \AA}$, in **40** are slightly shorter than corresponding bonds in the starting ligand **35**, P–N(exo): $1.648(9)\text{ \AA}$, P–N(endo): $1.787(10)$ and $1.743(10)\text{ \AA}$.³³ This is probably due to the fact that the phosphorus atoms in **40** are P(V) as opposed to the P(III) atoms in **35**. The two identical exocyclic P–N bonds in **40** are almost perpendicular to the P_2N_2 ring. The endocyclic P–N bonds in **40** are longer than those in *cis*- $[\text{PdCl}_2\{^t\text{BuNP}(\text{OCH}_2\text{CH}_2\text{SCH}_3)\}_2]$ ($1.6555(15)$ – $1.7374(14)\text{ \AA}$),⁷⁹ and $\{[\text{Me}_2\text{Si}(\mu\text{-N}^t\text{Bu})_2\text{P}=(\text{N-}i\text{p-tolyl})(\text{NHPH})]-0.5\text{C}_6\text{H}_5\text{Me}\}$ ($1.653(2)$ and $1.561(3)\text{ \AA}$).¹¹³

Due to symmetry there are two identical Hf–N(amido) bonds in **40**, $2.1066(9)\text{ \AA}$, which are shorter than those in $(\text{Me}_4\text{taen})\text{Hf}(\text{NMe}_2)_2$, $2.1816(5)\text{ \AA}$,¹¹¹ and $[\text{HfCp}_2(\text{Me})\{\text{NH}_2\text{B}(\text{C}_6\text{F}_5)_3\}]$, $2.270(2)\text{ \AA}$,¹¹⁴ but they are longer than those in $[\{\mu\text{-NC}(\text{NMe}_2)_2\}\{\text{NC}(\text{NMe}_2)_2\}_2\text{HfCl}_2]$ (P–N(av): $2.0765(5)\text{ \AA}$),¹¹⁵ $\{[(\text{MeSiN}^t\text{Bu})_2(\text{N}^t\text{Bu})_2]\text{HfCl}_2\}$, $2.084(4)$ and $2.075(4)\text{ \AA}$, and $\{[(\text{MeSiN}^t\text{Bu})_2(\text{N}^t\text{Bu})_2]\text{HfMe}_2\}$, $2.080(1)\text{ \AA}$, reported by Stahl and co-workers.¹¹⁶ There

are weak dative interactions, 2.555(3) and 2.537(2) Å, between the hafnium atom and each of the ring-nitrogen atoms.

The two almost identical Hf–Cl bonds in **40**, 2.3506(10) and 2.3551(10) Å, are comparable to that in **37**, 2.3685(5) Å,³³ but they are shorter than the Hf–Cl bond in $\{(\text{Me}_3\text{Si})_2\text{N}\}_3\text{HfCl}$, 2.436(5) Å.¹¹⁷ The two identical P=S bonds in **40**, 1.9097(8) Å, are slightly shorter than the P=S bonds in $[(4\text{-CN-PhO})(\text{S})\text{P}(\mu\text{-N}^t\text{Bu})_2]$ (1.9118(8)–1.918(2) Å),¹¹⁸ $\text{C}_6\text{H}_4\text{N}_2[\text{P}(\text{S})(\text{NEt}_2)_2]_2\text{PNEt}_2$ (1.940(2) and 1.936(2) Å),¹¹⁹ $[(\text{C}_6\text{H}_5\text{NH})\text{P}(\text{S})\text{NC}_6\text{H}_5]_2$ (1.925(4) Å),¹²⁰ and $[\text{Me}_2\text{Si}(\mu\text{-N}^t\text{Bu})_2\text{P}=\text{S}(\text{NHPH})]$ (1.938(2) Å).¹¹³ Just like its zirconium analogue **39**, the P_2N_2 ring in **40** is slightly puckered, angle sum = 357°.

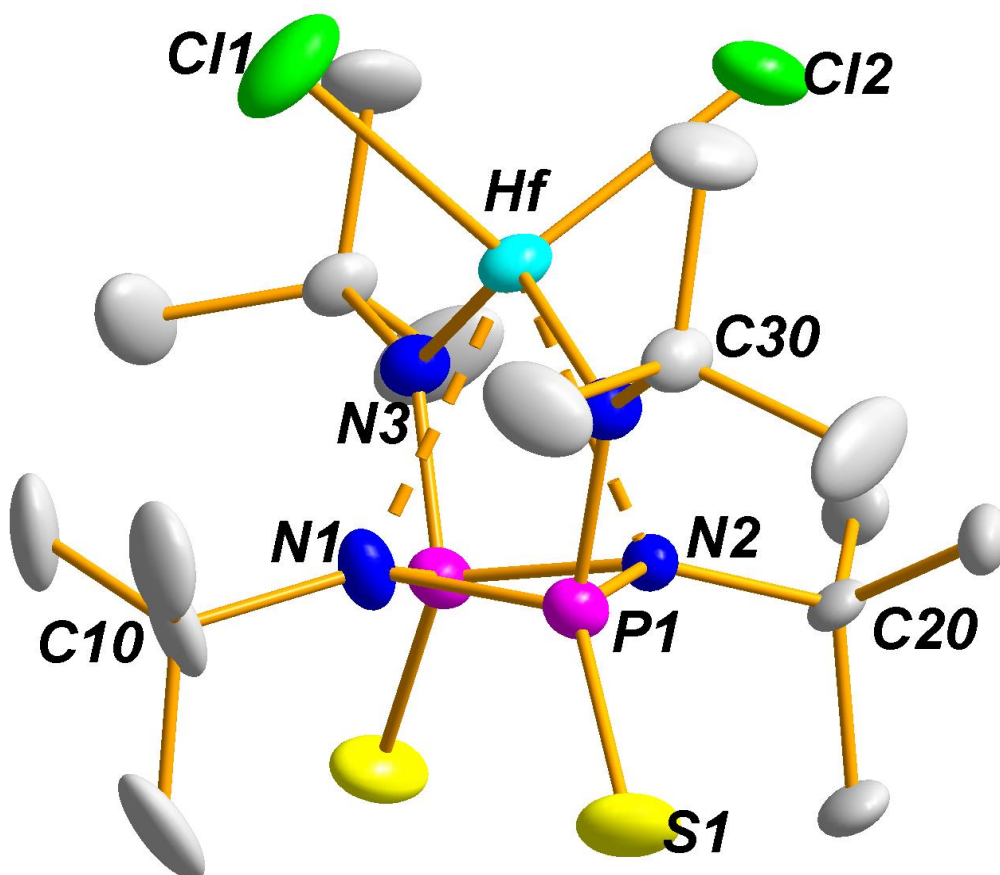


Figure 26. Solid-state structure and partial labelling scheme of **40**. With the exception of carbon (35 %) all atoms are drawn at the 50 % probability level.

Table 7. Crystal and structure refinement data for compound **40**.

Chemical Formula	C ₂₄ H ₅₄ Cl ₂ N ₄ P ₂ S ₂ Hf
fw	659.91
T/K	173(2)
$\lambda/\text{\AA}$	0.71073
Crystal system	Orthorhombic
Space group	<i>Pbcm</i>
$a/\text{\AA}$	13.4904(6)
$b/\text{\AA}$	13.7347(6)
$c/\text{\AA}$	13.9586(6)
$\alpha/^\circ$	90
$\beta/^\circ$	90
$\gamma/^\circ$	90
$V/\text{\AA}^3$	2586.2(2)
<i>Z</i>	4
$\rho(\text{calc}) \text{ g cm}^{-3}$	1.695
μ/mm^{-1}	4.535
F(000)	1312
Completeness (%)	99.9
Reflections collected	19190
Independent reflections	3913 [$R_{\text{int}} = 0.0398$]
$R_w(F^2)^b$ [$I > 2\sigma(I)$]	$R_1 = 0.0251$, $wR_2 = 0.0660$
$R(F)^a$ (all data)	$R_1 = 0.0273$, $wR_2 = 0.0673$

^a $R = \sum |F_o - F_c| / \sum |F_o|$. ^b $R_w = \{ [\sum w(F_o^2 - F_c^2)] / [\sum w(F_o^2)^2] \}^{1/2}$; $w = 1 / [\sigma^2(F_o)^2 + (xP)^2 + yP]$, where $P = (F_o^2 + 2F_c^2) / 3$.

Table 8. Selected bond lengths (Å) and angles (°) for **40**.

Bond Lengths			
Hf1–Cl1	2.3506(10)	P1–N1	1.7354(18)
Hf1–Cl2	2.3551(10)	P1–N2	1.7416(18)
Hf1–N3	2.1066(19)	P1–S1	1.9097(8)
Hf1–N2	2.537(2)	N1–P1#	1.7354(18)
Hf1–N1	2.555(3)	N2–C20	1.505(4)
Hf1–P1	2.7993(6)	N1–C10	1.516(5)
P1–N3	1.6363(19)	N3–C30	1.497(3)
Bond Angles			
N3#–Hf1–N3	127.11(10)	Cl2–Hf1–P1	121.50(3)
N3–Hf1–Cl1	106.27(5)	Cl2–Hf1–P1#	121.50(3)
N3#–Hf1–Cl2	105.32(5)	Cl1–Hf1–P1	123.82(3)
Cl1–Hf1–Cl2	104.63(4)	P1#–N1–P1	98.49(13)
N3–Hf1–N2	66.49(5)	N3–P1–N1#	99.77(11)
Cl1–Hf1–N2	155.41(6)	N1–P1–N2	80.42(9)
Cl2–Hf1–N2	99.96(6)	N2–P1–S1	122.26(9)
N3–Hf1–N1	66.38(5)	N3–P1–S1	123.41(8)
Cl2–Hf1–N1	152.27(7)	N1–P1–S1	122.08(10)
N2–Hf1–N1	52.31(8)	N3–P1–N2	99.53(12)
N3–Hf1–P1#	91.56(5)	N2–P1–N1#	79.37(10)

5. Polymerization Studies

Compound **39** was tested for its productivity as a polyolefin catalyst in duplicate reactions. The tests were done in an argon-flushed, 250-mL, mechanically-stirred, glass-lined, stainless-steel Parr pressure vessel (250 mL, Parr Inst.). Initially 10 μmol of pre-catalyst dissolved in toluene (40 mL) was injected. Then 1000 molar equivalents of a standard MAO solution were added by syringe and the vessel was pressurized (8.0 bar) with ethylene. The stirred reaction mixture was then heated (55 °C) for 0.5 hour. After completion of the reaction, the vessel was vented and the polymer mass was washed and dried. Under the above-described conditions **39** produced 9.2×10^3 kg PE/mol catalyst·h. Under identical conditions the analogous phosphorus(III) compound **33** produced 1.2×10^3 kg PE/mol catalyst·h. These crude experiments do not allow a separation of activity and catalyst lifetime.

6. Summary and Conclusion

The reactions of Group 4 metal bis(*tert*-butylamido)cyclodiphosph(III)azanes dichlorides with elemental sulfur and sodium *tert*-butoxide have been studied. We have synthesized the first alkoxide derivatives of Group 4 metal (Zr, Hf) bis(*tert*-butylamido)cyclodiphosph(III)azanes, **35** and **36**, by treating sodium *tert*-butoxide with the corresponding bis(*tert*-butylamido)cyclodiphosph(III)azanes dichloride. Both compounds **35** and **36** are monomeric in solution however, they crystallized twinned preventing the solution of their solid-state structures. Notwithstanding, the oxidation of compounds **35** and **36** with elemental sulfur resulted in the bis(*tert*-butylamido)cyclodiphosph(V)azane derivatives **37** and **38**, which crystallized isostructurally in the orthorhombic space group *Cmc*2(1).

In contrast to oxidation of compounds **35** and **36**, the oxidation of **33** and **34** with elemental sulfur required more forcing conditions (refluxing in toluene for 5 days) to give compounds **39** and **40**. This is because the chloride groups in the latter are more electron-withdrawing than the *tert*-butoxy groups in the former, which results in the lone pairs of electrons on the ring P atoms in bis(*tert*-butylamido)cyclodiphosph(III)azanes metal dichlorides less available for oxidation. Both compounds, **39** and **40**, crystallized isostructurally in the orthorhombic space group *Pbcm*. Our results indicate a similarity in the reactivity of Group 4 bis(*tert*-butylamido)cyclodiphosph(III)azanes, because all compounds formed for zirconium were analogous to those formed for hafnium. Compounds **35–40** are all air- and moisture-sensitive, and they are all soluble in organic solvents such as toluene and hexanes. The activity of **39** towards ethylene polymerization is higher (9.2×10^3 kg PE/mol catalyst·h) than that of the phosphorus(III) analogous compound **33** (1.2×10^3 kg PE/mol catalyst·h).

CHAPTER III

**REACTIONS OF DIANIONIC
BIS(ALKYLAMIDO)CYCLODIPHOSPH(III)AZANES WITH
ELECTROPHILES: *N* VERSUS *P* ELECTROPHILIC ATTACK**

1. Introduction

Cyclodiphosphazanes are versatile ligands in coordination chemistry that can be used as either anionic or neutral ligands for metal complexes, forming mononuclear, dinuclear, and tetranuclear complexes.^{27-35, 121-127} This versatility is largely due to their flexible bite angle and multidentate nature. The coordination behavior of cyclodiphosphazanes depends on both steric and electronic attributes which can be readily altered by changing the substituents on the phosphorus atoms.¹²⁸⁻¹³²

Cyclodiphosphazane ligands usually bind through a variety of coordination modes as illustrated in Figure 27. These coordination sites can either be terminal and bridging N-donor atoms (**41–43**), which allows for the incorporation of s-, p-, or d-block elements with a variety of sizes and oxidation states; or through the “hard” N and “soft” E centers (**44–47**). The latter coordination mode has been used to obtain different coordination polymers.^{38, 44} Compounds which are chelated as represented in compound **43** have idealized C_{2v} symmetry while those represented by compound **41** are C_s -symmetric. Compounds similar to **42** are C_{2v} -symmetric if the metal (M) or element bears two identical exocyclic substituents, but they are C_s -symmetric if the element bears two different groups.³⁸

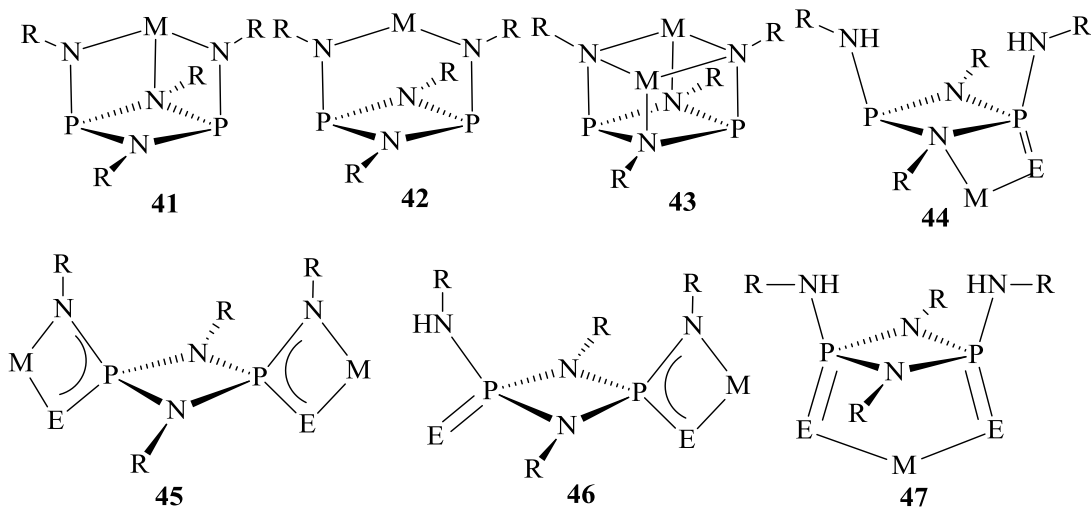
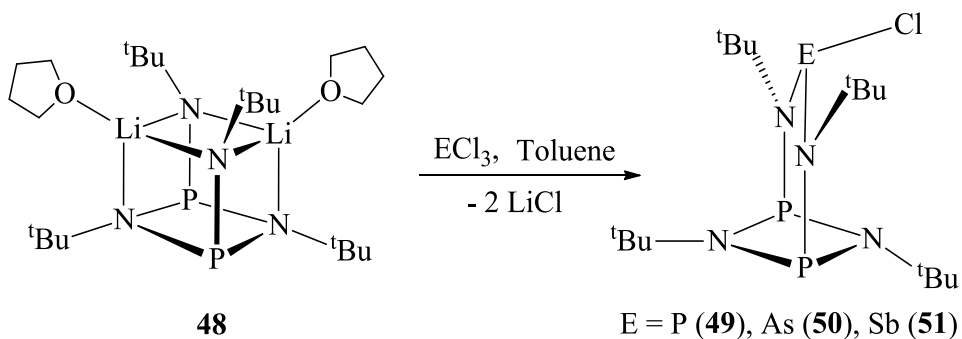


Figure 27. Coordination modes of cyclodiphosphazanes.

The type of chelation observed depends on a combination of factors including, the size of the metal (covalent radius), the steric bulk around the metal- and amido substituents, the electron donating abilities of the amido nitrogen atoms, and the hard-soft-acid-base (HSAB) considerations of both the metal and ligand fragment.^{30, 112} Large metals ($r_{\text{cov}} > 1.25 \text{ \AA}$) prefer to coordinate to the ligand through the amido nitrogen atoms in a bis(amido) (N, N') mode (cf. **41** and **42**), although sometimes the metal may coordinate to the cyclodiphosphazane ligand laterally (cf. **45–46**).^{32, 51} The reason for the bis(amido) coordination preference is the larger N–N interatomic distance, versus the smaller N, E lateral coordination site. Consequently, large metals experience more steric repulsion in the lateral N, E coordination site than in the N, N' amido coordination site. However, large metals with sterically crowded ancillary ligands will preferably coordinate to the cyclodiphosphazane laterally because there will be significant repulsion between the amido substituents in the cyclodiphosphazane and the ligands of the metal.⁵⁴

To establish the above mentioned coordination modes of cyclodiphosphazanes, their reactions have been studied by different investigators.^{32, 38, 47, 54, 93, 121, 133-135} In these

complexes the metals serve as electrophiles. There are very few reported studies in which the reaction chemistry of these molecules with non-metallic electrophiles was investigated (Scheme 18). In one such example, Stahl and coworkers,³⁵ used a salt-elimination method (Scheme 18) for the introduction of phosphorus, arsenic, and antimony into **48**, giving rise to the first fully-characterized mono-arsenic, mono-antimony, and mono-phosphorus derivatives of bis(alkylamino)cyclodiphosphazanes.



Scheme 18. Syntheses of **49**, **50**, and **51**.

Although these heterocycles have been known for over fifty years, recent research on the compounds have focused mainly on their roles as *P* and *N* donor ligands.^{27, 31, 35, 37, 38, 44, 52, 121, 135, 136} We were particularly interested in investigating the *P*, *N* ambidenticity of these heterocycles. In this work we set out to study the reactions of bis(amido)cyclodiphosph(III)azanes, such as **48** and **54**, with electrophiles like methyl iodide, phosphorus trichloride, and chlorophosphines. In order to expand the scope of this study, we were also interested in finding out how the bis(alkylamido)cyclodisilazane $\{(\text{MeSiN}^t\text{Bu})_2(\text{N}^t\text{BuLi}\cdot\text{THF})_2\}$, which is isoelectronic to **48**, will react with similar electrophiles.

2. Experimental

Description of Techniques and Chemicals Used

General

All experimental procedures were carried out under an atmosphere of argon, using standard Schlenk lines. Prior to use, all solvents were dried and freed of molecular oxygen by distillation under a nitrogen atmosphere from sodium- or potassium benzophenone ketyl.

Chemicals used

Phosphorus trichloride, chlorodiphenylphosphine, *n*-butyllithium (2.5 M in hexanes), and methyl iodide, were purchased from either Sigma Aldrich or Alfa Aesar, and they were used without further purification. The compounds *cis*-[(^tBuNP)₂(CyNH)₂],⁵⁰ *cis*-[(^tBuNP)₂(^tBuNLi·thf)₂],³⁷ *trans*-1,3-di(*tert*-butylamino)-2,4-dimethylcyclodisilazane,¹³⁷ and *cis*-[(MeSiN^tBu)₂(N^tBuLi·thf)₂],¹³⁷ were synthesized according to published procedures.

Description of Instrumentation

NMR spectra were recorded on a Bruker AVANCE-500 NMR spectrometer. The ¹H and ¹³C NMR spectra were referenced relative to C₆D₅H (7.15 ppm) and C₆D₆ (128.0 ppm), respectively, as internal standards, while the ³¹P spectra were referenced relative to P(OEt)₃ (137.0 ppm) as external standard in C₆D₆. In all cases positive chemical shift values represent higher frequencies and downfield shifts. Melting points were recorded on Mel-Temp melting point apparatus; they are uncorrected. Elemental analyses on crystalline samples were performed by ALS Life Sciences Division Environmental, Tucson, AZ.

X-ray Crystallography

Suitable, single crystals were coated with Paratone oil, affixed to Mitegen or Litholoop crystal holders, and centered on the diffractometer in a stream of cold nitrogen. Reflection intensities were collected with a Bruker Apex diffractometer, equipped with an Oxford Cryosystems, 700 Series Cryostream cooler, operating at 173 K. Data were measured using ω scans of 0.3° per frame for 20 seconds until a complete hemisphere of data had been collected. Cell parameters were retrieved using SMART⁹⁷ software and refined with SAINT⁹⁸ on all observed reflections. Data were reduced with SAINTplus, which corrects for Lorentz polarization effects and crystal decay. Empirical absorption corrections were applied with SADABS.⁹⁹ The structures were solved by direct methods with SHELXS-90¹⁰⁰ program and refined by full-matrix least squares methods on F² with SHELXL-97¹⁰¹ incorporated in SHELXTL Version 5.10.¹⁰²

3. Syntheses of Compounds

Synthesis of [(PPh₂)^tBuNP(μ -N^tBu)₂PN^tBu(PPh₂)], **52A** and **52B**

Chlorodiphenylphosphine (1.58 g, 7.15 mmol), was dissolved in 10 mL of THF in a 100 mL two-necked flask equipped with a gas inlet and magnetic stirbar. This flask was then cooled to 0 °C in an ice bath. A solution of *cis*-[(^tBuNP)₂(^tBuNLi·thf)₂, **48**, (1.81 g, 3.58 mmol) in 15 mL of THF was added dropwise to the chlorodiphenylphosphine solution. After the reaction mixture had warmed to room temperature, it was stirred at 50 °C overnight. All THF was removed *in vacuo* and the residue was dissolved in 40 mL of toluene. A white precipitate of LiCl appeared instantly after the addition of compound **48**. The LiCl was then filtered off after 1 h and the filtrate was concentrated and stored at -12 °C. The next day, colorless, tiny, bar-shaped crystals of **52A** were isolated and the

supernatant was concentrated and stored again at $-12\text{ }^{\circ}\text{C}$. After 3 days colorless, block-shaped crystals of **52B** were isolated.

52A – Yield: (3.69 g, 5.15 mmol), 72 %. Mp: 178–180 $^{\circ}\text{C}$. ^1H NMR (500.1 MHz, benzene- d_6 , 25 $^{\circ}\text{C}$): 8.18 (t, $J_{\text{HH}} = 7.70$ Hz, 2H, Ph), 7.92 (t, $J_{\text{HH}} = 8.65$ Hz, 2H, Ph), 7.04 (t, $J_{\text{HH}} = 7.45$ Hz, 1H, Ph), 1.83 (s, 9H, N^tBu), 1.40 (s, 9H, N^tBu), 1.20 (s, 18H, N^tBu). $^{13}\text{C}\{^1\text{H}\}$ NMR (125.8 MHz, benzene- d_6 , 25 $^{\circ}\text{C}$): 135.8 (dd, $J_{\text{PC}} = 5.89$ Hz; 27.8 Hz, Ph), 135.3 (m, Ph), 129.4 (t, $J_{\text{PC}} = 22.0$, Ph), 128.4 (d, $J_{\text{PC}} = 2.82$ Hz, Ph), 63.24 (dd, $J_{\text{PC}} = 9.91$ Hz, 28.1 Hz, N^tBu), 53.57 (d, $J_{\text{PC}} = 11.6$ Hz, N^tBu), 53.01 (d, $J_{\text{PC}} = 14.9$ Hz, N^tBu), 34.82 (d, $J_{\text{PC}} = 9.26$ Hz, N^tBu) 32.52 (d, $J_{\text{PC}} = 3.31$ Hz, N^tBu), 31.64 (d, $J_{\text{PC}} = 14.5$ Hz, N^tBu). $^{31}\text{P}\{^1\text{H}\}$ NMR (202.5 MHz, benzene- d_6 , 25 $^{\circ}\text{C}$): 87.33 (t, $J_{\text{PP}} = 28.6$ Hz), 48.04 (d, $J_{\text{PP}} = 37.1$ Hz), -8.72 (d, $J_{\text{PP}} = 0.978$ Hz), -45.26 (dd, $J_{\text{PP}} = 25.1$ Hz, 201 Hz). Anal. Calcd for $\text{C}_{40}\text{H}_{56}\text{N}_4\text{P}_4$: C, 67.02; H, 7.88; N, 7.82. Found: C, 67.42; H, 8.10; N, 7.38.

52B – Yield: (1.41 g, 1.97 mmol), 27 %. Mp: 156–158 $^{\circ}\text{C}$. ^1H NMR (500.1 MHz, benzene- d_6 , 25 $^{\circ}\text{C}$): 8.56 (t, $J_{\text{HH}} = 7.20$ Hz, 2H, Ph), 7.12 (t, $J_{\text{HH}} = 7.40$ Hz, 2H, Ph), 7.02 (t, $J_{\text{HH}} = 7.20$ Hz, 1H, Ph), 1.64 (s, 18H, N^tBu), 1.19 (s, 18H, N^tBu). $^{13}\text{C}\{^1\text{H}\}$ NMR (125.8 MHz, benzene- d_6 , 25 $^{\circ}\text{C}$): 138.3 (m, Ph), 136.6 (dt, $J_{\text{PC}} = 12.8, 6.63$, Ph), 129.6 (s, Ph), 53.72 (m, N^tBu), 34.46 (t, $J_{\text{PC}} = 5.31$ Hz, N^tBu), 33.42 (s, N^tBu). $^{31}\text{P}\{^1\text{H}\}$ NMR (202.5 MHz, benzene- d_6 , 25 $^{\circ}\text{C}$): -16.53 (d, $J_{\text{PP}} = 1.20$ Hz), -37.08 (d, $J_{\text{PP}} = 1.25$ Hz). Anal. Calcd for $\text{C}_{40}\text{H}_{56}\text{N}_4\text{P}_4$: C, 67.02; H, 7.88; N, 7.82. Found: C, 67.42; H, 8.10; N, 7.38.

Synthesis of *cis*-[$(^t\text{BuNP})_2(\text{CyNLi}\cdot\text{thf})_2$], **54**

Exactly 3.77 g (9.40 mmol) of *cis*-[$(^t\text{BuNP})_2(\text{CyNH})_2$], **53**, was dissolved in 45 mL of THF in a 100 mL three-neck flask equipped with a magnetic stirring bar, two gas

inlets, and a dropping funnel. Via addition funnel, 7.50 mL (18.8 mmol) of 2.50 M *n*-butyllithium solution was added dropwise to the cooled (0 °C) reaction flask. After the reaction mixture had reached RT, it was refluxed for 1 h, allowed to cool, and concentrated in vacuo. It was then stored at –20 °C. The next day, large, colorless rhombic crystals of **54** were isolated and the supernatant was concentrated and stored again at –20 °C. Yield: (4.05 g, 7.28 mmol), 77 %.

Mp: 118–120 °C. ¹H NMR (500.1 MHz, benzene-d₆, 25 °C): 3.58 (t, 8H, OCH₂), 1.94 (t, 2 H, Cy), 1.76 (m, 4H, Cy), 1.68 (m, 4H, Cy), 1.55 (s, 18 H, N^tBu), 1.39 (q, 8H, CH₂), 1.30 (m, 4H, Cy), 1.13 (m, 8H, Cy). ¹³C{¹H} NMR (125.8 MHz, benzene-d₆, 25 °C): 67.94 (s, OCH₂), 54.98 (t, *J* = 18.42 Hz, N^tBu), 41.36 (br s, Cy), 30.56 (t, *J* = 7.19 Hz, Cy), 30.01 (t, *J* = 8.09 Hz, N^tBu), 27.21 (s, Cy), 26.03 (s, Cy), 25.68 (s, CH₂). ³¹P{¹H} NMR (202.5 MHz, benzene-d₆, 25 °C): 130.8 (s). Anal. Calcd for C₂₈H₅₆Li₂N₄O₂P₂: C, 60.42; H, 10.07; N, 10.14. Found: C, 59.98; H, 9.85; N, 9.92.

Synthesis of *cis*-{[P(μ-N^tBu)]₂(CyNPCl₂)₂}, **55**

A 100 mL two-neck flask equipped with a stirbar and gas inlet was charged with PCl₃ (0.318 g, 2.31 mmol) dissolved in 5 mL of toluene and cooled to 0 °C. A solution of compound **54** (1.29 g, 2.31 mmol) dissolved in 15 mL of toluene was added dropwise to the PCl₃ solution. After the reaction mixture had warmed to RT, it was stirred at 50 °C overnight. The reaction mixture was cooled to RT for 1 h and filtered with a medium-porosity frit. The filtrate was concentrated *in vacuo* and stored at –20 °C. After two days, colorless, bar-shaped crystals of **55** were isolated. Yield: (1.04 g, 1.73 mmol), 75 %.

Mp: 138–140 °C. ¹H NMR (500.1 MHz, benzene-d₆, 25 °C): 1.95 (m, 2H, Cy), 1.81 (m, 4H, Cy), 1.43 (m, 4H, Cy), 1.36 (s, 18H, N^tBu), 1.21 (m, 4H, Cy), 0.95 (m, 8H,

Cy). $^{13}\text{C}\{^1\text{H}\}$ NMR (125.8 MHz, benzene- d_6 , 25 °C): 61.56 (br s, Cy), 54.68 (t, $J = 14.49$ Hz, N^tBu), 36.46 (br s, Cy), 31.80 (t, $J = 7.18$ Hz, N^tBu), 26.97 (s, Cy), 25.91 (s, Cy). $^{31}\text{P}\{^1\text{H}\}$ NMR (202.5 MHz, benzene- d_6 , 25 °C): 172.6 (s), 112.2 (s). Anal. Calcd for $\text{C}_{20}\text{H}_{40}\text{Cl}_4\text{N}_4\text{P}_4$: C, 39.89; H, 6.69; N, 9.30. Found: C, 40.09; H, 7.15; N, 9.11.

Synthesis of *cis*-[(MeSiN^tBu)₂(N^tBuPCL₂)₂], **57**

To a cooled (0 °C) solution of PCl_3 (1.69 g, 12.3 mmol) in 22 mL of toluene was added dropwise 0.700 g (1.70 mmol) of *cis*-[(MeSiN^tBu)₂(N^tBuLi·thf)₂], **56**, dissolved in 40 mL of toluene. Upon addition of **56**, a white precipitate of LiCl formed. The cloudy solution was allowed to warm to room temperature, stirred at 50 °C overnight and filtered through a medium-porosity frit. The resulting light-yellow solution was concentrated *in vacuo* and stored at -20 °C. After three days, colorless block-shaped crystals were isolated. Yield: (4.96 g, 8.63 mmol), 70 %.

Mp: 168–170 °C. ^1H NMR (500.1 MHz, benzene- d_6 , 25 °C): 1.57 (s, 18H, N^tBu), 1.30 (s, 18H, N^tBu), 0.61 (s, 6H, SiMe). $^{13}\text{C}\{^1\text{H}\}$ NMR (125.8 MHz, benzene- d_6 , 25 °C): 64.8 (s, $\text{NC}(\text{CH}_3)_3$, amido), 51.34 (s, $\text{NC}(\text{CH}_3)_3$, imido), 33.7 (s, $\text{NC}(\text{CH}_3)_3$, amido), 32.81 (s, $\text{NC}(\text{CH}_3)_3$, imido), 11.5 (t, $J_{\text{PC}} = 3.17$ Hz, SiMe). $^{31}\text{P}\{^1\text{H}\}$ NMR (202.5 MHz, benzene- d_6 , 25 °C): 167.1 (s). Anal. Calcd for $\text{C}_{18}\text{H}_{42}\text{Cl}_4\text{N}_4\text{P}_2\text{Si}_2$: C, 37.63; H, 7.37; N, 9.75. Found: C, 37.52; H, 7.77; N, 9.61.

Synthesis of *cis*-[(^tBuNPMe)₂(^tBuN)₂Li₂I₂], **58**

Exactly 1.99 g (3.93 mmol) of *cis*-[(^tBuNP)₂(^tBuNLi·thf)₂], **46**, was dissolved in 30 mL of toluene in a 100 mL 3-necked flask equipped with a gas inlet, a magnetic stirring bar, and a dropping funnel, and cooled to 0 °C. Exactly 7.86 mL of 1.00 M methyl iodide was dissolved in 15 mL of toluene and added dropwise to the cold solution

of **46**. After the reaction had been stirred at RT for 24 h, the resulting colorless solution was then concentrated *in vacuo* and stored at $-12\text{ }^{\circ}\text{C}$ for 2 d. This yielded colorless, plate-shaped crystals of **57**. Yield: (2.86 g, 3.63 mmol), 92 %.

Mp: 184–186 $^{\circ}\text{C}$. ^1H NMR (500.1 MHz, THF- d_8 , 25 $^{\circ}\text{C}$): 1.68 (d, J_{PH} 16.1 Hz, 6H, CH₃), 1.49 (s, 18H, N^tBu), 1.27 (s, 18H, N^tBu). $^{13}\text{C}\{^1\text{H}\}$ NMR (125.8 MHz, THF- d_8 , 25 $^{\circ}\text{C}$): 54.14 (s, NC(CH₃)₃, amido), 51.87 (s, NC(CH₃)₃, imido), 35.15 (t, $J_{\text{PC}} = 0.044$ Hz, NC(CH₃)₃, amido), 31.88 (t, $J_{\text{PC}} = 0.038$ Hz, NC(CH₃)₃, imido), 23.13 (d, $J_{\text{PC}} = 1.00$ Hz, CH₃). $^{31}\text{P}\{^1\text{H}\}$ NMR (202.5 MHz, THF- d_8 , 25 $^{\circ}\text{C}$): -48.78 (s).

Synthesis of *trans*-[(MeSiN^tBu)₂(N^tBu(Li·(thf)₂)₂)]₂, **60**

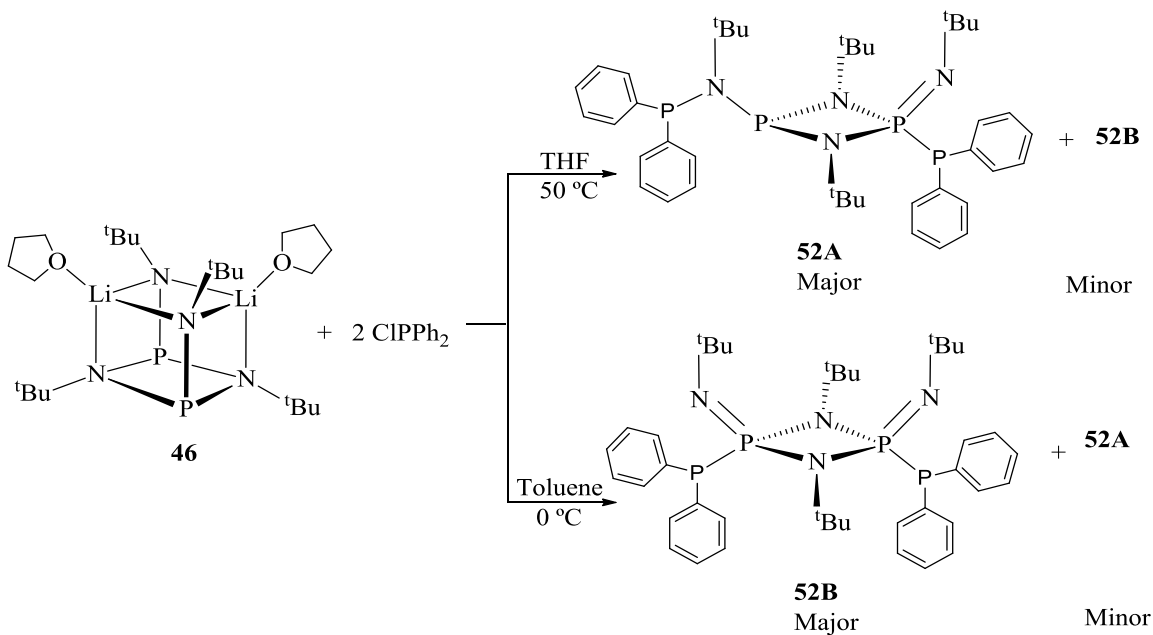
A 250 mL two-necked flask equipped with a stir bar, dropping funnel, and two gas inlets was charged with 3.56 g (9.55 mmol) of *trans*-1,3-di(*tert*-butylamino)-2,4-dimethylcyclodisilazane, **58**, dissolved in 35 mL of THF and cooled to 0 $^{\circ}\text{C}$. Exactly 8.44 mL of 2.5 M *n*-butyllithium was then added dropwise to this solution. Upon reaching room temperature the light-yellow solution was refluxed for 3 h, cooled and then reduced to 15 mL *in vacuo*. After the solution had been stored for 3 d at $-12\text{ }^{\circ}\text{C}$, colorless, flat hexagonal crystals of **60** were isolated. Yield: (5.59 g, 8.31 mmol), 87 %.

Mp: 176–178 $^{\circ}\text{C}$. ^1H NMR (500.1 MHz, benzene- d_6 , 25 $^{\circ}\text{C}$): 3.55 (s, 16H, OCH₂), 1.68 (s, 18H, N^tBu), 1.63 (s, 18H, N^tBu), 1.30 (s, 16H, CH₂), 0.72 (s, 6H, SiMe). $^{13}\text{C}\{^1\text{H}\}$ NMR (125.8 MHz, benzene- d_6 , 25 $^{\circ}\text{C}$): 68.65 (s, OCH₂), 51.19 (s, NC(CH₃)₃, amido), 51.17 (s, NC(CH₃)₃, imido), 38.98 (s, NC(CH₃)₃, amido), 34.07 (s, NC(CH₃)₃, imido), 25.33 (s, OCH₂CH₂), 9.62 (s, SiMe). Anal. Calcd for C₃₄H₇₄Li₂N₄O₄Si₂: C, 60.67; H, 11.51; N, 8.32. Found: C, 60.36; H, 11.51; N, 8.09.

4. Results and Discussions

Synthesis and Spectroscopic Analysis of [(PPh₂)^tBuNP(μ-N^tBu)₂PN^tBu(PPh₂)] **52A** and **52B**)

The synthesis of **52A** and **52B** was carried out through the addition of *cis*-[(^tBuNP)₂(^tBuNLi·thf)₂, **46** to two equivalents of chlorodiphenylphosphine (Scheme 19). Two isomers of this compound that illustrate two different coordination modes were isolated and characterized. Both isomers were separated by fractional crystallization. Isomer **52A** was isolated as colorless, bar-shaped crystals while **52B** formed colorless, rhombic crystals.



Scheme 19. Syntheses of **52A** and **52B**.

The relative ratios of isomer produced depended on specific experimental conditions. Higher temperature (50 °C), longer reaction times and THF solvent always favored the formation of isomer **52A** as the major product and **52B** as the minor product in a ratio of 60 to 40 %. On the other hand, isomer **52B** was favored at lower temperature

(0 °C), shorter reaction times and toluene solvent. Isomer **52A** is therefore the thermodynamic product while isomer **52B** is the kinetic product.

Figures 28 and 29 show the ^1H and $^{31}\text{P}\{^1\text{H}\}$ NMR spectrum of a reaction mixture containing both isomers respectively.

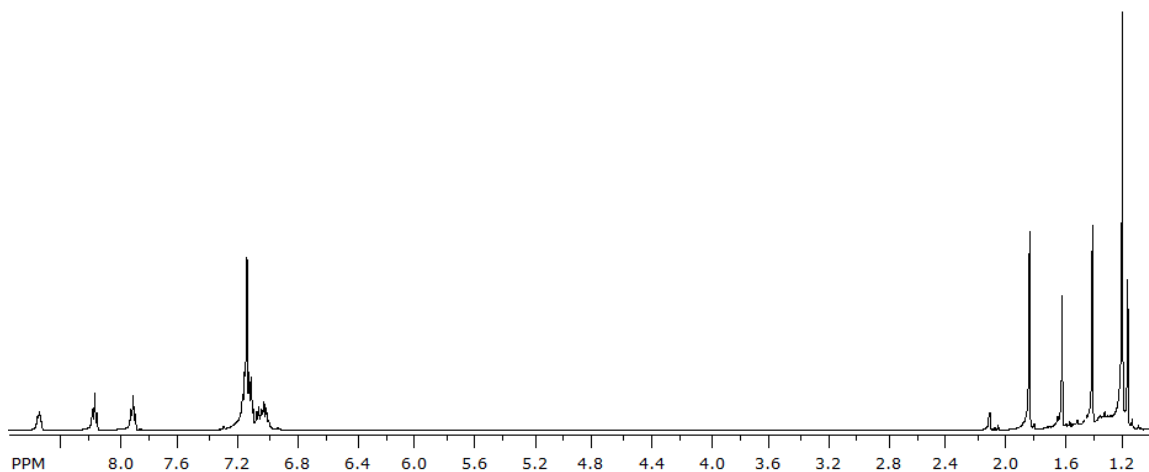


Figure 28. ^1H NMR Spectrum of **52** showing both isomers present.

The ratio of 60 to 40 for isomers **52A** and **52B** can easily be verified from the $^{31}\text{P}\{^1\text{H}\}$ spectrum of the mixtures of isomers shown in Figure 29.

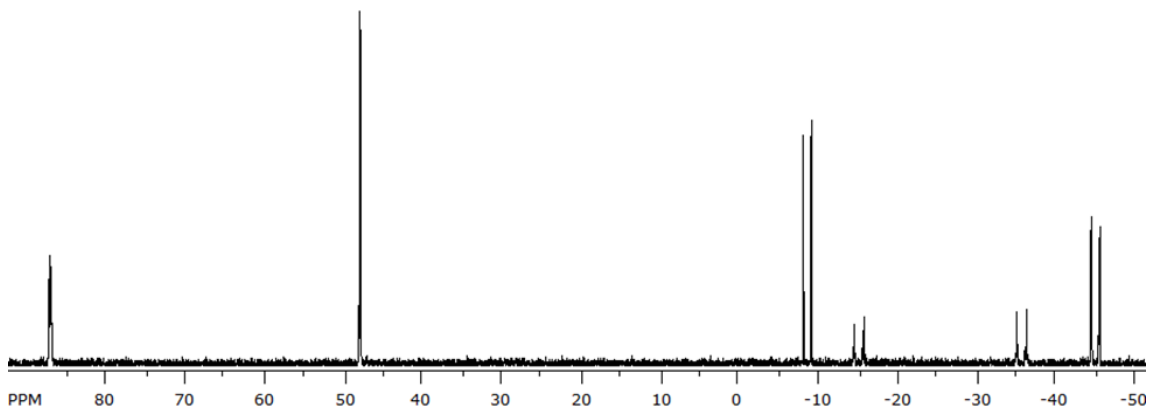


Figure 29. $^{31}\text{P}\{^1\text{H}\}$ NMR Spectrum of **52** showing both isomers present.

Isomer **52A** is less symmetrical than isomer **52B** as illustrated in the ^1H and $^{31}\text{P}\{^1\text{H}\}$ NMR spectra of isomer **52A**, shown in Figures 30 and 31 respectively. There are

three triplets in the aromatic region of the proton NMR spectrum of **52A** which represent the three different types of aromatic protons. The ^1H NMR spectrum of **52A** also shows three distinct peaks in the aliphatic region in a ratio of 2:1:1. The two *tert*-butylamido protons in the (P–N)₂ ring are identical and therefore appear at the same chemical shift of 1.20 ppm. Whereas the two different *tert*-butylimido protons appear at 1.83 and 1.40 ppm, which represents the *tert*-butyl protons attached to the nitrogen atom bearing the diphenyl phosphine group and those of the nitrogen atom without the diphenyl phosphine group, respectively. These protons are chemically and magnetically inequivalent due to the different coordination modes of their nitrogen atoms. This inequivalence is a result of the fact that one PPh₂ is bound to a nitrogen atom on one side of the molecule and to a phosphorus atom on the other side of the molecule. As a consequence, isomer **52A** has four different phosphorus atoms as can be seen in its $^{31}\text{P}\{^1\text{H}\}$ NMR spectrum.

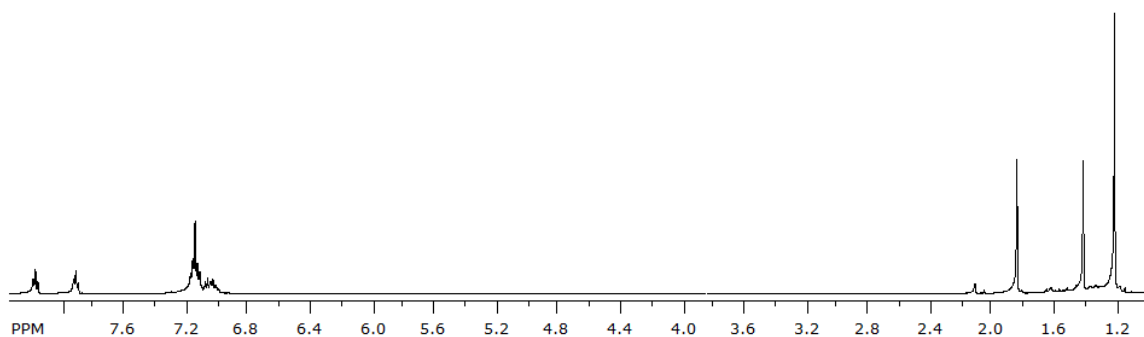


Figure 30. ^1H NMR Spectrum of **52A**.

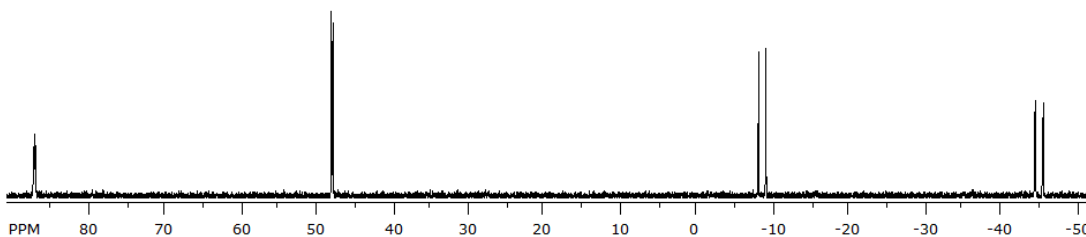


Figure 31. $^{31}\text{P}\{^1\text{H}\}$ NMR Spectrum of **52A**.

The $^{13}\text{C}\{^1\text{H}\}$ NMR spectrum of **52A** is shown in Figure 32 and it depicts seven signals. The phenyl carbons resonate between 135.8 and 128.4 ppm, while the *tert*-butyl carbons appear between 63.24 and 31.66 ppm.

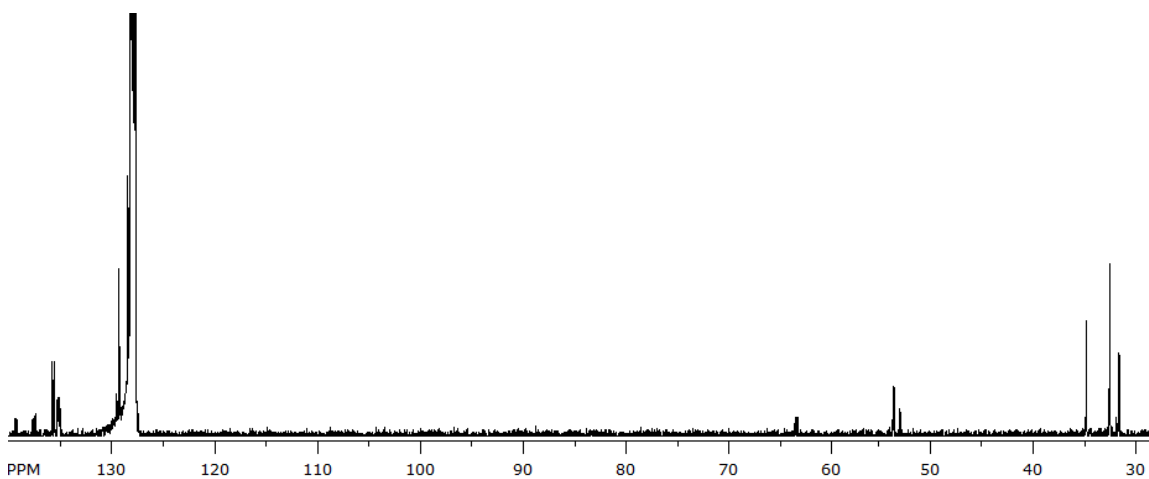


Figure 32. $^{13}\text{C}\{^1\text{H}\}$ NMR Spectrum of **52A**.

Isomer **52B**, has C_2 symmetry because each PPh_2 is attached to a phosphorus atom on either side of the molecule. This results in only two kinds of *tert*-butyl protons, and these appear at 1.64 and 1.79 ppm, and two types of phosphorus atoms as shown in the ^1H and $^{31}\text{P}\{^1\text{H}\}$ NMR spectra of **52B** (Figures 33 and 34, respectively). The $^{13}\text{C}\{^1\text{H}\}$ NMR spectrum of **52B**, as shown in Figure 35, is made up of six signals. The phenyl

carbons resonate between 138.3 and 129.6 ppm while peaks for the aliphatic carbons appear between 53.7 and 33.4 ppm. Isomers **52A** and **52B** demonstrates rare examples of structural isomerism in cyclodiphosphazane compounds.

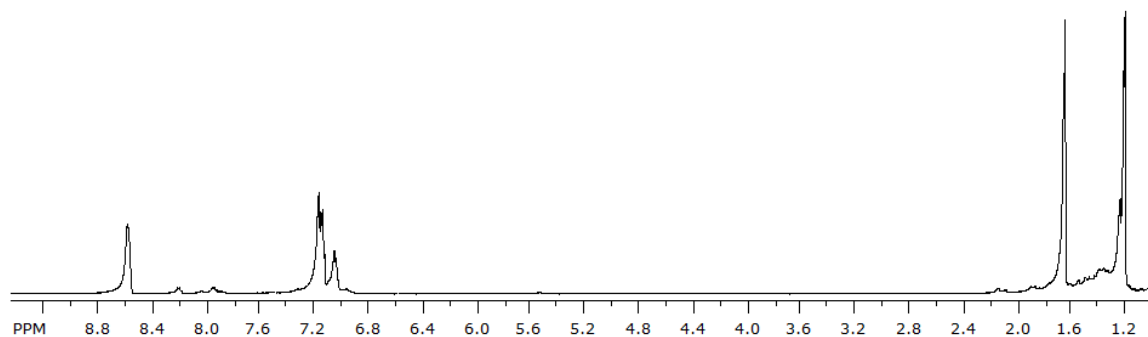


Figure 33. ^1H NMR Spectrum of **52B**.

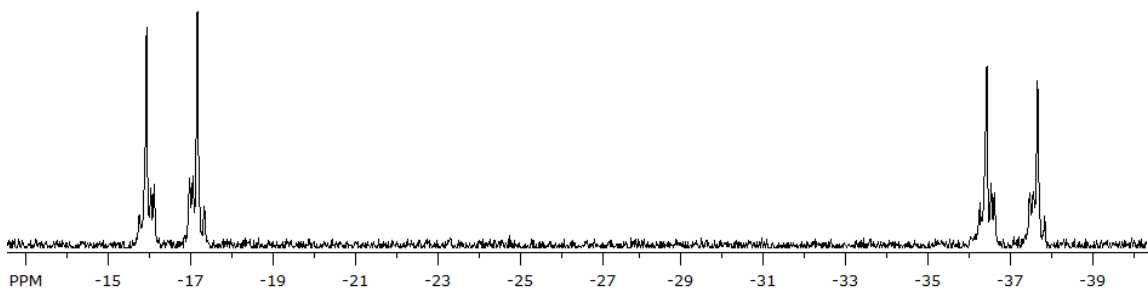


Figure 34. $^{31}\text{P}\{^1\text{H}\}$ NMR Spectrum of **52B**.

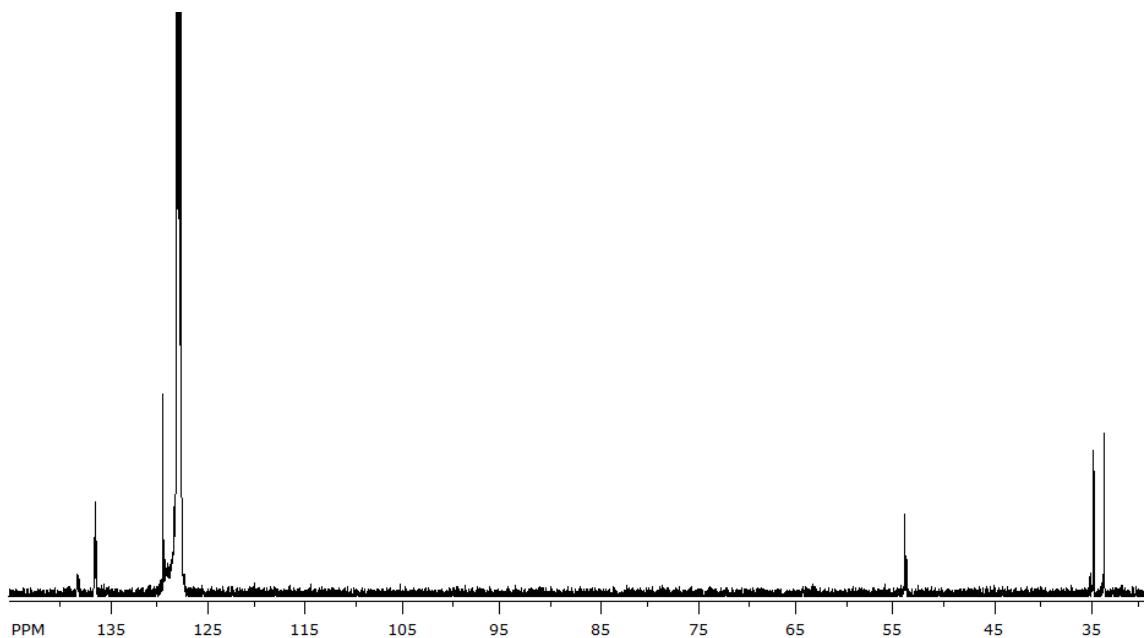


Figure 35. $^{13}\text{C}\{^1\text{H}\}$ NMR Spectrum of **52B**.

Kinetic Studies for the Conversion of Isomer **52B** to Isomer **52A**

During the synthesis of isomers **52A** and **52B**, we observed that the formation of the former is favored by higher temperature while the latter is favored by lower temperature. We proceeded to study the kinetics of this isomerization. We heated a sample of isomer **52B** in a sealed NMR tube at 70 °C while taking NMR readings after every one hour. A graph of the rate of change of the concentration of isomer **52B** with time is shown in Figure 36. As the concentration of isomer **52B** is decreasing, the concentration of isomer **52A** is increasing.

The graph suggests that the isomerization of isomer **52B** to isomer **52A** is a first order process. The half-life of the process is 120 minutes and the rate constant, k , is $9.63 \times 10^{-5} \text{ s}^{-1}$. In order to confirm the first order kinetics, we plotted a graph of the natural logarithm of the concentration of isomer **52B** against time (Figure 37) throughout the conversion process. The graph is a straight line with exactly the same half-life and rate

constant, which confirms that the isomerization process is truly a first order process. The rate equations for the process are shown in equation 3.1 (linear) and equation 3.2 (exponential):

$$\ln[\text{isomer } \mathbf{52B}] = \ln[\text{Isomer } \mathbf{52B}]_o - kt \quad (3.1)$$

$$[\text{Isomer } \mathbf{52B}] = [\text{Isomer } \mathbf{52B}]_o e^{-kt} \quad (3.2)$$

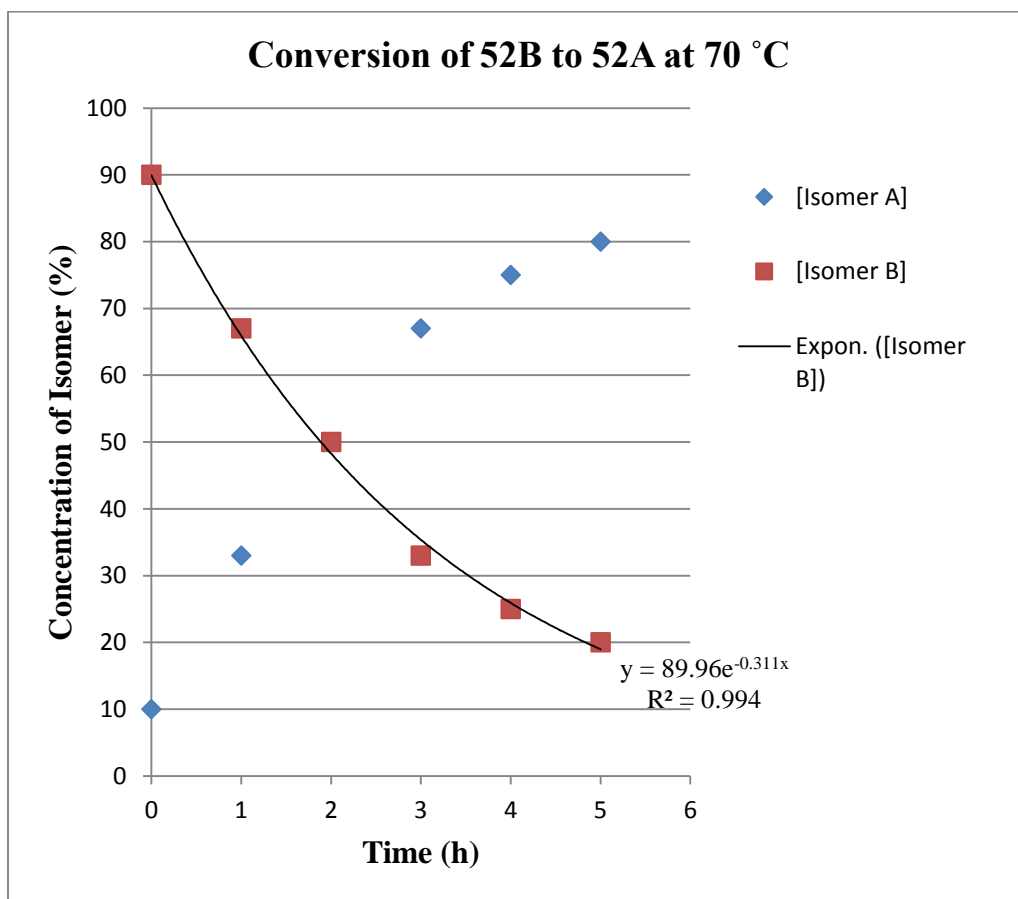


Figure 36. Conversion of isomer **52B** to isomer **52A** at 70 °C.

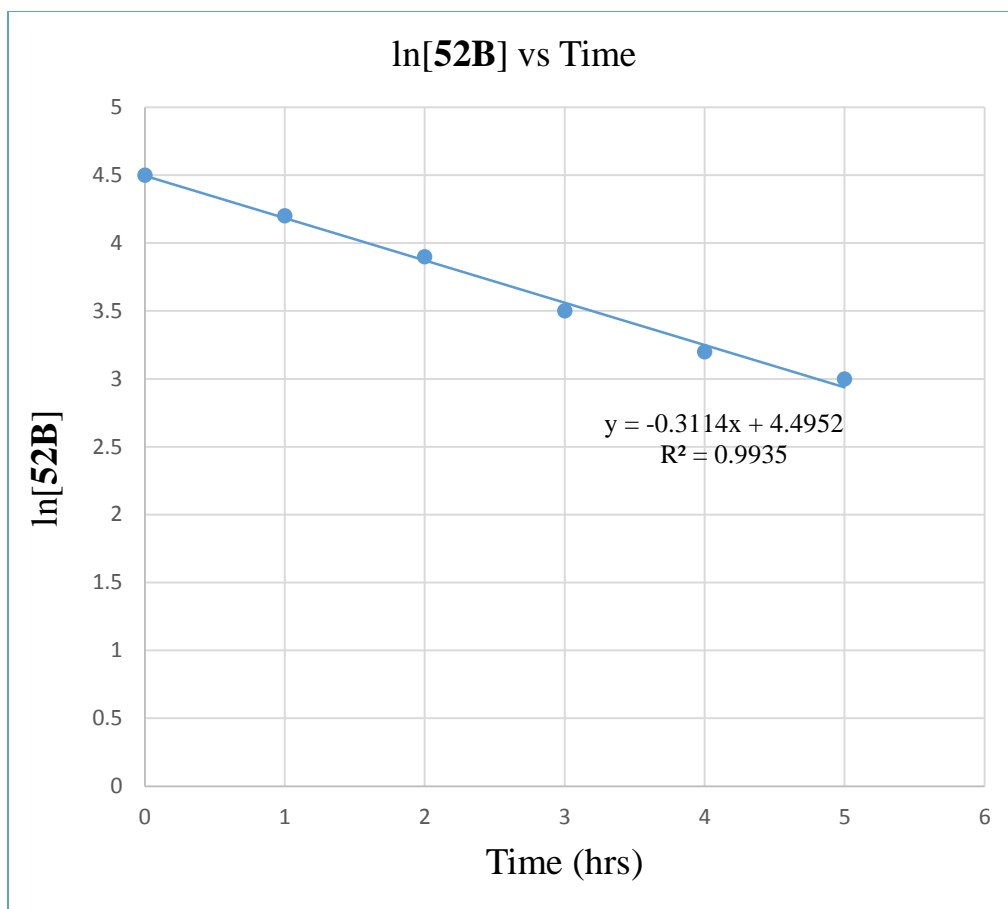


Figure 37. Graph of ln[isomer **52B**] against time.

In order to calculate the activation energy (E_a) for this isomerization, we carried out the same process at a different temperature ($T_2 = 60\text{ }^\circ\text{C}$) and obtained the rate constant ($k_2 = 2.75 \times 10^{-5}\text{ s}^{-1}$) at this temperature. Then, using equation 3.3–3.5 we found the activation energy for this process to be 119 kJ/mol or 28.4 kcal/mol.

$$k = Ae^{-\frac{E_a}{RT}} \quad 3.3$$

k = rate constant

A = frequency factor

E_a = Activation energy

R = Gas constant

T = Temperature

After rearranging equation 3.3, equations 3.4 and 3.5 were obtained from which E_a was calculated.

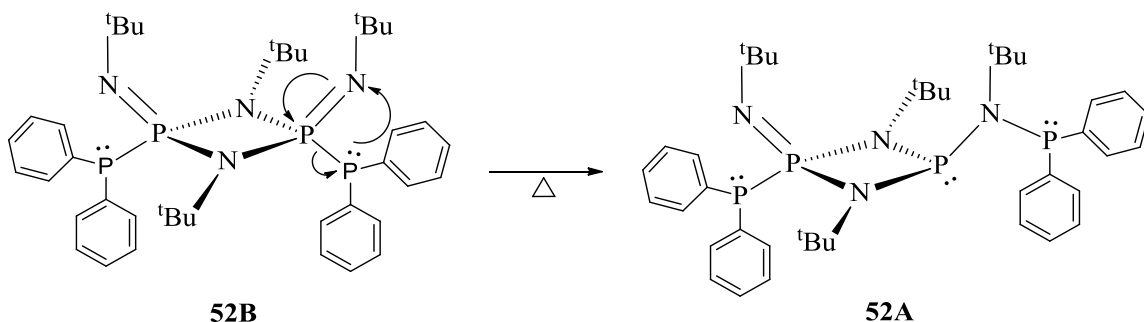
$$\ln\left(\frac{k_1}{k_2}\right) = \frac{E_a}{R} \left(\frac{1}{T_2} - \frac{1}{T_1}\right) \quad 3.4$$

$$E_a = \frac{R \ln\left(\frac{k_2}{k_1}\right)}{\left(\frac{1}{T_2} - \frac{1}{T_1}\right)} \quad 3.5$$

In comparison, Holm and co-workers¹³⁸ studied the kinetics of intramolecular isomerization of tris(5-methylhexane-2,4-dionato)cobalt(III) from the *cis*- to the *trans* isomer and vice versa at 90 °C. They found the rate constant and activation energy for *cis* to *trans* isomerization to be $5.73 \times 10^{-5} \text{ s}^{-1}$ and 32.9 kcal/mol, respectively. While the rate constant and activation energy for the *trans* to *cis* isomerization was $2.75 \times 10^{-5} \text{ s}^{-1}$ and 32.9 kcal/mol. Therefore, the intramolecular isomerization of **52B** to **52A** follows a similar first order kinetics with comparable rate constants to that observed by Holm's group. However, the activation energy of the intramolecular isomerization of **52B** to **52A**, 28.4 kcal/mol, is slightly lower than the values observed by Holm's group.

We believe the conversion from **52B** to **52A** takes place through intramolecular nucleophilic attack, in which the lone pair of electrons on the phosphorus atom of the diphenyl-phosphine attacks the imino nitrogen atom close to it, as shown in Scheme 20. This rearrangement takes place only on one side of the molecule while the other side of the molecule still retains its P–P coordination. This is because both diphenyl-phosphine and *tert*-butyl groups binding to each imino nitrogen atom on both sides of the molecule will possibly result in steric crowding. To the best of our knowledge, this is the first

observation of an intramolecular nucleophilic attack in a bis(amino)cyclodiphosphazane molecule.



Scheme 20. Isomerization of **52B** to **52A** via intramolecular nucleophilic attack.

Solid-state Structure of **52A**

X-ray quality crystals of **52A** were isolated from THF as tiny, colorless bars. The solid-state structure of **52A** with a partial atom numbering scheme is shown in Figure 38, while the crystal data and selected bond parameters are listed in Tables 9 and 10 respectively. Compound **52A** crystallizes in the triclinic space group $P\bar{1}$ (#2) with two molecules per unit cell. The compound is a non-symmetrical cyclodiphosphazane, having one diphenyl-phosphine substituent bonded to one of the phosphorus atom of the P_2N_2 , and the other diphenyl-phosphine group bonded to one of the exocyclic nitrogen atoms.

The endocyclic P–N bonds in **52A**, 1.7057(16) and 1.7426(7) Å, are similar to those in isomer **52B**, 1.7100(15) Å and those for $[(1,10\text{-phen})_2\text{Cu}_2\text{I}_2\{[{}^t\text{BuNP}(\text{NC}_4\text{H}_8\text{O})]_2\}]$ (1.6654(16) and 1.7265(15) Å),¹²⁶ but they are longer than those reported for $[(\text{Me}_3\text{Si})_2\text{NP}(\mu\text{-NSiMe}_3)]_2$ (1.640(7) and 1.699(7) Å),¹³⁹ and shorter than the exocyclic P–N bonds, P2–N4: 1.9286(7) Å and P4A–N4: 1.7641(18) Å. The shortness of the P1–N3 bond, 1.5217(7) Å is a reflection of π -bonding between the two atoms, while

the very long P2–N4 bond is due to the fact that N4 is sandwiched between P2 and P4 meaning the electron cloud around N4 is shared by more atoms than that around N3.

The P–P bond in **52A**, 2.2336(8) Å, is similar to that in isomer **52B** (2.2312(9) Å), and that in $\text{Me}_2\text{Si}(\mu\text{-N}^t\text{Bu})_2\text{P}(=\text{NPh})\text{PPh}_2$ (2.2092(7) Å),¹⁴⁰ $\{[(\text{Me}_3\text{Si})_2\text{N}]_2\text{Sn}(\text{Cl})\text{P}(\text{Ph})\}_2$ (2.2360(10) Å).¹⁴¹ It is also similar to the P–P bond lengths reported for the dications, $[\text{R}_3\text{P-PR}'\text{-PR}'\text{-PR}_3]^{2+}$ (2.2041(9) – 2.2583(10) Å), reported by Decken et al.,¹⁴² and the dianionic tetraphosphorus chains $[\text{CyP-CyP-PCy-PCy}]^{2-}$ and $[\text{PhP-PhP-PPh-PPh}]^{2-}$, (2.177(1) – 2.244(3) Å), reported by Grützmacher and co-workers.^{143, 144} Although the P₂N₂ ring in isomer **52B** is planar (angle sum = 359.9°), that in **52A** is slightly puckered (angle sum = 356.6°).

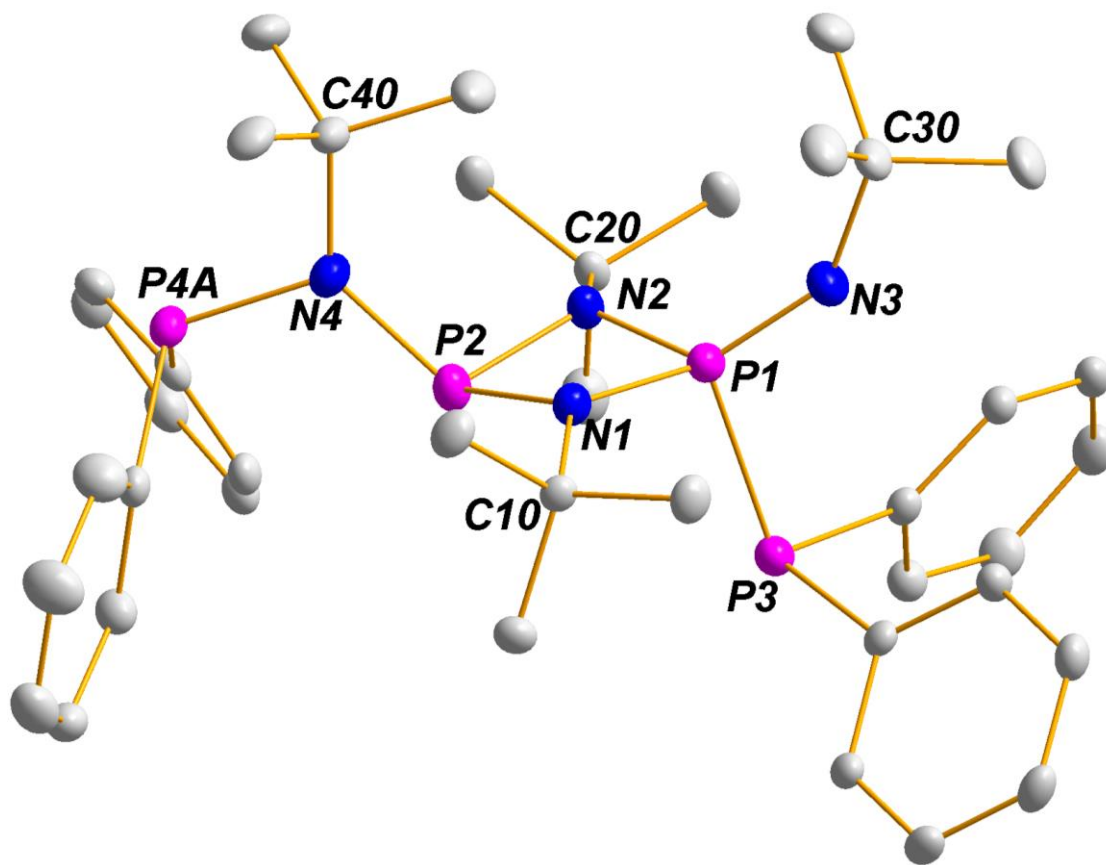


Figure 38. Solid-state structure and partial labelling scheme of **52A**. With the exception of carbon (35 %) all atoms are drawn at the 50 % probability level.

Table 9. Crystal and structure refinement data for compound **52A**.

Chemical Formula	C ₄₀ H ₅₆ N ₄ P ₄
fw	716.77
T/K	100.04
$\lambda/\text{\AA}$	0.71073
Crystal system	Triclinic
Space group	<i>P</i> -1 (#2)
<i>a</i> /\AA	9.6038(3)
<i>b</i> /\AA	13.3765(3)
<i>c</i> /\AA	16.9285(4)
$\alpha/^\circ$	97.9385(14)
$\beta/^\circ$	92.7290(15)
$\gamma/^\circ$	102.0334(15)
<i>V</i> /\AA ³	2099.99(10)
<i>Z</i>	2
$\rho(\text{calc}) \text{ g cm}^{-3}$	1.200
μ/mm^{-1}	0.215
F(000)	811.1
Completeness (%)	99.97
Reflections collected	35472
Independent reflections	9670 [<i>R</i> _{int} = 0.0480]
<i>R</i> _w (<i>F</i> ²) ^b [<i>I</i> > 2 σ (<i>I</i>)]	<i>R</i> ₁ = 0.0498, w <i>R</i> ₂ = 0.1125
<i>R</i> (<i>F</i>) ^a (all data)	<i>R</i> ₁ = 0.0685, w <i>R</i> ₂ = 0.1287

^a $R = \sum |F_o - F_c| / \sum |F_o|$. ^b $R_w = \{ [\sum w(F_o^2 - F_c^2)] / [\sum w(F_o^2)^2] \}^{1/2}$; $w = 1 / [\sigma^2(F_o)^2 + (xP)^2 + yP]$, where $P = (F_o^2 + 2F_c^2) / 3$.

Table 10. Selected bond lengths (Å) and angles (°) for **52A**.

Bond Lengths			
P1–P3	2.2336(8)	P4A–N4	1.7641(18)
P1–N1	1.7062(18)	P3–C50	1.847(2)
P1–N2	1.7052(17)	P4A–C70	1.841(2)
P1–N3	1.5217(18)	N1–C10	1.493 (3)
P2–N1	1.7402(17)	N2–C20	1.497(23)
P2–N2	1.7451(17)	N3–C30	1.464(3)
P2–N4	1.9286(7)	N4–C40	1.531(3)
Bond Angles			
N1–P1–P3	105.58(6)	C50–P3–P1	104.04(7)
N2–P1–P3	103.59(7)	C60–P3–C50	99.05(9)
N2–P1–N1	82.70(8)	C70–P4A–N4	108.16(9)
N3–P1–P3	108.68(8)	C80–P4A–C70	108.16(9)
N3–P1–N1	125.92(10)	C10–N1–P1	131.78(14)
N3–P1–N2	126.30(9)	P2–N2–P1	96.56(9)
N2–P2–N1	80.58(8)	C20–N2–P1	130.85(14)
N4–P2–N1	112.72(9)	C30–N3–P1	144.68(16)
N2–P2–N2	111.19(9)	C40–N4–P2	133.62(15)

Solid-state Structure of **52B**

Crystals of **52B** were isolated from toluene as colorless, rhombic blocks. The solid-state structure of **52B** with a partial atom numbering scheme is shown in Figure 39, while the crystal data and selected bond parameters are listed in Tables 11 and 12 respectively. Unlike **52A**, compound **52B** crystallizes in the monoclinic space group $C2/c$ with four molecules per unit cell. The compound possesses a crystallographic C_2 symmetry that lies on the two-fold axis. Each phosphorus atom in the P_2N_2 has a distorted tetrahedral geometry and bears a diphenyl-phosphine substituent. It is surprising that the phosphorus atoms of the PPh_2 moiety are highly pyramidalized with bond angles, which range from 99.89(8) to 105.38(6) Å, compared to angles in PPh_3 , 101.82(14) to 102.57(14).¹⁴⁵ Each exocyclic nitrogen atom has a geometry that is mid-way between linear and bent (angle = 143.7°) and bears a *tert*-butyl group that lies above and almost perpendicular to the plane of the P_2N_2 .

The endocyclic P–N bonds in **52B**, 1.7100(15) are similar to those in isomer **52A**, but longer than the exocyclic P–N bonds, 1.522(4) (See discussion above). As mentioned earlier, the short exocyclic P–N bonds are a reflection of the P=N double bond. The two identical P–P bonds in **52B**, 2.2312(9) Å, are similar in length to the P–P bond in the dianion of 2,6-bis(trimethylsilyl)-3,5-dimethylphosphinine, 2.286(2) Å,¹⁴⁶ $Me_2Si(\mu-N^tBu)_2P(=NPh)PPh_2$ (2.2092(7) Å),¹⁴⁰ and that in bis(cyclenphosphorane), 2.264(2) Å, and $Mn_2-(CO)_8[P_2(t-BuN)_2P_2(t-BuN)_2]$, 2.234(2) Å, reported by the groups of Holmes,¹⁴⁷ and Paine,¹⁴⁸ respectively. However, the P–P bond in both compounds **52A** and **52B**, is longer than the P–P single bond of 2.194 Å in P_4 ,^{149, 150} and the P–P bonds in $[1,2,4-(^tBu_3C_5H_2Co)_2P_4Sm(C_5Me_4R)_2]$ (2.149(1)–2.150(2) Å), reported by Roesky and

co-workers.¹⁵¹ The P₂N₂ ring in **52B** is perfectly planar with angle sum = 359.9°.

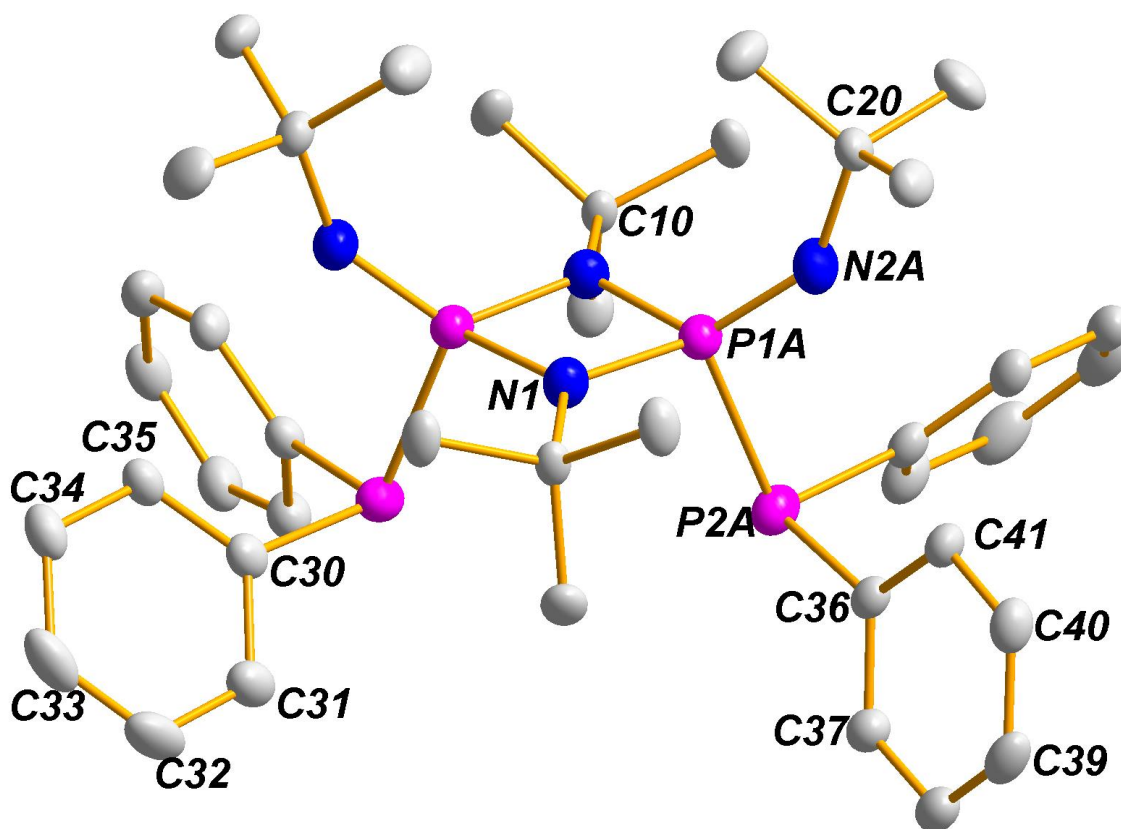


Figure 39. Solid-state structure and partial labelling scheme of **52B**. With the exception of carbon (35 %) all atoms are drawn at the 50 % probability level.

Table 11. Crystal and structure refinement data for compound **52B**.

Chemical Formula	C ₄₀ H ₅₆ N ₄ P ₄
fw	716.77
T/K	173(2)
$\lambda/\text{\AA}$	0.71073
Crystal system	Monoclinic
Space group	C2/c
$a/\text{\AA}$	16.9400(3)
$b/\text{\AA}$	9.8845(2)
$c/\text{\AA}$	24.8587(5)
$\alpha/^\circ$	90
$\beta/^\circ$	105.2670(10)
$\gamma/^\circ$	90
$V/\text{\AA}^3$	4015.53(13)
Z	4
$\rho(\text{calc}) \text{ g cm}^{-3}$	1.186
μ/mm^{-1}	0.220
F(000)	1536
Completeness (%)	100
Reflections collected	57946
Independent reflections	5853 [R _{int} = 0.0321]
$R_w(F^2)^b$ [I>2 σ (I)]	R ₁ = 0.0522, wR ₂ = 0.1594
$R(F)^a$ (all data)	R ₁ = 0.0551, wR ₂ = 0.1650

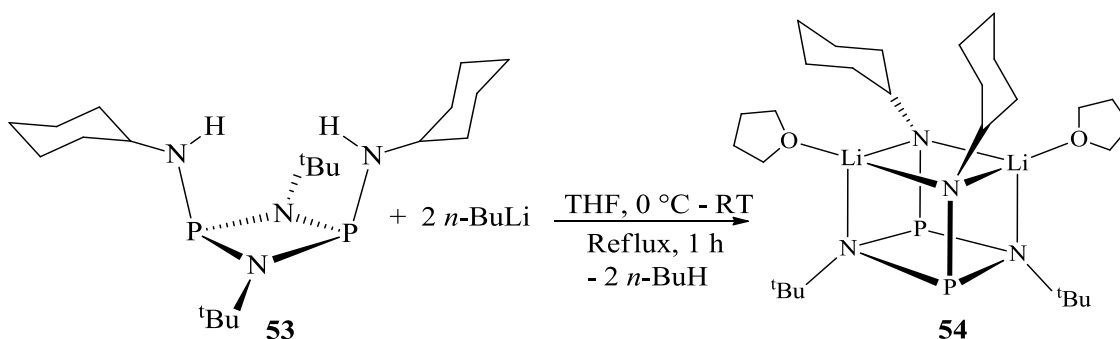
^a $R = \sum |F_o - F_c| / \sum |F_o|$. ^b $R_w = \{ [\sum w(F_o^2 - F_c^2)] / [\sum w(F_o^2)^2] \}^{1/2}$; $w = 1 / [\sigma^2(F_o)^2 + (xP)^2 + yP]$, where $P = (F_o^2 + 2F_c^2) / 3$.

Table 12. Selected bond lengths (Å) and angles (°) for **52B**.

Bond Lengths			
P1A–P2A	2.2312(9)	P2A–C36	1.8457(17)
P1A–N1	1.7100(15)	N1–P1A#	1.7109(15)
P1A–N1#	1.7109(15)	N1–C10	1.4859(19)
P1A–N2A	1.522(4)	N2A–C20	1.443(4)
P2A–C30	1.8478(19)	N1–P1B	1.781(8)
Bond Angles			
N1–P1A–P2A	105.21(6)	P1A–N1–P1A#	97.66(7)
N1#–P1A–P2A	107.28(6)	P1A–N1–P1B#	96.7(3)
N1–P1A–N1#	82.27(7)	P1A#–N1–P1B	96.9(3)
N2A–P1A–P2A	107.92(11)	P1B#–N1–P1B	91.8(4)
N2A–P1A–N1#	124.91(14)	C10–N1–P1A#	130.61(11)
N2A–P1A–N1	125.89(15)	C20–N2B–P2B	116.3(2)
C30–P2A–P1A	102.91(6)	C20–N2B–P1B	133.6(13)
C36–P2A–P1A	105.38(6)	P2B–N2B–P1B	110.6(16)
C36–P2A–C30	99.89(8)	C20–N2A–P1A	143.7(2)

Synthesis and Spectroscopic Analysis of *cis*-[(^tBuNP)₂(CyNLi·thf)₂], **54**

Compound **54** was synthesized by the lithiation of *cis*-[(^tBuNP)₂(CyNH)₂], **53** with two equivalents of a 2.5 M *n*-butyllithium solution (Scheme 21). The lithiation was complete after 1 h of refluxing and the dilithio salt **54** was isolated as large, colorless rhombic crystals in spectroscopically and analytically pure form in 77 % yield. We synthesized compound **54** to ascertain if the less-bulky cyclohexyl substituents (as compared to *tert*-butyl groups in **46**) on the amido nitrogen atoms will affect the reactivity with electrophiles.



Scheme 21. Synthesis of **54**.

Due to the presence of the cyclohexyl substituents on the amido nitrogen atoms, the ¹H and ¹³C NMR spectra of **54** are somewhat complex. The ¹H NMR spectrum of **54**, shown in Figure 40, exhibits eight signals, all of which are in the aliphatic region as expected. The OCH₂ and CH₂ protons of THF resonate at 3.58 and 1.39 ppm, respectively. The cyclohexyl protons are observed as multiplets in the range of 1.94–1.12 ppm, while the *tert*-butylimido protons resonate as a singlet at 1.55 ppm.

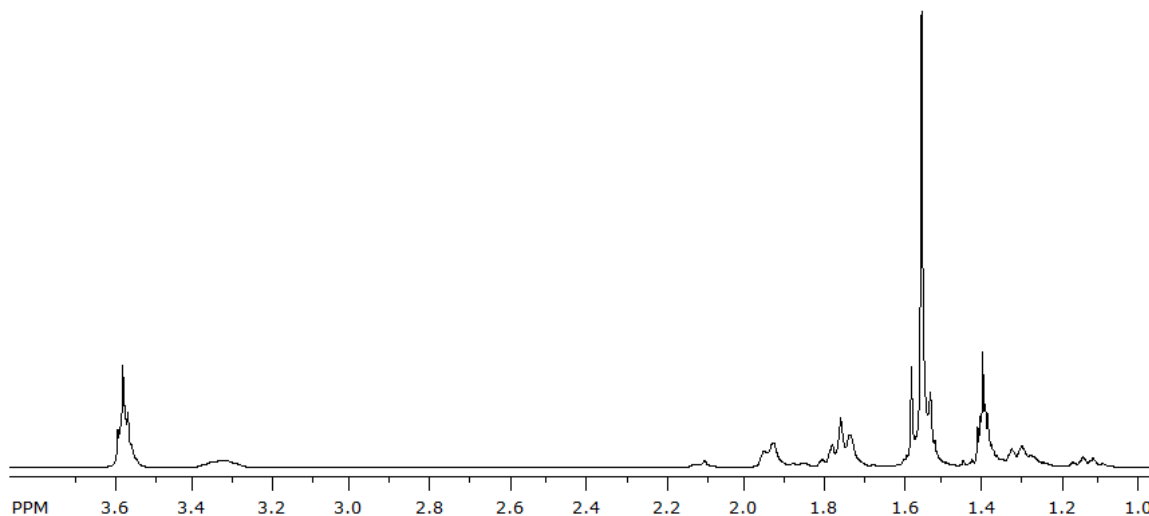


Figure 40. ^1H NMR Spectrum of **54**.

The $^{13}\text{C}\{^1\text{H}\}$ NMR spectrum of **54** (Figure 41) shows eight signals. The OCH_2 and CH_2 carbons of THF resonate at 67.94 and 25.68 ppm, respectively. The quaternary and primary *tert*-butylimido carbons are observed as triplets at 54.98 and 30.02 ppm, respectively. The signals are split into triplets because of phosphorus coupling. The tertiary cyclohexyl carbons attached to the amino nitrogen atoms are observed as a broad singlet at 41.36 ppm. The remaining cyclohexyl carbons are observed between 30.56 and 26.03 ppm. As expected, the ^{31}P NMR spectrum of **54** (Figure 42) shows just one singlet at 130.8 ppm, which is within the range of P(III) centers.

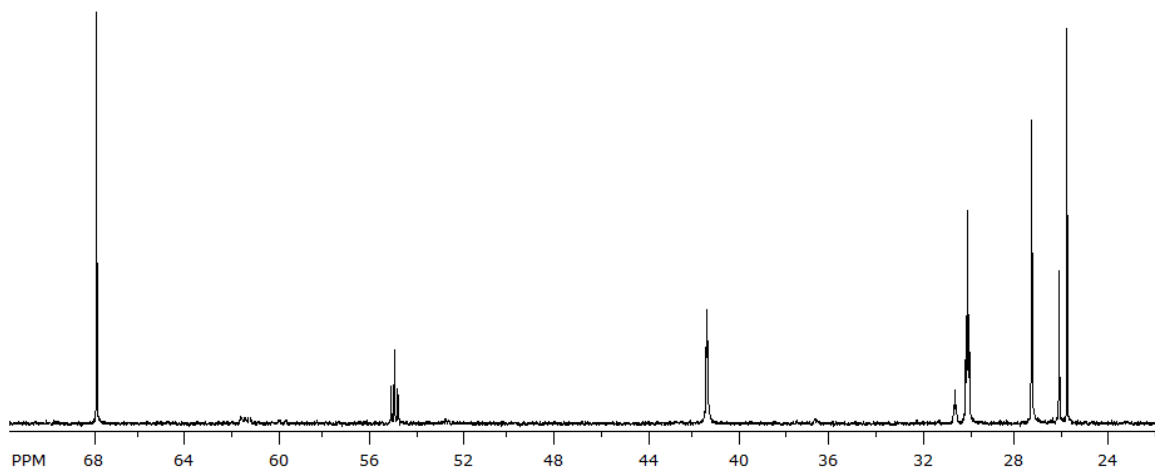


Figure 41. The $^{13}\text{C}\{^1\text{H}\}$ NMR Spectrum of **54**.

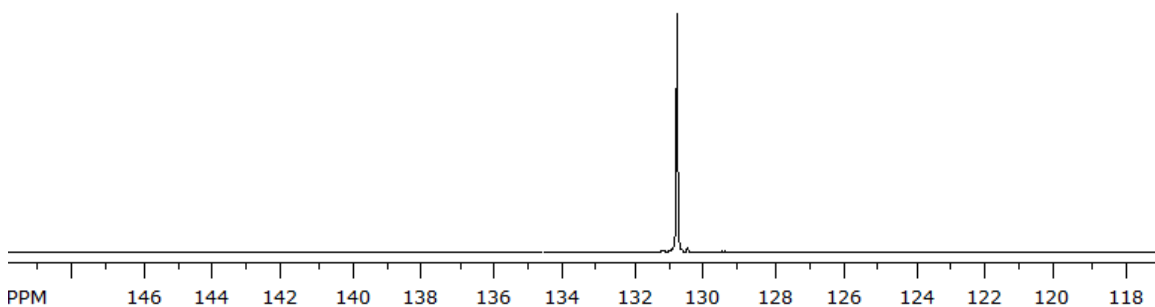


Figure 42. The $^{31}\text{P}\{^1\text{H}\}$ NMR spectrum of **54**.

Solid-state Structure of *cis*-[$(^t\text{BuNP})_2(\text{CyNLi}\cdot\text{THF})_2$], **54**

Suitable crystals of **54** for X-ray crystallography were isolated from a concentrated THF solution as large, colorless, rhombic crystals. The solid-state structure of **54** with a partial atom numbering scheme is shown in Figure 43, while the crystal data and selected bond parameters of **54** are listed in Tables 13 and 14, respectively. The compound crystallizes in the monoclinic space group $P2_1/c$ (#14) with four molecules per unit cell. The crystal structure of **54** shows it is an inorganic heterocube bearing an approximate C_{2v} symmetry. It is made up of alternating nitrogen, phosphorus, and lithium

atoms that are surrounded by a shell of organic groups. All atoms within the cube, except the phosphorus atoms, are four-coordinate, and these atoms achieve an electron octet through formation of covalent bonds, donor bonds, or lone pairs. The endocyclic P–N bonds of **54** are longer, 1.7785(9) and 1.7651(9) Å, than the exocyclic P–N bonds, 1.6533(9) and 1.6518(9) Å. Although the exocyclic bonds in **54** are similar to those in the starting ligand **53**, the endocyclic bonds are slightly longer. This is likely due to steric congestion associated with the incorporation of Li–THF moieties. This is not unusual in lithiated cyclodiphosphazanes because similar observations have been reported before.³⁷ As in the starting ligand **53**, both cyclohexyl groups in **54** adopt a chair conformation and lie above the (P–N)₂ ring in exo orientations.

There are four Li–N bonds with bond lengths ranging from 2.077(2) to 2.125(2) Å, that form the (Li–N)₂ ring. These bond lengths are similar to those in LiN(SiMe₃)₂ (2.00(1) Å),¹⁵² {Li[N(SiMe₃)₂](OEt₂)₂} (2.06(1) Å),¹⁵³ and related lithium amides.^{154, 155} While the (P–N)₂ ring is perfectly planar, angle sum = 359.7°, the (Li–N)₂ ring is highly puckered with angle sum of 351.4°. This highly puckered (Li–N)₂, which is caused by the presence of the large lithium atoms, makes the heterocube distorted. This heterocube distortion has been observed in similar bis(THF) dilithio salts by Stahl *et al.*,^{33, 37, 137} and Chivers *et al.*¹⁵⁶

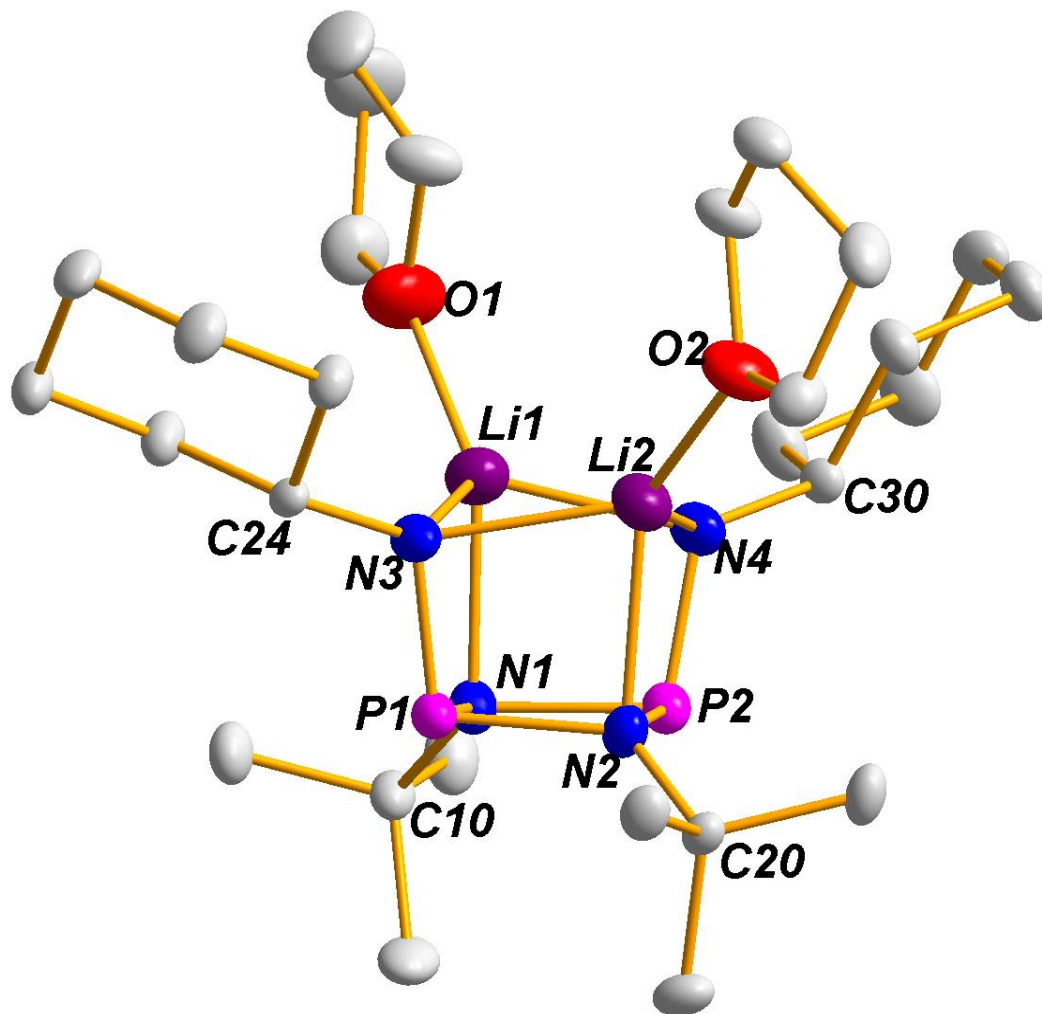


Figure 43. Solid-state structure and partial labelling scheme of **54**. With the exception of carbon (35 %) all atoms are drawn at the 50 % probability level.

Table 13. Crystal and structure refinement data for compound **54**.

Chemical Formula	C ₂₈ H ₅₆ Li ₂ N ₄ O ₂ P ₂
fw	556.60
T/K	173(2)
$\lambda/\text{\AA}$	0.71073
Crystal system	Monoclinic
Space group	<i>P</i> 2 ₁ / <i>c</i> (#14)
<i>a</i> /\AA	18.8882(6)
<i>b</i> /\AA	10.0899(3)
<i>c</i> /\AA	19.7056(6)
$\alpha/^\circ$	90
$\beta/^\circ$	118.0191(9)
$\gamma/^\circ$	90
<i>V</i> /\AA ³	3315.32(18)
<i>Z</i>	4
$\rho(\text{calc}) \text{ g cm}^{-3}$	1.099
μ/mm^{-1}	0.180
F(000)	1536
Completeness (%)	99.30
Reflections collected	62162
Independent reflections	11816 [<i>R</i> _{int} = 0.0293]
$R_w(F^2)^b$ [<i>I</i> > 2 σ (<i>I</i>)]	<i>R</i> ₁ = 0.0378, <i>wR</i> ₂ = 0.0958
$R(F)^a$ (all data)	<i>R</i> ₁ = 0.0508, <i>wR</i> ₂ = 0.1049

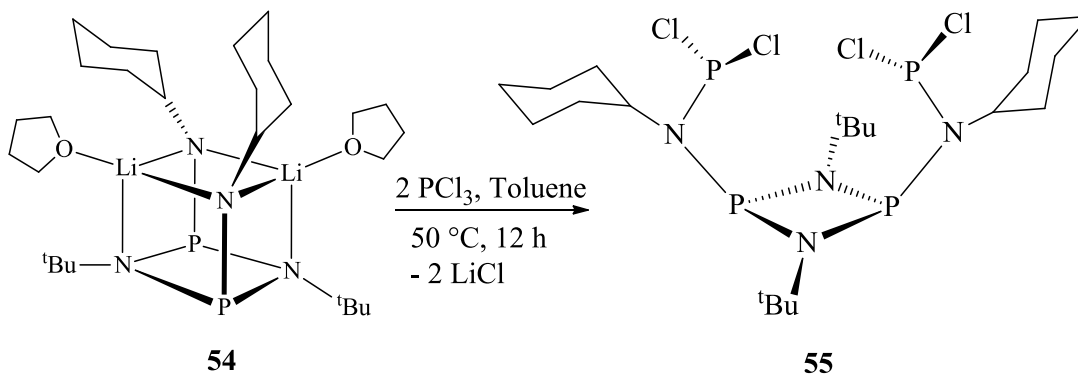
^a $R = \sum |F_o - F_c| / \sum |F_o|$. ^b $R_w = \{ [\sum w(F_o^2 - F_c^2)] / [\sum w(F_o^2)^2] \}^{1/2}$; $w = 1 / [\sigma^2(F_o)^2 + (xP)^2 + yP]$, where $P = (F_o^2 + 2F_c^2) / 3$.

Table 14. Selected bond lengths (Å) and angles (°) for **54**.

Bond Lengths			
P1–N1	1.7785(9)	Li1–N1	2.097(2)
P1–N2	1.7651(9)	Li1–N3	2.125(2)
P1–N3	1.6533(9)	Li1–N4	2.077(2)
P2–N1	1.7780(9)	Li2–O2	1.939(2)
P2–N2	1.7675(9)	Li2–N2	2.101(2)
P2–N4	1.6518(9)	Li2–N3	2.100(2)
Li1–O1	1.926(2)	Li2–N4	2.086(2)
Bond Angles			
N2–P1–N1	82.20(4)	Li1–N3–P1	92.41(7)
N3–P1–N1	100.18(4)	Li2–N3–P1	93.17(7)
N3–P1–N2	99.59(4)	Li2–N3–Li1	73.61(8)
N2–P2–N1	82.15(4)	Li1–N4–P2	93.22(7)
N4–P2–N1	99.68(4)	Li2–N4–P2	93.41(7)
N4–P2–N2	99.52(4)	Li2–N4–Li1	74.90(8)
P2–N1–P1	97.21(4)	N4–Li1–N3	101.14(9)
Li1–N1–P1	89.87(7)	N4–Li1–N1	77.85(8)
Li1–N1–P2	88.98(7)	N3–Li1–N1	77.18(8)
P2–N2–P1	98.10(4)	N4–Li2–N2	77.18(7)
Li2–N2–P1	89.97(6)	N4–Li2–N3	101.79(9)
Li2–N2–P2	89.63(6)	N3–Li2–N2	76.90(7)

Synthesis and Spectroscopic Analysis of *cis*-{[P(μ -N^tBu)]₂(CyNPCL₂)₂}, **55**

Treatment of compound **54** with PCl₃ in toluene at 50 °C gave bis(dichlorophosphino)-bis(cyclohexylamido)cyclodiphosphazane **55** (Scheme 22). The reaction was complete after 12 h and compound **55** was isolated in 75 % yield.



Scheme 22. Synthesis of **55**.

As mentioned earlier, the presence of the cyclohexyl substituents on the amido nitrogen atoms of **55** makes its ¹H and ¹³C NMR spectra slightly complex and similar to the spectra of the lithiated ligand **54**. The ¹H NMR spectrum of **55** shown in Figure 44 depicts six signals, all of which appear in the aliphatic region as expected. The *tert*-butylimino protons appear as a singlet at 1.36 ppm. The cyclohexyl protons are observed as multiplets in the range of 1.95–0.95 ppm.

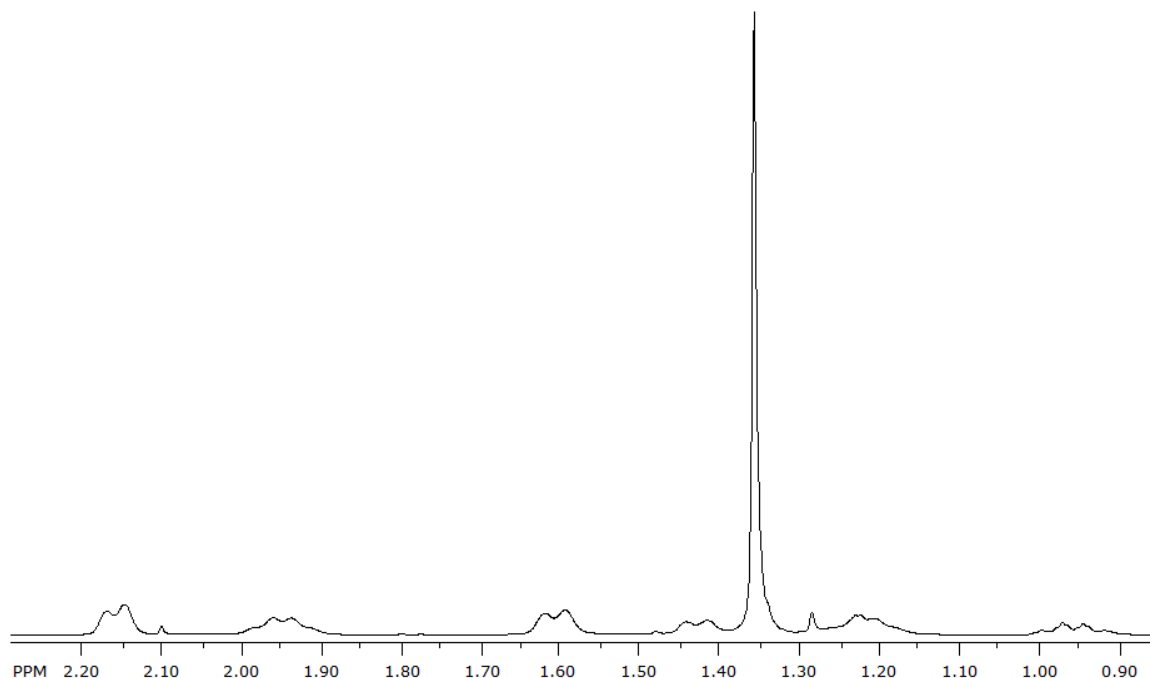


Figure 44. ^1H NMR Spectrum of **55**.

The $^{13}\text{C}\{^1\text{H}\}$ NMR spectrum of **55** (Figure 45) shows six signals. The quaternary and primary *tert*-butylimino carbons are observed as triplets at 54.68 and 31.80 ppm, respectively. The signals are split into triplets because of coupling with the two phosphorus atoms in the P_2N_2 ring. The tertiary cyclohexyl carbons attached to the amino nitrogen atoms are observed as a broad singlet at 61.56 ppm. The remaining cyclohexyl carbons are observed as singlets between 36.46 and 25.91 ppm. The ^{31}P NMR spectrum of **55** (Figure 46) shows two broad singlets at 172.6 and 112.2 ppm, which represents the phosphorus bearing the chlorine atoms and the phosphorus atoms in the P_2N_2 ring, respectively. Both signals are within the range of P(III) derivatives.

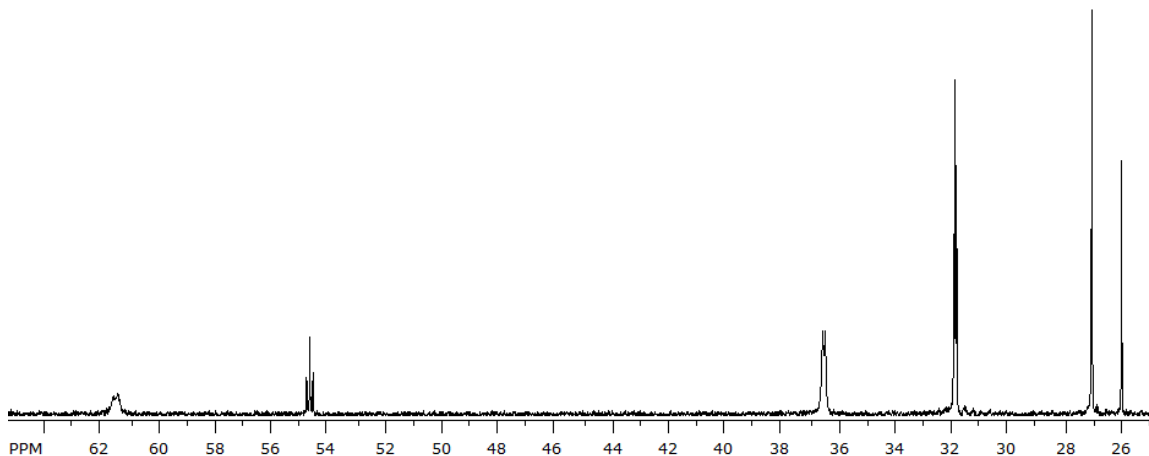


Figure 45. $^{13}\text{C}\{^1\text{H}\}$ NMR Spectrum of **55**.

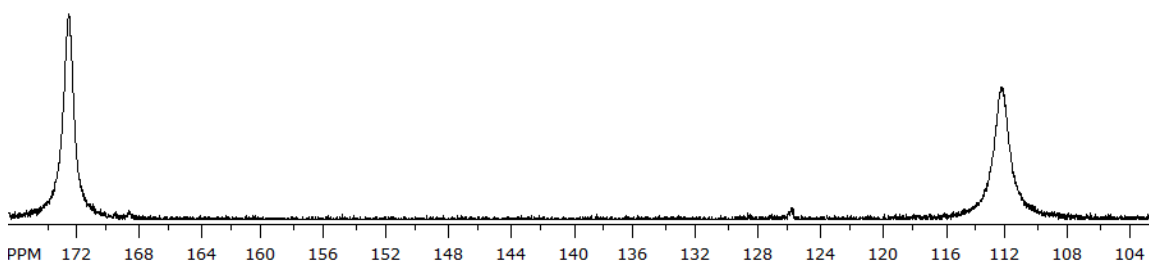


Figure 46. $^{31}\text{P}\{^1\text{H}\}$ NMR Spectrum of **55**.

Solid-state Structure of *cis*- $\{[\text{P}(\mu\text{-N}^t\text{Bu})]_2(\text{CyN}(\text{P}(\text{Cl})_2)_2)\}_2$, **55**

Single crystals of **55** for X-ray studies were isolated as colorless, bar-shaped crystals from a concentrated solution of toluene. The solid-state structure of **55** with a partial atom numbering scheme is shown in Figure 47, while the crystal data and selected bond parameters are listed in Tables 15 and 16, respectively. The compound crystallizes in the monoclinic space group $C2/c$ with 8 molecules per unit cell. There are four equivalent $\text{P-N}_{\text{imino}}$ and two $\text{P-N}_{\text{amino}}$ bonds in **55**. Unlike in compound **54**, the $\text{P-N}_{\text{imino}}$ bonds (1.7160(5) Å) in **55** are slightly shorter than the $\text{P-N}_{\text{amino}}$ bonds (1.7474(6) Å). As explained above, there is more steric crowding in **54** that results in the lengthening of the

P–N_{imino} bonds. However, the P–N bonds in both **54** and **55** are shorter than P–N single bonds, 1.79 Å.¹ Both amino nitrogen atoms in **55** are planar (angle sum = 359.8°). The shortness of the P–N bonds with the planarity of the exocyclic N atoms, may be indicative of partial double bond character. This partial double-bond character is also reflected in the fact that the P–N bonds in N–P–Cl (1.6653(6) Å) are significantly shorter than other P–N bonds in the molecule, and are similar to those observed for compound **57** (1.6643(8) Å) below.

The P–Cl bonds in **55** (2.0086(2) Å) are similar those in its silicon analogue **57**, however, they are shorter than those in structurally related heterocycles *cis*-1,3-di-*tert*-butyl-2,4-dichlorocyclodiphosphazane (2.105(9) Å),¹⁵⁷ and {[(^tBuNP)₂(^tBuN)₂]PCl} (2.244(3) Å).³⁵ Compared to the planar Si₂N₂ ring (angle sum = 359.2°) in compound **57**, the P₂N₂ ring in **55** is slightly puckered with angle sum = 356.2°. The ring puckering in **55** is due to the smaller phosphorus atom causing more angle strain than silicon. The cyclohexyl substituents in compound **55** are parallel to the P₂N₂ and they reside in the chair conformation.

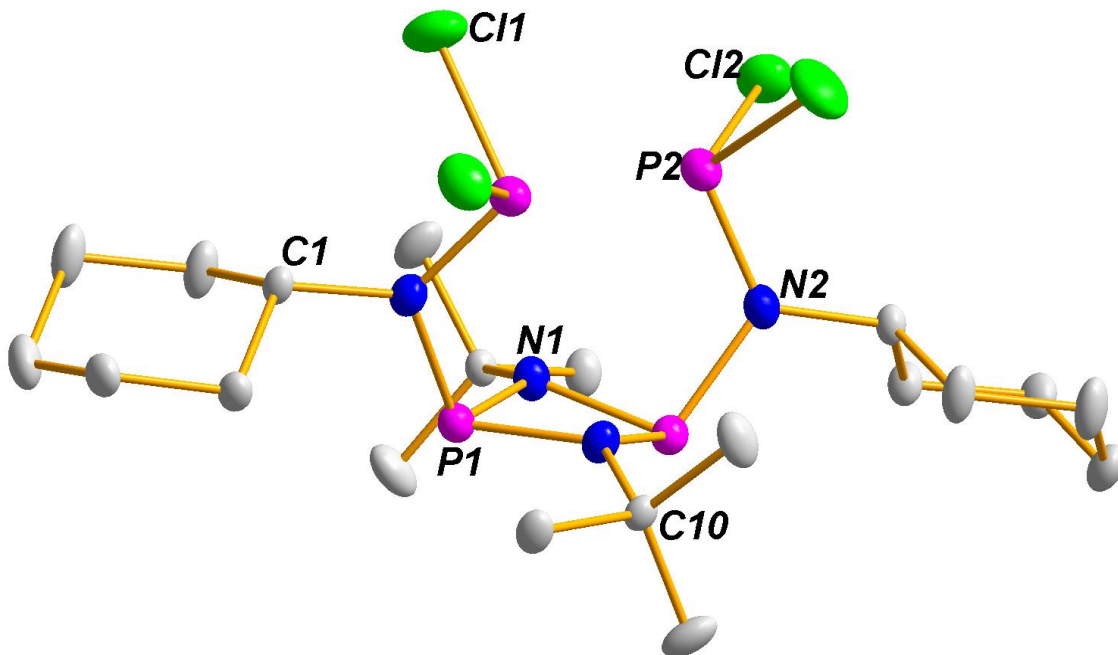


Figure 47. Solid-state structure and partial labelling scheme of **55** With the exception of carbon (35 %) all atoms are drawn at the 50 % probability level.

Table 15. Crystal and structure refinement data for compound **55**.

Chemical Formula	C ₂₀ H ₄₀ Cl ₄ N ₄ P ₄
fw	602.27
T/K	173(2)
$\lambda/\text{\AA}$	0.71073
Crystal system	Monoclinic
Space group	<i>C2/c</i>
$a/\text{\AA}$	14.4427(5)
$b/\text{\AA}$	12.4838(4)
$c/\text{\AA}$	16.5416(5)
$\alpha/^\circ$	90
$\beta/^\circ$	98.8660(10)
$\gamma/^\circ$	90
$V/\text{\AA}^3$	2946.81(17)
<i>Z</i>	8
$\rho(\text{calc}) \text{ g cm}^{-3}$	1.357
μ/mm^{-1}	0.636
F(000)	1264
Completeness (%)	99.6
Reflections collected	34066
Independent reflections	9328 [<i>R</i> _{int} = 0.0259]
$R_w(F^2)^b$ [<i>I</i> > 2 σ (<i>I</i>)]	<i>R</i> ₁ = 0.0275, <i>wR</i> ₂ = 0.0748
$R(F)^a$ (all data)	<i>R</i> ₁ = 0.0339, <i>wR</i> ₂ = 0.0797

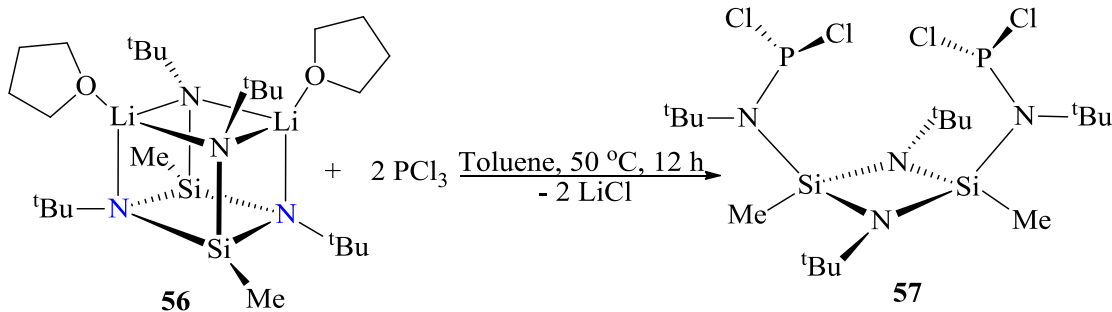
^a $R = \sum |F_o - F_c| / \sum |F_o|$. ^b $R_w = \{ [\sum w(F_o^2 - F_c^2)] / [\sum w(F_o^2)] \}^{1/2}$; $w = 1 / [\sigma^2(F_o)^2 + (xP)^2 + yP]$, where $P = (F_o^2 + 2F_c^2) / 3$.

Table 16. Selected bond lengths (Å) and angles (°) for compound **55**.

Bond Lengths			
P1–N1	1.7160(5)	N1–P1#	1.7337(5)
P1–N1#	1.7337(5)	N2–C1	1.4991(8)
P1–N2	1.7474(6)	N1–C10	1.4896(7)
P2–N2	1.6653(6)	P2–Cl2	2.1021(2)
P2–Cl1	2.0886(2)	C10–C11	1.5281(9)
Bond Angles			
N1–P1–N2	102.68(3)	N2–P2–Cl2	101.95(2)
N1#–P1–N2	110.03(3)	N2–P2–Cl1	101.72(2)
N1–P1–N1#	81.17(3)	P2–N2–P1	119.34(3)
Cl1–P2–Cl2	96.538(11)	C1–N2–P1	118.09(4)
P1–N1–P1#	96.99(3)	C1–N2–P2	122.33(4)
C10–N1–P1	127.04(4)	C10–N1–P1#	127.11(4)

Synthesis and Spectroscopic Analysis of *cis*-[(MeSi^tBu)₂(N^tBuPCl₂)₂], **57**

Treatment of the lithium salt of bis(*tert*-butylamido)cyclodisilazane, **56** with PCl₃ in toluene (Scheme 18) overnight yielded the bis(dichlorophosphino)-di-*tert*-butylamidocyclodisilazane **57**, which was isolated as colorless, block-shaped crystals. Although **56** is isoelectronic with **48**, we observed that the reaction of **56** with PCl₃ yielded a tetrachlorodiphosphinocyclodisilazane **57**, different from the monochloromonophosphino compound **49** observed by Stahl *et al.*³⁵ We think that the slightly larger size of Si compared to P may have played a role in creating more space above the Si₂N₂ that allowed the incorporation of the second P–Cl moiety.



Scheme 23. Synthesis of **57**.

The proton NMR spectrum of **57** (Figure 48) features three distinct singlets. The singlets at 1.57 and 1.30 ppm are assigned to the two different *tert*-butyl protons and the singlet at 0.61 ppm is due to the methyl protons.

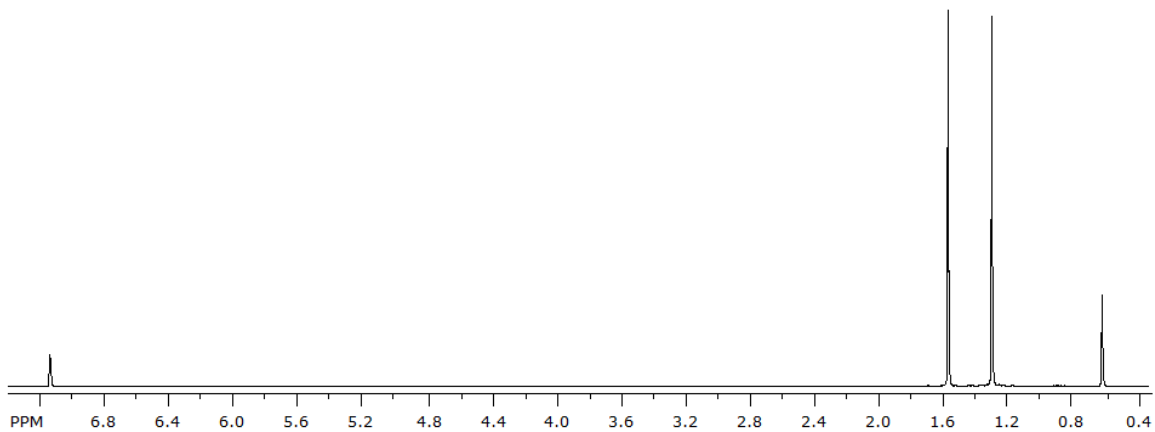


Figure 48. ^1H NMR Spectrum of **57**.

As expected, the $^{13}\text{C}\{^1\text{H}\}$ NMR spectrum of **57** (Figure 49) shows four singlets representing the four different types of carbon atoms, while the $^{31}\text{P}\{^1\text{H}\}$ NMR (Figure 50) of **57** depicts just one singlet at 167.1 ppm. The presence of the electron withdrawing chlorine atoms on the P(III) centers clearly shifts this value downfield.

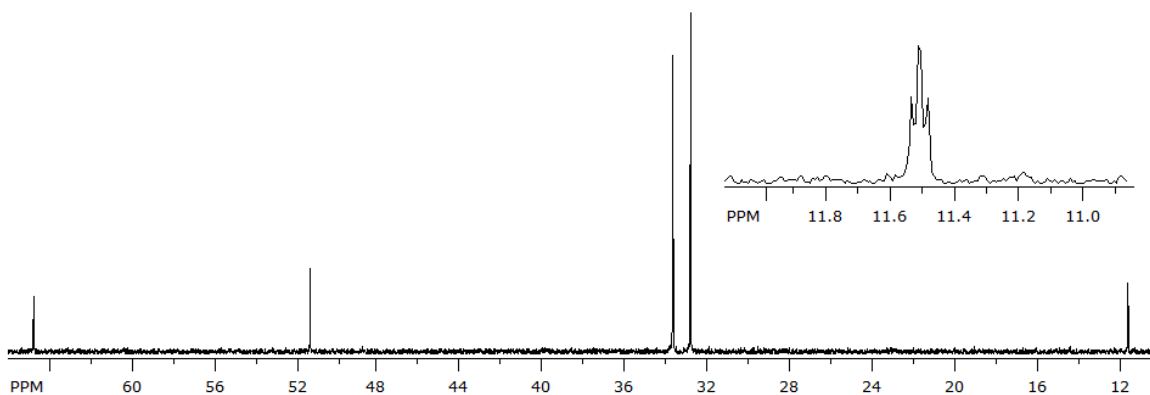


Figure 49. $^{13}\text{C}\{^1\text{H}\}$ NMR Spectrum of **57**.

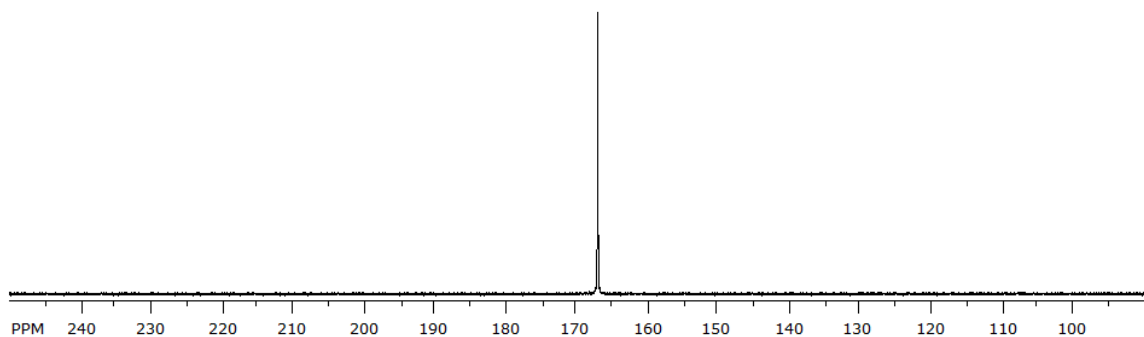


Figure 50. $^{31}\text{P}\{^1\text{H}\}$ NMR Spectrum of **57**.

Solid-state Structure of *cis*-[(MeSiN^tBu)₂(N^tBuPCl₂)₂], **57**

Compound **57** was isolated as colorless, block-shaped crystals from a concentrated toluene solution. The solid-state structure of **57** with a partial atom numbering scheme is shown in Figure 51, while the crystal data and selected bond parameters are listed in Tables 17 and 18, respectively. The compound crystallizes in the monoclinic space group $P2_1/c$ (#14) with four molecules per unit cell. With the exception of the bond to the silicon atoms, all structural parameters of **57** are similar to those of **55**.

The Si–N bonds in **57** range from 1.7324(9) to 1.7984(10) Å, and they are similar to those of related heterocycles reported before.^{52, 103, 116} The endocyclic Si–N bonds in **57**, 1.7324(9) and 1.7365(10) Å, are longer than those reported for 1,2-{Me₂Si(μ -N^tBu)₂PNH}₂C₆H₄ (1.713(3) and 1.715(3) Å,¹³⁵ but they are shorter than the exocyclic Si–N bonds, 1.7984(10) and 1.7942(10) Å. The P–Cl bonds in **57** range from 2.0901(4) to 2.1063(4) Å, and they are similar to those observed for **55** above and another related molecule reported elsewhere.¹⁵⁷ Unlike the slightly puckered P₂N₂ ring in **55** (angle sum = 356.2°), the Si₂N₂ ring in **57** is planar with angle sum = 359.2°.

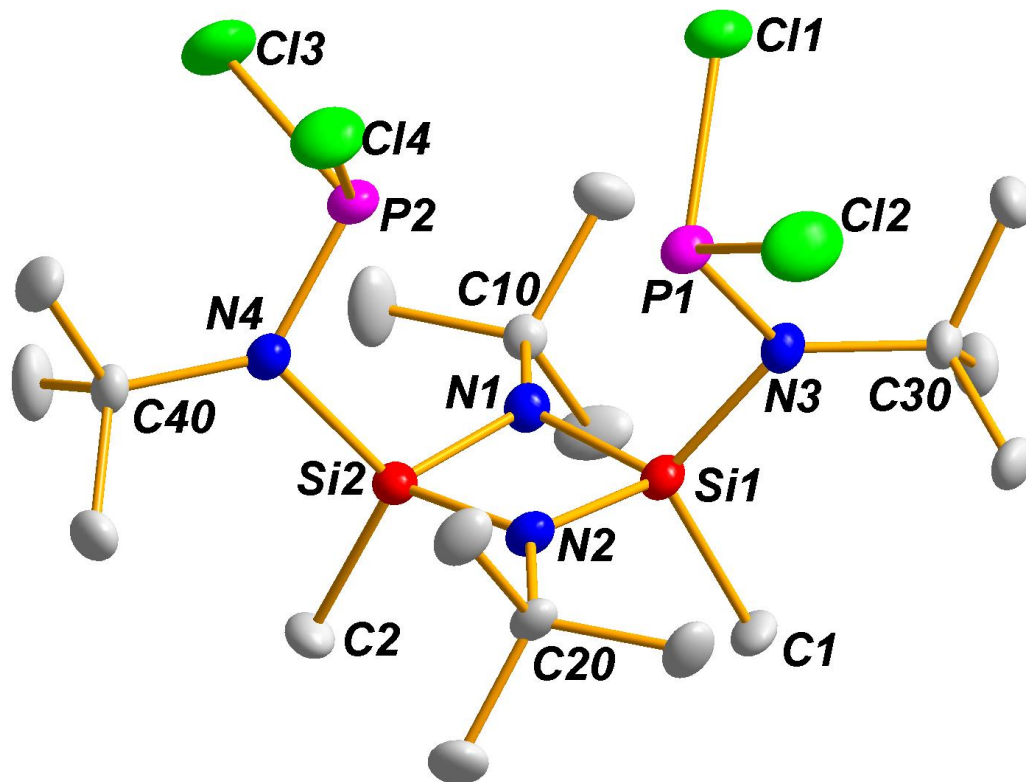


Figure 51. Solid-state structure and partial labelling scheme of **57**. With the exception of carbon (35 %) all atoms are drawn at the 50 % probability level.

Table 17. Crystal and structure refinement data for compound **57**.

Chemical Formula	C ₁₈ H ₄₂ Cl ₄ N ₄ P ₂ Si ₂
fw	574.48
T/K	173(2)
$\lambda/\text{\AA}$	0.71073
Crystal system	Monoclinic
Space group	<i>P</i> 2 ₁ / <i>c</i> (#14)
<i>a</i> /\AA	10.4522(2)
<i>b</i> /\AA	18.2055(4)
<i>c</i> /\AA	16.2317(3)
$\alpha/^\circ$	90
$\beta/^\circ$	107.346(1)
$\gamma/^\circ$	90
<i>V</i> /\AA ³	2948.22(18)
<i>Z</i>	4
$\rho(\text{calc}) \text{ g cm}^{-3}$	1.294
μ/mm^{-1}	0.606
F(000)	1216
Completeness (%)	99.70
Reflections collected	40706
Independent reflections	10231 [<i>R</i> _{int} = 0.0231]
$R_w(F^2)^b$ [<i>I</i> > 2 σ (<i>I</i>)]	<i>R</i> ₁ = 0.0308, <i>wR</i> ₂ = 0.0782
$R(F)^a$ (all data)	<i>R</i> ₁ = 0.0382, <i>wR</i> ₂ = 0.0835

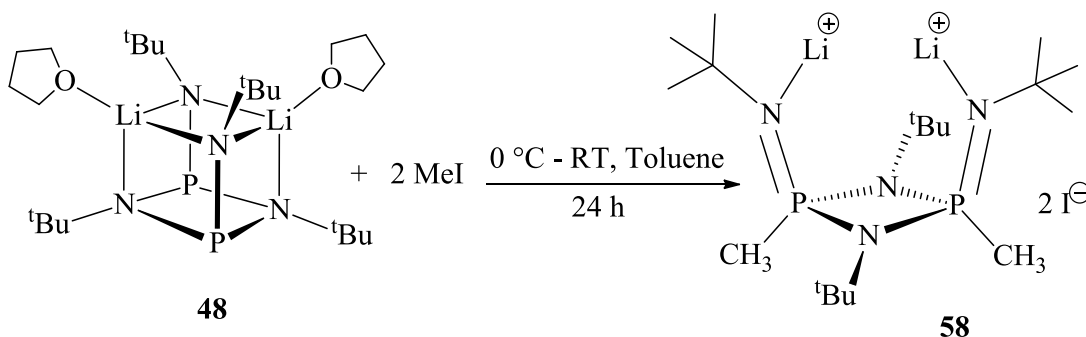
^a $R = \sum |F_o - F_c| / \sum |F_o|$. ^b $R_w = \{ [\sum w(F_o^2 - F_c^2)] / [\sum w(F_o^2)] \}^{1/2}$; $w = 1 / [\sigma^2(F_o)^2 + (xP)^2 + yP]$, where $P = (F_o^2 + 2F_c^2) / 3$.

Table 18. Selected bond lengths (Å) and angles (°) for **57**.

Bond Lengths			
Si1–N1	1.7324(9)	Si2–C2	1.8619(13)
Si1–N2	1.7365(10)	P1–N3	1.6638(9)
Si1–N3	1.7984(10)	P1–Cl2	2.0986(4)
Si1–C1	1.8666(12)	P1–Cl1	2.1004(4)
Si2–N1	1.7342(10)	P2–N4	1.6648(10)
Si2–N2	1.7388(9)	P2–Cl4	2.0901(4)
Si2–N4	1.7942(9)	P2–Cl3	2.1063(4)
Bond Angles			
N1–Si1–N2	86.82(4)	N3–P1–Cl2	105.69(4)
N1–Si1–N3	115.16(5)	N3–P1–Cl1	107.80(4)
N2–Si1–N3	114.45(5)	Cl1–P1–Cl2	96.964(19)
N1–Si1–C1	113.41(5)	N4–P2–Cl4	107.27(4)
N2–Si1–C1	110.79(6)	N4–P2–Cl3	105.61(4)
N3–Si1–C1	113.49(5)	Cl4–P2–Cl3	97.237(19)
N1–Si2–N2	86.69(4)	Si2–N1–Si1	92.97(5)
N1–Si2–N4	113.72(5)	C10–N1–Si2	132.85(7)
N2–Si2–N4	116.43(4)	Si2–N2–Si1	92.67(5)
N2–Si2–C2	113.89(6)	C20–N2–Si2	133.65(8)
N1–Si2–C2	110.49(6)	C30–N3–P1	128.78(8)
N4–Si2–C2	112.94(5)	C40–N4–P2	128.28(8)
P1–N3–Si1	106.14(5)	P2–N4–Si2	107.25(5)

Synthesis and Spectroscopic Analysis of *cis*-{[(*t*BuNPMe)₂(*t*BuN)₂Li₂I₂]}, **58**

Addition of two equivalents of methyl iodide to a cooled (0 °C) solution of compound **48** and stirring at RT for 24 h afforded compound **58** in 92 % yield (Scheme 24). This reaction produced the same result when carried out in THF solvent. However, compound **58** was isolated in toluene due to its lower solubility in toluene compared to its very high solubility in THF.



Scheme 24. Synthesis of **58**.

The ¹H NMR spectrum of **58** depicts three distinct signals (Figure 52). The *tert*-butylamido and *tert*-butylimido protons are represented by the signals at 1.49 and 1.27 ppm, respectively. The methyl protons resonate as a doublet at 1.68 ppm. This signal appears as a doublet due to coupling with the phosphorus center to which each methyl group is attached. The ³¹P{¹H} NMR spectrum of **58**, as shown on Figure 53, depicts only one signal at -48.79 ppm, which is consistent with equivalent P(V) centers in the molecule.

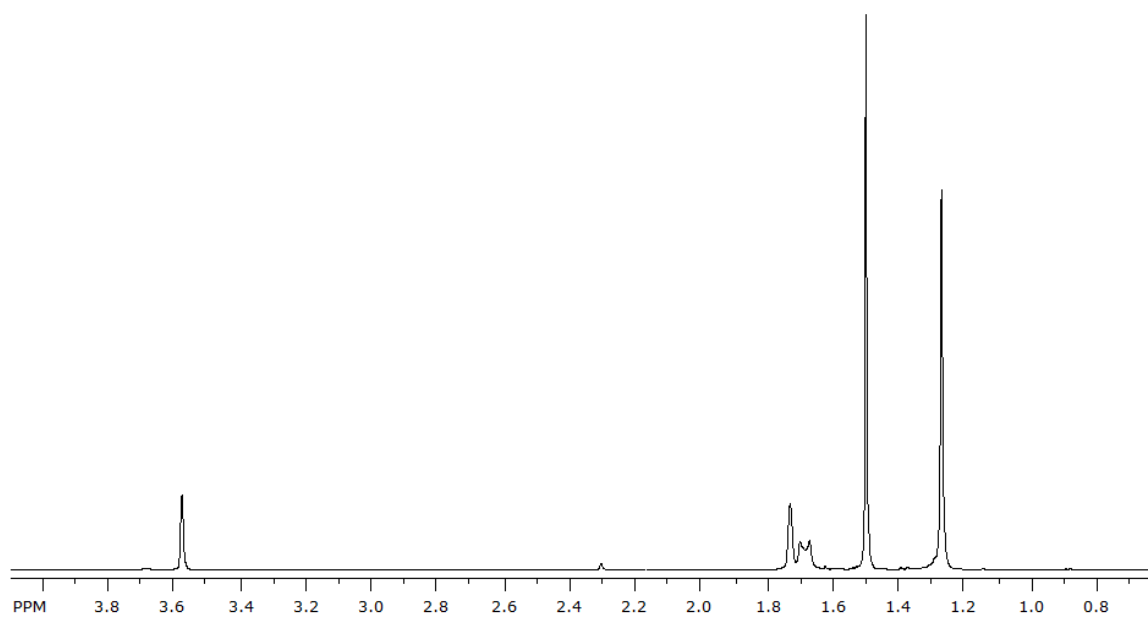


Figure 52. ^1H NMR Spectrum of **58**.

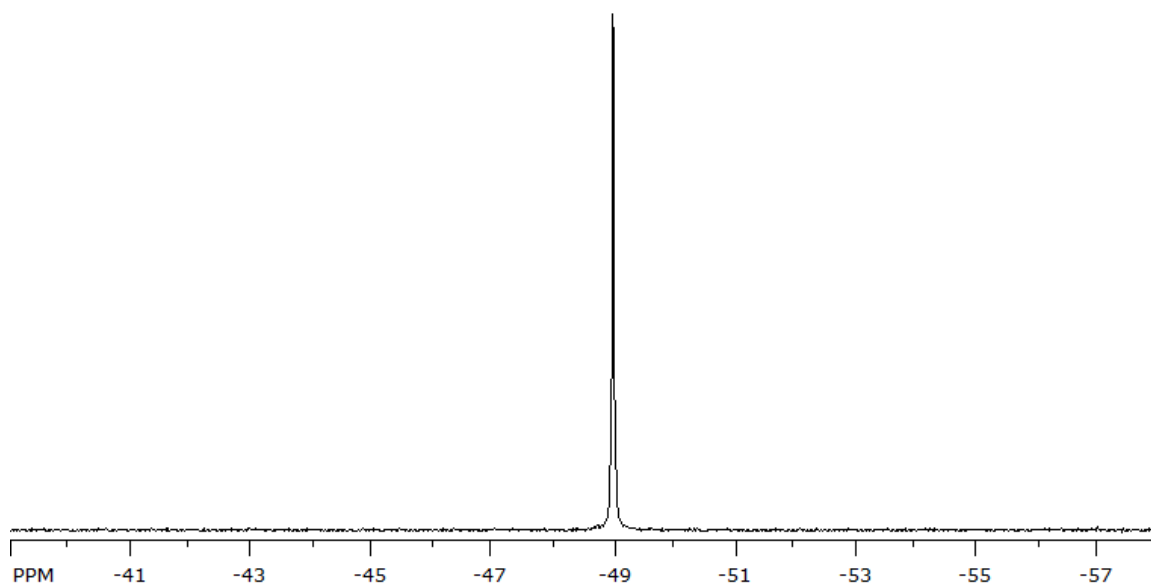
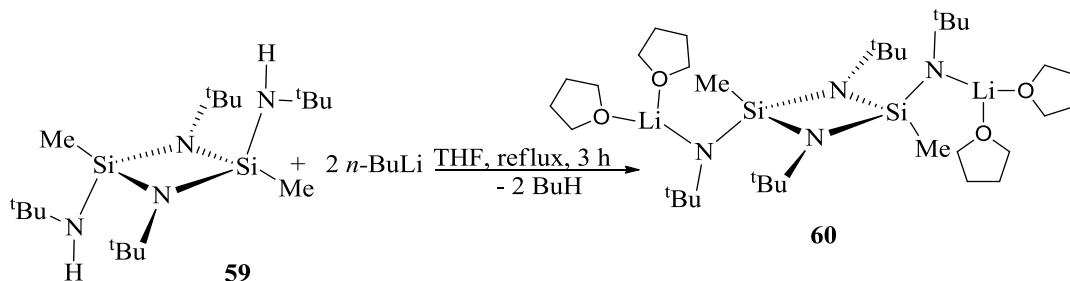


Figure 53. $^{31}\text{P}\{^1\text{H}\}$ NMR Spectrum of **58**.

Synthesis and Spectroscopic Analysis of *trans*-[(MeSi^{*t*}Bu)₂(N^{*t*}Bu(Li·(thf)₂)₂)]**60**

Refluxing compound **59** and a THF solution of 2 equivalents of *n*-BuLi produces compound **60** (Scheme 25) in 87 % yield.



Scheme 25. Synthesis of **60**.

The proton NMR spectrum of **60** shows five distinct singlets (Figure 54). The OCH₂ and CH₂ protons appear at 3.55 and 1.30 ppm, respectively, while the two different types of *tert*-butyl protons appear at 1.68 and 1.63 ppm. The methyl protons appear at 0.72 ppm.

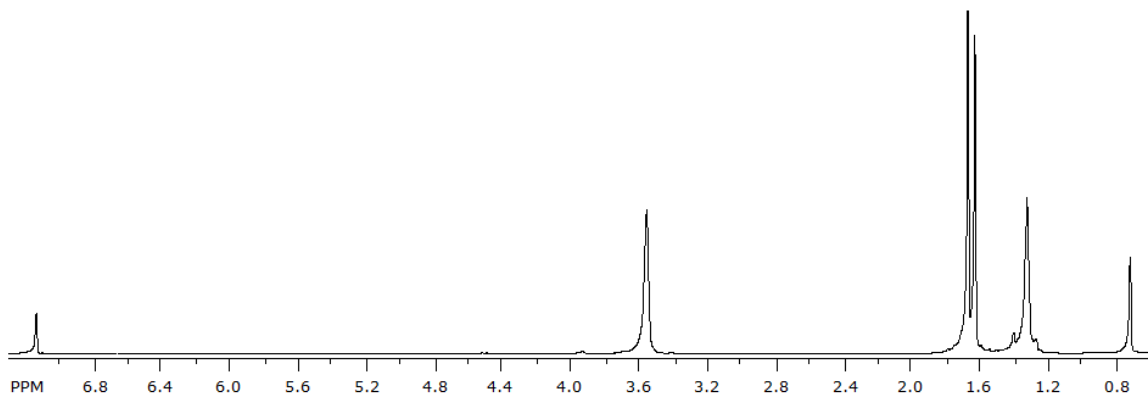


Figure 54. ¹H NMR Spectrum of **60**.

The ¹³C{¹H} NMR spectrum of **60** (Figure 55) shows seven singlets. The OCH₂ and OCH₂CH₂ carbons of the THF moiety appear at 68.65 and 25.33 ppm respectively. The singlet at 9.62 ppm is for the SiMe carbons. The quaternary *tert*-butylamido and *tert*-

butylimido carbons appear at 51.19 and 51.17 ppm respectively, while the primary carbons of these groups resonate at 38.94 and 34.07 ppm, respectively.

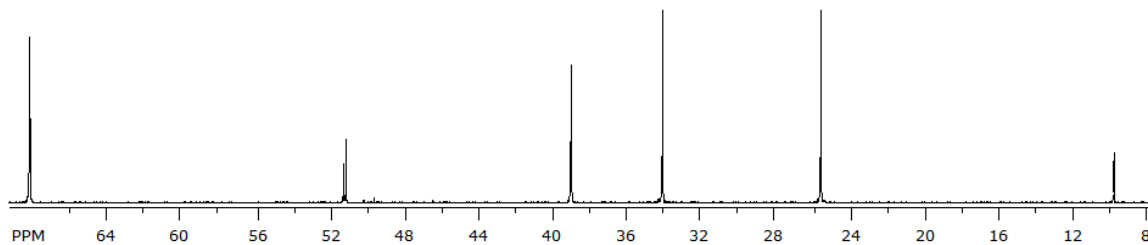


Figure 55. $^{13}\text{C}\{^1\text{H}\}$ NMR spectrum of **60**.

Solid-state Structure of *trans*-[(MeSiⁿBu)₂(NⁿBuLi·thf)₂], **60**

Colorless, hexagonal crystals of **60** were isolated from a concentrated THF solution at $-20\text{ }^{\circ}\text{C}$. The solid-state structure of **60** with a partial atom numbering scheme is shown in Figure 56, while the crystal data and selected bond parameters are listed in Tables 19 and 20, respectively. The compound crystallizes in the triclinic space group of $P-1(\#2)$ with one molecule per unit cell.

The solid-state structure of **60** depicts a tetrahedral geometry around the silicon atoms. Unlike in compound **57**, the endocyclic Si–N bonds in **60** (Av. = 1.7537(11) Å) are longer than the exocyclic Si–N bonds (Av. = 1.6656(11) Å). These Si–N bond lengths are similar to those observed for *cis*-[^tBuNP(μ -^tBuN)₂PN^tBu]SiCl₂ (1.7543(16) Å),⁵² but they are shorter than the Si–N bonds for {[Me₃Si)₂N]₂Sn(Cl)P(Ph)₂]₂, 2.0464(16) Å.¹⁴¹ The Li–O bonds, 1.964(3) and 1.943(3), are similar to those reported elsewhere.^{37, 52, 156}

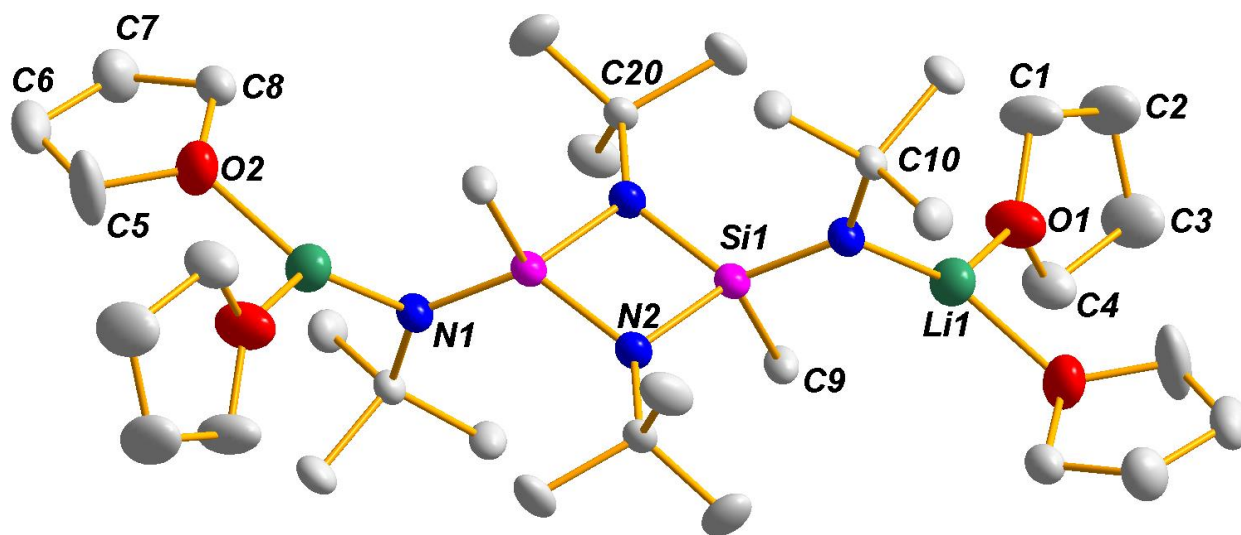


Figure 56. Solid-state structure and partial labelling scheme of **60**. With the exception of carbon (35 %) all atoms are drawn at the 50 % probability level.

Table 19. Crystal and structure refinement data for compound **60**.

Chemical Formula	C ₃₄ H ₇₄ Li ₂ N ₄ O ₄ Si ₂
fw	673.04
T/K	173(2) K
$\lambda/\text{\AA}$	0.71073 \AA
Crystal system	Triclinic
Space group	<i>P</i> –1(#2)
<i>a</i> / \AA	9.8329(2) \AA
<i>b</i> / \AA	11.1403(3) \AA
<i>c</i> / \AA	11.2861(3) \AA
$\alpha/^\circ$	100.227(1) $^\circ$
$\beta/^\circ$	103.119(1) $^\circ$
$\gamma/^\circ$	114.538(1) $^\circ$
<i>V</i> / \AA^3	1042.47(5) \AA^3
<i>Z</i>	1
$\rho(\text{calc}) \text{ g cm}^{-3}$	1.072 g/cm^3
μ/mm^{-1}	0.122 mm^{-1}
F(000)	372.3
Completeness (%)	99.61
Reflections collected	17417
Independent reflections	4753 [<i>R</i> _{int} = 0.0193]
$R_w(F^2)^b$ [<i>I</i> > 2 σ (<i>I</i>)]	<i>R</i> ₁ = 0.0456, <i>wR</i> ₂ = 0.1271
$R(F)^a$ (all data)	<i>R</i> ₁ = 0.0497, <i>wR</i> ₂ = 0.1321

^a $R = \sum |F_o - F_c| / \sum |F_o|$. ^b $R_w = \{ [\sum w(F_o^2 - F_c^2)] / [\sum w(F_o^2)^2] \}^{1/2}$; $w = 1 / [\sigma^2(F_o)^2 + (xP)^2 + yP]$, where $P = (F_o^2 + 2F_c^2) / 3$.

Table 20. Selected bond lengths (Å) and angles (°) for **60**.

Bond Lengths			
Si1–N1	1.6656(11)	Li1–N1	1.894(3)
Si1–N2	1.7537(11)	Li1–O1	1.964(3)
Si1–N2#	1.7575(11)	Li1–O2	1.943(3)
Si1–C9	1.9059(14)	N1–C10	1.4521(17)
Si1–N1	2.5913(7)	N2–C20	1.4622(16)
Bond Angles			
N1–Si1–N2#	125.44(6)	N1–Li1–O2	123.52(16)
N1–Si1–N2	124.63(5)	Li1–N1–Si1	105.20(11)
C9–Si1–N1	101.64(6)	C10–N1–Si1	133.25(9)
C9–Si1–N2	109.86(6)	C10–N1–Li1	120.47(12)
O2–Li1–O1	98.61(13)	C20–N2–Si1#	131.76(9)
N1–Li1–O1	135.20(16)	C20–N2–Si1	132.58(9)

5. Summary and Conclusion

The attack of two equivalents of the electrophiles Ph₂PCl, PCl₃, and CH₃I on the dianionic bis(alkylamido)cyclodiphosph(III)azanes, {R = *tert*-butyl (**48**), cyclohexyl (**54**)} was studied. We found out that PCl₃ attacked the cyclodiphosph(III)azanes exclusively at the exocyclic nitrogen atoms resulting in compound **49** and **55**. Although the reaction of **48** with PCl₃ resulted in the monophosphorus derivative **49**, the reaction of **54** with PCl₃ yielded a tetrachloro diphosphorus derivative **55**. The reason is probably steric rather than electronic. The cyclohexyl groups on the amido nitrogen atoms in **54** are less bulky than their *tert*-butyl counterpart in compound **48**. This probably results in more space above the P₂N₂ ring that can accommodate two phosphorus atoms as seen in compound **55**.

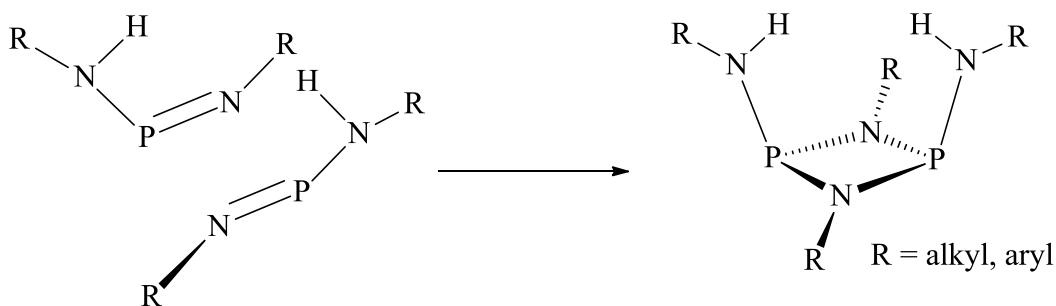
Similarly, CH₃I attacked the heterocycles exclusively at both phosphorus(III) centers, thus yielding in each case symmetrical products. In its reaction with bis(*tert*-butylamino)cyclodiphosph(III)azane Ph₂PCl, by contrast, initially furnished a symmetric P, P substituted heterocycle, **52B**, which then rearranged to an asymmetric P, N product, **52A**. Compound **52A** is the thermodynamic product while compound **52B** is the kinetic product. Kinetic studies of the isomerization of **52B** to **52A** were carried out at 70 °C and the results reveal that the process follows first-order kinetics with a rate constant, $k = 9.63 \times 10^{-5} \text{ s}^{-1}$ and a half-life of 120 minutes. We also determined the activation energy for this isomerization process to be 119 kJ/mol or 28.4 kcal/mol. We found that while The P₂N₂ ring in **52B** is perfectly planar with angle sum = 359.9°, that in **52A** is slightly puckered with angle sum = 356.6°.

CHAPTER IV

SYNTHESES AND CHARACTERIZATION OF CYCLODIPHOSPHAZANE COMPLEXES OF PHOSPHORUS AND ANTIMONY

1. Introduction

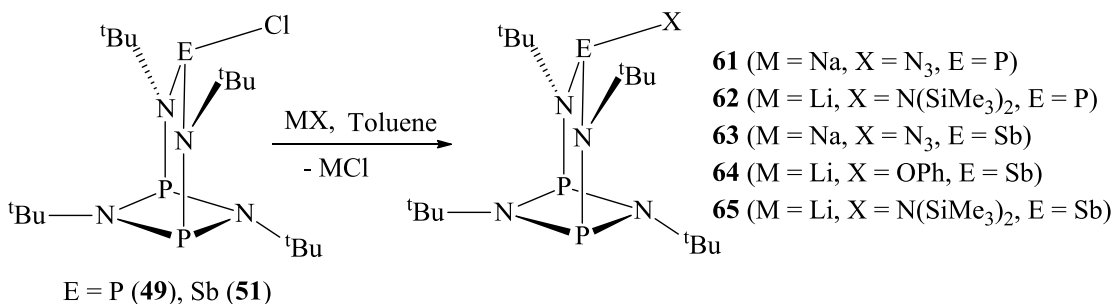
Phosphorus-nitrogen bonds are typically formed by the transamination or aminolysis of P–Cl bonds.¹⁵⁸ Bis(amino)cyclodiphosphazanes are products of the formal [2 + 2] cycloaddition of two aminophosphazenes,¹⁵⁹ as shown in Scheme 26.



Scheme 26. Synthesis of bis(amino)cyclodiphosphazanes from two aminophosphazenes.

In this project, we were investigating the synthetic derivatives of bis(amino)cyclodiphosphazane complexes of phosphorus and antimony. While phosphorus amides are a well-known class of inorganic compounds,¹⁶⁰ few analogues of antimony exist. The synthesis of the first fully characterized mono-phosphorus, **49** and mono-antimony, **51** complexes of bis(amino)cyclodiphosphazanes were reported by Stahl and co-workers.^{34, 35} However, the reaction chemistry of these compounds has not been fully exploited.

There are very few reported derivatives of compounds **49** and **51** (Scheme 27).^{21,}
^{34, 35} We sought therefore to expand the scope of reactivity and structural variations of these compact and electron-rich four-membered heterocycles by studying the reactions of **49** and **51** with a variety of reagents in order to determine the extent to which these compounds can be functionalized.



Scheme 27. Syntheses of **61–65** reported previously.^{21, 34, 35}

Our first goal for studying the synthetic derivatives compounds, **49** and **51** is to seek an understanding of the bond variation that may occur with novel substitution reactions. Secondly, new insight into the reactivity and selectivity of the rigid heterocyclic P₂N₂ system may be applied to other systems such as the isoelectronic cyclodisilazanes.¹¹⁶ Also, the fact that bis(amino)cyclodiphosphazanes can be easily modified at both the N- and P-donor sites makes them an attractive candidate to investigate. In addition, novel syntheses and full characterization of bis(amino)cyclodiphosphazane derivatives will furnish the scientific literature with more understanding of the steric and electronic properties of the P₂N₂ moiety.

2. Experimental

Description of Techniques and Chemicals Used

General

All experimental procedures were carried out under an atmosphere of argon, using standard Schlenk lines. Prior to use, all solvents were dried and freed of molecular oxygen by distillation under a nitrogen atmosphere from sodium- or potassium benzophenone ketyl.

Chemicals used

Phosphorus trichloride, SbCl_3 , PhMgCl , NaO^tBu , AgSO_3CF_3 and sulfur were purchased from either Sigma Aldrich or Alfa Aesar, and they were used without further purification. The compounds *cis*- $[(^t\text{BuNP})_2(^t\text{BuNLi}\cdot\text{thf})_2]$,³⁷ $\{[(^t\text{BuNP})_2(^t\text{BuN})_2]\text{PCl}\}$,³⁵ and $\{[(^t\text{BuNP})_2(^t\text{BuN})_2]\text{SbCl}\}$,³⁴ were synthesized according to published procedures.

Description of Instrumentation

NMR spectra were recorded on a Bruker AVANCE-500 NMR spectrometer. The ^1H and ^{13}C NMR spectra were referenced relative to $\text{C}_6\text{D}_5\text{H}$ (7.15 ppm) and C_6D_6 (128.0 ppm), respectively, as internal standards, while the ^{31}P spectra were referenced relative to $\text{P}(\text{OEt})_3$ (137.0 ppm) as external standard in C_6D_6 . In all cases positive chemical shift values represent higher frequencies and downfield shifts. Melting points were recorded on Mel-Temp melting point apparatus; they are uncorrected. Elemental analyses on crystalline samples were performed by ALS Life Sciences Division Environmental, Tucson, AZ.

X-ray Crystallography

Suitable, single crystals were coated with Paratone oil, affixed to Mitegen or Litholoop crystal holders, and centered on the diffractometer in a stream of cold nitrogen. Reflection intensities were collected with a Bruker Apex diffractometer, equipped with an Oxford Cryosystems, 700 Series Cryostream cooler, operating at 173 K. Data were measured using ω scans of 0.3° per frame for 20 seconds until a complete hemisphere of data had been collected. Cell parameters were retrieved using SMART⁹⁷ software and refined with SAINT⁹⁸ on all observed reflections. Data were reduced with SAINTplus, which corrects for Lorentz polarization effects and crystal decay. Empirical absorption corrections were applied with SADABS.⁹⁹ The structures were solved by direct methods with SHELXS-90¹⁰⁰ program and refined by full-matrix least squares methods on F² with SHELXL-97¹⁰¹ incorporated in SHELXTL Version 5.10.¹⁰²

3. Syntheses of Compounds

Synthesis of [(^tBuNP=S)₃N], 66

In a 100-mL three-necked flask, equipped with a gas inlet and magnetic stir bar, samples of {[(^tBuNP)₂(^tBuN)₂]PCl}, **49**, (0.420 g, 1.01 mmol) and excess sulfur (0.100 g, 3.13 mmol) were combined in 30 mL of toluene and refluxed for 2 d. After the reaction had been allowed to cool to RT, unreacted sulfur was filtered off using a medium-porosity frit and the light-yellow solution concentrated in *vacuo* and stored at -12 °C. After several days, colorless, tiny, rod-shaped crystals were isolated. Yield: (0.310 g, 0.730 mmol), 73 %.

Mp: 236–238 °C. ¹H NMR (500.1 MHz, benzene-d₆, 25 °C): 1.40 (s, 27H, N^tBu).
¹³C{¹H} NMR (125.8 MHz, benzene-d₆, 25 °C): 58.13 (s, NC(CH₃)₃), 30.23 (s,

NC(CH₃)₃). ³¹P{¹H} NMR (202.5 MHz, benzene-d₆, 25 °C): 35.6 (s). Anal. Calcd for C₁₂H₂₇N₄P₃S₃: C, 34.61; H, 6.63; N, 13.45. Found: C, 35.06; H, 6.88; N, 12.98.

Synthesis of [(^tBuNP)₂(^tBuN)₂P]⁺SO₃CF₃⁻, **67**

A 100 mL two-necked flask equipped with a magnetic stir bar and gas inlet was charged with a solution of AgSO₃CF₃ (0.250 g, 0.970 mmol) in 7 mL of THF and cooled to 0 °C. A solution of {[(^tBuNP)₂(^tBuN)₂]PCl}, **49**, (0.400 g, 0.970 mmol) in 20 mL of THF was then added dropwise and a white precipitate formed instantly. The reaction mixture was stirred at 0 °C for 30 minutes, and the AgCl was filtered off with a medium-porosity frit. The ensuing colorless solution was concentrated *in vacuo* and stored at -20 °C. After 24 h, colorless, needle-shaped crystals were isolated. Yield: (0.460 g, 0.860 mmol), 89 %.

Mp: 119–121 °C. ¹H NMR (500.1 MHz, CD₂Cl₂, 25 °C): 1.73 (s, 9H, N^tBu), 1.46 (s, 27H, N^tBu). ¹³C{¹H} NMR (125.8 MHz, CD₂Cl₂, 25 °C): 60.65 (q, *J*_{PC} = 8.48 Hz, NC(CH₃)₃), 57.23 (t, *J*_{PC} = 7.82 Hz, NC(CH₃)₃), 31.30 (t, *J*_{PC} = 5.79 Hz, NC(CH₃)₃), 22.81 (q, *J*_{PC} = 5.21 Hz, NC(CH₃)₃). ³¹P{¹H} NMR (202.5 MHz, CD₂Cl₂, 25 °C): 210.4 (s, 3P). Anal. Calcd for C₁₇H₃₆F₃N₄O₃P₃S: C, 38.78; H, 6.89; N, 10.64. Found: C, 38.63; H, 7.19; N, 10.33.

Synthesis of {[(^tBuNP)₂(^tBuN)₂]PPh}, **68**

To a cooled (0 °C) solution of {[(^tBuNP)₂(^tBuN)₂]PCl}, **49**, (0.700 g, 1.70 mmol) in 25 mL of toluene was added dropwise 0.870 mL (1.83 mmol) of PhMgCl and stirred at RT for 24 h. MgCl₂ was then filtered off using a medium-porosity frit and the ensuing light-yellow solution was concentrated *in vacuo* and stored at -12 °C. After several days, colorless plate-like crystals were isolated. Yield: (0.670 g, 1.49 mmol), 88 %.

Mp: 126–128 °C. ^1H NMR (500.1 MHz, benzene- d_6 , 25 °C): 7.82 (td, 2H, $J = 6.20, 1.75$ Hz, Ph), 7.21 (td, 2H, $J = 7.60, 2.15$ Hz, Ph), 7.06 (td, 1H, $J = 7.30, 1.10$ Hz, Ph), 1.62 (s, 18H, N^tBu , amino), 1.29 (s, 9H, N^tBu , imino, N1), 1.00 (s, 9H, N^tBu , imino, N2). $^{13}\text{C}\{^1\text{H}\}$ NMR (125.8 MHz, benzene- d_6 , 25 °C): 152.0 (d, $J_{\text{PC}} = 21.4$ Hz, C–P, Ph), 129.3 (d, $J_{\text{PC}} = 19.2$ Hz, CH, Ph), 126.5 (d, $J_{\text{PC}} = 1.86$ Hz, CH, Ph), 57.38 (dd, $J_{\text{PC}} = 27.0, 15.1$ Hz, $\text{NC}(\text{CH}_3)_3$, amino), 32.79 (dt, $J_{\text{PC}} = 39.6, 16.3$ Hz, $\text{NC}(\text{CH}_3)_3$, imino) 32.48 (t, $J_{\text{PC}} = 11.9$ Hz, $\text{NC}(\text{CH}_3)_3$, amino), 31.04 (t, $J_{\text{PC}} = 6.50$ Hz, $\text{NC}(\text{CH}_3)_3$, imino, N1), 28.88 (t, $J_{\text{PC}} = 6.51$ Hz, $\text{NC}(\text{CH}_3)_3$, imino, N2). $^{31}\text{P}\{^1\text{H}\}$ NMR (202.5 MHz, benzene- d_6 , 25 °C): 203.05 (d, $J_{\text{PP}} = 6.13$ Hz), 69.67 (s). Anal. Calcd for $\text{C}_{22}\text{H}_{41}\text{N}_4\text{P}_3$: C, 58.14; H, 9.09; N, 12.33. Found: C, 57.84; H, 9.30; N, 12.61.

Synthesis of $\{[(^t\text{BuNP})_2(^t\text{BuN})_2](\text{P}=\text{S})\text{Ph}\}$, **69**

In a 50-mL two-necked flask equipped with a gas inlet and magnetic stir bar, samples of $\{[(^t\text{BuNP})_2(^t\text{BuN})_2]\text{PPh}\}$, **68**, (0.23 g, 0.510 mmol) and sulfur (0.0180 g, 0.550 mmol) were dissolved in 20 mL of toluene and stirred at RT for 24 h. Unreacted sulfur was filtered off using a medium-porosity frit and the resulting colorless solution was concentrated *in vacuo* and stored at -12 °C. After 3 days, colorless, block-shaped crystals were isolated. Yield: (0.180 g, 0.360 mmol), 71 %.

Mp: 226–228 °C. ^1H NMR (500.1 MHz, benzene- d_6 , 25 °C): 8.69 (q, $J = 7.30$, Hz, Ph), 7.07 (t, $J = 7.20$ Hz, Ph), 7.06 (t, $J = 7.01$ Hz, Ph), 1.49 (s, 9H, N^tBu , imino, N1), 1.43 (s, 18H, N^tBu , amino), 1.40 (s, 9H, N^tBu , imino, N2). $^{13}\text{C}\{^1\text{H}\}$ NMR (125.8 MHz, benzene- d_6 , 25 °C): 133.13 (d, $J_{\text{PC}} = 13.2$ Hz, C–P, Ph), 130.23 (d, $J_{\text{PC}} = 2.64$ Hz, CH, Ph), 127.60 (d, $J_{\text{PC}} = 13.4$ Hz, CH, Ph), 61.30 (m, $\text{NC}(\text{CH}_3)_3$, amino), 54.06 (t, $J_{\text{PC}} = 12.6$ Hz, $\text{NC}(\text{CH}_3)_3$, imino, N1), 53.06 (t, $J_{\text{PC}} = 7.25$ Hz, $\text{NC}(\text{CH}_3)_3$, imino, N2), 32.75

(m, NC(CH₃)₃, amino), 30.54 (t, $J_{PC} = 5.99$ Hz, NC(CH₃)₃, imino, N1), 29.98 (t, $J_{PC} = 7.06$ Hz, NC(CH₃)₃, imino, N2). ³¹P{¹H} NMR (202.5 MHz, benzene-d₆, 25 °C): 193.27 (d, $J_{pp} = 21.8$ Hz), 53.43 (t, $J_{pp} = 21.4$ Hz). Anal. Calcd for C₂₂H₄₁N₄P₃S: C, 54.31; H, 8.49; N, 11.51. Found: C, 53.86; H, 8.70; N, 11.22.

Synthesis of {[^tBuNP)₂(^tBuN)₂]PO^tBu}, 70

In a 100-mL two-necked flask equipped with a gas inlet and magnetic stir bar, samples of {[^tBuNP)₂(^tBuN)₂]PCl}, **49**, (0.680 g, 1.64 mmol) and NaO^tBu (0.160 g, 1.66 mmol) were dissolved in 35 mL of toluene and stirred at 70 °C for 24 h. After the reaction had been allowed to cool to RT for 1 h, NaCl was filtered off using a medium-porosity frit. The resulting colorless solution was concentrated *in vacuo* to about 10 mL and stored at -12 °C for 3 days. This produced colorless, block-shaped crystals. Yield: (0.660 g, 1.46 mmol), 89 %.

Mp: 186–188 °C. ¹H NMR (500.1 MHz, benzene-d₆, 25 °C): 1.55 (s, 18H, N^tBu, amino), 1.51 (s, 9H, O^tBu), 1.42 (s, 9H, N^tBu, imino, N1), 1.392 (s, 9H, N^tBu, imino, N2). ¹³C{¹H} NMR (125.8 MHz, benzene-d₆, 25 °C): 76.68 (d, $J_{PC} = 15.7$ Hz, OC(CH₃)₃), 57.13 (m, NC(CH₃)₃, amino), 53.00 (t, $J_{PC} = 7.12$ Hz, NC(CH₃)₃, imino, N1), 32.79 (t, $J_{PC} = 12.9$ Hz, NC(CH₃)₃, imino, N2), 31.81 (d, $J_{PC} = 7.27$ Hz, OC(CH₃)₃), 30.09 (t, $J_{PC} = 6.72$ Hz, NC(CH₃)₃, amino), 29.19 (t, $J_{PC} = 6.15$ Hz, NC(CH₃)₃, imino). ³¹P{¹H} NMR (202.5 MHz, benzene-d₆, 25 °C): 200.2 (d, $J_{pp} = 12.9$ Hz), 117.8 (t, $J_{pp} = 12.0$ Hz). Anal. Calcd for C₂₀H₄₅N₄OP₃: C, 53.32; H, 10.07; N, 12.44. Found: C, 53.07; H, 10.41; N, 12.03.

Synthesis of $\{[(^t\text{BuNP})_2(^t\text{BuN})_2]\text{SbPh}\}$, **71**

0.820 mL (1.16 mmol) of PhMgCl solution was added dropwise to a cooled (0 °C) solution of $\{[(^t\text{BuNP})_2(^t\text{BuN})_2]\text{SbCl}\}$, **51**, (0.58 g, 1.16 mmol) in 20 mL of toluene and stirred at RT for 24 h. A white precipitate of MgCl₂ was then filtered off using a medium-porosity frit and the ensuing colorless solution was concentrated *in vacuo* and stored at -12 °C. After 24 h, colorless, hexagonal crystals were isolated. Yield: (0.57 g, 1.05 mmol), 90 %.

Mp: 162–164 °C. ¹H NMR (500.1 MHz, benzene-d₆, 25 °C): 8.21 (d, 2H, $J_{\text{HH}} = 7.30$ Hz, Ph), 7.29 (t, 2H, $J_{\text{HH}} = 7.35$ Hz, Ph), 7.13 (t, 1 H, $J_{\text{HH}} = 1.45$ Hz, 1 Hz, Ph), 1.48 (s, 9 H, N^tBu, imino, N2), 1.45 (s, 9H, N^tBu, imino, N2), 1.20 (s, 18 H, N^tBu, amino). ¹³C{¹H} NMR (125.8 MHz, benzene-d₆, 25 °C): 156.4 (s, Cq, Ph), 136.2 (s, CH, Ph), 128.7 (s, CH, Ph), 128.3 (s, CH, Ph), 57.27 (d, $J_{\text{PC}} = 17.0$ Hz, NC(CH₃)₃, amino), 53.75 (t, $J_{\text{PC}} = 13.3$ Hz, NC(CH₃)₃, imino, N1), 52.88 (t, $J_{\text{PC}} = 13.6$ Hz, NC(CH₃)₃, imino, N2), 33.63 (d, $J_{\text{PC}} = 11.4$ Hz, NC(CH₃)₃, amino) 30.95 (t, $J_{\text{PC}} = 7.14$ Hz, NC(CH₃)₃, imino, N1), 29.03 (t, $J_{\text{PC}} = 7.14$ Hz, NC(CH₃)₃, imino, N2). ³¹P{¹H} NMR (202.5 MHz, benzene-d₆, 25 °C): 138.3 (s). Anal. Calcd for C₂₂H₄₁N₄P₂Sb: C, 48.46; H, 7.58; N, 10.27. Found: C, 48.66; H, 7.89; N, 10.10.

Synthesis of $\{[(^t\text{BuNP})_2(^t\text{BuN})_2]\text{SbO}^t\text{Bu}\}$, **72**

A 100-mL two-necked flask equipped with a gas inlet and magnetic stir bar, was charged with samples of $\{[(^t\text{BuNP})_2(^t\text{BuN})_2]\text{SbCl}\}$, **51**, (0.540 g, 1.07 mmol) and NaO^tBu (0.10 g, 1.07 mmol). The reagents were dissolved in 30 mL of toluene and the reaction mixture was stirred at 70 °C for 24 h. After the reaction had been allowed to cool to RT for 1 h, NaCl was filtered off using a medium-porosity frit. The resulting colorless

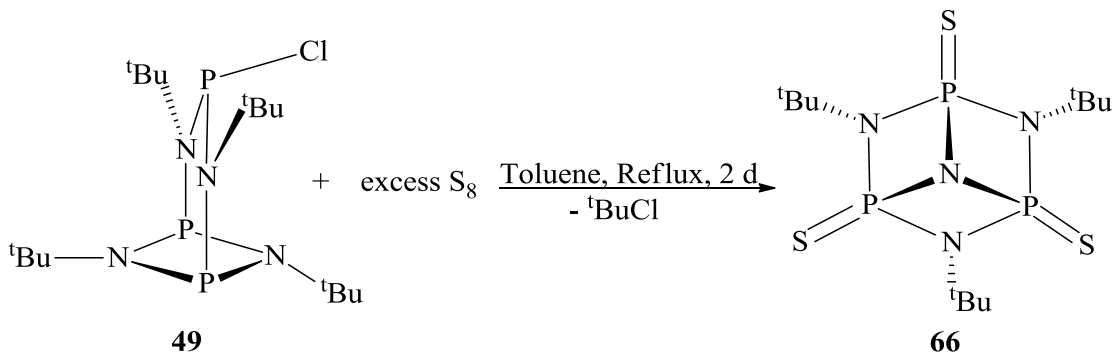
solution was concentrated *in vacuo* to about 10 mL and stored at $-12\text{ }^{\circ}\text{C}$ for 3 days. This produced colorless, block-shaped crystals. Yield: (0.460 g, 0.913 mmol), 79 %.

Mp: 114–116 $^{\circ}\text{C}$. ^1H NMR (500.1 MHz, benzene- d_6 , 25 $^{\circ}\text{C}$): 1.54 (s, 18H, N^tBu, amino), 1.49 (s, 9H, O^tBu), 1.43 (s, 9H, N^tBu, imino, N1), 1.41 (s, 9H, N^tBu, imino, N2). $^{13}\text{C}\{^1\text{H}\}$ NMR (125.8 MHz, benzene- d_6 , 25 $^{\circ}\text{C}$): 74.04 (s, OC(CH₃)₃), 56.80 (d, $J_{\text{PC}} = 15.5\text{ Hz}$, NC(CH₃)₃, amino), 53.29 (t, $J_{\text{PC}} = 12.3\text{ Hz}$, NC(CH₃)₃, imino, N1), 52.61 (t, $J_{\text{PC}} = 9.21\text{ Hz}$, NC(CH₃)₃, imino, N2), 34.52 (d, $J_{\text{PC}} = 13.3\text{ Hz}$, NC(CH₃)₃, amino), 34.15 (s, OC(CH₃)₃), 30.98 (t, $J_{\text{PC}} = 5.97\text{ Hz}$, NC(CH₃)₃, imino, N1), 27.95 (t, $J_{\text{PC}} = 7.32\text{ Hz}$, NC(CH₃)₃, imino, N1). $^{31}\text{P}\{^1\text{H}\}$ NMR (202.5 MHz, benzene- d_6 , 25 $^{\circ}\text{C}$): 158.1 (s). Anal. Calcd for C₂₀H₄₅N₄OP₂Sb: C, 44.38; H, 8.38; N, 10.35. Found: C, 44.25; H, 8.76; N, 9.90.

4. Results and Discussions

Synthesis and Spectroscopic Analysis of [(^tBuNP=S)₃N], **66**

The reaction of **49** with excess sulfur yield the nitridocyclodiphosphazane, **66**, after two days of refluxing in toluene (Scheme 28). Although we expected a compound in which all three phosphorus atoms would be oxidized by sulfur, we obtained **66** instead. We believe that the high refluxing temperatures led to the elimination of *tert*-butyl chloride resulting in thermally stable **66**. It is difficult to say whether it is the *tert*-butyl group of the P₂N₂ ring N or that of the amino N that is lost during this elimination process. However, we think the amino *tert*-butyl group is likely the group that is lost owing to the stability of the P₂N₂ ring which may result in the ring *tert*-butyl being held more tightly. Notwithstanding, we are currently investigating this detail.



Scheme 28. Synthesis of **66**.

Owing to the highly symmetrical nature of **66** its ^1H , $^{13}\text{C}\{^1\text{H}\}$, and $^{31}\text{P}\{^1\text{H}\}$ NMR spectra are very simple, and are shown in Figures 57, 58, and 59 respectively. All *tert*-butyl protons and all phosphorus atoms are equivalent resulting in just one singlet at 1.40 ppm in the ^1H spectrum, two singlets at 58.13 and 30.23 ppm in the $^{13}\text{C}\{^1\text{H}\}$ spectrum, and one singlet at 35.6 ppm in the $^{31}\text{P}\{^1\text{H}\}$ spectrum indicative of a P(V) center.

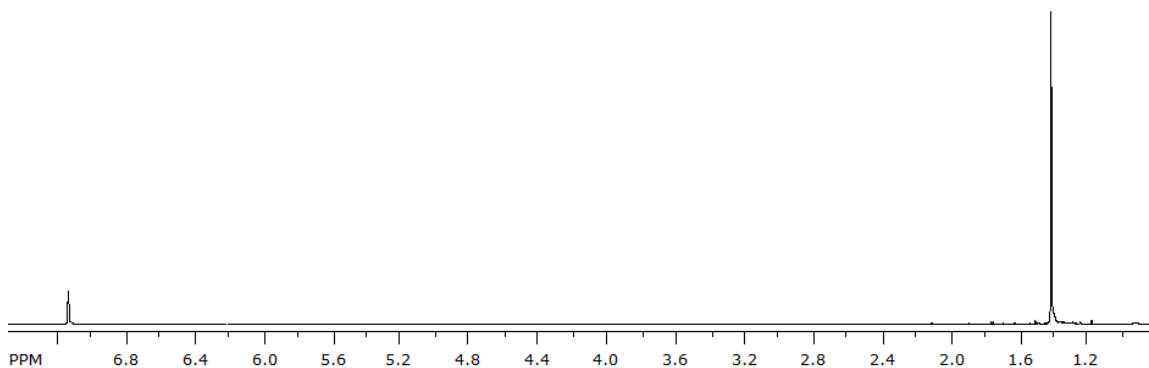


Figure 57. ^1H NMR Spectrum of **66**.

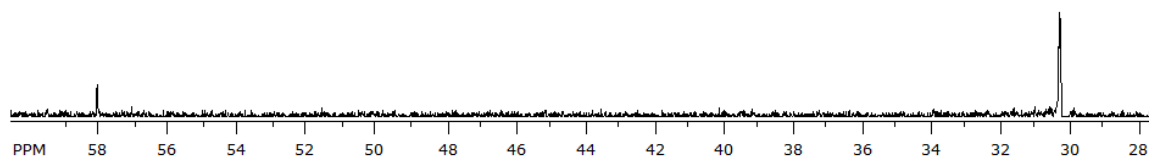


Figure 58. $^{13}\text{C}\{^1\text{H}\}$ NMR Spectrum of **66**.

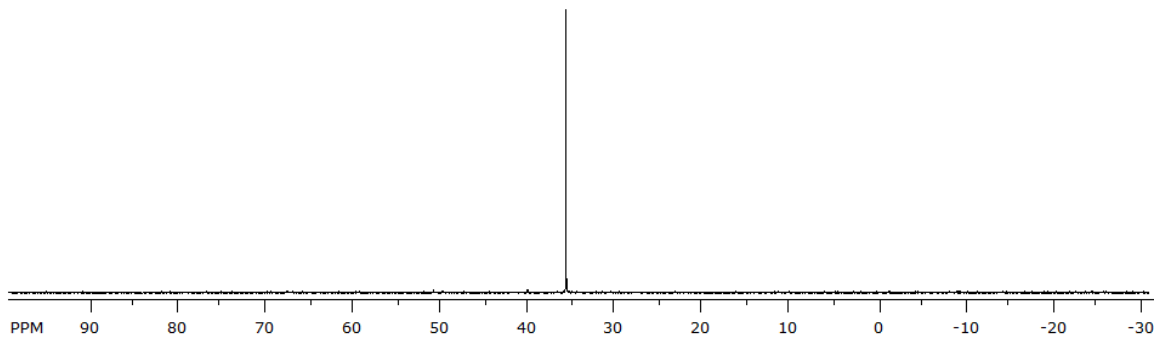


Figure 59. $^{31}\text{P}\{^1\text{H}\}$ NMR Spectrum of **66**.

Solid-state Structure of $[^t\text{BuNP}=\text{S})_3\text{N}]$, **66**

X-ray quality crystals of **66** were isolated as colorless, tiny, rod-shaped crystals from a cold ($-12\text{ }^\circ\text{C}$), concentrated solution of toluene. The solid-state structure of **66** with a partial atom numbering scheme is shown in Figure 60, while the crystal data and selected bond parameters are listed in Tables 21 and 22, respectively. The compound crystallizes in the orthorhombic space group $Pnma$ (#62), with four molecules per unit cell. The solid-state structure of **66** depicts a pyramidal nitrogen atom (N1) at the center of the molecule to which are bonded all three phosphorus atoms. Each phosphorus atom is a P(V) center and it is bonded to sulfur. The compound can also be viewed as constituted of three slightly puckered (angle sum = 358.4° , 358.3° , 358.7°) P_2N_2 rings fused together with the pyramidal nitrogen atom (N1) being a part of all three rings. Each of the other three nitrogen atoms (N2, N3, N3#) is part of only one P_2N_2 ring and bears a *tert*-butyl substituent. The top view of **66** as shown in Figure 61 reveals the C_s symmetry of the compound having a crystallographic mirror plane containing S2, P2, N1, N2, C20, and bisecting one of the P_2N_2 rings. This compound can serve as a tridentate chelating ligand in which a metal atom binds to each of the three N atoms at the base of the pyramid.

The P–N bonds in **66**, 1.6945(8)–1.7292 (12) Å, are longer than the average P–N bond length in the nitrides β -HP₄N₇, 1.6295(2) Å, and P₃N₅, 1.6700(2) Å, reported by Schnick and co-workers.^{161, 162} The molecule has two almost identical P–N1 bonds, 1.7275(8) and 1.7292(12) Å, which are longer than the other P–N bonds, 1.6945(8) – 1.6973(8) Å. Whereas N2 and N3 are almost planar, the central nitrogen (N1) atom is highly pyramidalized (277.5°).

There are two identical P=S bonds, 1.8995(3) Å, and one slightly longer P=S bond, 1.9021(5) Å in compound **66**. These P=S bonds are comparable to the P=S bonds in compounds **39** (1.9080(5) Å), and **40** (1.9097(8) Å), but they are shorter than those in compounds **37** (1.9284(7) Å), and **38** (1.9269(13) Å).

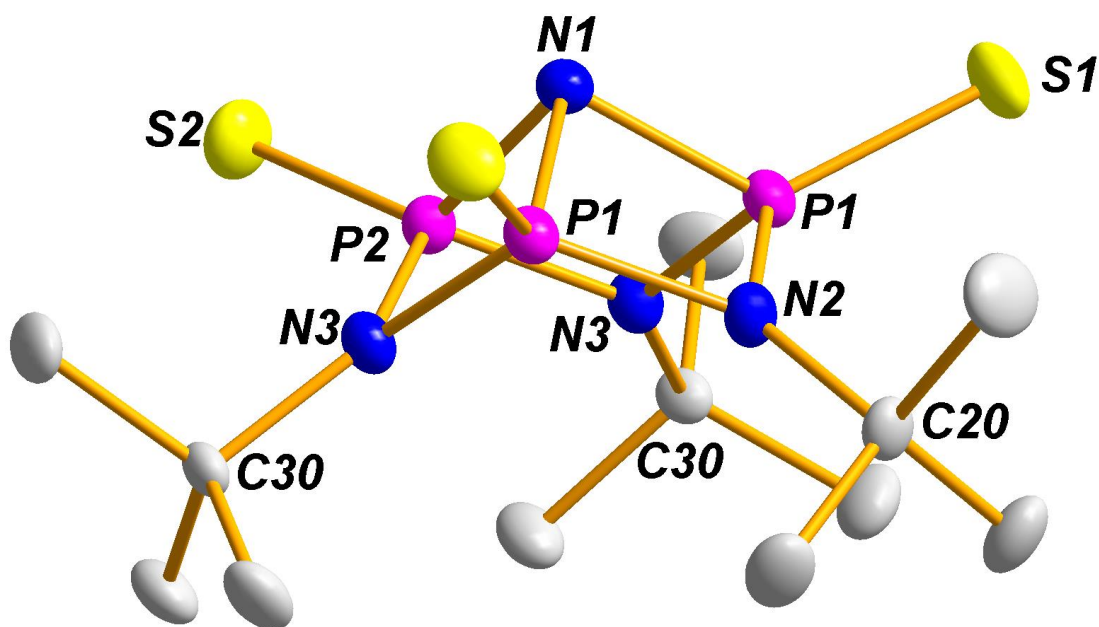


Figure 60. Solid-state structure and partial labelling scheme of **66**. With the exception of carbon (35 %) all atoms are drawn at the 50 % probability level.

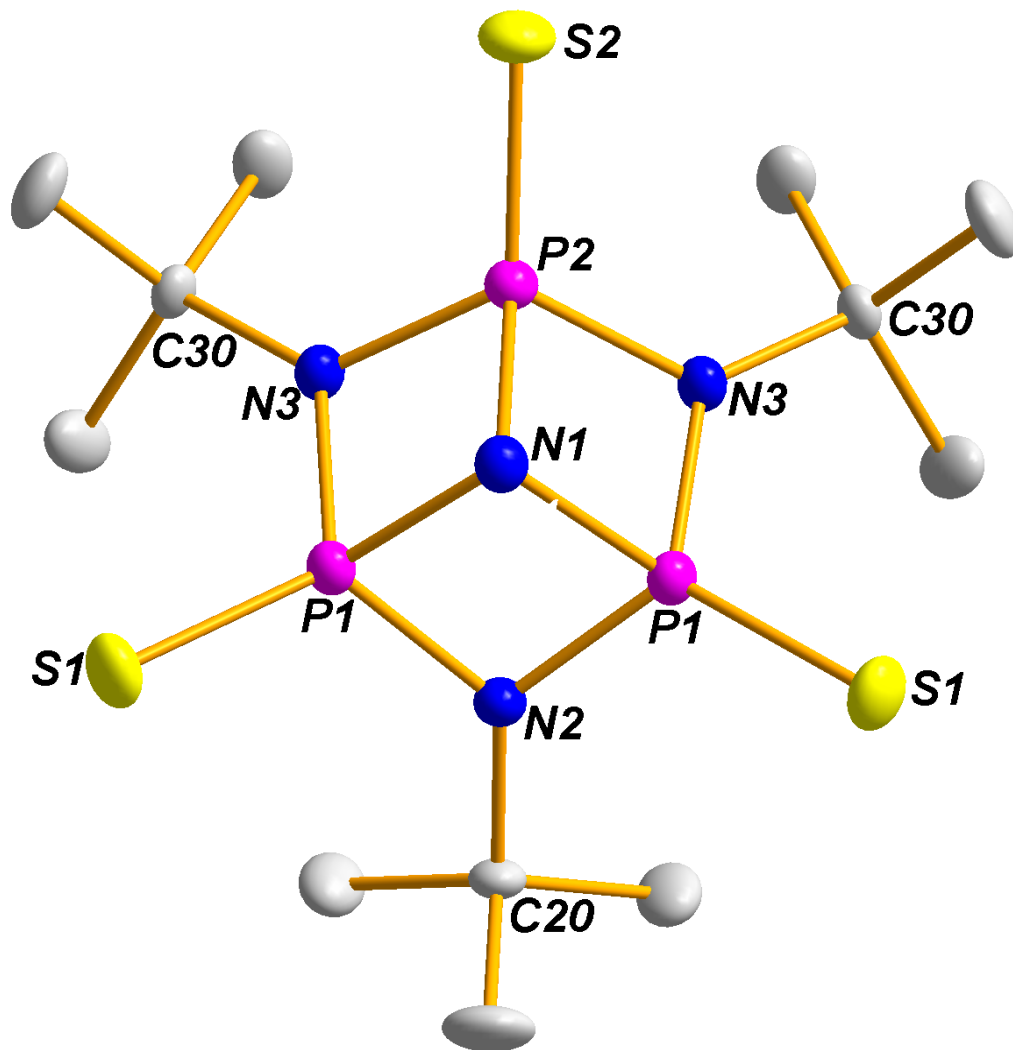


Figure 61. Top view of **66** showing C_s symmetry.

Table 21. Crystal and structure refinement data for compound **66**.

Chemical Formula	C ₁₂ H ₂₇ N ₄ P ₃ S ₃
fw	416.47
T/K	173(2)
$\lambda/\text{\AA}$	0.71073
Crystal system	Orthorhombic
Space group	<i>Pnma</i> (#62)
$a/\text{\AA}$	11.9485(3)
$b/\text{\AA}$	17.2722(5)
$c/\text{\AA}$	10.2091(3)
$\alpha/^\circ$	90
$\beta/^\circ$	90
$\gamma/^\circ$	90
$V/\text{\AA}^3$	2106.92(10)
<i>Z</i>	4
$\rho(\text{calc}) \text{ g cm}^{-3}$	1.313
μ/mm^{-1}	0.581
F(000)	880
Completeness (%)	99.90
Reflections collected	15851
Independent reflections	3773 [$R_{\text{int}} = 0.0190$]
$R_w(F^2)^b$ [$I > 2\sigma(I)$]	$R_1 = 0.0262$, $wR_2 = 0.0699$
$R(F)^a$ (all data)	$R_1 = 0.0315$, $wR_2 = 0.0742$

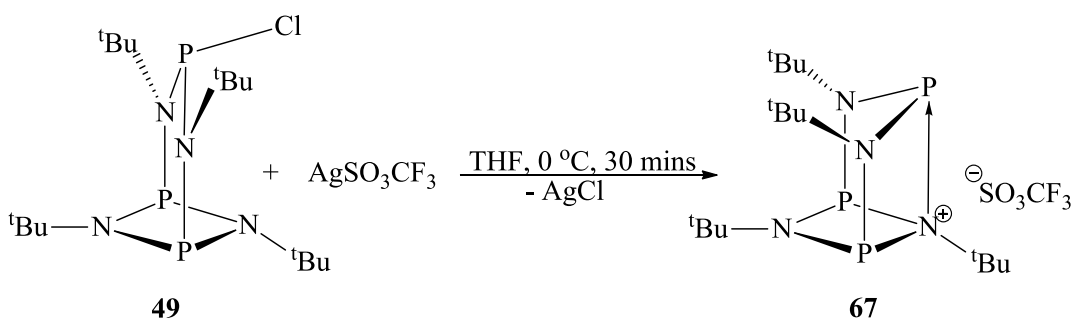
^a $R = \sum |F_o - F_c| / \sum |F_o|$. ^b $R_w = \{ [\sum w(F_o^2 - F_c^2)] / [\sum w(F_o^2)^2] \}^{1/2}$; $w = 1 / [\sigma^2(F_o)^2 + (xP)^2 + yP]$, where $P = (F_o^2 + 2F_c^2) / 3$.

Table 22. Selected bond lengths (Å) and angles (°) for **66**.

Bond Lengths			
P1–N1	1.7275(8)	P2–N1	1.7292(12)
P1–N2	1.6973(8)	P2–N3	1.6945(8)
P1–S1	1.8995(3)	P2–S2	1.9021(5)
P1–P2	2.4946(4)	N2–C20	1.4977(18)
P1–N3	1.6981(8)	N3–C30	1.5031(12)
P1–P1#	2.5001(5)	N1–P1#	1.7275(8)
Bond Angles			
P1–N2–P1#	94.86(6)	P1–N1–P1#	92.70(6)
P1–N2–C20	132.39(3)	P1–N1–P2	92.38(5)
N2–P1–N3	111.03(5)	N3#–P2–N3	111.66(6)
N2–P1–S1	120.30(4)	N3–P2–P1#	95.43(3)
N2–P1–N1	85.43(4)	S2–P2–P1	144.293(13)
N1–P1–S1	126.07(4)	N1–P2–S2	126.31(4)
N3–P1–S1	119.60(3)	N3–C30–C31	108.90(8)
P2–N3–P1	94.66(4)	N2–C20–C21	108.90(9)
C30–N3–P1	132.45(7)	C30–N3–P2	131.98(7)

Synthesis and Spectroscopic Analysis of $[(^t\text{BuNP})_2(^t\text{BuN})_2\text{P}]^+\text{SO}_3\text{CF}_3^-$, **67**

Reaction of **49** with silver triflate in THF for 30 minutes yielded compound **67** (Scheme 29). The flask containing the reaction mixture was wrapped with aluminum foil to prevent the photo-reduction of Ag(I) to Ag(0). We experienced polymerization of THF which introduced unexpected difficulties in the synthesis and isolation of **67**. This is probably caused by the presence of silver(I) salts (AgCl and AgOTf), which have previously been observed to cause polymerization of THF.¹⁶³ Compound **67** is an ammonium salt of cyclodiphosphazanes because the formal positive charge is on one of the nitrogen atoms since this nitrogen atom donates its lone pair of electrons to form a dative bond with the phosphorus atom from which the chloride was lost.



Scheme 29. Synthesis of **67**.

The ¹H NMR spectrum of **67** (Figure 62) shows two peaks at 1.73 and 1.46 ppm for the corresponding quaternary and primary *tert*-butyl groups in a 1 to 3 ratio. The *tert*-butyl group on the ammonium nitrogen is different from the other three *tert*-butyl groups. This splitting pattern shows that the positive charge is certainly localized on one nitrogen atom in solution. The ¹³C{¹H} NMR spectrum of **67** (Figure 63) shows two quartets at 60.65 and 22.81 ppm and two triplets at 57.23 and 31.20 ppm. The quartet at 22.81 ppm likely represents the triflate carbon due to coupling to 3 fluorine atoms. All three

phosphorus atoms in Compound **67** are chemically and magnetically equivalent making them identical and thus giving rise to only one peak at 210.4 ppm in the $^{31}\text{P}\{^1\text{H}\}$ NMR spectrum (Figure 64).

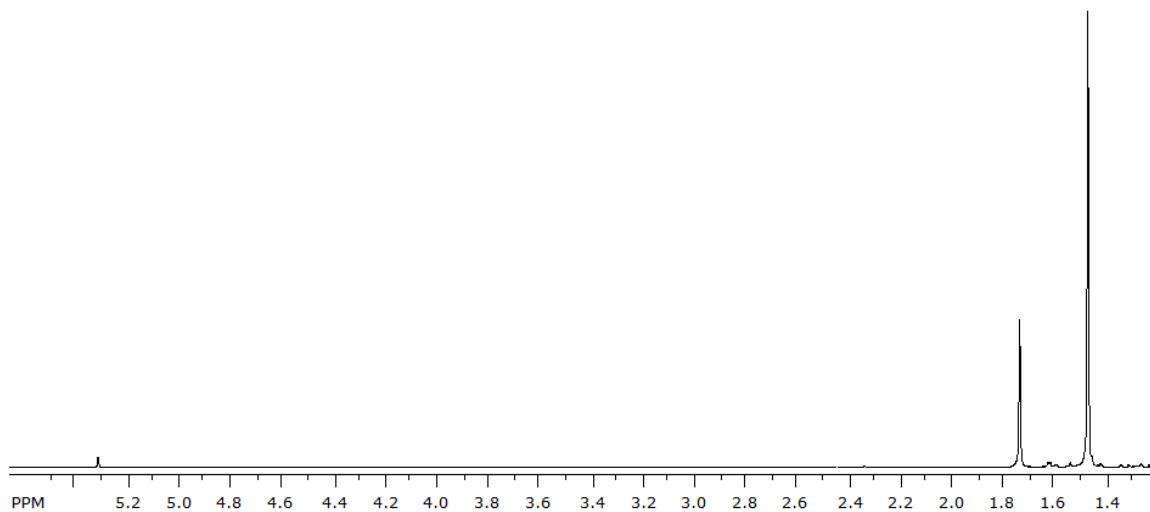


Figure 62. ^1H NMR Spectrum of **67**.

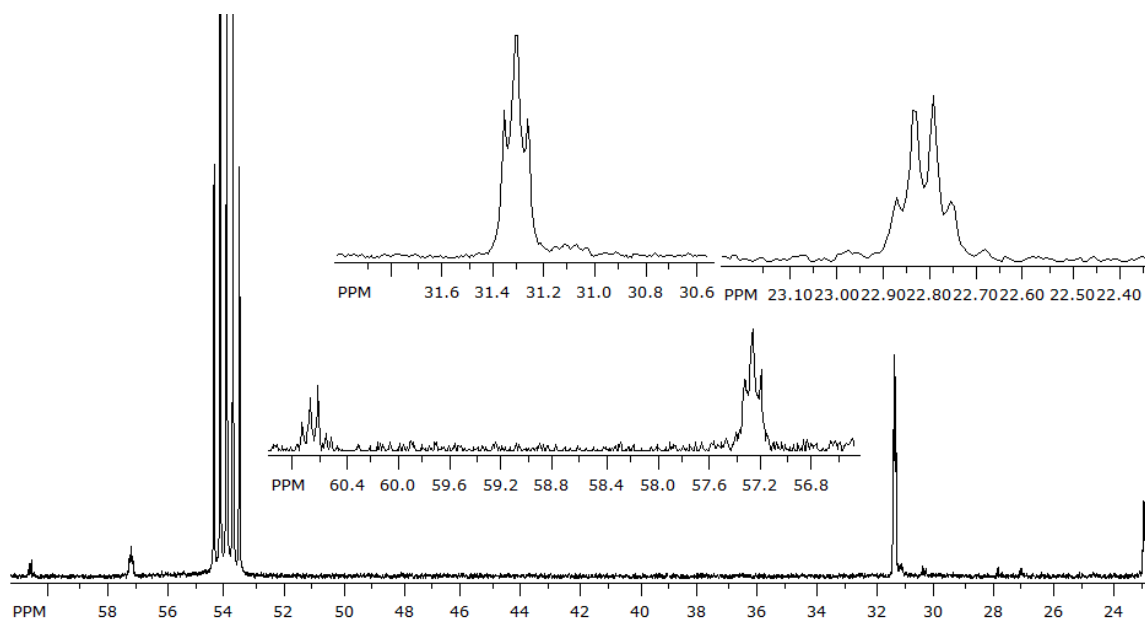


Figure 63. $^{13}\text{C}\{^1\text{H}\}$ NMR Spectrum of **67**.

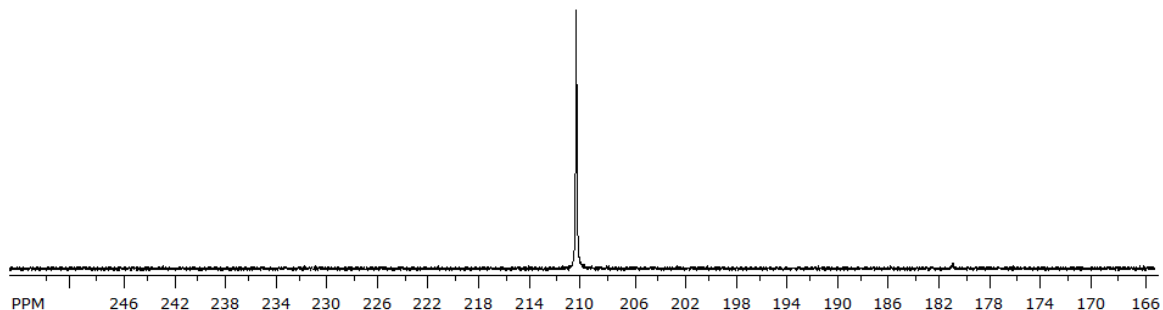


Figure 64. $^{31}\text{P}\{^1\text{H}\}$ NMR Spectrum of **67**.

Solid-state Structure of $[(^t\text{BuNP})_2(^t\text{BuN})_2\text{P}]^+ \text{SO}_3\text{CF}_3^-$, **67**

Compound **67** was isolated as colorless, needle-shaped crystals from a cold (-20 °C) concentrated THF solution. The solid-state structure of **67** with a partial atom numbering scheme is shown in Figure 65, while the crystal data and selected bond parameters are listed in Tables 23 and 24, respectively. The compound crystallizes in the cubic space group $P2_13$ (#189) with four molecules per unit cell. The crystal structure of **67** depicts three P_2N_2 rings fused together which is likely also stabilized by the electrostatic interactions between the ammonium cation center and the negative charge from the triflate ion.

The molecule sits on a three-fold axis which goes through C20, N2, and P1. However, **67** is not C_3 -symmetric because of a crystallographic disorder. Due to this disorder the molecule is missing a P2 atom at the corner of what would have been a cube. It is safe to argue that compound **67** possesses a pseudo- C_3 symmetry (Figure 66). Each of the four nitrogen atoms in the molecule has a *tert*-butyl substituent and it is also bonded to two phosphorus atoms. The ammonium nitrogen atom is crystallographically identical to all the other three nitrogen atoms, while each of the three phosphorus atoms is bonded to three nitrogen atoms in the polycyclic cage.

The P–N bonds in **67**, 1.749(4)–1.842(5) Å, are comparable to the P–N bonds in [4,4′-bipyridine·P(OCH₂CF₃)₂=NSiMe₃]OTf (1.777(3) and 1.800(3) Å),¹⁶⁴ but they are longer than the P–N bonds in [(*i*-Pr₂N)₂P]⁺ (1.611(4) and 1.615(4) Å),¹⁶⁵ [(Me₃SiNP)₂[(Me₃Si)₂N]₂]⁺[SbF₆][−] (1.640(7) and 1.697(7) Å),¹³⁹ and [P(PhN)₂C₁₀H₆]OTf (1.635(2) and 1.632(2) Å).¹⁶⁶

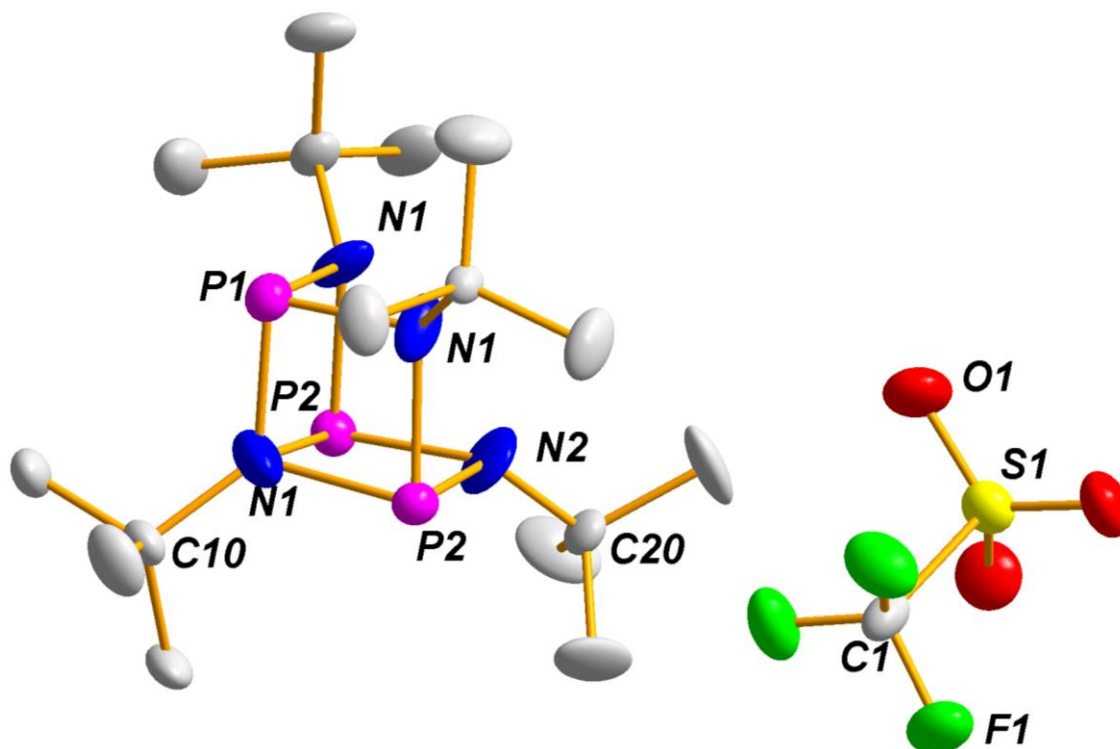


Figure 65. Solid-state structure and partial labelling scheme of **67**. With the exception of carbon (35 %) all atoms are drawn at the 50 % probability level.

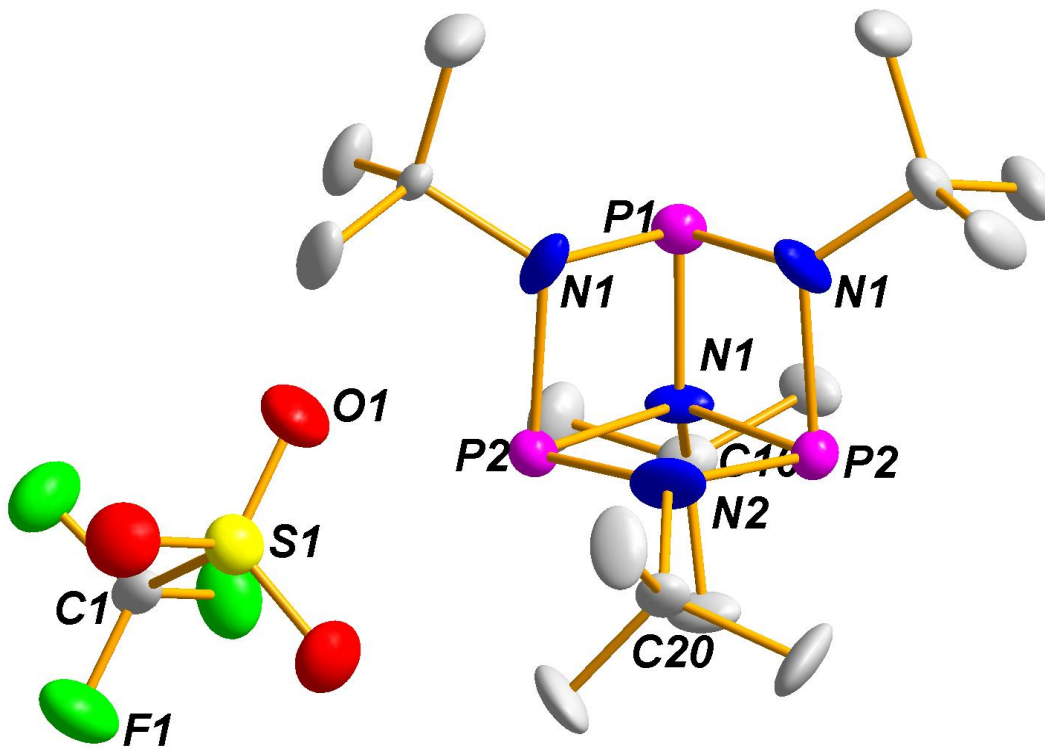


Figure 66. Solid-state structure of **67** showing its pseudo- C_3 symmetry.

Table 23. Crystal and structure refinement data for compound **67**.

Chemical Formula	C ₁₇ H ₃₆ F ₃ N ₄ O ₃ P ₃ S
fw	526.47
T/K	173(2)
$\lambda/\text{\AA}$	0.71073
Crystal system	Cubic
Space group	<i>P</i> 2 ₁ 3 (#189)
<i>a</i> /\AA	13.7390(2)
<i>b</i> /\AA	13.7390(2)
<i>c</i> /\AA	13.7390(2)
$\alpha/^\circ$	90
$\beta/^\circ$	90
$\gamma/^\circ$	90
<i>V</i> /\AA ³	2593.38(7)
<i>Z</i>	4
$\rho(\text{calc}) \text{ g cm}^{-3}$	1.348
μ/mm^{-1}	0.356
F(000)	1112
Completeness (%)	99.90
Reflections collected	28648
Independent reflections	2033 [<i>R</i> _{int} = 0.0269]
$R_w(F^2)^b$ [<i>I</i> > 2σ(<i>I</i>)]	<i>R</i> ₁ = 0.0635, <i>wR</i> ₂ = 0.1683
$R(F)^a$ (all data)	<i>R</i> ₁ = 0.0665, <i>wR</i> ₂ = 0.1721

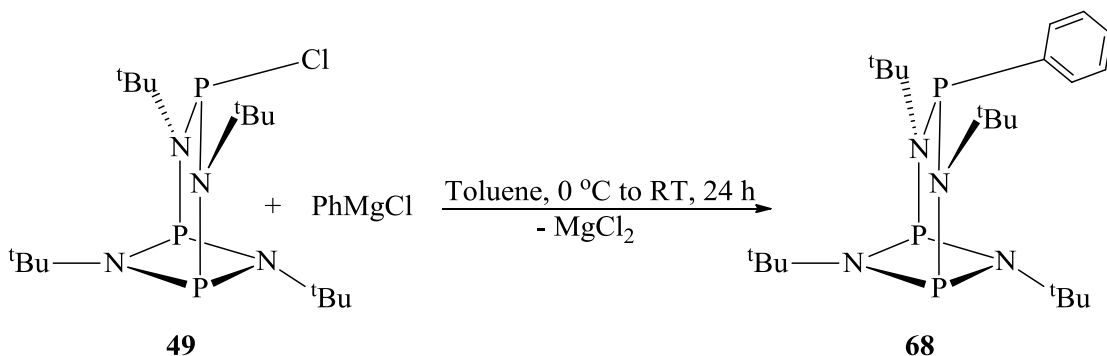
^a $R = \sum |F_o - F_c| / \sum |F_o|$. ^b $R_w = \{ [\sum w(F_o^2 - F_c^2)] / [\sum w(F_o^2)] \}^{1/2}$; $w = 1 / [\sigma^2(F_o)^2 + (xP)^2 + yP]$, where $P = (F_o^2 + 2F_c^2) / 3$.

Table 24. Selected bond lengths (Å) and angles (°) for **67**.

Bond Lengths			
P1–N1	1.749(4)	P2–N1	1.871(4)
P1–N1#	1.749(4)	P2–N2	1.842(5)
P1–P2	2.6575(16)	P2–N1#	1.881(5)
S1–O1	1.409(4)	N1–C10	1.482(4)
S1–O1#	1.409(4)	N2–C20	1.385(9)
S1–C1	1.932(8)	C10–C11	1.480(7)
F1–C1	1.289(4)	C20–C21	1.479(7)
Bond Angles			
O1#–S1–O1	115.83(13)	N2–P2–N1#	87.2(2)
O1–S1–C1	101.94(19)	N1–P2–N1#	82.0(2)
O1#–S1–C1	101.94(19)	N2–P2–P1	87.1(2)
N1–P1–N1#	89.49(17)	N1–P2–P2#	86.74(13)
P2–P1–P2#	60.63(5)	C10–N1–P1	126.6(3)
N2–P2–N1	87.5(2)	P1–N1–P2	94.41(19)
F1–C1–S1	107.6(4)	C20–N2–P2	122.8(2)
F1–C1–F1#	111.3(3)	P2–N2–P2#	93.5(3)

Synthesis and Spectroscopic Analysis of $\{[(^t\text{BuNP})_2(^t\text{BuN})_2]\text{PPh}\}$, **68**

The reaction of compound **49** with PhMgCl at RT in toluene yielded compound **68** in 88 % yield (Scheme 30). We attempted previously to synthesize **68** from the interaction of **48** with PhPCl_2 and instead obtained the previously reported diphenyldiphosphine.⁵⁵ Compound **68** is the first example of a phenyl-substituted mono-phosphorus derivative of cyclodiphosphazanes.



Scheme 30. Synthesis of **68**.

The ^1H NMR spectrum of **68** (Figure 67) shows three singlets at 1.62, 1.29, and 1.00 ppm in the ratio of 2:1:1, respectively representing the three different *tert*-butyl protons. The *tert*-butylamino protons appear at 1.62 ppm. The location of the phenyl group on the phosphorus atom above the P_2N_2 ring makes the *tert*-butyl substituents of the imino nitrogen atoms diastereotopic, resulting in two proton NMR signals. The *tert*-butylimino protons that are located on the same side as the phenyl group appear at 1.00 ppm, while the other *tert*-butylimino protons resonate at 1.29 ppm. The three different aromatic protons appear as three sets of triplets of doublets at 7.82, 7.21 and 7.06 ppm. This is because the *ortho* protons couple to the P atom and to the *meta* protons, while the *meta* protons couple to both the *ortho* and the *para* protons, and the *para* proton couple to the *meta* protons. There are eight signals in the $^{13}\text{C}\{^1\text{H}\}$ NMR spectrum of **68** as shown

in Figure 68. The phenyl carbons appear as three sets of doublets at 152.0, 129.3, and 126.5 ppm. The respective quaternary *tert*-butylamino and *tert*-butylimino carbons appear as doublet of doublets at 57.38 ppm and as doublet of triplets at 32.79 ppm. While the primary *tert*-butylamino and *tert*-butylimino carbons appear respectively as triplets at 32.48 and 31.04 ppm. The $^{31}\text{P}\{^1\text{H}\}$ NMR spectrum of **68** (Figure 69) shows two peaks: a doublet at 203 ppm for the two equivalent phosphorus atoms in the P_2N_2 ring and a singlet at 69.7 ppm for the P atom bearing the phenyl group. All attempts so far to obtain single crystals of compound **68** for X-ray studies have proved futile.

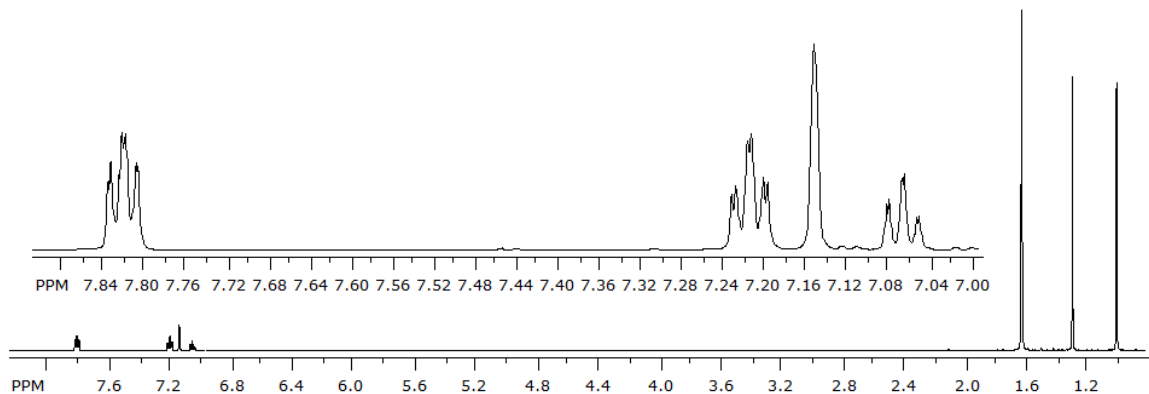


Figure 67. ^1H NMR Spectrum of **68**.

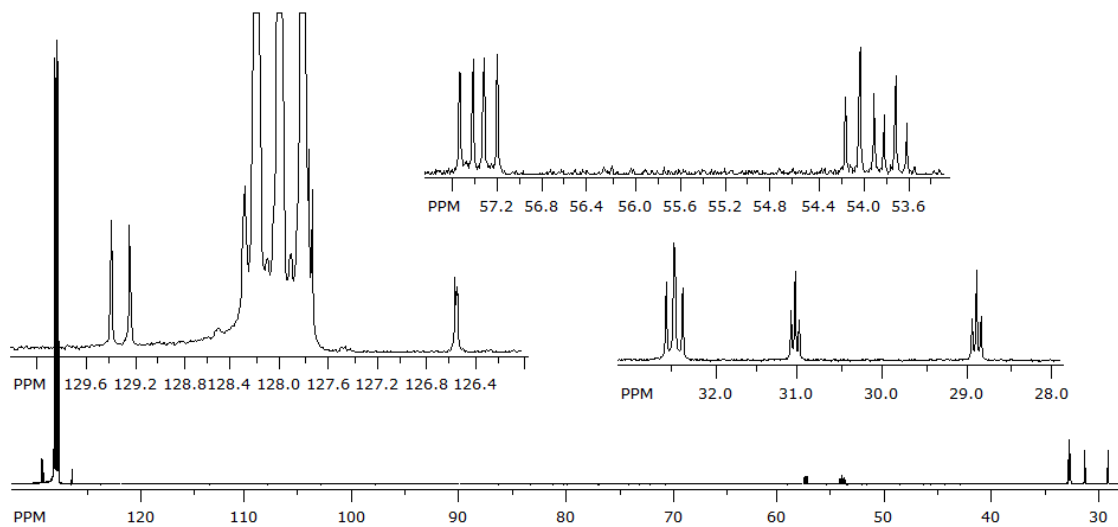


Figure 68. $^{13}\text{C}\{^1\text{H}\}$ NMR Spectrum of **68**.

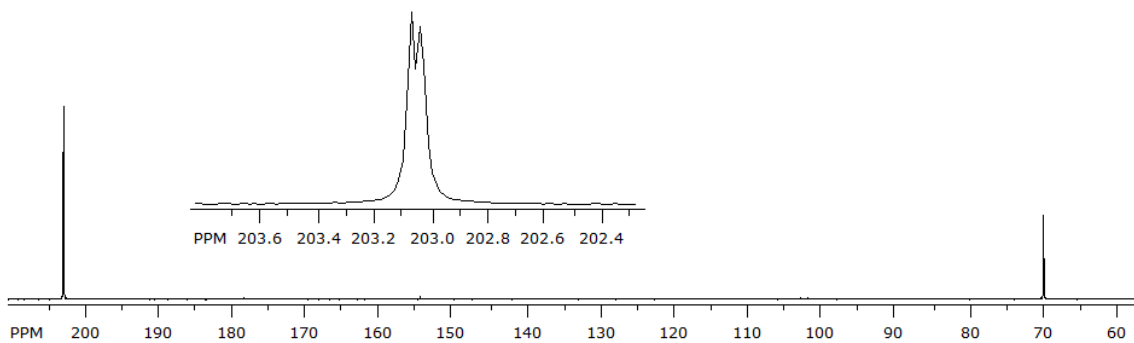
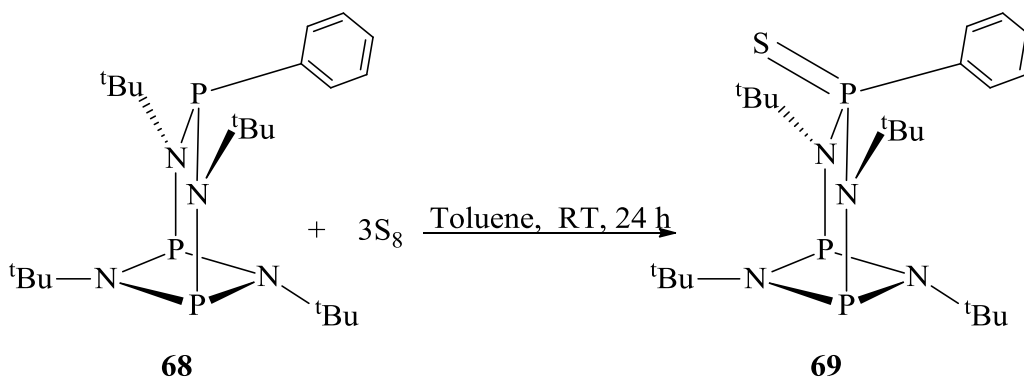


Figure 69. $^{31}\text{P}\{^1\text{H}\}$ NMR Spectrum of **68**.

Synthesis and Spectroscopic Analysis of $\{[(^t\text{BuNP})_2(^t\text{BuN})_2](\text{P}=\text{S})\text{Ph}\}$, **69**

Oxidation of compound **68** with 3 equivalents of sulfur at RT in toluene for 24 h gave compound **69** in 71 % yield (Scheme 31). Only the phosphorus atom bearing the phenyl group was oxidized.



Scheme 31. Synthesis of **69**.

The ^1H NMR spectrum of **69** shown in Figure 70 depicts three singlets at 1.48, 1.43, and 1.40 ppm in the ratio of 1:2:1, respectively representing the three different *tert*-butyl protons. The *tert*-butylamino protons appear at 1.43 ppm. The location of the phenyl group and the sulfide group on the phosphorus atom above the P_2N_2 ring makes the *tert*-butyl substituents of the imino nitrogen atoms diastereotopic, resulting in two proton NMR signals. The *tert*-butylimino protons that are located on the same side as the phenyl group appear at 1.40 ppm, while the other *tert*-butylimino protons resonate at 1.48 ppm. Meanwhile the three different aromatic protons appear as a doublet of doublets at 8.69 ppm, and two triplets at 7.07, and 7.06 ppm. The doublet of doublets at 8.69 ppm represents the *ortho* protons because they couple to the *meta* protons and the phosphorus atom. The two triplets at 7.07 and 7.06 ppm represents the *meta* and *para* protons, respectively.

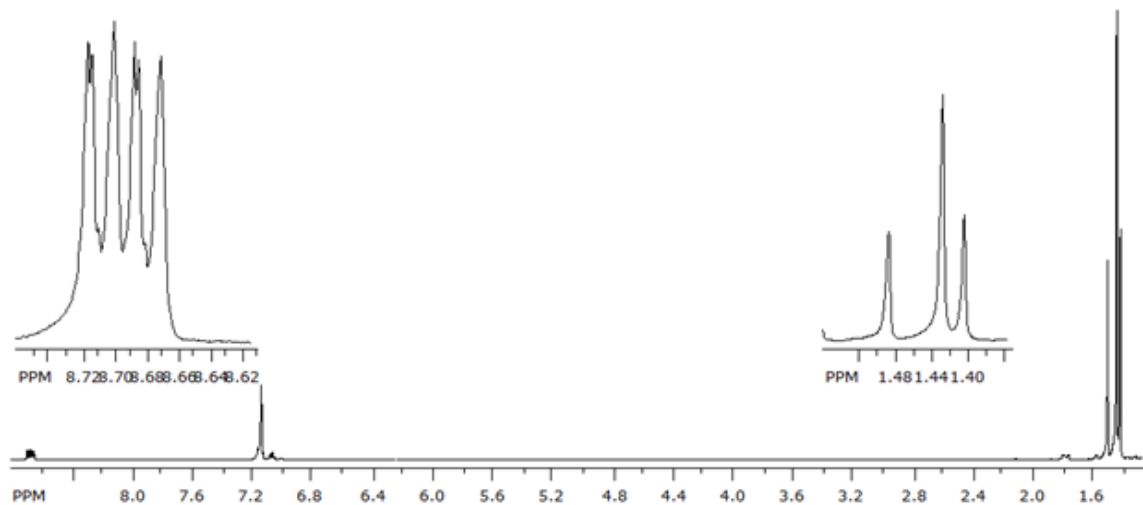


Figure 70. ^1H NMR Spectrum of **69**.

The $^{13}\text{C}\{^1\text{H}\}$ spectrum of **69** as shown in Figure 71 has eight signals that resonate between 133.1 and 29.98 ppm. The phenyl carbons appear as three sets of doublets at 133.3, 130.2, and 127.6 ppm. The respective quaternary and primary *tert*-butylamino carbons appear as a doublet of triplets at 61.30 ppm and as a multiplet at 32.75 ppm. The quaternary *tert*-butylimino carbons appear as triplets at 54.06 and 53.06 ppm, while the primary *tert*-butylimino carbons also appear as triplets at 30.54 and 29.98 ppm. The $^{31}\text{P}\{^1\text{H}\}$ NMR spectrum of **69** (Figure 72) shows two peaks: a doublet at 193.3 ppm representing the two identical phosphorus atoms in the P_2N_2 ring and a triplet at 53.44 ppm representing the P(V) atom bearing the phenyl group and sulfur.

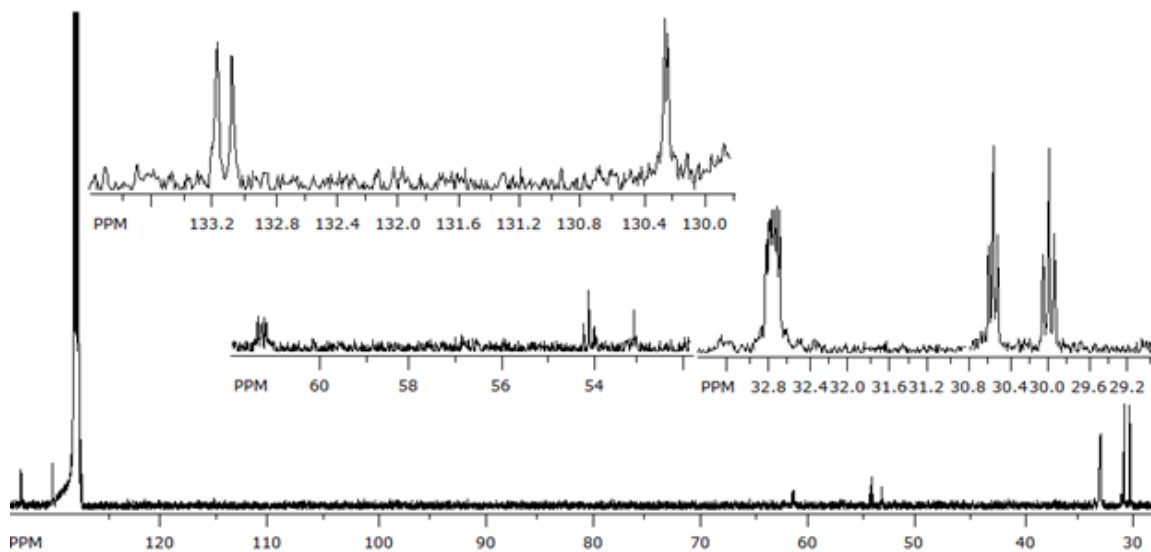


Figure 71. $^{13}\text{C}\{^1\text{H}\}$ NMR Spectrum of **69**.

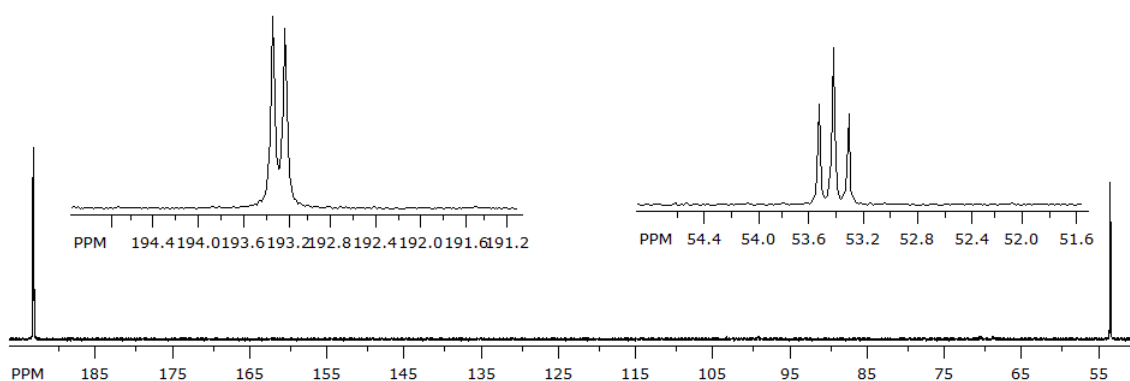


Figure 72. $^{31}\text{P}\{^1\text{H}\}$ NMR Spectrum of **69**.

Solid-state Structure of $\{[(^t\text{BuNP})_2(^t\text{BuN})_2](\text{P}=\text{S})\text{Ph}\}$, **69**

Colorless, block-shaped crystals of **69** were grown from a concentrated toluene solution. The solid-state structure of **69** with a partial atom numbering scheme is shown in Figure 73, while the crystal data and selected bond parameters are listed in Tables 25 and 26, respectively. Compound **69** crystallizes in the triclinic space group $P\bar{1}$ (#2) with one independent molecule per unit cell. One of the ring phosphorus atoms is partially (8%) oxidized. Compound **69** is a non-crystallographic C_s -symmetric molecular cage, made up of a slightly puckered P_2N_2 ring (angle sum = 355.5°) and a polycyclic core,

which is composed entirely of nitrogen and phosphorus atoms. The crystallographic mirror plane, which contains the central bridgehead phosphorus atom, the phenyl substituent, and the sulfur atom bisects the slightly puckered P₂N₂ ring. The bridgehead phosphorus(V) atom has a pseudo-tetrahedral geometry and it is coordinated to two planar exocyclic nitrogen atoms, a phenyl group, and a sulfur atom. The P₂N₂ ring contains two almost perpendicular *tert*-butylamido groups bonded to the phosphorus atoms and two *tert*-butyl substituents bonded to the nitrogen atoms of the ring. The *tert*-butyl group on N1 is almost coplanar with the P₂N₂ ring, while the *tert*-butyl substituent of N2 is slightly bent below the P₂N₂ ring because of the steric interaction between this group and the phenyl substituent on the bridgehead phosphorus atom. This steric interaction makes N2 pyramidal, whereas the other three nitrogen atoms are almost perfectly planar.

The P–N bonds in **69**, 1.6989(12)–1.7391(12) Å, are comparable to the P–N bonds in {[^tBuNP)₂(^tBuN)₂]PCl}, 1.689(4)–1.733(4) Å,³⁵ {[^tBuNP)₂(^tBuN)₂]Ga(^tBuNPN^tBu)}, 1.694(4)–1.742(3) Å,³⁶ and [(PhNH)P₂(NPh)₂]₂NPh, 1.659(8)–1.732(6) Å,⁴¹ but they are shorter than P–N single bonds, 1.79 Å.¹ The phenyl substituent on the bridgehead phosphorus atom is perfectly planar with angle sum around C90 = 359.9°. The P–C bond in **69**, 1.8234(5) Å, is midway between the P–C bond lengths in PPh₃, 1.828(3)–1.839(3) Å,¹⁴⁵ but slightly shorter than the two almost identical P–C bonds in compound **52B**, 1.8478(19) and 1.8457(17) Å, and tris(3,5-dimethyl-4-methoxyphenyl)-phosphine, 1.844(6) and 1.840(5) Å.¹⁶⁷ Meanwhile the P=S bond in **58**, 1.9442(5) Å, is longer than the P=S bonds in compounds **37** (1.9283(7) Å), **38** (1.9268(10) Å), **39** (1.9080(5) Å), and **40** (1.9097(8) Å).

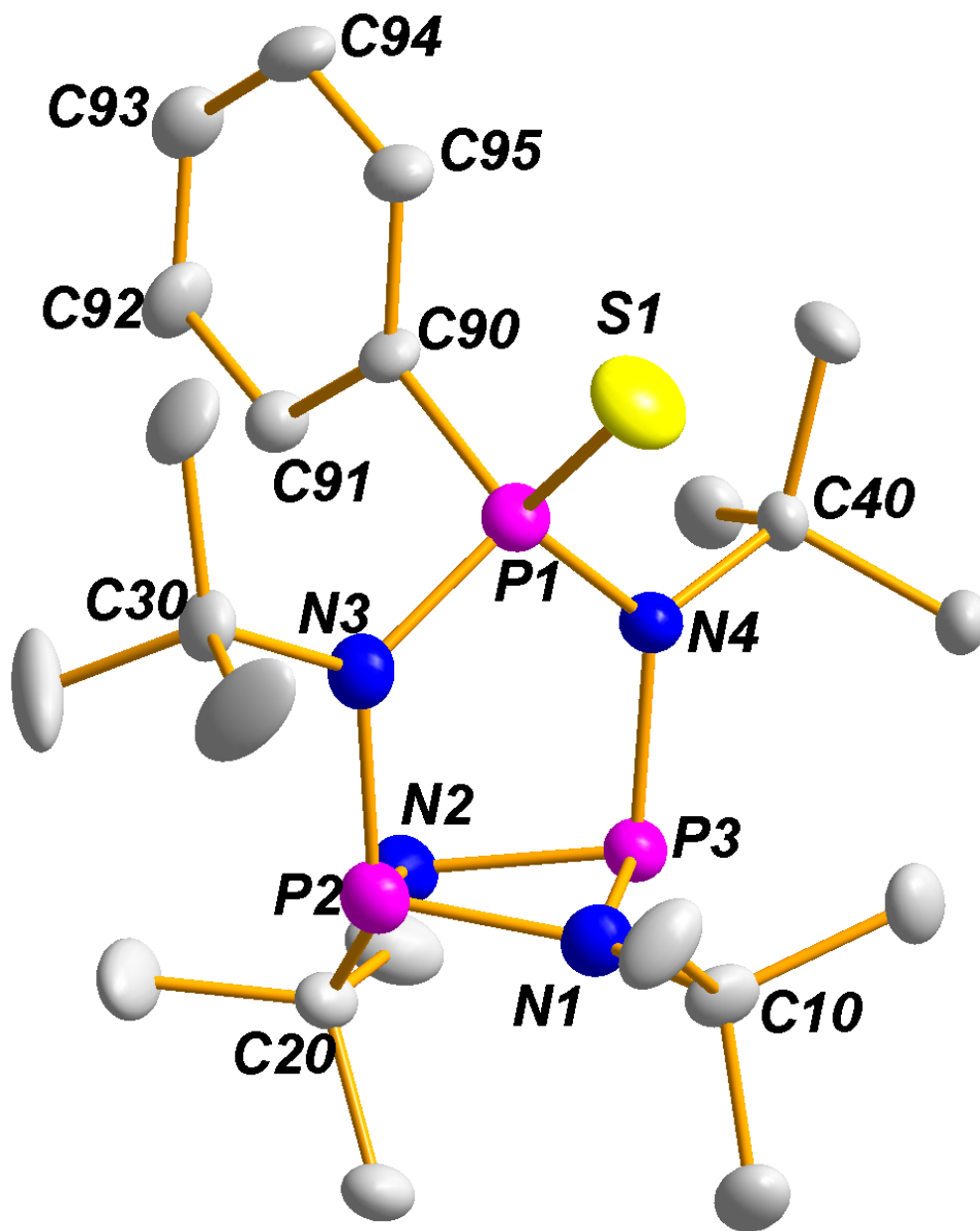


Figure 73. Solid-state structure and partial labelling scheme of **69**. With the exception of carbon (35 %) all atoms are drawn at the 50 % probability level.

Table 25. Crystal and structure refinement data for compound **69**.

Chemical Formula	C ₂₂ H ₄₁ N ₄ P ₃ S
fw	486.57
T/K	173(2)
$\lambda/\text{\AA}$	0.71073
Crystal system	Triclinic
Space group	P-1 (#2)
$a/\text{\AA}$	9.8617(3)
$b/\text{\AA}$	10.4953(3)
$c/\text{\AA}$	14.3072(5)
$\alpha/^\circ$	75.326(2)
$\beta/^\circ$	73.407(2)
$\gamma/^\circ$	71.557(2)
$V/\text{\AA}^3$	1324.45(8)
Z	1
$\rho(\text{calc}) \text{ g cm}^{-3}$	1.250
μ/mm^{-1}	0.322
F(000)	537.0
Completeness (%)	99.40
Reflections collected	41763
Independent reflections	10989 [$R_{\text{int}} = 0.0261$]
$R_w(F^2)^b$ [$I > 2\sigma(I)$]	$R_1 = 0.0511$, $wR_2 = 0.1515$
$R(F)^a$ (all data)	$R_1 = 0.0609$, $wR_2 = 0.1671$

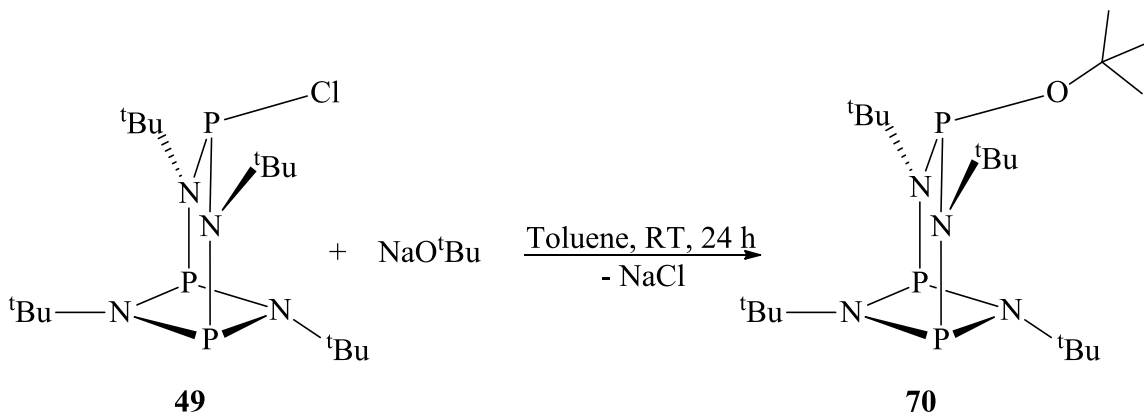
^a $R = \sum |F_o - F_c| / \sum |F_o|$. ^b $R_w = \{ [\sum w(F_o^2 - F_c^2)] / [\sum w(F_o^2)^2] \}^{1/2}$; $w = 1 / [\sigma^2(F_o)^2 + (xP)^2 + yP]$, where $P = (F_o^2 + 2F_c^2) / 3$.

Table 26. Selected bond lengths (Å) and angles (°) for **69**.

Bond Lengths			
P1–N3	1.7009(12)	P3–N1	1.7114(12)
P1–N4	1.6989(12)	P3–N4	1.7243(11)
P1–C90	1.8234(15)	P3–N2	1.7391(12)
P1–S1	1.9442(5)	N1–C10	1.4811(19)
P2–N1	1.7031(13)	N2–C20	1.4900(17)
P2–N2	1.7359(12)	N3–C30	1.5340(18)
P2–N3	1.7262(13)	N4–C40	1.5322(18)
Bond Angles			
N3–P1–N4	106.07(6)	P3–N1–C10	130.92(11)
N3–P1–S1	113.73(5)	P2–N1–C10	132.92(11)
N4–P1–S1	114.64(5)	P2–N2–C20	121.39(11)
N3–P1–C90	104.03(6)	P3–N2–C20	120.79(9)
N4–P1–C90	104.87(6)	P2–N2–P3	92.69(6)
N1–P2–N3	103.51(6)	P1–N3–P2	123.24(7)
N1–P2–N2	83.99(6)	P2–N3–C30	114.71(10)
N3–P2–N2	97.90(6)	P1–N3–C30	121.88(10)
N1–P3–N4	101.56(6)	P1–N4–P3	123.45(7)
N1–P3–N2	94.85(6)	P3–N4–C40	113.65(9)
N4–P3–N2	100.06(6)	P1–N4–C40	122.54(9)
P2–N1–P3	94.85(6)	N2–C20–C23	112.42(12)

Synthesis and Spectroscopic Analysis of $\{[(^t\text{BuNP})_2(^t\text{BuN})_2]\text{PO}^t\text{Bu}\}$, **70**

Compound **70** was obtained in 89 % yield by the reaction of compound **49** with one equivalent of NaO^tBu in toluene for 24 h (Scheme 32). The synthesis involved the straight forward replacement of the chloride group by the *tert*-butoxy group followed by filtration of NaCl from the reaction mixture using a medium-porosity frit.



Scheme 32. Synthesis of **70**.

The ^1H NMR spectrum of **70** as shown in Figure 74 depicts four singlets at 1.55, 1.51, 1.42, and 1.39 ppm representing the four different *tert*-butyl protons. The *tert*-butylamino protons appear at 1.55 ppm. The location of the *tert*-butoxy group on the phosphorus atom above the P_2N_2 ring makes the *tert*-butyl substituents of the imino nitrogen atoms diastereotopic, resulting in two proton NMR signals. The *tert*-butylimino protons that are located on the same side as the *tert*-butoxy group appear at 1.39 ppm, while the other *tert*-butylimino protons resonate at 1.42 ppm, while the *tert*-butoxy protons appear at 1.51 ppm. The $^{13}\text{C}\{^1\text{H}\}$ NMR spectrum of **70** (Figure 75) shows seven signals that resonate between 76.68 and 29.19 ppm. The quaternary and primary *tert*-butoxy carbons appear as doublets at 76.68 and 31.81 ppm, respectively. The doublets are a result of coupling with the bridgehead phosphorus atom. The quaternary and primary

tert-butylamino carbons resonate as a multiplet at 57.13 ppm and a triplet 30.00 ppm, respectively. This is due to coupling with the two phosphorus atom of the ring. The quaternary and primary *tert*-butylimino carbons resonate as triplets at 53.00 and 29.19 ppm, respectively. This is due to coupling with the two phosphorus atom of the ring. As expected, the $^{31}\text{P}\{^1\text{H}\}$ NMR spectrum of **70** (Figure 76) shows two peaks: a doublet at 200.2 ppm representing the two identical phosphorus atoms in the P_2N_2 ring and a triplet at 117.8 ppm representing the P atom bearing the *tert*-butoxy group. Single X-ray crystal analysis of compound **70** was attempted, but the data could not be refined because of crystallographic disorder.

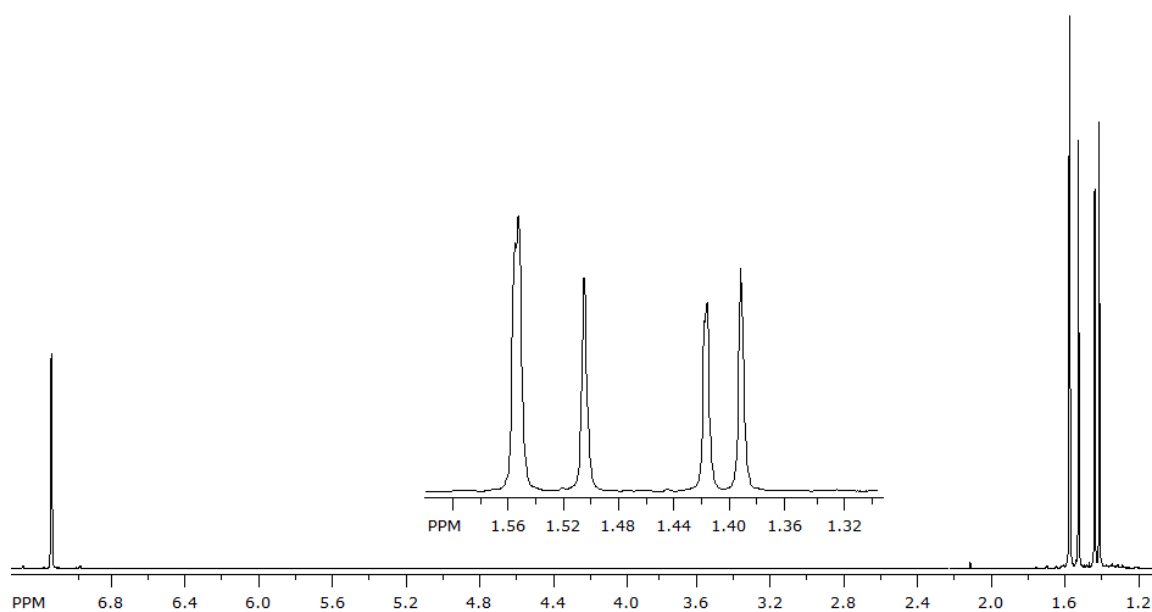


Figure 74. ^1H NMR Spectrum of **70**.

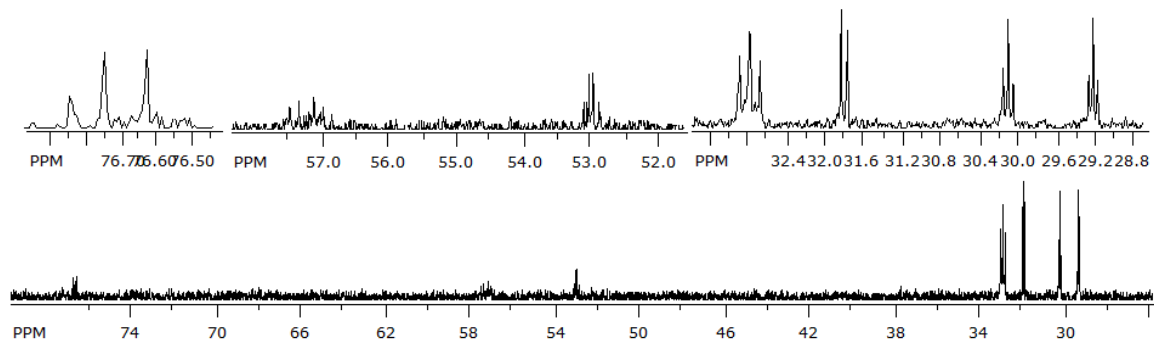


Figure 75. $^{13}\text{C}\{^1\text{H}\}$ NMR Spectrum of **70**.

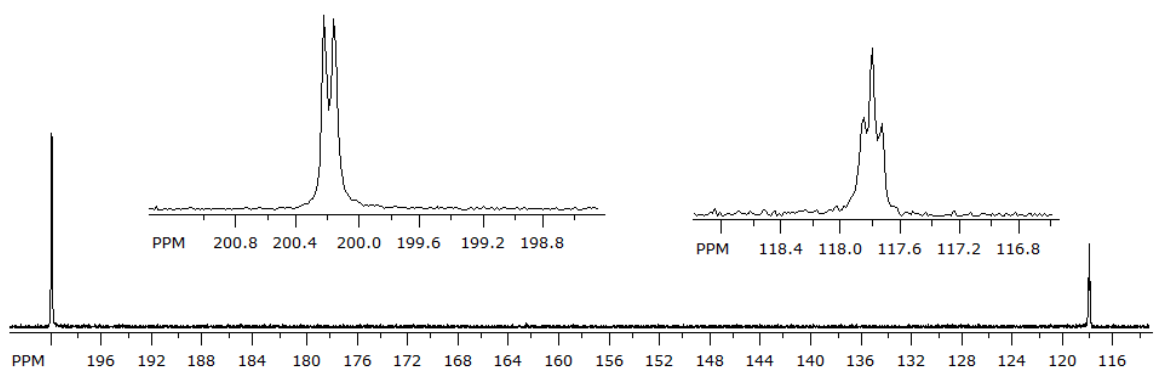
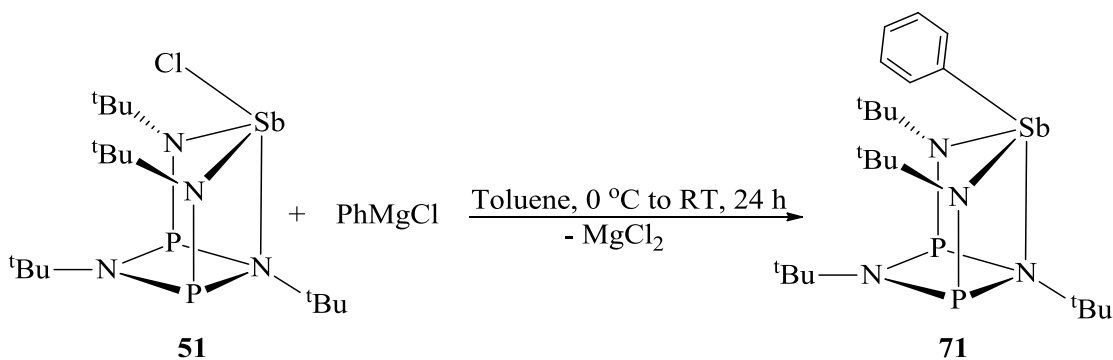


Figure 76. $^{31}\text{P}\{^1\text{H}\}$ NMR Spectrum of **70**.

Synthesis and Spectroscopic Analysis of $\{[(^t\text{BuNP})_2(^t\text{BuN})_2]\text{SbPh}\}$, **71**

The reaction of compound **51** with PhMgCl at RT in toluene yielded compound **71** in 90 % yield (Scheme 33). Magnesium chloride was filtered out of the reaction mixture with a medium-porosity frit. The synthesis of compound **71** was similar to that of its phosphorus analogue, **68**. Although both compounds **68** and **71** were isolated from toluene, compound **68** crystallized as colorless plates, whereas compound **71** crystallized as colorless, hexagonal crystals. Compound **71** is the first example of a phenyl-substituted antimony derivative of a cyclodiphosphazane.



Scheme 33. Synthesis of **71**.

The ^1H NMR spectrum of **71** (Figure 77) shows six different signals. There are three singlets in the aliphatic region at 1.48, 1.45, and 1.20 ppm in the ratio of 1:1:2, respectively representing the three different *tert*-butyl protons. The location of the phenyl group on the antimony atom above the P_2N_2 ring makes the *tert*-butyl substituents of the imino nitrogen atoms diastereotopic, resulting in two proton NMR signals. The three different aromatic protons appear as a doublet at 8.21 ppm representing the *ortho* protons and two triplets at 7.29 and 7.13 ppm representing the *meta* and *para* protons, respectively. This is because unlike the analogous compound **71**, the *ortho* protons couple only to the *meta* protons resulting in a doublet. Meanwhile the *meta* protons couple to both the *ortho* and the *para* protons, and the *para* proton couples to the *meta* protons giving rise to a set of triplets in each case.

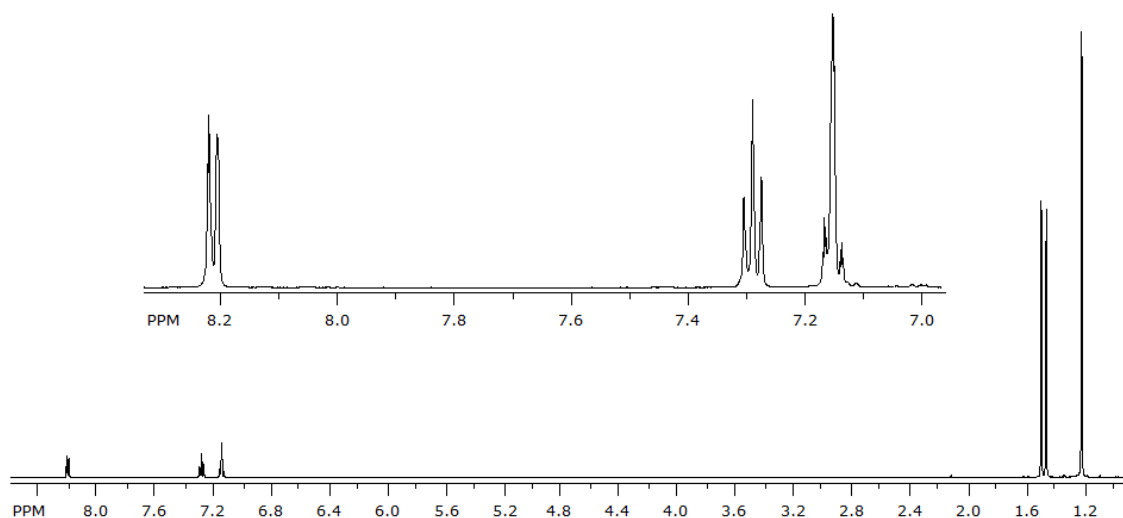


Figure 77. ^1H NMR Spectrum of **71**.

There are nine signals in the $^{13}\text{C}\{^1\text{H}\}$ NMR spectrum of **71** as shown in Figure 78. The phenyl carbons resonate between 156.4 and 128.3 ppm. The respective quaternary and primary *tert*-butylamino carbons appear as doublets at 57.27 and 33.63 ppm due to coupling to one phosphorus center. The quaternary *tert*-butylimino carbons appear as two sets of triplets at 53.75 and 52.88 ppm, while the primary *tert*-butylimino carbons also appear as two sets of triplets at 30.95 and 29.03 ppm. This is due to the coupling of each *tert*-butylimino carbon with two phosphorus centers in the P_2N_2 ring.

The $^{31}\text{P}\{^1\text{H}\}$ NMR spectrum of **71** (Figure 79) shows a singlet at 138.3 ppm, indicating the presence of two equivalent phosphorus atoms in the P_2N_2 ring.

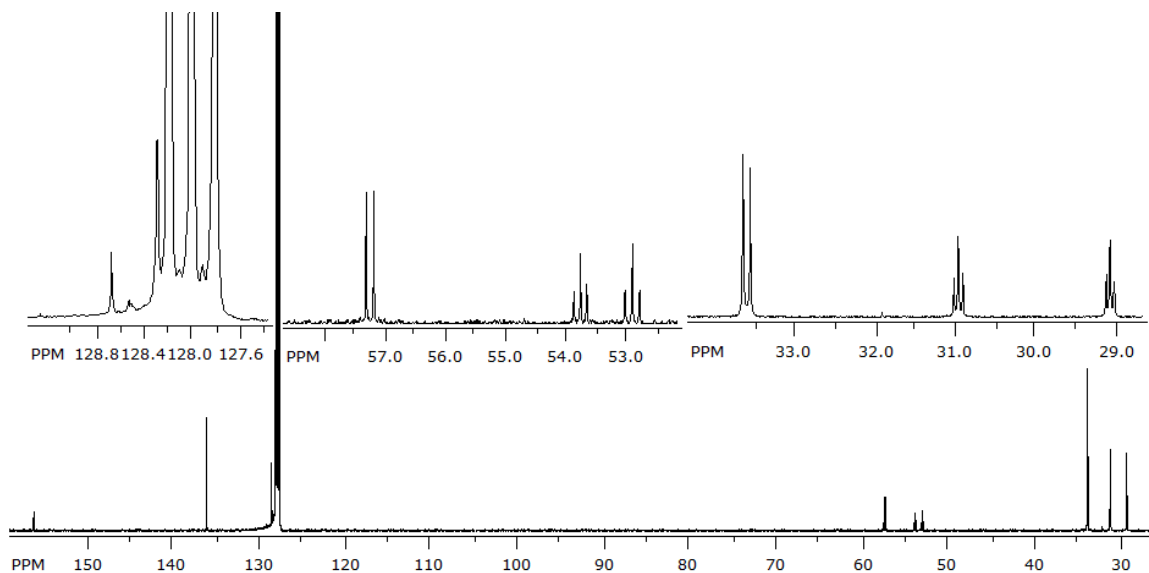


Figure 78. $^{13}\text{C}\{^1\text{H}\}$ NMR Spectrum of **71**.

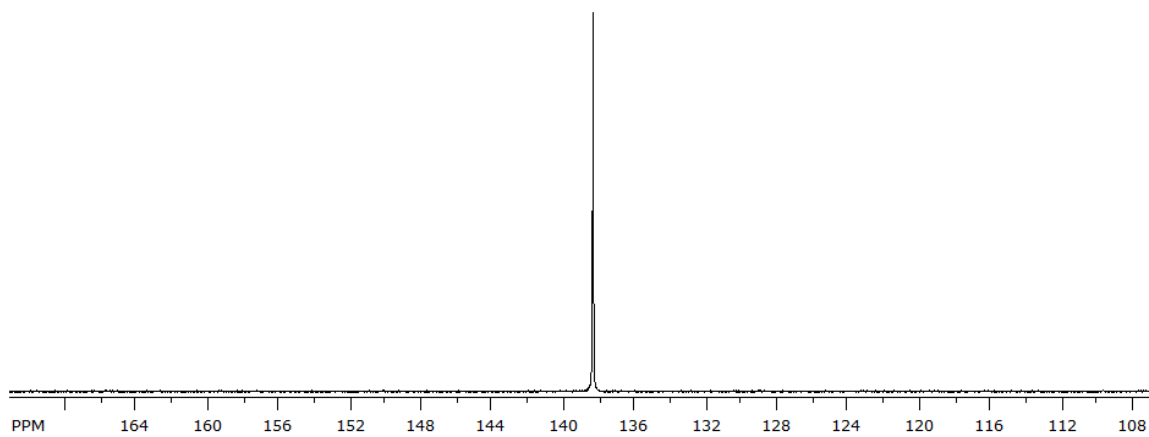


Figure 79. $^{31}\text{P}\{^1\text{H}\}$ NMR Spectrum of **71**.

Solid-state Structure of $\{[(^t\text{BuNP})_2(^t\text{BuN})_2]\text{SbPh}\}$, **71**

Colorless, block-shaped crystals of **71** were isolated from a concentrated toluene solution. The solid-state structure of **71** with a partial atom numbering scheme is shown in Figures 80 and 81, while the crystal data and selected bond parameters are listed in Tables 29 and 30, respectively. Compound **71** crystallizes in the monoclinic space group

$P2_1/n$ (#14) with four molecules per unit cell. The compound is a C_s -symmetric molecular cage, made up of a slightly puckered P_2N_2 ring (angle sum = 355.5°) and a polycyclic core, which is composed entirely of nitrogen, phosphorus, and antimony atoms. The molecule has a crystallographic mirror plane, which contains the central antimony atom and the phenyl substituent, and it bisects the slightly puckered P_2N_2 ring. The P_2N_2 ring contains two almost perpendicular *tert*-butylamino groups bonded to the phosphorus atoms and two *tert*-butyl substituents bonded to the nitrogen atoms of the ring. The antimony atom has a distorted pyramidal geometry and it is coordinated to two planar exocyclic nitrogen atoms, a phenyl group, and one ring-nitrogen atom through a weak dative bond.

The two almost identical Sb–N bonds, 2.1113(10) and 2.1057(10) Å, are comparable to those in the starting compound **51**, 2.100(6) and 2.089(4) Å, $\{[\{PN^tBu\}_2(N^tBu)_2]SbOPh\}$, 2.104(8) and 2.080(8) Å, and $\{[\{PN^tBu\}_2(NPh)_2]SbCl\}$, 2.084(2) and 2.093(2), but they are slightly shorter than the Sb–N bonds in $\{[\{PN^tBu\}_2(N^tBu)_2]SbN(SiMe_3)_2\}$, 2.123(2) and 2.120(2) Å, reported previously.³⁴ Similarly to that in **51**, the dative bond between the antimony atom and the ring-nitrogen atom, 2.774(5) Å, is very long.

Just like in similar C_s -symmetric cyclodiphosphazane compounds,^{26, 27, 116} the endocyclic P–N bonds in **71**, 1.7416(10) and 1.7371(9) Å, are longer than the almost identical exocyclic P–N bonds, 1.6682(10) and 1.6734(10) Å. The phenyl substituent on the antimony atom is perfectly planar with angles around $C1 = 360^\circ$. The Sb–C bond in **71**, 2.1635(12) Å, is slightly longer than that in $[(TPP)Sb(CH_3)(F)]^+PF_6^-$, 2.115(6) Å, and $[(OEP)SbMe_2]^+PF_6^-$, 2.0910(8) Å.¹⁶⁸

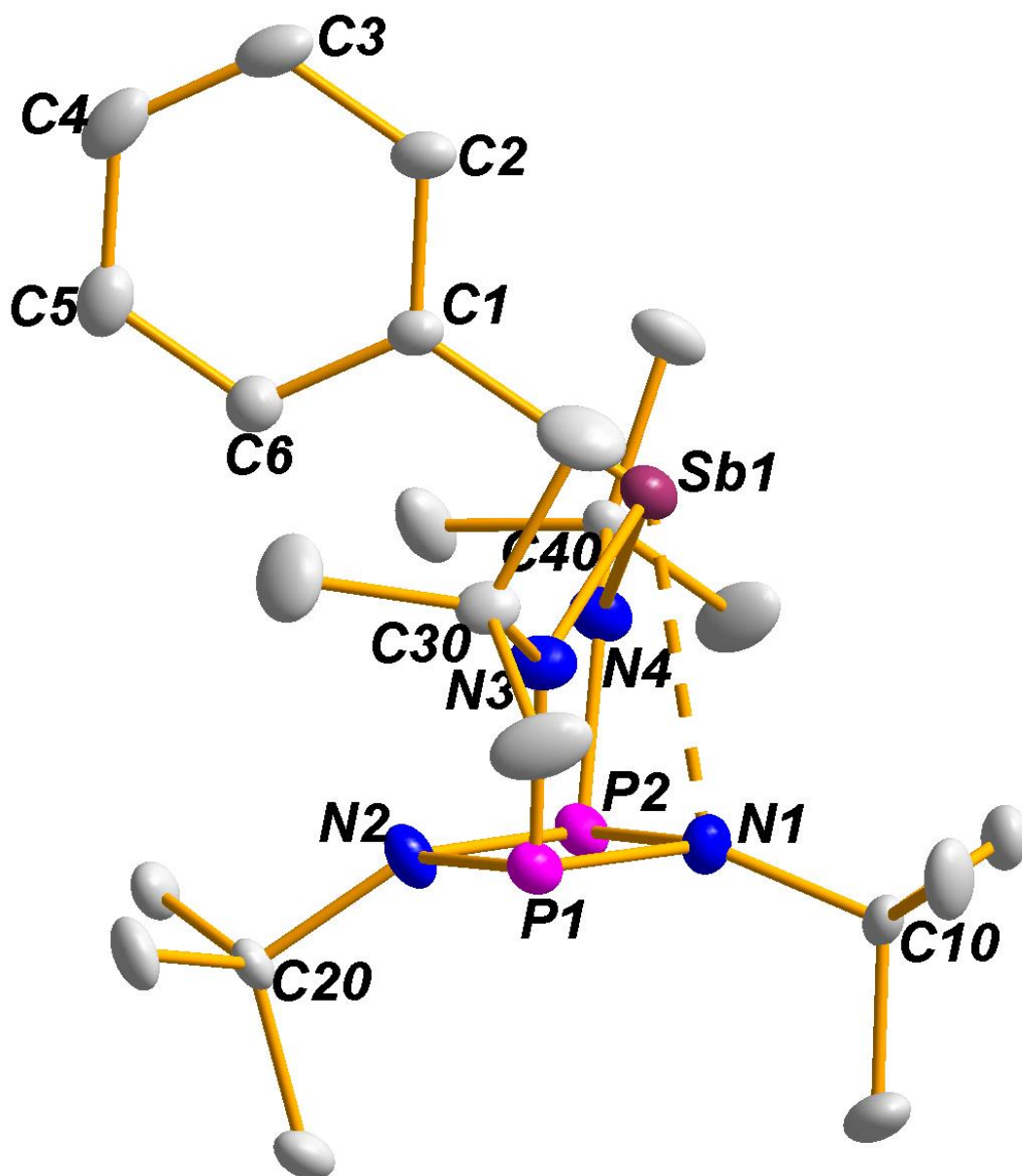


Figure 80. Solid-state structure and partial labelling scheme of **71**. With the exception of carbon (35 %) all atoms are drawn at the 50 % probability level.

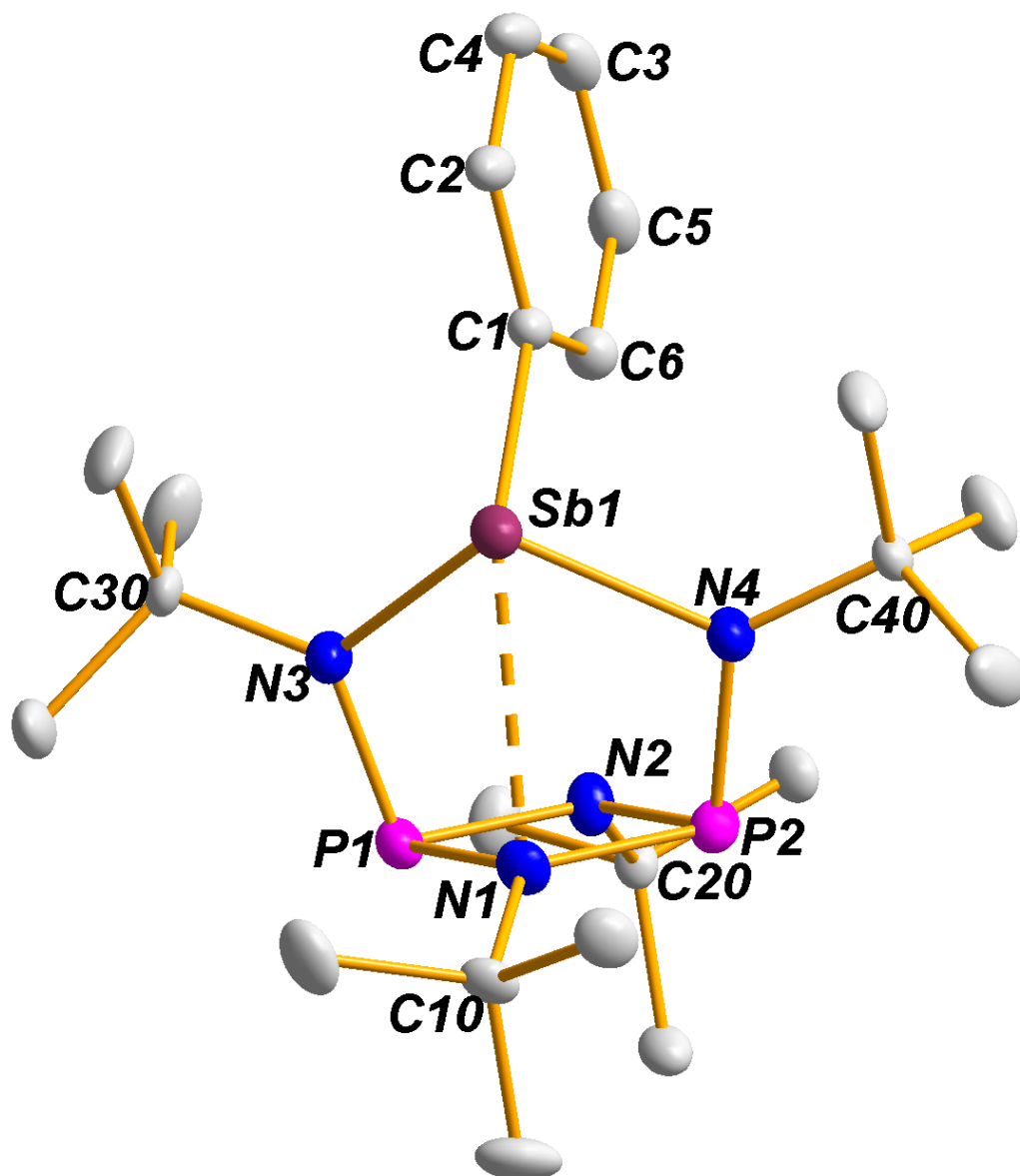


Figure 81. Front view of **71** showing C_s symmetry.

Table 27. Crystal and structure refinement data for compound **71**.

Chemical Formula	C ₂₂ H ₄₁ N ₄ P ₂ Sb
fw	545.31
T/K	100.0
$\lambda/\text{\AA}$	0.71073
Crystal system	Monoclinic
Space group	<i>P</i> 2 ₁ / <i>n</i> (#14)
<i>a</i> /\AA	16.0322(6)
<i>b</i> /\AA	9.6090(4)
<i>c</i> /\AA	18.2097(7)
$\alpha/^\circ$	90
$\beta/^\circ$	110.3634(14)
$\gamma/^\circ$	90
<i>V</i> /\AA ³	2629.88(18)
<i>Z</i>	4
$\rho(\text{calc}) \text{ g cm}^{-3}$	1.377
μ/mm^{-1}	1.186
F(000)	1126.7
Completeness (%)	99.98
Reflections collected	36559
Independent reflections	9401 [<i>R</i> _{int} = 0.0217]
$R_w(F^2)^b$ [<i>I</i> > 2 σ (<i>I</i>)]	<i>R</i> ₁ = 0.0205, <i>wR</i> ₂ = 0.0498
$R(F)^a$ (all data)	<i>R</i> ₁ = 0.0231, <i>wR</i> ₂ = 0.0519

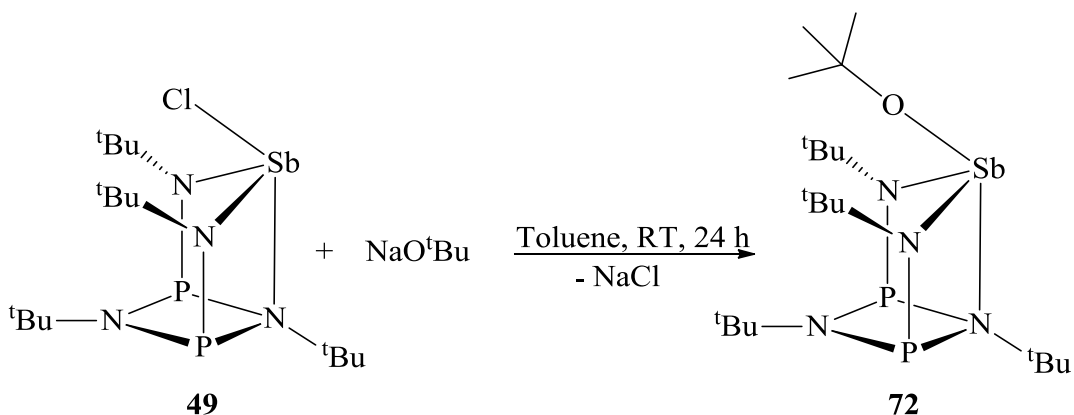
^a $R = \sum |F_o - F_c| / \sum |F_o|$. ^b $R_w = \{ [\sum w(F_o^2 - F_c^2)] / [\sum w(F_o^2)^2] \}^{1/2}$; $w = 1 / [\sigma^2(F_o)^2 + (xP)^2 + yP]$, where $P = (F_o^2 + 2F_c^2) / 3$.

Table 28. Selected bond lengths (Å) and angles (°) for **71**.

Bond Lengths			
Sb1–N3	2.1113(10)	P1–P2	2.6252(4)
Sb1–N4	2.1057(10)	P2–N2	1.7390(9)
Sb1–C1	2.1635(12)	P2–N4	1.6734(10)
P1–N1	1.7371(9)	N1–C10	1.4768(15)
P1–N2	1.7395(10)	N2–C20	1.4778(14)
P1–N3	1.6682(10)	N3–C30	1.4909(15)
P2–N1	1.7416(10)	N4–C40	1.4911(6)
Bond Angles			
N4–Sb1–N3	105.04(4)	P2–N1–P1	97.99(5)
C1–Sb1–N3	94.01(4)	P2–N2–P1	98.00(5)
C1–Sb1–N4	93.51(4)	P1–N3–Sb1	111.78(5)
N2–P1–N1	82.06(5)	P2–N4–Sb1	111.74(5)
N3–P1–N1	95.21(5)	C10–N1–P1	125.42(8)
N3–P1–N2	104.11(5)	C20–N2–P1	123.56(7)
N1–P2–N2	81.95(5)	C30–N3–Sb1	124.08(7)
N4–P2–N1	95.35(5)	C40–N4–Sb1	124.65(7)
N4–P2–N2	103.82(5)	C40–N4–P2	123.10(8)

Synthesis and Spectroscopic Analysis of $\{[(^t\text{BuNP})_2(^t\text{BuN})_2]\text{SbO}^t\text{Bu}\}$, **72**

In a manner similar to the synthesis of **70**, compound **72** was obtained in 79 % yield by the reaction of compound **49** with 1 eq. of NaO^tBu in toluene for 24 h (Scheme 34). This similarity in synthesis is due the fact that **72** is the antimony analogue of **70**. Both compounds were isolated from toluene after filtering off NaCl from the reaction mixture using a medium-porosity frit.



Scheme 34. Synthesis of **72**.

Just like that of its phosphorus analogue **70**, the ^1H NMR spectrum of **72** as shown in Figure 82 depicts four singlets at 1.54, 1.49, 1.43, and 1.41 ppm representing the four different *tert*-butyl protons. Due to the fact that the *tert*-butoxy group above the P_2N_2 ring is bent towards one of the imino nitrogen atoms, the protons of the *tert*-butyl group on this nitrogen atom are chemically and magnetically non-equivalent to those on the other imino *tert*-butyl group. Hence, two separate peaks are observed for each of the *tert*-butylimino protons at 1.49 and 1.41 ppm. The *tert*-butylamino protons and the *tert*-butoxy protons appear as singlets at 1.54 and 1.43 ppm, respectively.

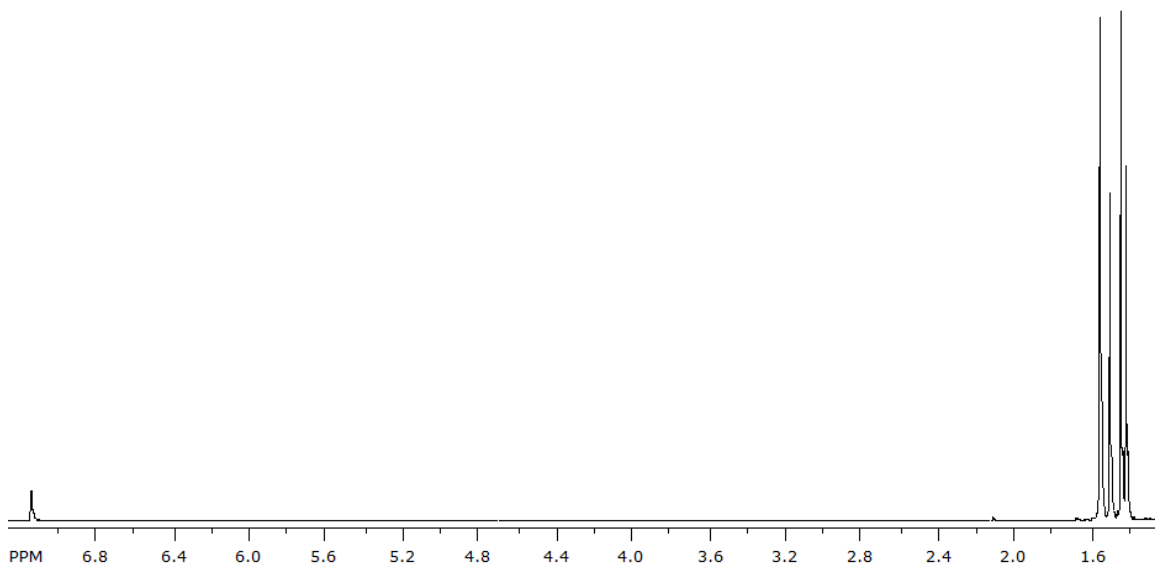


Figure 82. ^1H NMR Spectrum of **72**.

The $^{13}\text{C}\{^1\text{H}\}$ NMR spectrum of **72** (Figure 83) shows eight signals that resonate between 74.01 and 27.95 ppm. The quaternary and primary *tert*-butoxy carbons resonate as singlets at 74.04 and 34.15 ppm, respectively. While the quaternary imino carbons appear as triplets at 53.29 and 52.61 ppm; the primary *tert*-butylimino carbon appear as triplets at 30.98 and 27.95 ppm. These imino carbons all appear as triplets due to their coupling with the two phosphorus atoms in the P_2N_2 ring. On their part, the quaternary and primary *tert*-butylamino carbons resonate as doublets at 56.80 and 32.52 ppm, respectively. These doublets are a result of coupling with just one phosphorus atom in the P_2N_2 ring.

As expected, the $^{31}\text{P}\{^1\text{H}\}$ NMR spectrum of **72** (Figure 84) shows just one signal at 158.1 ppm for the two identical phosphorus atoms in the P_2N_2 ring. This chemical shift is indicative of a phosphorus(III) derivative.

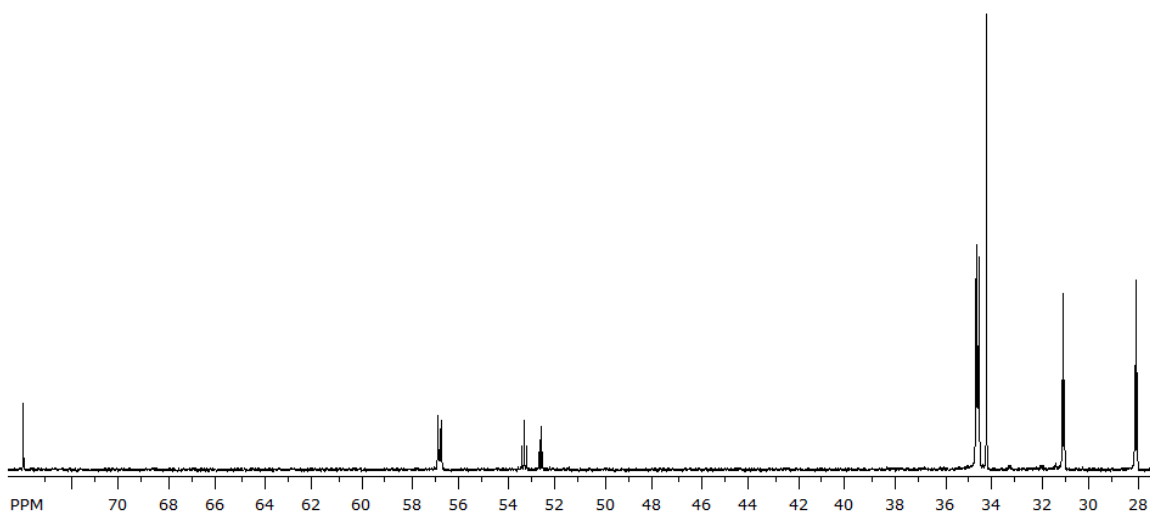


Figure 83. $^{13}\text{C}\{^1\text{H}\}$ NMR Spectrum of **72**.

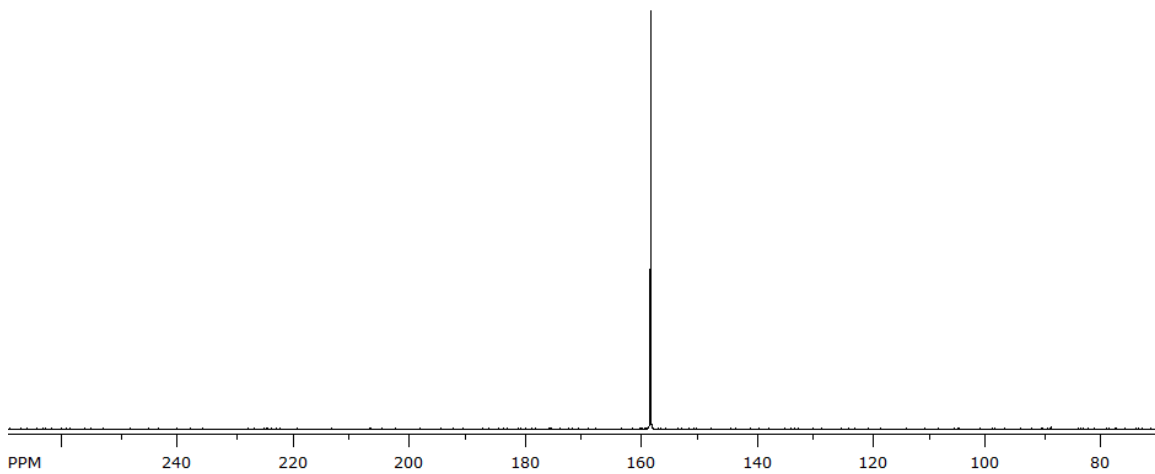


Figure 84. $^{31}\text{P}\{^1\text{H}\}$ NMR Spectrum of **72**.

5. Summary and Conclusion

The reactions of $\{[(^t\text{BuNP})_2(^t\text{BuN})_2]\text{ECl}\}$, $\text{E} = \text{P}, \text{Sb}$, with various reagents was studied. The reaction of $\{[(^t\text{BuNP})_2(^t\text{BuN})_2]\text{PCl}\}$, **49**, with excess sulfur, AgSO_3CF_3 , PhMgCl , and NaO^tBu gave compounds $[(^t\text{BuNP}=\text{S})_3\text{N}]$, **66**, $[(^t\text{BuNP})_2(^t\text{BuN})_2]\text{P}^+\text{SO}_3\text{CF}_3^-$, **67**, $\{[(^t\text{BuNP})_2(^t\text{BuN})_2]\text{PPh}\}$, **68**, and $\{[(^t\text{BuNP})_2(^t\text{BuN})_2]\text{PO}^t\text{Bu}\}$, **70**, respectively. Compound **66** is a C_s -symmetric, high-thermally stable molecule with the potential to be a tridentate ligand. It was obtained after the elimination of *tert*-butyl chloride during the high temperature oxidation of compound **49**. While compound **67** is an ammonium ion derivative of cyclodiphosph(III)azanes obtained by the chloride abstraction of **49** with silver triflate. This ammonium ion is insoluble in non-polar organic solvents like toluene and hexanes, but it was expectedly soluble in polar solvents such as tetrahydrofuran. Compounds **68** and **70** are the first examples of phenyl and *tert*-butoxy mono-phosphorus derivatives, respectively, of cyclodiphosph(III)azanes. Oxidation of compound **68** with elemental sulfur resulted in $\{[(^t\text{BuNP})_2(^t\text{BuN})_2](\text{P}=\text{S})\text{Ph}\}$, **69**.

Also, the reaction of $\{[(^t\text{BuNP})_2(^t\text{BuN})_2]\text{SbCl}\}$, **51** (the antimony analogue of compound **49**), with PhMgCl yielded $\{[(^t\text{BuNP})_2(^t\text{BuN})_2]\text{SbPh}\}$, **71**. Although the X-ray structure of compound **68** could not be properly refined due to crystallographic disorder, NMR data and the X-ray structure of compound **71** suggest that the two compounds are structurally similar. The only difference is that in **71**, one of the imido nitrogen atom of the P_2N_2 ring is datively bonded to the antimony atom but there is no such interaction in **68**. These observations show that compounds **49** and **51** can undergo a wide range of reactions such as elimination, substitution and oxidation reactions, and that at very high

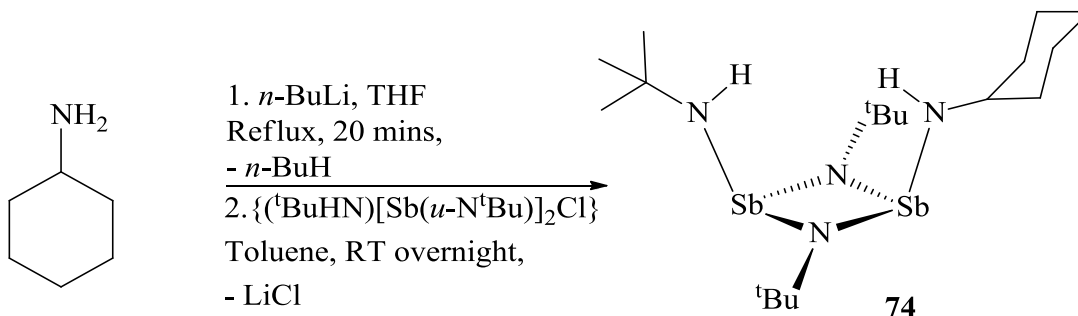
temperatures there is potential for rearrangement in cyclodiphosphazanes to give more thermally stable compounds. We also found that oxidation of the P₂N₂ ring P atoms is more difficult than that of the P atoms above the ring. The ease of oxidation of P atoms above the ring is due to the availability of the electron pair. In the ring the lone pair has more s character, making the P atoms more difficult to oxidize.

APPENDICES

APPENDIX I

Synthesis and Spectroscopic Analysis of $\{({}^t\text{BuHN})[\text{Sb}(\mu\text{-N}^t\text{Bu})]_2(\text{CyNH})\}$, **74**

The synthesis of **74** is a two-step process (Scheme 35). First, cyclohexylamine was deprotonated with one equivalent of *n*-BuLi. Then, the resulting lithium salt was treated with one equivalent of $\{({}^t\text{BuHN})[\text{Sb}(\mu\text{-N}^t\text{Bu})]_2\text{Cl}\}$, **73**, to obtain compound **74** in 78 % yield. We synthesized **74** in an attempt to understand which *tert*-butyl group is eliminated during the high temperature oxidation of **49** to obtain **66**. Work in this area is currently in progress.



Scheme 35. Synthesis of **74**.

The ${}^1\text{H}$ NMR spectrum of **74** (Figure 85) depicts nine peaks. The two types of *tert*-butyl protons appear as singlets at 1.23 and 1.08 ppm, while the *tert*-butylamino hydrogen atom appears as a broad singlet at 1.68 ppm. The cyclohexylamino hydrogen atom appear as a broad multiplet at 4.76 ppm, while the cyclohexyl protons appear as sets of multiplet between 2.53 and 1.00 ppm.

The $^{13}\text{C}\{^1\text{H}\}$ spectrum of **74** is made up of ten different singlets (Figure 86). The primary *tert*-butylamido and *tert*-butylimido carbons appear at 27.25 and 34.95 ppm, respectively; while the quaternary *tert*-butylamido and *tert*-butylimido carbons appear at 43.64 and 42.84 ppm, respectively. The six different cyclohexyl carbons appear at 58.98, 55.19, 54.83, 26.59, 26.49, and 26.21 ppm.

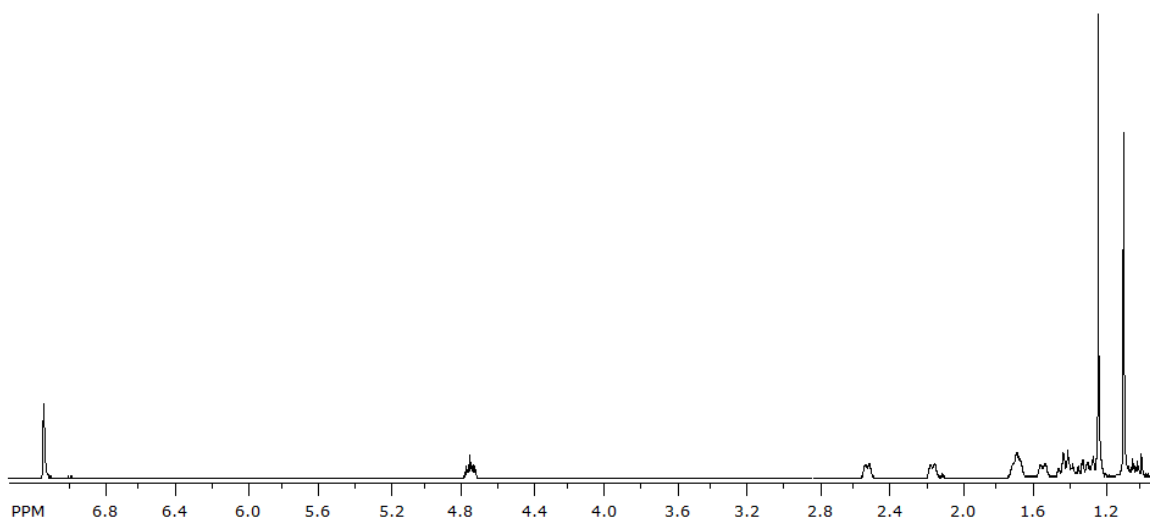


Figure 85. ^1H NMR Spectrum of **74**.

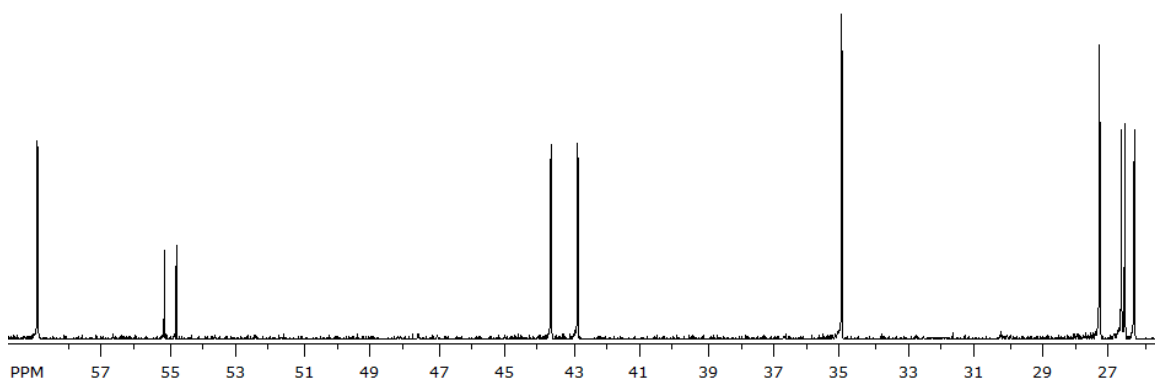


Figure 86. $^{13}\text{C}\{^1\text{H}\}$ NMR Spectrum of **74**.

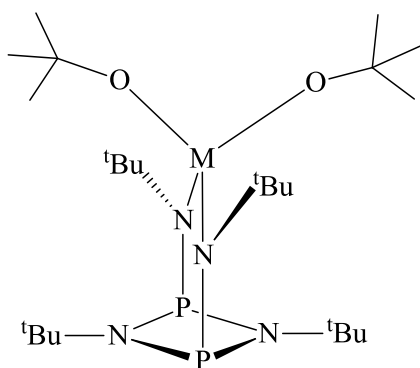
APPENDIX II

Table 29. Crystal and structure refinement data for compounds, **35** and **36**.

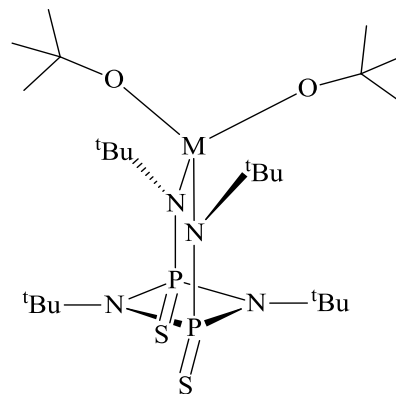
Chemical Formula	C ₂₄ H ₅₄ N ₄ O ₂ P ₂ Zr (35)	C ₂₄ H ₅₄ HfN ₄ O ₂ P ₂ (36)
fw	583.88	671.15
T/K	173(2)	173(2)
$\lambda/\text{\AA}$	0.71073	0.71073
Crystal system	Monoclinic	Monoclinic
Space group	<i>Cm</i>	<i>Cm</i>
$a/\text{\AA}$	28.8773(16)	28.8773(3)
$b/\text{\AA}$	17.0979(9)	17.048(2)
$c/\text{\AA}$	9.8969(5)	9.8591(11)
$\alpha/^\circ$	90	90
$\beta/^\circ$	94.962(2)	94.956(5)
$\gamma/^\circ$	90	90
$V/\text{\AA}^3$	4868.2(5)	4834.9(9)
<i>Z</i>	8	8
$\rho(\text{calc}) \text{ g cm}^{-3}$	0.2512	0.7619
μ/mm^{-1}	0.304	5.455
F(000)	329.2	929.7
Completeness (%)	92.21	93.77
Reflections collected	30481	21283
Independent reflections	9857 [$R_{\text{int}} = 0.0203$]	9904 [$R_{\text{int}} = 0.0193$]

APPENDIX III

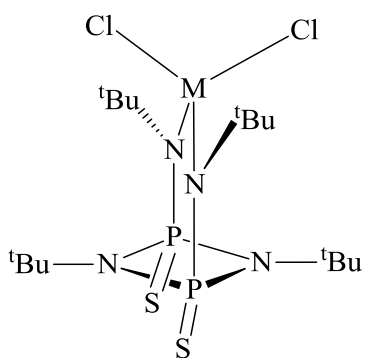
List of Synthesized Compounds



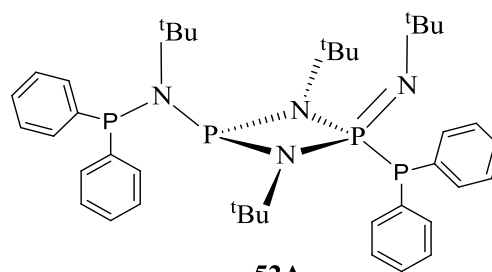
M = Zr (35), Hf (36)



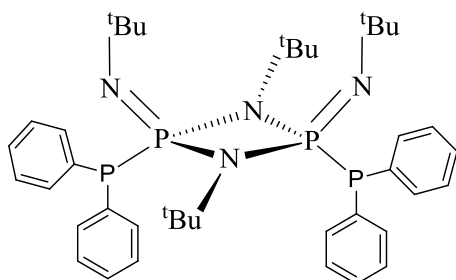
M = Zr (37), Hf (38)



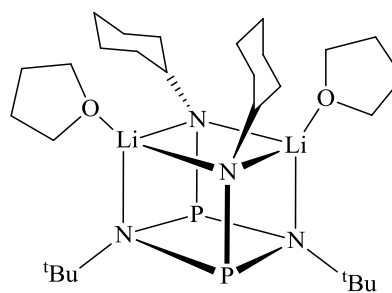
M = Zr (39), Hf (40)



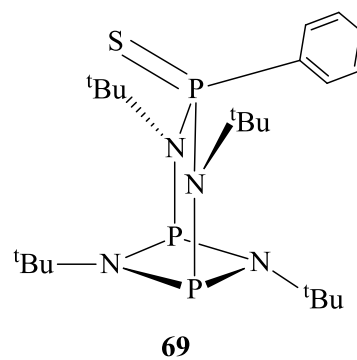
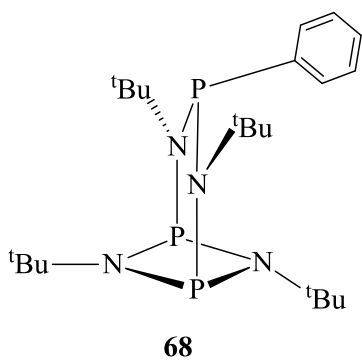
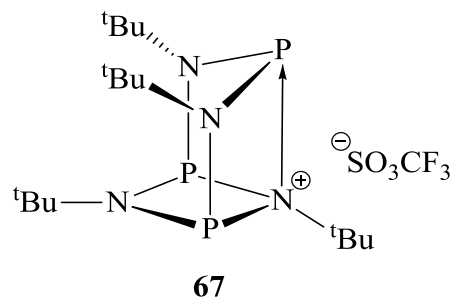
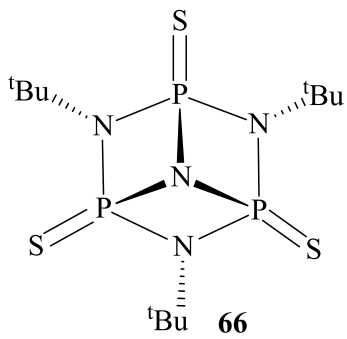
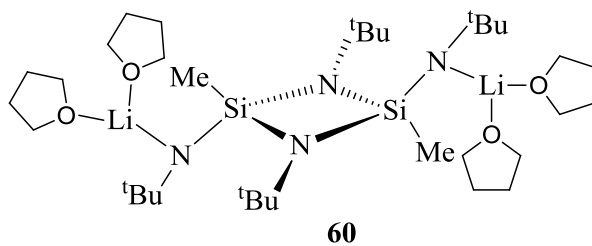
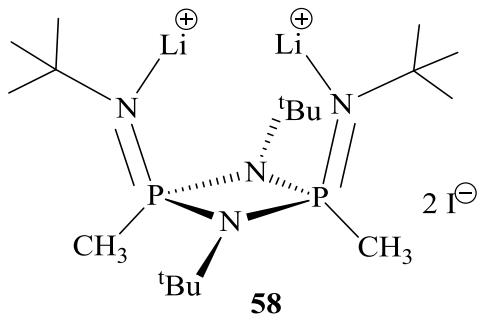
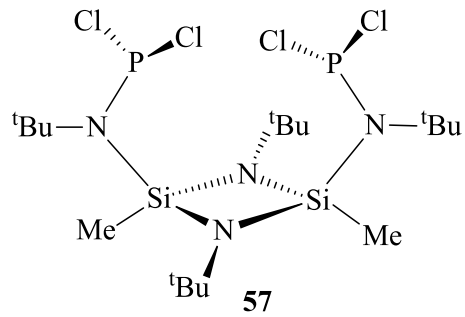
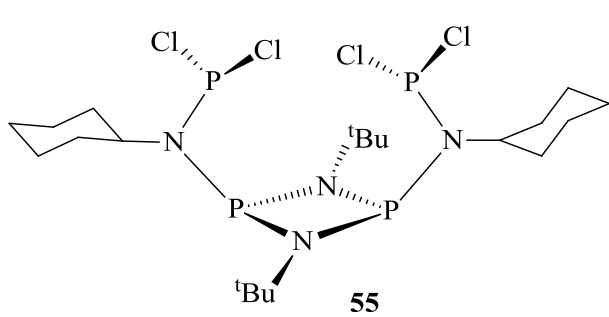
52A

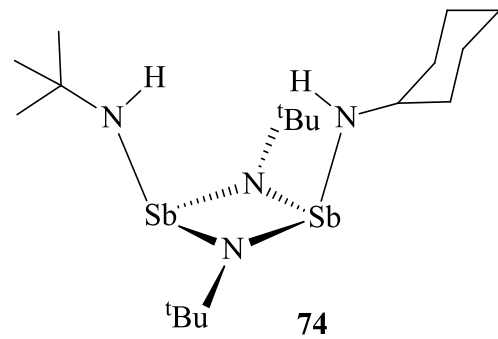
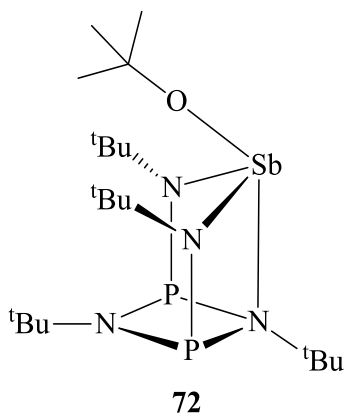
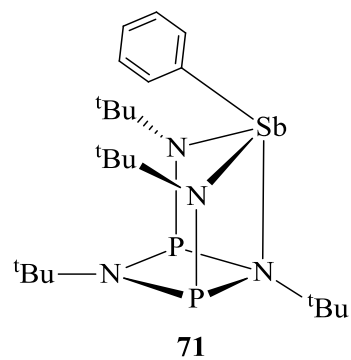
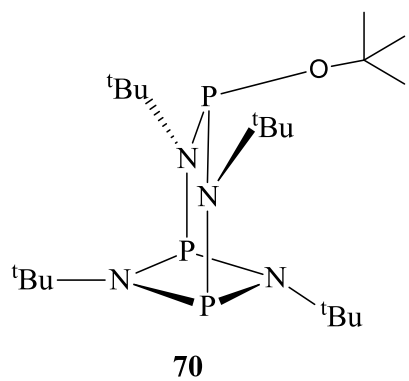


52B



54





REFERENCES

1. Corbridge, D. E. C. *Phosphorus: An Outline of its Chemistry, Biochemistry and Technology*. 5th ed.; Elsevier: Amsterdam, **1995**.
2. Greenwood, N. N. E. *Chemistry of the Elements*. 2nd ed.; Butterworth-Heinemann: Oxford, **1998**.
3. Allen, C. W. *Coord.Chem. Rev.* **1994**, *130*, 137–173.
4. Potin, P.; De Jaeger, R. *Euro. Polym. J.* **1991**, *27*, 341–348.
5. Neilson, R. H.; Wisian-Neilson, P. *Chem. Rev.* **1988**, *88*, 541–562.
6. Allen, C. W. *The Chemistry of Inorganic Homo- and Heterocycles*. Academic Press: London, **1987**.
7. Holmes, R. R.; Forstner, J. A. *Inorg. Chem.* **1963**, *2*, 380–384.
8. Hill, T. G.; Haltiwanger, R. C.; Thompson, M. L.; Katz, S. A.; Norman, A. D. *Inorg. Chem.* **1994**, *33*, 1770–1777.
9. Kumaravel, S. S.; Krishnamurthy, S. S.; Cameron, T. S.; Linden, A. *Inorg. Chem.* **1988**, *27*, 4546–4550.
10. Dou, D.; Duesler, E. N.; Paine, R. T. *Inorg. Chem.* **1999**, *38*, 788–793.
11. Scherer, O. J.; Schnabl, G. *Angew. Chem. Int. Ed. Eng.* **1976**, *15*, 772–772.
12. Davies, A. R.; Dronsfield, A. T.; Haszeldine, R. N.; Taylor, D. R. *J. Chem. Soc. Perkin Trans. 1* **1973**, 379–385.
13. Michaelis, M.; Schroeter, G. *Chem. Ber.* **1894**, *27*, 490.

14. Holmes, R. R. *J. Am. Chem. Soc.* **1961**, *83*, 1334–1336.
15. Jefferson, R.; Nixon, J. F.; Painter, T. M. *J. Chem. Soc. D: Chem. Comm.* **1969**, 622–623.
16. Muir, K. W.; Nixon, J. F. *J. Chem. Soc. D: Chem. Comm.* **1971**, 1405–1406.
17. Keat, R. *Top. Curr. Chem.* **1982**, *102*, 89–116.
18. Keat, R.; Rycroft, D. S.; Thompson, D. G. *J. Chem. Soc. Dalton Trans.* **1979**, 1224–1230.
19. Keat, R.; Rycroft, D. S.; Thompson, D. G. *J. Chem. Soc. Dalton Trans.* **1980**, 321–326.
20. Niecke, E.; Flick, W.; Pohl, S. *Angew. Chem. Int. Ed. Eng.* **1976**, *15*, 309–310.
21. Scherer, O. J.; Wolmershäuser, G.; Conrad, H. *Angew. Chem. Int. Ed. Eng.* **1983**, *22*, 404–405.
22. Balakrishna, M. S.; Mague, J. T. *Organometallics* **2007**, *26*, 4677–4679.
23. Balakrishna, M. S.; Mague, J. T. *Inorg. Chem.* **2009**, *48*, 1398–1406.
24. Chandrasekaran, P.; Mague, J. T.; Balakrishna, M. S. *Inorg. Chem.* **2005**, *44*, 7925–7932.
25. Chandrasekaran, P.; Mague, J. T.; Balakrishna, M. S. *Organometallics* **2005**, *24*, 3780–3783.
26. Grocholl, L.; Schranz, I.; Stahl, L.; Staples, R. J. *Inorg. Chem.* **1998**, *37*, 2496–2499.
27. Grocholl, L.; Stahl, L.; Staples, R. J. *Chem. Commun.* **1997**, 1465–1466.
28. Kumar, N. N. B.; Swamy, K. C. K. *Polyhedron* **2007**, *26*, 883–890.

29. Lief, G. R.; Carrow, C. C.; Moser, D. F.; Stahl, L. *Phosphorus, Sulfur, Silicon Relat. Elts.* **2001**, *168–169*, 157–162.
30. Lief, G. R.; Carrow, C. J.; Stahl, L.; Staples, R. J. *Organometallics* **2001**, *20*, 1629–1635.
31. Lief, G. R.; Moser, D. F.; Stahl, L.; Staples, R. J. *J. Organomet. Chem.* **2004**, *689*, 1110–1121.
32. Moser, D. F.; Carrow, C. J.; Stahl, L.; Staples, R. J. *J. Chem. Soc. Dalton Trans.* **2001**, 1246–1252.
33. Moser, D. F.; Grocholl, L.; Stahl, L.; Staples, R. J. *Dalton Trans.* **2003**, 1402–1410.
34. Moser, D. F.; Schranz, I.; Gerrety, M. C.; Stahl, L.; Staples, R. J. *J. Chem. Soc. Dalton Trans.* **1999**, 751–757.
35. Schranz, I.; Grocholl, L. P.; Stahl, L.; Staples, R. J.; Johnson, A. *Inorg. Chem.* **2000**, *39*, 3037–3041.
36. Schranz, I.; Moser, D. F.; Stahl, L.; Staples, R. J. *Inorg. Chem.* **1999**, *38*, 5814–5819.
37. Schranz, I.; Stahl, L.; Staples, R. J. *Inorg. Chem.* **1998**, *37*, 1493–1498.
38. Stahl, L. *Coord. Chem. Rev.* **2000**, *210*, 203–250.
39. Briand, G. G.; Chivers, T.; Parvez, M.; Schatte, G. *Inorg. Chem.* **2002**, *42*, 525–531.
40. Gangadhararao, G.; Kumara, S. K. C. *J. Chem. Sci.* **2015**, *127*, 197–207.
41. Thompson, M. L.; Tarassoli, A.; Haltiwanger, R. C.; Norman, A. D. *Inorg. Chem.* **1987**, *26*, 684–689.

42. Chandrasekaran, P.; Mague, J. T.; Balakrishna, M. S. *Eur. J. Inorg. Chem.* **2011**, 2264–2272.
43. Chen, H. J.; Haltiwanger, R. C.; Hill, T. G.; Thompson, M. L.; Coons, D. E.; Norman, A. D. *Inorg. Chem.* **1985**, 24, 4725–4730.
44. Briand, G. G.; Chivers, T.; Krahn, M. *Coord. Chem. Rev.* **2002**, 233-234, 237–254.
45. Axenov, Kirill V.; Klinga, M.; Leskelä, M.; Kotov, V.; Repo, T. *Eur. J. Inorg. Chem.* **2004**, 2004, 4702–4709.
46. Siddiqui, M. M.; Mague, J. T.; Balakrishna, M. S. *J. Organomet. Chem.* **2015**, 794, 81–87.
47. Hursthouse, M. B.; Parkes, H. G.; Shaw, L. S.; Shaw, R. A.; Watkins, D. A. *Phosphorus, Sulfur, Rel. Elts.* **1986**, 28, 221–227.
48. Haagensohn, D. C.; Lief, G. R.; Stahl, L.; Staples, R. J. *J. Organomet. Chem.* **2008**, 693, 2748–2754.
49. Chivers, T.; Fedorchuk, C.; Krahn, M.; Parvez, M.; Schatte, G. *Inorg. Chem.* **2001**, 40, 2547–2553.
50. Chivers, T.; Krahn, M.; Parvez, M. *Chem. Commun.* **2000**, 463–464.
51. Chivers, T.; Fedorchuk, C.; Krahn, M.; Parvez, M.; Schatte, G. *Inorg. Chem.* **2001**, 40, 1936–1942.
52. Schranz, I.; Stahl, L. *Inorg. Chim. Acta* **2010**, 363, 975–980.
53. Axenov, K. V.; Leskelä, M.; Repo, T. *J. Catal.* **2006**, 238, 196–205.

54. Lief, G. R. Synthesis and Characterization of Bis(1^o-amino)-cyclodiphosph(V)azanes, Bis(diazasilaphosphetidines), and some of their Metal Complexes. Ph.D. Dissertation, University of North Dakota, Grand Forks, **2003**.
55. Linti, D.; Noth, H.; Schneider, E.; Storch, W. *Chem. Ber.* **1993**, *126*, 619–626.
56. Balakrishna, M. S.; Eisler, D. J.; Chivers, T. *Chem. Soc. Rev.* **2007**, *36*, 650–664.
57. Kommana, P.; Kumara Swamy, K. C. *Inorg. Chem.* **2000**, *39*, 4384–4385.
58. Bashall, A.; Doyle, E. L.; Tubb, C.; Kidd, S. J.; McPartlin, M.; Woods, A. D.; Wright, D. S. *Chem. Comm.* **2001**, 2542–2543.
59. Garcia, F.; Goodman, J. M.; Kowenicki, R. A.; McPartlin, M.; Riera, L.; Silva, M. A.; Wirsing, A.; Wright, D. S. *Dalton Trans.* **2005**, 1764–1773.
60. Chandrasekaran, P.; Mague, J. T.; Balakrishna, M. S. *Dalton Trans.* **2009**, 5478–5486.
61. Brask, J. K.; Chivers, T. *Angew. Chem. Int. Ed.* **2001**, *40*, 3960–3976.
62. Beswick, M. A.; Mosquera, M. E. G.; Wright, D. S. *J. Chem. Soc. Dalton Trans.* **1998**, 2437–2444.
63. Fleischer, R.; Stalke, D. *Coord. Chem. Rev.* **1998**, *176*, 431–450.
64. Calera, S. G.; Wright, D. S. *Dalton Trans.* **2010**, *39*, 5055–5065.
65. Suresh, D.; Balakrishna, M. S.; Mague, J. T. *Dalton Trans.* **2008**, 3272–3274.
66. Siddiqui, M. M.; Mague, J. T.; Balakrishna, M. S. *Inorg. Chem.* **2015**, *54*, 1200–1202.
67. Doyle, Emma L.; Riera, L.; Wright, Dominic S. *Eur. J. Inorg. Chem.* **2003**, 3279–3289.

68. Zhang, K.; Prabhavathy, J.; Yip, J. H. K.; Koh, L. L.; Tan, G. K.; Vittal, J. J. *J. Am. Chem. Soc.* **2003**, *125*, 8452–8453.
69. Bai, G.; Roesky, H. W.; Lobinger, P.; Noltemeyer, M.; Schmidt, H.-G. *Angew. Chem. Int. Ed.* **2001**, *40*, 2156–2159.
70. Bashall, A.; Bond, A. D.; Doyle, E. L.; García, F.; Kidd, S.; Lawson, G. T.; Parry, M. C.; McPartlin, M.; Woods, A. D.; Wright, D. S. *Chem. Eur. J.* **2002**, *8*, 3377–3385.
71. García, F.; Goodman, J. M.; Kowenicki, R. A.; Kuzu, I.; McPartlin, M.; Silva, M. A.; Riera, L.; Woods, A. D.; Wright, D. S. *Chem. Eur. J.* **2004**, *10*, 6066–6072.
72. Gianneschi, N. C.; Bertin, P. A.; Nguyen, S. T.; Mirkin, C. A.; Zakharov, L. N.; Rheingold, A. L. *J. Am. Chem. Soc.* **2003**, *125*, 10508–10509.
73. van Delden, R. A.; Hurenkamp, J. H.; Feringa, B. L. *Chem. Eur. J.* **2003**, *9*, 2845–2853.
74. Schalley, C. A. *Angew. Chem. Int. Ed.* **2002**, *41*, 1513–1515.
75. Surry, D. S.; Buchwald, S. L. *Angew. Chem. Int. Ed.* **2008**, *47*, 6338–6361.
76. Corbet, J.-P.; Mignani, G. *Chem. Rev.* **2006**, *106*, 2651–2710.
77. Schlummer, B.; Scholz, U. *Adv. Synth. Catal.* **2004**, *346*, 1599–1626.
78. Yang, B. H.; Buchwald, S. L. *J. Organomet. Chem.* **1999**, *576*, 125–146.
79. Suresh, R. R.; Swamy, K. C. K. *Tetrahedron Lett.* **2009**, *50*, 6004–6007.
80. Miyaura, N.; Suzuki, A. *Chem. Rev.* **1995**, *95*, 2457–2483.
81. Punji, B.; Mague, J. T.; Balakrishna, M. S. *Inorg. Chem.* **2007**, *46*, 10268–10275.
82. Punji, B.; Mague, J. T.; Balakrishna, M. S. *Inorg. Chem.* **2007**, *46*, 11316–11327.

83. Punji, B.; Mague, J. T.; Balakrishna, M. S. *Inorg. Chem.* **2006**, *45*, 9454–9464.
84. Balakrishna, M. S.; Suresh, D.; Mague, J. T. *Inorg. Chim. Acta* **2011**, *372*, 259–265.
85. Widegren, J. A.; Bennett, M. A.; Finke, R. G. *J. Am. Chem. Soc.* **2003**, *125*, 10301–10310.
86. Kumara Swamy, K. C.; Gangadhararao, G.; Rama Suresh, R.; Bhuvan Kumar, N. N.; Chakravarty, M. *J. Organomet. Chem.* **2010**, *695*, 1042–1051.
87. Gangadhararao, G.; Kumara Swamy, K. C. *J. Chem. Sci.* **2015**, *127*, 197–207.
88. Bhuvan Kumar, N. N.; Chakravarty, M.; Kumara Swamy, K. C. *New J. Chem.* **2006**, *30*, 1614–1617.
89. Lu X, Z. C.; Xu, Z. *Acc. Chem. Res.* **2001**, *34*, 535–542.
90. Kumara Swamy, K. C.; Bhuvan Kumar, N. N.; Balaraman, E.; Pavan Kumar, K. V. P. *Chem. Rev.* **2009**, *109*, 2551–2559.
91. Abd-Ellah, I. M.; El-Bassyouni, M.; Farag, R. S.; El-Khazandar, A. N. *Egypt. J. Microbiol.* **1994**, *29*, 69–72.
92. Suresh, D.; Balakrishna, M. S.; Rathinasamy, K.; Panda, D.; Mobin, S. M. *Dalton Trans.* **2008**, 2812–2814.
93. Balakrishna, M. S. *J. Organomet. Chem.* **2010**, *695*, 925–936.
94. Hegedus, L.; Aris, R.; T., B. A.; Boudart, M.; Chen, N. Y.; Gates, B. C.; Haag, W. O.; Somorjai, G. A.; Wei, J. *Catalyst Design: Progress and Perspectives*. John Wiley & Sons: New York, **1987**.
95. Axenov, K. V.; Klinga, M.; Leskelae, M.; Kotov, V.; Repo, T. *Eur. J. Inorg. Chem.* **2004**, 4702–4709.

96. Axenov, K. V.; Klinga, M.; Leskelae, M.; Repo, T. *Organometallics* **2005**, *24*, 1336–1343.
97. Siemens Analytical X-ray Systems. Madison, WI, **1995**.
98. Sheldrick, G. M. *Acta Cryst.* **2008**, *A64*, 112–122.
99. SADABS Program for Absorption Corrections Using the Bruker CCD Detector System. Based on: Blessing, R. H. *Acta Cryst.* **1995**, *A51*, 33–38.
100. Sheldrick, G. M., SHELXS-90, Program for the Solution of Crystal Structures. University of Gottingen, Gottingen, Germany, **1990**.
101. SHELXTL 5.10 (PC-Version), Siemens Analytical X-Ray Instruments, Inc. Madison, WI, **1998**.
102. SHELXTL NT Version 5.10, Program Library for Structure Solution and Molecular Graphics, Bruker Analytical X-ray Systems. Madison, WI, **1999**.
103. Schranz, I.; Lief, G. R.; Midstokke, S. J.; Stahl, L. *Inorg. Chem.* **2002**, *41*, 6919–6927.
104. Schrock, R. R.; Casado, A. L.; Goodman, J. M.; Liang, L. C.; Bonitatebus, P. J.; Davies, W. M. *Organometallics* **2000**, *19*, 5325–5334.
105. Fan, M.; Duesler, E. N.; Janik, J. F.; Paine, R. T. *J. Inorg. Organomet. Polym. Mat.* **2007**, *17*, 423–437.
106. Wu, Z.; Diminnie, J.; Xue, Z. *J. Am. Chem. Soc.* **1999**, *121*, 4300–4301.
107. Starikova, Z. A.; Turevskaya, E. P.; Kozlova, N. I.; Turova, N. Y.; Berdyev, D. V.; Yanovsky, A. I. *Polyhedron* **1999**, *18*, 941–947.
108. Spijksma, G. I.; Seisenbaeva, G. A.; Bouwmeester, H. J. M.; Blank, D. H. A.; Kessler, V. G. *Polyhedron* **2013**, *53*, 150–156.

109. Njua, E. Y.; Steiner, A.; Stahl, L. *J. Organomet. Chem.* **2011**, *696*, 3301–3303.
110. Perrotin, P.; El-Zoghbi, I.; Oguandinma, P. O.; Schaper, F. *Organometallics* **2009**, *28*, 4912–4922.
111. Black, D. G.; Jordan, R. F.; Rogers, R. D. *Inorg. Chem.* **1997**, *36*, 103–108.
112. Briand, G. G.; Chivers, T.; Schatte, G. *Inorg. Chem.* **2002**, *41*, 1958–1965.
113. Haagenson, D. C.; Moser, D. F.; Stahl, L. *Inorg. Chem.* **2002**, *41*, 1245–1253.
114. Mountford, A. J.; Clegg, W.; Coles, S. J.; Harrington, R. W.; Horton, P. N.; Humphrey, S. M.; Hursthouse, M. B.; Wright, J. A.; Lancaster, S. J. *Chem. Eur. J.* **2007**, *13*, 4535–4547.
115. Milanov, A.; Bhakta, R.; Baunemann, A.; Becker, H.-W.; Thomas, R.; Ehrhart, P.; Winter, M.; Devi, A. *Inorg. Chem.* **2006**, *45*, 11008–11018.
116. Grocholl, L.; Huch, V.; Stahl, L.; Staples, R. J.; Steinhart, P.; Johnson, A. *Inorg. Chem.* **1997**, *36*, 4451–4457.
117. Airoidi, C.; Bradley, D. C.; Chudzynska, H.; Hursthouse, M. B.; Malik, K. M. A.; Raithby, P. R. *J. Chem. Soc. Dalton Trans.* **1980**, 2010–2015.
118. Shi, Y. X.; Liang, R. Z.; Martin, K. A.; Weston, N.; Gonzalez-Calera, S.; Ganguly, R.; Li, Y.; Lu, Y.; Ribeiro, A. J. M.; Ramos, M. J.; Fernandes, P. A.; Garcia, F. *Inorg. Chem.* **2015**, *54*, 6423–6432.
119. Barendt, J. M.; Bent, E. G.; Haltiwanger, R. C.; Norman, A. D. *Inorg. Chem.* **1989**, *28*, 2334–2339.
120. Chang, C. C.; Haltiwanger, C.; Thompson, M. L.; Chen, H. J. *Inorg. Chem.* **1979**, *18*, 1899–1904.

121. Balakrishna, M. S.; Chandrasekaran, P.; Venkateswaran, R. *J. Organomet. Chem.* **2007**, *692*, 2642–2648.
122. Rastaetter, M.; Roesky, P. W. *Eur. J. Inorg. Chem.* **2008**, 5287–5291.
123. Rastaetter, M.; Roesky, P. W.; Gudat, D.; Deacon, G. B.; Junk, P. C. *Chem. Eur. J.* **2007**, *13*, 7410–7415.
124. Ananthnag, G. S.; Kuntavalli, S.; Mague, J. T.; Balakrishna, M. S. *Inorg. Chem.* **2012**, *51*, 5919–5930.
125. Balakrishna, M. S.; Suresh, D.; Mague, J. T. *J. Chem. Sci.* **2011**, *123*, 861–868.
126. Balakrishna, M. S.; Suresh, D.; Rai, A.; Mague, J. T.; Panda, D. *Inorg. Chem.* **2010**, *49*, 8790–8801.
127. Chandrasekaran, P.; Mague, J. T.; Balakrishna, M. S. *Dalton Trans.* **2007**, 2957–2962.
128. Balakrishna, M. S.; Suresh, D.; Mague, J. T. *Eur. J. Inorg. Chem.* **2010**, 4201–4210.
129. Chandrasekaran, P.; Mague, J. T.; Venkateswaran, R.; Balakrishna, M. S. *Eur. J. Inorg. Chem.* **2007**, 4988–4997.
130. Suresh, D.; Balakrishna, M. S.; Mague, J. T. *Tetrahedron Lett.* **2007**, *48*, 2283–2285.
131. Chandrasekaran, P.; Mague, J. T.; Balakrishna, M. S. *Inorg. Chem.* **2006**, *45*, 5893–5897.
132. Chandrasekaran, P.; Mague, J. T.; Balakrishna, M. S. *Inorg. Chem.* **2006**, *45*, 6678–6683.

133. Balakrishna, M. S.; Reddy, V. S.; Krishnamurthy, S. S.; Nixon, J. F.; Burckett, J. C. T. R. *Coord. Chem. Rev.* **1994**, *129*, 1–90.
134. El-Khazandar, A. N.; Farag, R. S.; Abd-Ellah, I. M. *Proc. Indian Natl. Sci. Acad. Part A* **1994**, *60*, 793–801.
135. Schranz, I.; Lief, G. R.; Carrow, C. J.; Haagenson, D. C.; Grocholl, L.; Stahl, L.; Staples, R. J.; Boomishankar, R.; Steiner, A. *Dalton Trans.* **2005**, 3307–3318.
136. Siddiqui, M. M.; Mobin, S. M.; Mague, J. T.; Balakrishna, M. S. *Polyhedron* **2015**, *101*, 179–184.
137. Grocholl, L.; Stahl, L. *Inorg. Chem.* **1998**, *37*, 5036–5038.
138. Gordon, J. G.; Holm, R. H. *J. Am. Chem. Soc.* **1970**, *92*, 5319–5332.
139. Su, Y.; Zheng, X.; Wang, X.; Zhang, X.; Sui, Y.; Wang, X. *J. Am. Chem. Soc.* **2014**, *136*, 6251–6254.
140. Anagho, L. E.; Bickley, J. F.; Steiner, A.; Stahl, L. *Angew. Chem. Int. Ed.* **2005**, *44*, 3271–3275.
141. West, J.; Stahl, L. *Organometallics* **2012**, *31*, 2042–2052.
142. Dyker, C. A.; Burford, N.; Lumsden, M. D.; Decken, A. *J. Am. Chem. Soc.* **2006**, *128*, 9632–9633.
143. Geier, J.; Harmer, J.; Grützmacher, H. *Angew. Chem. Int. Ed.* **2004**, *43*, 4093–4097.
144. Stein, D.; Dransfeld, A.; Flock, M.; Rügger, H.; Grützmacher, H. *Eur. J. Inorg. Chem.* **2006**, 4157–4167.
145. Kooijman, H.; Spek, A. L.; Bommel, K. J. C.; Verboom, W.; Reinhoudt, D. N. *Acta Cryst. C.* **1998**, *54*, 1695–1698.

146. Cataldo, L.; Choua, S.; Berclaz, T.; Geoffroy, M.; Mezailles, N.; Ricard, L.; Mathey, F.; Floch, P. L. *J. Am. Chem. Soc.* **2001**, *123*, 6654–6661.
147. Richman, J. E.; Day, R. O.; Holmes, R. R. *Inorg. Chem.* **1981**, *20*, 3378–3381.
148. DuBois, D. A.; Duesler, E. N.; Paine, R. T. *Inorg. Chem.* **1985**, *24*, 3–5.
149. Haser, M.; Treutler, O. *J. Chem. Phys.* **1995**, *102*, 3703–3711.
150. Maxwell, L. R.; Hendricks, S. B.; Mosley, V. M. *J. Chem. Phys.* **1935**, *3*, 699–709.
151. Li, T.; Arleth, N.; Gamer, M. T.; Koppe, R.; Augenstein, T.; Dielmann, F.; Scheer, M.; Konchenko, S. N.; Roesky, P. W. *Inorg. Chem.* **2013**, *52*, 14231–14236.
152. Rogers, R. D.; Atwood, J. L.; Gruning, R. *J. Organomet. Chem.* **2008**, *157*, 229–237.
153. Lappert, M. F.; Slade, M. J.; Singh, A. *J. Am. Chem. Soc.* **1983**, *105*, 302–304.
154. Chivers, T.; Krahn, M.; Parvez, M.; Schatte, G. *Chem. Commun.* **2001**, 1922–1923.
155. Kruger, T.; Ruffer, T.; Lang, H.; Wagner, C.; Steinborn, D. *Inorg. Chem.* **2008**, *47*, 1190–1195.
156. Eisler, J. D. C., T. *Inorg. Chem.* **2006**, *45*, 10734–10742.
157. Muir, K. W. *J. Chem. Soc. Dalton Trans.* **1975**, 259–262.
158. Lappert, M. F.; Sanger, A. R.; Srivastava, R. C.; Power, P. P. *Metal And Metalloid Amides*. Ellis Horwood: U.K. **1981**.
159. Boeske, J.; Niecke, E.; Nieger, M.; Ocando, E.; Majoral, J. P.; Bertrand, G. *Inorg. Chem.* **1989**, *28*, 499–504.

160. Lappert, M. F.; Sanger, A. R.; Srivastava, R. C.; Power, P. P. *Metal And Metalloid Amides*. Ellis Horwood: Chichester, **1980**.
161. Baumann, D.; Schnick, W. *Inorg. Chem.* **2014**, *53*, 7977–7982.
162. Schnick, W.; Lucke, J.; Krumeich, F. *Chem. Mat.* **1996**, *8*, 281–286.
163. Lee, D. P.; Dreyfuss, P. *J. Polym. Sci. Part A: Polym. Chem.* **1980**, *18*, 1627–1632.
164. Huynh, K.; Rivard, E.; Lough, A. J.; Manners, I. *Inorg. Chem.* **2007**, *46*, 9979–9987.
165. Spinney, H. A.; Korobkov, I.; DiLabio, G. A.; Yap, G. P. A.; Richeson, D. S. *Organometallics* **2007**, *26*, 4972–4982.
166. Romain, J. K.; Ribblett, J. W.; Byrn, R. W.; Snyder, R. D.; Storhoff, B. N.; Huffman, J. C. *Organometallics* **2000**, *19*, 2047–2050.
167. Kadish, K. M.; Autret, M.; Ou, Z.; Akiba, K.-y.; Masumoto, S.; Wada, R.; Yamamoto, Y. *Inorg. Chem.* **1996**, *35*, 5564–5569.
168. Akiba, K.; Onzuka, Y.; Itagaki, M.; Hirota, H.; Yamamoto, Y. *Organometallics* **1994**, *13*, 2800–2803.